

AFAPL-TR-71-55

Details of illustrations in
this document may be better
studied on microfiche

651132
AD 731156

PROPELLER NOISE AT LOW TIP SPEEDS

DAVID BROWN

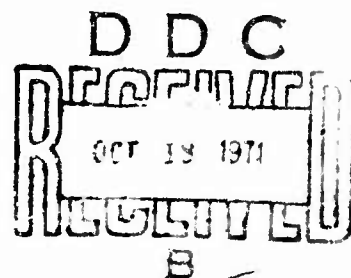
J. B. OLLERHEAD

WYLE LABORATORIES

HAMPTON, VIRGINIA

TECHNICAL REPORT AFAPL-TR-71-55

SEPTEMBER 1971



"This document has been approved for public release
and sale; its distribution is unlimited."

Reproduced by
NATIONAL TECHNICAL
INFORMATION SERVICE
Springfield, Va. 22151

AIR FORCE AERO PROPULSION LABORATORY
AIR FORCE SYSTEMS COMMAND
WRIGHT-PATTERSON AIR FORCE BASE, OHIO

**BLANK PAGES
IN THIS
DOCUMENT
WERE NOT
FILMED**

UNCLASSIFIED

Security Classification

DOCUMENT CONTROL DATA - R&D

(Security classification of title, body of abstract and indexing annotation must be entered when the overall report is classified)

1. ORIGINATING ACTIVITY (Corporate author) WYLE LABORATORIES 7800 Governors Drive, West Huntsville, Alabama 35807		2a. REPORT SECURITY CLASSIFICATION UNCLASSIFIED	
		2b. GROUP N/A	
3. REPORT TITLE PROPELLER NOISE AT LOW TIP SPEEDS			
4. DESCRIPTIVE NOTES (Type of report and inclusive dates) FINAL			
5. AUTHOR(S) (Last name, first name, initial) Brown, David Ollerhead, John B.			
6. REPORT DATE September 1971	7a. TOTAL NO. OF PAGES 212	7b. NO. OF REFS 38	
8a. CONTRACT OR GRANT NO. F33615-70-C-1135 b. PROJECT NO. 9356 Project 3066		9a. ORIGINATOR'S REPORT NUMBER(S) Wyle Laboratories - Research Staff Report WR 71-9	
c. d.		9b. OTHER REPORT NO(S) (Any other numbers that may be assigned this report) AFAPL-TR-71-55	
10. AVAILABILITY/LIMITATION NOTICES "This document has been approved for public release and sale; its distribution is unlimited."			
11. SUPPLEMENTARY NOTES Do not Do not of illustrations in this document may be better studied on microfiche		12. SPONSORING MILITARY ACTIVITY Air Force Aero Propulsion Laboratory Air Force Systems Command Wright-Patterson Air Force Base, Ohio 45433	
13. ABSTRACT This study comprises an analytical and experimental investigation of the "vortex" noise generated by low-tip speed propellers. Initially, the treatment of the subject is focussed on an examination of the origins of broadband noise and the methods by which these can be analytically represented. Subsequent noise measurements on simple-design propellers indicated that the typical spectra in the Strouhal frequency range are significantly influenced by an extensive range of high order harmonics of the blade passage frequency, and a treatment of this harmonic content is included in this study report. The broadband and harmonic components of noise data, obtained from propellers with blade number and blade angle variations, have been analyzed in detail and noise prediction methods have been derived for each. The primary findings of the study are: (i) that the harmonic content due to unsteady blade loads (augmenting the Gutin terms) is essentially constant in amplitude up to harmonic orders (m) given by $mB = 30$ to 40, and decays at rates between 6 and 12 dB per octave, depending on blade tip speed, at higher orders; (ii) the broadband noise characteristic spectrum has a maximum at frequencies given by a Strouhal number of 0.85 based on blade chord; (iii) the fluctuating blade airloads responsible for both harmonic and random radiation appear to be proportional to the steady forces divided by the square root of the number of blades. It is postulated that the noise source mechanisms may be associated with unstable laminar flow separation (or transition) at the blade surfaces. The report also includes a set of graphical procedures by which both harmonic and random spectral details of the radiated noise can be calculated by tip Mach numbers in the range 0.2 to 0.6.			

DD FORM 1473

1 JAN 64

UNCLASSIFIED

Security Classification

NOTICE

When Government drawings, specifications, or other data are used for any purpose other than in connection with a definitely related Government procurement operation, the United States Government thereby incurs no responsibility nor any obligation whatsoever; and the fact that the government may have formulated, furnished, or in any way supplied the said drawings, specifications, or other data, is not to be regarded by implication or otherwise as in any manner licensing the holder or any other person or corporation, or conveying any rights or permission to manufacture, use, or sell any patented invention that may in any way be related thereto.

ACCESSION NO.	
CFSTI	WHITE SECTION <input checked="" type="checkbox"/>
DOC	GRAY SECTION <input type="checkbox"/>
UNCLASSIFIED	<input type="checkbox"/>
JUSTIFICATION	
BY	
REVIEWER/REVIEWER'S NAME	
DOC.	DATE, NAME, SERIAL
A	

- Copies of this report should not be returned unless return is required by security considerations, contractual obligations, or notice on a specific document.

UNCLASSIFIED
Security Classification

DOCUMENT CONTROL DATA - R&D		
<small>(Security classification of title, body of abstract and indexing annotation must be entered when the overall report is classified)</small>		
1. ORIGINATING ACTIVITY (Corporate author) WYLE LABORATORIES 7800 Governors Drive, West Huntsville, Alabama 35897		2a. REPORT SECURITY CLASSIFICATION UNCLASSIFIED
		2b. GROUP N/A
3. REPORT TITLE PROPELLER NOISE AT LOW TIP SPEEDS		
4. DESCRIPTIVE NOTES (Type of report and inclusive dates) FINAL		
5. AUTHOR(S) (Last name, first name, initial) Brown, David Ollerhead, John B.		
6. REPORT DATE September 1971	7a. TOTAL NO. OF PAGES 212	7b. NO. OF REFS 38
8a. CONTRACT OR GRANT NO. F33615-70-C-1135 b. PROJECT NO. 9356 Project 3066	9a. ORIGINATOR'S REPORT NUMBER(S) Wyle Laboratories - Research Staff Report WR 71-9	
c. d.	9b. OTHER REPORT NO(S) (Any other numbers that may be assigned this report) AFAPL-TR-71-55	
10. AVAILABILITY/LIMITATION NOTICES "This document has been approved for public release and sale; its distribution is unlimited."		
11. SUPPLEMENTARY NOTES DO NOT Illustrations in this document may be better studied on microfiche	12. SPONSORING MILITARY ACTIVITY Air Force Aero Propulsion Laboratory Air Force Systems Command Wright-Patterson Air Force Base, Ohio 45433	
13. ABSTRACT This study comprises an analytical and experimental investigation of the "vortex" noise generated by low-tip speed propellers. Initially, the treatment of the subject is focussed on an examination of the origins of broadband noise and the methods by which these can be analytically represented. Subsequent noise measurements on simple-design propellers indicated that the typical spectra in the Strouhal frequency range are significantly influenced by an extensive range of high order harmonics of the blade passage frequency, and a treatment of this harmonic content is included in this study report. The broadband and harmonic components of noise data, obtained from propellers with blade number and blade angle variations, have been analyzed in detail and noise prediction methods have been derived for each. The primary findings of the study are: (i) that the harmonic content due to unsteady blade loads (augmenting the Gutin terms) is essentially constant in amplitude up to harmonic orders (m) given by $mB = 30$ to 40, and decays at rates between 6 and 12 dB per octave, depending on blade tip speed, at higher orders; (ii) the broadband noise characteristic spectrum has a maximum at frequencies given by a Strouhal number of 0.85 based on blade chord; (iii) the fluctuating blade airloads responsible for both harmonic and random radiation appear to be proportional to the steady forces divided by the square root of the number of blades. It is postulated that the noise source mechanisms may be associated with unstable laminar flow separation (or transition) at the blade surfaces. The report also includes a set of graphical procedures by which both harmonic and random spectral details of the radiated noise can be calculated by tip Mach numbers in the range 0.2 to 0.6.		

DD FORM 1 JAN 64 1473

UNCLASSIFIED
Security Classification

PROPELLER NOISE AT LOW TIP SPEEDS

**David Brown
J. B. Ollerhead**

**"This document has been approved for public release
and sale; its distribution is unlimited."**

FOREWORD

The research effort reported herein was conducted by Wyle Laboratories Research Staff under Contract F33 615-70-C-1135 for the Air Force Aero Propulsion Laboratory, Wright-Patterson Air Force Base, Ohio, under Project 3066, Task 12. The present study is part of a continuing program sponsored by the Air Force Aero Propulsion Laboratory which is aimed at reducing propulsion system noise with minimum performance and weight penalties. This study is concerned specifically with propeller noise radiation with emphasis on the relatively high frequency component known as vortex noise. The experimental content of the program, and the test facility design and fabrication, was conducted at Wyle Laboratories Testing Division, Huntsville, Alabama, under the supervision of Mr. J. Robertson. Other major contributors to the experimental program were Mr. J. A. Cockburn and Dr. Tu. The data analysis and theoretical content of the program were conducted by the authors at Wyle Laboratories Hampton Division, Hampton, Virginia. The principal investigator was J. B. Ollerhead.

Dr. M. V. Lowson of the University of Loughborough, England, participated in this program in a consultative capacity.

Mr. J. Robertson of Wyle Laboratories contributed Appendix I of the report.

Captain Paul A. Shahady of the U.S.A.F. was the contract monitor and project engineer during the program, which was conducted during the period November 1969 to March 1971. This report was submitted by the authors in June 1971.

Publication of this report does not constitute Air Force approval of the report's findings or conclusions. It is published only for the exchange and stimulation of ideas.


ERNEST C. SIMPSON

Director
Turbine Engine Division
Air Force Aero Propulsion Laboratory

ABSTRACT

This study comprises an analytical and experimental investigation of the "vortex" noise generated by low-tip speed propellers. Initially, the treatment of the subject is focussed on an examination of the origins of broadband noise and the methods by which these can be analytically represented. Subsequent noise measurements on simple-design propellers indicated that the typical spectra in the Strouhal frequency range are significantly influenced by an extensive range of high order harmonics of the blade passage frequency, and a treatment of this harmonic content is included in this study report.

The broadband and harmonic components of noise data, obtained from propellers with blade number and blade angle variations, have been analyzed in detail and noise prediction methods have been derived for each. The primary findings of the study are: (i) that the harmonic content due to unsteady blade loads (augmenting the Gutin terms) is essentially constant in amplitude up to harmonic orders (m) given by $mB = 30$ to 40 , and decays at rates between 6 and 12 dB per octave, depending on blade tip speed, at higher orders; (ii) the broadband noise characteristic spectrum has a maximum at frequencies given by a Strouhal number of 0.85 based on blade chord; (iii) the fluctuating blade airloads responsible for both harmonic and random radiation appear to be proportional to the steady forces divided by the square root of the number of blades. It is postulated that the noise source mechanisms may be associated with unstable laminar flow separation (or transition) at the blade surfaces.

The report also includes a set of graphical procedures by which both harmonic and random spectral details of the radiated noise can be calculated for tip Mach Numbers in the range 0.2 to 0.6 .

TABLE OF CONTENTS

	<u>Page</u>
I. INTRODUCTION	1
II. PROPELLER NOISE THEORY	5
1. Analytical Considerations	5
2. Sound Generated by Turbulent Flow	10
a. Radiation Due to External Turbulence	12
b. Boundary Layer Radiation	14
c. Vortex Shedding Noise	15
3. Comparison with Previous Experimental Data	15
4. Noise Radiation by Rotating Random Forces	16
a. Theory	16
b. Discussion of Results	20
c. Computation	21
III. EXPERIMENTAL PROGRAM	23
1. Objectives	23
2. Test Blade Geometries and Propeller Design	25
3. Wind Tunnel Tests	26
a. Wake Turbulence Definitions	26
b. Blade Surface Pressure Measurements	29
4. Propeller Noise Measurement Program	31
a. Procedures	31
b. Noise Data Analysis	32
c. Discussion of Test Results	33
d. Propeller Noise Characteristics	35
IV. CORRELATION OF THEORY AND EXPERIMENT	40
1. Broadband Noise Radiation	40
2. Harmonic Noise Radiation	43
3. The Origins of the Fluctuating Airloads	45
a. Random Pressure Fluctuations	46
b. Harmonic Pressure Fluctuations	48
4. Prediction of Propeller Noise Radiation	49
5. Effects of Forward Speed	50
6. Design Requirements for a Quiet Propeller	53

TABLE OF CONTENTS (Concluded)

	<u>Page</u>
V. CONCLUSIONS AND RECOMMENDATIONS	54
1. Theoretical Analysis	54
2. Experiments	55
3. Correlation of Theory and Experiment	56
4. Prediction	57
5. Noise Control	58
6. Recommendations	58
7. Addendum	59
REFERENCES	60
APPENDIX I: DESCRIPTION OF THE EXPERIMENTS	123
APPENDIX II: EXPERIMENTAL DATA	151
APPENDIX III: METHODS FOR PREDICTING THE NOISE OF LOW SPEED PROPELLERS	173
APPENDIX IV: ADDITIONAL EXPERIMENTS ON PROPELLER NOISE CONTROL	189

LIST OF ILLUSTRATIONS

<u>Figure</u>		<u>Page</u>
1.	Narrow Band Analysis of Propeller Noise - Bandwidth $\sim f_o/10$	67
2.	Relative Contributions from Steady Dipole and Quadrupole Sources	68
3.	Coordinate System for Propeller Noise Analysis	68
4.	Noise Radiated from a Plate in a Turbulent Airstream (after Sharland, Reference 16)	69
5.	Directionality Patterns for Combined Load in Any One Harmonic	70
6.	The Variation of $10 \log_{10} J_{\text{mB}}^2$ (mB M sin θ) with Order and Argument Showing Cut-Off Effect	71
7.	Propeller Tip Geometries Employed in Test Program	72
8.	Sensenich W60LK18 Propeller Configuration	73
9.	Thrust Grading on Whirl Test Propellers	73
10.	Coordinate Convention for Wake Turbulence Measurements	74
11.	Turbulence Intensity at Tip Vortex of Tunnel Blade	75
12.	One-Third Octave Band Spectrum of Wind Tunnel Blade Wake Turbulence	76
13.	Turbulence Intensity Contours in Wake of Wind Tunnel Blades	77
14.	Variation of Maximum Turbulence Intensity in Wake with Respect to Maximum Mean Flow Defect	80
15.	Relationship Between Mean Flow Defect and Distance from Trailing Edge of Blade	81
16.	Comparison of Wake Dimensions with Silverstein Theory	82
17.	Arrangement of Tandem Blades in Wind Tunnel	83
18.	Measured Surface Pressures on Wind Tunnel Blades	84

LIST OF ILLUSTRATIONS (Continued)

<u>Figure</u>		<u>Page</u>
19.	One Third Octave Band Spectra of Wind Tunnel Blade Surface Pressures, Measured for Single and Tandem Blade Arrangements	86
20.	Measurement Error of 1/8-Inch Diameter Pressure Transducers	90
21.	Propeller Whirl Test Facility	91
22.	Propeller Configurations	92
23.	On-Axis One Third Octave Band Noise Spectra of Test Propellers	93
24.	One Third Octave Band Spectrum of Sensenich Propeller Noise	94
25.	Installation of Pressure Transducers on Propeller Blade	95
26.	One Third Octave Spectra of Measured Propeller Blade Pressures	95
27.	Narrow Band Spectrum of High Frequency Noise Content	98
28.	Narrow Bandwidth (25 Hz) Spectra of Test Propeller Noise at Various Tip Angle Settings	99
29.	Narrow Band (25 Hz) Spectrum of Sensenich Propeller Noise	102
30.	1 % Bandwidth Spectra of Test Propeller Noise	103
31.	Variation of High Frequency Noise Level with Propeller Geometry	104
32.	Effect of Wind Gusts on Propeller Noise Analyzed in 1/3 Octave Bands	105
33.	One Third Octave Broadband Noise Levels at $\theta = 0^\circ$ (on-axis)	106
34.	One Third Octave Broadband Noise Levels at $\theta = 30^\circ$ (relative to axis)	107
35.	One Third Octave Broadband Noise Levels at $\theta = 60^\circ$ (relative to axis)	108
36.	One Third Octave Broadband Noise Levels of Sensenich Propeller	109
37.	Characteristics of Measured Broadband Noise Content	110

LIST OF ILLUSTRATIONS (Continued)

<u>Figure</u>		<u>Page</u>
38.	Variation of Measured Blade Surface Pressures with Velocity	112
39.	Harmonic Levels of Test Propeller Noise Spectra (on-axis)	113
40.	Harmonic Content of Sensenich Propeller Noise	115
41.	Variation of Harmonic Decay Rate with C_T and M_t	116
42.	Characteristics of Measured Harmonic Noise Content	117
43.	Strouhal Number for Axially Radiated Broadband Noise	119
44.	Dependence of Broadband Noise Radiation upon Blade Thrust Coefficient and Number of Blades	119
45.	Dependence of Low Harmonic On-Axis Levels upon Disc Thrust Coefficient and Blade Number	120
46.	Computed Effect of Forward Speed on Overall Broadband Noise Relative to Instantaneous Position of Propeller	121
I-1.	Arrangement of the Wind Tunnel in the Aerodynamic Laboratory	130
I-2.	Schematic of the Wind Tunnel Model Installation	131
I-3.	Photograph of the Wind Tunnel Model Installation showing a Typical Propeller Blade and the Hot-Wire Probe	132
I-4.	Plan View of Wind Tunnel Blade Configurations, Airfoil Section — NACA 0012	133
I-5.	Photograph of the Free-Field Propeller Test Facility	140
I-6.	Schematic of the Free-Field Propeller Test Facility	141
I-7.	Schematic of the Motor Drive Assembly for the Free-Field Propeller Test Facility	142
I-8.	Details of a Typical Wyle Propeller Blade	143
I-9.	Photograph of the Wyle 2-Blade Propeller Configuration	144

LIST OF ILLUSTRATIONS (Concluded)

<u>Figure</u>		<u>Page</u>
I-10.	Photograph of the Wyle 4-Blade Propeller Configuration	145
I-11.	Photograph of the Wyle 6-Blade Propeller Configuration	146
I-12.	Photograph of the Wyle 2-Blade Propeller showing the Amplifier Package and Slip-Ring Assembly	147
I-13.	Photograph of Wyle Propeller Blades showing the Three Tip Configurations	148
I-14.	Photograph of the Sensenich Propeller	149
II-1.	Turbulence Intensity Distributions at Different Stations Behind a Standard Blade-Tip Assembly. Wind Tunnel Data; $U_{\infty} = 150$ fps, $c = 3$ inch	169
III-1.	Harmonic Noise Levels Due to Unsteady Blade Forces	179
III-2.	Bessel Function Term $10 \log_{10} J_{mB}^2$ (mB M sin θ)	183
III-3.	Spectrum Level (1 Hz Bandwidth) of Random Noise Radiation	184
III-4.	Example Calculation of Propeller Noise Spectrum	188
IV-1.	Comparison of Model Propeller Noise Levels (with Blade Surface Modifications)	190
IV-2.	One Third Octave Band Noise Spectra of Model Propellers at 9000 rpm Speed	191

LIST OF TABLES

<u>Table</u>		<u>Page</u>
I	Pressure Correlation Areas in a Turbulent Boundary Layer	63
II	Estimated Performance of Test Propellers	63
III	Propeller Configurations Tested in Noise Measurement Program	64
IV	Measured Center Frequencies for Broadband Noise. ($\theta = 0^\circ$)	65
II-1	Maximum Streamwise Components of Turbulence Intensity in Wake of Wind Tunnel Test Blade	153
II-2	Maximum Streamwise Components of Turbulence Intensity in Wake of Swept and Trapezoidal Tip Blades	154
II-3	Maximum Components of Turbulence Intensity in Direction Normal to Blade Surface	155
II-4	One-Third Octave Band Levels of Model Propeller Broadband Noise at 12 ft Radius from Hub	156
II-5	One-Third Octave Band Levels of Sensenich Propeller Broadband Noise at 12 ft Radius	161
II-6	One-Third Octave Band Levels of Model Propeller Broadband Noise on Axis at 12 ft Radius from Hub	162
II-7	Harmonic Levels of Model Propeller Noise Spectra at 12 ft Radius from Hub	163
II-8	Harmonic Levels of Sensenich Propeller Noise Spectra at 12 ft Radius from Hub	168

LIST OF SYMBOLS

a_0	Velocity of sound (fps)
A	Propeller disc area (πR^2); also used as plate surface area of integration in Section II.2
A_b	Total blade area (ft ²)
A_c	Correlation area (ft ²)
A_0	Effective correlation area on blades (ft ²)
B	Number of blades
c	Blade chord (ft)
C_{d_0}	Profile drag coefficient
$ C_n $	Modulus of Gutin-term sound pressure of n-th harmonic (lb/ft ²)
C_F	Blade force coefficient (= Acoustic Stress/ $\rho_0 \Omega^2 R^2 Rc$)
C_L	Lift coefficient (= Lift force/ $\frac{1}{2} \rho_0 U_t^2$)
C_S	Reynolds stress coefficient (= $T/\rho_0 r^2 R^2 Rc$)
C_T	Thrust coefficient based on disc area (= $T_0/\frac{1}{2} \rho_0 U_t^2 A$)
C_{T_b}	Thrust coefficient based on blade area (= $T_0/\frac{1}{2} \rho_0 U_t^2 A_b$)
d	Typical blade dimension relative to turbulence generation (ft)
D	Drag force (lb)
f	Frequency (Hz)
f_c	Center frequency of broadband noise spectrum maximum (Hz)
f_0	Disc frequency (= $\Omega/2\pi$ (Hz))

F	Blade loading force or dipole force (lb)
F_i	Dipole force tensor (per unit volume) (lb/ft ³)
G_μ, G_ν	Acoustic transfer function (defined in equation (38))
J_{mB}	Bessel function of first kind and order (mB)
K	Empirical constant
l	Typical turbulence scale length (ft)
l_c	Correlation length (ft)
L	Lift per unit span (lb/ft)
m	Blade passage harmonic number
M	Source Mach number
M_r	Source Mach number in direction of observation point
n	(= mB)
n_c	Value of n at which harmonic level decay occurs
N_S	Strouhal Number based on chord (= f_c/U)
p	Sound pressure (lb/ft ²)
p_n, p_{mB}	Sound pressure of n -th harmonic
p_H, p_B	Harmonic and Broadband sound pressures (lb/ft ²)
p_M, p_D, p_Q	Monopole, Dipole and Quadrupole sound pressures (lb/ft ²)
P	Effective rms differential pressure at blade (lb/ft ²)
$q' = \frac{\partial Q}{\partial t}$	Rate of change of mass introduction (lb sec ² /ft ⁴ /sec ²)

q_t	Dynamic pressure at blade tip ($= \frac{1}{2} \rho_0 U_t^2$)
q_∞	Free stream dynamic pressure ($= \frac{1}{2} \rho_0 U_\infty^2$ (lb/ft ²))
r_i	Radius of observation point from propeller center (ft)
r, r'	Distance between acoustic source and observer (ft)
r_v	Vortex core radius (ft)
R	Propeller Radius (ft)
Re	Reynolds number
S_c	Boundary layer surface pressure correlation area (ft ²)
SPL	Sound pressure level (dB re: 0.0002 microbar)
t	Blade thickness (ft)
t_w	Wake thickness (ft)
T_{ij}	Acoustic stress tensor ($= \rho v_i v_j + p_{ij} - \rho_0^2 \rho \delta_{ij}$) (lb/ft ²)
T_0	Steady thrust load (lb)
T_n	rms thrust component of n-th harmonic (lb)
u, \tilde{u}	Velocity perturbation (fps)
U	Velocity (fps)
\overline{U}	Mean wake velocity (fps)
U_t	Blade tip velocity (fps)
U_∞	Free-stream flow velocity (fps)
v_i, v_j	Local velocity fluctuation tensors (fps)

\tilde{v}	Perturbation velocity in blade wake (fps)
V, V'	Volume (ft ³)
$w(f)$	Power spectral density of sound pressure (lb/ft ²) ² /Hz
$w_p(f)$	Power spectral density of blade surface pressure (lb/ft ²) ² /Hz
$w_L(f)$	Blade loading function ($\approx w_p(f) c $)
W	Sound power (ft lb/sec)
x, y, z	Cartesian coordinates

Greek:

α	Blade pitch angle (degrees)
δ_b	Boundary layer thickness (feet)
δ^*	Boundary layer displacement thickness (feet)
$\bar{\xi}$	Nondimensional shed wake thickness
η, η'	Blade spanwise coordinates (feet)
$\bar{\eta}$	Dynamic pressure loss in airfoil wake
$\bar{\theta}$	Angle between observer and direction of source motion (degrees)
θ	Angle between observer and forward propeller axis (degrees)
λ	Blade loading harmonic number
μ	Summation parameter ($n - \lambda$)
ξ	Blade spanwise coordinate increment (feet)
$\bar{\xi}$	Nondimensional distance behind blade trailing edge
ρ	Air density perturbation amplitude (lb sec ² /ft ⁴)
ρ_0	Mean density of air (lb sec ² /ft ⁴)

σ	Propeller solidity A_b/A
τ	Retarded (source) time $(t - r/a_0)$ (sec)
ω	Radian frequency
Ω	Propeller rotational frequency (rads/sec)

SECTION I

INTRODUCTION

Many different descriptions and definitions of rotor or propeller noise have emerged with the consequence that some confusion exists as to what constitutes each particular form of noise. For a propeller, only two forms of noise radiation are generally recognized, "rotational" noise and "vortex" noise. "Rotational" noise is regarded as that component which would be generated by the propeller operating in an inviscid fluid (but including all the harmonic airloads introduced by unsteady potential flow); whereas, "vortex" noise is considered to be the additional noise which can be attributed, directly or indirectly, to fluid viscosity (boundary layer turbulence and separation, vortex shedding and airfoil encounters with the turbulent wake). Thus, "rotational" noise tends to be harmonic in form, appearing in a spectral analysis as a series of discrete frequency spikes; whereas, "vortex" noise has been regarded as having random characteristics with wide band spectral content.

These categorizations are somewhat complicated by the fact that several fundamental source mechanisms exist - the familiar monopoles, dipoles and quadrupoles of acoustic theory. These result from fluid displacement, aerodynamic blade loads and shear forces exerted on the fluid. Both steady and unsteady sources of each type exist and all can contribute to both the harmonic and random noise radiation. At subsonic speeds and low frequencies the dipole sources generally predominate and these have been the subject of most propeller noise research.

The predominance of the dipole sources has been understood, or at least known, since the pioneering work of Gutin in 1936 (Reference 1). He showed that the harmonically ordered noise of propellers could be attributed to the actions of the steady thrust and torque airloads on the blades. Representing the pressure distributions by point forces acting at the 70 percent radial stations, he developed an expression for the sound radiation patterns about the resulting dipole source and his results have been found to provide good agreement with experimental data for low order harmonics at high tip speeds.

At about the same time Stowell and Deming (Reference 2) were performing experiments with rotating rods using what was fairly advanced analysis equipment at that time. They argued, on the basis of the classical works of Strouhal and Rayleigh, that the modulated wideband noise generated by propellers was analogous to the "Aeolian tones" generated by wires in the wind. Their experiments showed that the Strouhal frequency corresponding to the conditions at rod tips (where the velocity was greatest) correlated very closely with the maximum frequency in the measured noise spectra. The mechanism behind this kind of noise generation is that eddies shed from the rod induce fluctuating pressures on the rod surface which in turn radiate noise; whence the expression "vortex noise". It was not until 1947 that Yudin (Reference 3) advanced the work of Stowell and Deming by developing an analytical expression for the "vortex" noise of rotating rods by integrating the acoustic power output along the rod length.

Yudin's work has formed the basis for most analytical/empirical analysis of the so-called vortex noise up to the present time. Hubbard (Reference 4) adapted Yudin's result to accommodate empirical correction factors which were based on experimental propeller noise data. Schlegel, et al. (Reference 5) further modified the Yudin/Hubbard formula for overall levels, proposed a normalized spectrum shape based on Strouhal numbers, and applied the resulting formulation to helicopter rotors. The spectral distribution was simply presented as a set of octave band levels relative to that in the band centered on the Strouhal frequency. Such a step is indeed consistent with Yudin's analysis with the exception that in dealing with airfoils instead of round rods, Schlegel, et al., substituted projected frontal blade thickness for rod diameters. Consequently, as blade angle of attack increased, so did the projected thickness so that frequency went down.

The latter results were obtained on the basis of experimental data obtained for helicopter rotors, on the assumption that all the acoustic energy within a wide frequency band is random in nature. As can be seen in figure 1, a detailed narrow band analysis of propeller noise over a corresponding frequency range reveals the presence of a significant amount of harmonically ordered noise. There is thus a strong possibility that the empirical formulae offered by References 5 through 7 are influenced, if not controlled, by periodic components of the spectrum.

The above discussions indicate some of the uncertainties which exist regarding the origins and nature of "vortex" noise. Fortunately, the problem of "rotational" noise is understood to a considerably higher degree and much of the work addressed at that subject is beginning to throw light on the problem of "vortex" noise radiation.

The classical theoretical result obtained by Gutin for the propeller noise radiated due to steady thrust and torque forces shows good correlation with experimental data, at least for the low order harmonics and has generally been adequate for prediction purposes. However, the theory grossly underestimates the higher order harmonic levels. In recent studies of the helicopter noise problem, Lowson and Ollerhead (Reference 8) essentially extended Gutin's analysis to include the effects of harmonic airloads. The solution contained a somewhat complex collection of Bessel functions and accounted for harmonics of lift, drag and radial force components.

The conclusions reached as a result of this study were numerous and will not be repeated here. However, the following examples are of particular relevance to the present study:

- (1) The range of airload frequencies which make significant contributions to any acoustic frequency f is approximately $(1 - M) f$ to $(1 + M) f$, where M is the rotational Mach number. Since M , for propellers, typically lies between 0.5 and 1, it is clear that very detailed aerodynamic data is required in order to make realistic calculations of audible noise radiation.
- (2) A narrow band analysis of helicopter noise showed a predominance of "rotational" noise harmonics to significantly higher frequencies than had previously been believed.

The second observation should be accompanied by a statement that here "rotational" noise is defined as "narrow band acoustic energy centered at harmonics of the blade passage frequency." It again brings us to the question of whether or not it is necessary, or justifiable, to distinguish between "rotational" and "vortex" noise. It has already been stated that both are the result of aerodynamic pressures in motion and that any differences are mainly a matter of spatial and temporal coherence. The low frequency noise is controlled by airloads which are functions of the gross dynamic and aerodynamic behavior of the rotor or propeller. In the case of the helicopter, the low airload harmonics are dominated by nonuniform inflow variations whose fluctuations are highly repetitive from revolution to revolution. As frequency increases, emphasis is transferred to airload variations which result from more randomly occurring phenomena such as wake instabilities. Such variations are not exactly repetitive during successive blade revolutions with the result that the airload spectrum, instead of containing discrete harmonic spikes, begins to exhibit "narrow band" peaks. This is reflected in the acoustic spectrum and exaggerated by the frequency broadening effects described above. Finally, at very high frequencies the pressure variations are very random, resulting from various turbulent flow phenomena. Thus, the narrow band peaks increase in width and eventually become a spectral continuum.

The background which led to the present investigation may be summarized as follows:

- (i) For high tip speeds and high power loadings, Gutin's formula provides reasonable estimates of the lower harmonics of rotational noise at least for radiation directions away from the axis of rotation;
- (ii) Harmonic source theories such as that of Lawson and Ollerhead give a good understanding of harmonic noise radiation mechanisms and account for the deficiencies of the Gutin formulation at higher frequencies. Unfortunately, lack of knowledge of the magnitude of the fluctuating source terms limits the usefulness of these methods for prediction purposes. In fact their greatest value is that they allow estimates of the source terms to be derived from the observed noise;
- (iii) Empirical formulae for the "vortex" noise radiation are consistent with experimental data for limited ranges of application but the detailed dependence of its spectral and directional characteristics upon propeller configuration and performance parameters are essentially unknown;
- (iv) Although the major design requirements for quiet propellers are known in principle (low disc loading, low tip speed, low blade loading), the theoretical benefits of these measures are not achieved in practice and theory seems particularly poor under low noise conditions. Available experimental data indicate that in this region, "vortex" noise assumes greater importance relative to the harmonic noise.

The objectives of this program were to perform a combined analytical and experimental study of propeller noise at low tip speeds in an attempt to fill some of the obvious gaps in present knowledge. In particular it was desired to extend the Lawson/Ollerhead analysis to the case of noise radiation by random sources, to measure some of the required aerodynamic input terms on airfoils in both uniform translation and rotation and to develop noise prediction procedures which may be used to optimize the design of quiet propellers with greater confidence than had hitherto been possible.

The work performed to meet these objectives is described in the following sections. Section II includes a review of propeller noise theory and presents the theoretical results for noise radiation by rotating, randomly fluctuating airloads. Section III describes experiments performed in a wind tunnel and a specially developed propeller test stand, and includes examples of the measured data and a discussion of the results. In Section IV the theoretical and experimental results are correlated to derive appropriate source terms for the acoustic equations. Section V reviews the major findings of the study and presents a number of recommendations for further work. Computations have been performed to prepare a set of charts and formulae which may be used to predict both the harmonic and broadband noise of low tip speed propellers. These, together with full instructions for their use, may be found in Appendix III. Appendices I and II are devoted to a description of the experimental facilities and tabulations of experimental data.

SECTION II

PROPELLER NOISE THEORY

1. ANALYTICAL CONSIDERATIONS

Although the primary objective of this study was to investigate the mechanisms underlying the generation of propeller broadband noise, it is practically impossible to divorce this component from the periodic "rotational" noise since the distinction between them is not always clear. Accordingly the arguments developed in this section cover the general problem of acoustic radiation by rotating blades. The distinctions between the two components is that rotational noise is that component attributable to potential flow effects, whereas broadband noise is the component resulting (directly or indirectly) from fluid viscosity. Note that the more commonly used expression "vortex" noise is generally avoided since although perfectly valid, it is really a legacy from early studies of Korman street effects. It will be shown that there are in fact several possible sources of broadband noise in the propeller case.

One of the earliest analytical studies of propeller noise generation was performed by Gutin, who revealed that accurate calculations could be made by considering only the actions of the steady thrust and torque forces upon the atmosphere. To derive this solution Gutin considered a simplified model consisting of a ring of discrete sources representing the propeller disc. The air at each point experiences a force as a blade passes by, and not at any other time. The resulting sound field was obtained by Fourier analysis of this force system and, as might be expected, turned out to have a periodic waveform with a fundamental frequency equal to the blade passage frequency. This theory provided a convenient solution, which for high tip speeds (typically 800-1000 ft. per second) proved satisfactory for practical use.

However, Gutin's equation proved to underestimate the higher harmonic levels for lower speed propellers and particularly helicopter rotors. These discrepancies prompted Loewy and Sutton (Reference 9), Schlegel, et al. (Reference 5), and others to examine the effects of fluctuating components of the blade airloads. They extended Gutin's analysis to cover models comprising surface distributions of sources which were energized at multiple harmonics of the blade passage frequency. Through numerical solutions, they were able to show that periodically fluctuating airloads of relatively small amplitude could be responsible for the observed acoustic harmonics. However, the calculations were still inaccurate at all but the lowest frequencies and in any case were of no value for estimating the apparently random higher frequency energy which becomes increasingly important at lower tip speeds.

The reasons for these inadequacies are easily traceable to oversimplification of the problem although these are equally easily excused. Unsteady aerodynamic phenomena associated with propellers and rotors are exceedingly complex and themselves defy mathematical analysis. Even those which are reasonably well understood lead to very complicated acoustic calculations and there is a very great temptation for the acoustician to simplify at every stage.

In order to assess the implications of some of these simplifications and assumptions it is necessary to return to the basic equation for the sound propagation in a perfect, stationary fluid. In this medium the pressure perturbation, p , satisfies the homogeneous wave equation (in tensor notation with implied summation over three dimensions).

$$\frac{\partial^2 p}{\partial t^2} - a_0^2 \frac{\partial^2 p}{\partial x_i^2} = 0 \quad (1)$$

Here a_0 is the speed of sound and the x_i are the three orthogonal displacement coordinates. In general, $p = a_0^2 \rho$ so that ρ and p are interchangeable in the above equation. Although not specified in these terms, Gutin's analysis were essentially a solution of this equation, for the region surrounding the propeller, in terms of the blade pressure distributions.

A more appropriate equation is the non-homogeneous (forced) equation:

$$\frac{\partial^2 \rho}{\partial t^2} - a_0^2 \frac{\partial^2 \rho}{\partial x_i^2} = \frac{\partial Q}{\partial t} - \frac{\partial F_i}{\partial x_i} + \frac{\partial^2 T_{ij}}{\partial x_i \partial x_j} \quad (2)$$

The three terms on the right hand side correspond to monopole, dipole and quadrupole sources which have been discussed at length in, for example, References 10 and 11. Very briefly, dQ/dt is the mass introduction term for a simple source, $\partial F_i / \partial x_i$ is the force distribution corresponding to surface dipole radiation, and $\partial^2 T_{ij} / \partial x_i \partial x_j$ is the volume distribution of "acoustic stress" responsible for quadrupole noise. Actually it represents all the effects due to fluid inhomogeneities not accounted for in the homogeneous wave equation, including temperature, refraction, diffraction and fluid motions. The latter has in fact the most practical significance and in general $T_{ij} \approx \rho v_i v_j$, the "Reynolds stress". The importance of T_{ij} is discussed in detail by Lighthill (Reference 11).

In making use of the above equation for present purposes, the question arises of what is the relative magnitude of the three terms. In many studies the first and third terms have been discussed as insignificant by comparison with the dipole term. Whereas this is probably true within certain limited ranges of conditions, it is most important to evaluate the inter-relationships in each and every situation.

For the case of sources which move in a straight line with uniform velocity the sound pressures generated by each type of source are (Reference 37) observed to be:

$$\begin{aligned}
 \text{Simple Source (Monopole): } p_M &= \left[\frac{q'}{4\pi r (1 - M \cos \bar{\theta})} \right] \\
 \text{Dipole: } p_D &= \left[\frac{\cos \bar{\theta}}{4\pi a_0 r (1 - M \cos \bar{\theta})^2} \frac{\partial F}{\partial t} \right] \\
 \text{Quadrupole: } p_Q &= \left[\frac{\cos^2 \bar{\theta}}{4\pi a_0^2 r (1 - M \cos \bar{\theta})^3} \frac{\partial^2 T}{\partial t^2} \right]
 \end{aligned} \tag{3}$$

where the square brackets denote evaluation at the retarded or source time $\tau = t - r/a_0$ (which is separated from the observer time, t , by the time of propagation r/a_0), $\bar{\theta}$ is the angle between the direction of motion and the observer at τ , and M is the source Mach number. The simple source parameter q' is $\partial Q/\partial t$. Since a typical source frequency may be assumed to vary with velocity U , each time differentiation of the source term introduces a factor U into the result so that the velocity dependencies of the three terms follow the proportionality

$$1 : \left(\frac{U \cos \bar{\theta}}{1 - M \cos \bar{\theta}} \right) : \left(\frac{U \cos \bar{\theta}}{1 - M \cos \bar{\theta}} \right)^2 \tag{4}$$

Thus we see that the multipole sources rapidly increase their radiation efficiencies as they move at greater speeds with quadrupoles increasing at a greater rate than the dipoles. This ratio of course reflects the well known velocity dependence of the three source types. Since q , F_i and T_{ij} all typically vary as the square of velocity U , the absolute sound pressures vary as $U^2:U^3:U^4$ and the sound intensities as $U^4:U^6:U^8$. This fact is frequently relied upon to identify source types in experiments in which the variation of acoustic power with velocity is measured.

For sources which follow a circular path, as do the blades of a propeller, the results become rather more complex since both the velocities and accelerations of the sources contribute to the sound field. Lowson derived expressions for the sound fields of rotating sources of constant strength and performed Fourier analyses to compute observed harmonic amplitudes. Following Lowson's analysis, it can be shown that the absolute magnitudes of the n -th harmonic (based on the rotational frequency Ω), are in each case:

$$\text{Monopole: } p_{M_n} = \frac{q'}{2\pi r} J_n(n M \sin \theta)$$

$$\text{Dipole: } p_{D_n} = \frac{n \Omega \cos \theta}{2\pi a_0 r} F J_n(n M \sin \theta) \quad (5)$$

$$\text{Quadrupole: } p_{Q_n} = \frac{n^2 \Omega^2 \cos^2 \theta}{2\pi a_0^2 r} T J_n(n M \sin \theta)$$

In these equations, which have been simplified by restricting the sources to single components, the Mach number effect appears in the argument of the Bessel function J_n (of the first kind and of order n). The angle θ is measured from the axis of rotation (positive in the thrust direction), r is the distance of the observer from the center of rotation, and M is the rotational Mach number of the source at radius R from the axis.

As recently demonstrated by Ffowcs-Williams and Hawkins (Reference 13), who compared the dipole and quadrupole sources for rotating machinery sources, the relative importance of the three terms can be assessed by making reasonable assumptions regarding the magnitude of the various parameters in the propeller case. First of all, the ratio of the three harmonic levels $p_{M_n} : p_{D_n} : p_{Q_n}$ is

$$q' : \frac{n \Omega \cos \theta F}{a_0} : \frac{n^2 \Omega^2 \cos^2 \theta T}{a_0^2} \quad (6)$$

The terms F and T are the dipole and quadrupole strengths, which, in the propeller case, are the thrust and integrated Reynolds stress components, respectively. The monopole term q' has been associated, in early studies of rotating blade noise, with the volume displacement of the fluid by the finite thickness of the blades. However, as there is no net input of air mass due to the thickness effect, it can be argued that the monopole strength must be zero in an ideal fluid. In the present work, the monopole term will be neglected.

As pointed out by Lighthill (Reference 11) the thickness effect does induce a net dipole strength, equal to $p_0 V_B \dot{u}$ where V_B is the blade volume and \dot{u} is the local blade acceleration.

The blade force dipole strength F may be written

$$F = C_F p_0 (\Omega R)^2 R c \quad (7)$$

where C_F is a force coefficient based on blade speed and planform area, and c is the blade chord. Thus, the ratio of thickness to thrust dipole components is

$$\frac{F(\text{thickness})}{F(\text{thrust})} = \frac{\rho_0 c t R (U^2/R)}{\rho_0 c R C_F U^2} = \frac{t}{C_F R} \quad (8)$$

where $U = \Omega R$ and t is the blade thickness.

This indicates that thickness noise will only be significant, relative to the thrust load term, for very thick blades at low loading conditions.

The Reynolds stress T can be expressed in a similar fashion since, as noted by Ffowcs-Williams and Hawkings, fluid velocity perturbations in the neighborhood of the blade may be assumed proportional to that of the blade itself. Thus

$$T = C_S \rho_0 \Omega^2 R^2 R c t \quad (9)$$

Substituting equations (7) and (9) into the ratio (6), we obtain the proportionality

$$P_{D_n} : P_{Q_n} = M C_F \cos \theta : n M^2 (t/R) C_S \cos^2 \theta \quad (10)$$

It may be assumed that C_F and C_S are of order unity, and for a propeller with B blades $n = mB$, where m is the harmonic number based on blade passage frequency. Thus the above ratio becomes, for $t/R = 0.01$,

$$M \cos \theta : 0.01 mB (M \cos \theta)^2 \quad (11)$$

This relationship is illustrated in Figure 2, where the relative sound pressure levels of the two source types are plotted as functions of harmonic number mB and the Mach number component $M \cos \theta$. This figure clearly illustrates the equal importance of both parameters showing that although at low Mach numbers, dipole (force) noise dominates the low frequency noise radiation, at high frequencies ($mB > 100$) and high Mach numbers the quadrupole (shear) component can exceed the dipole noise. In assessing these results it is of course important to remember that: (a) these results apply only to the specific case examined and that there is uncertainty regarding appropriate values for C_T and C_S ; (b) only one component each of force and shear have been considered, and other components modify the ratios; (c) the expressions used apply for steady flow conditions and both the quadrupole and dipole noise will be increased by unsteady flow effects. Despite these limitations, it may be concluded that for quiet propellers operating at tip speeds of less than about $M = 0.5$, quadrupole noise should not be expected to make significant contributions to the harmonic noise from $mB < 200$ even on the propeller axis. Furthermore, the relative contribution rapidly decreases with tip speed and as the observer moves away from the propeller axis ($M \cos \theta$ decreasing).

Although some of the previous discussions are appropriate for noise which is not harmonically related to disc frequency, it is most important to recognize that they have been based upon potential flow considerations. Random noise results mainly from viscous flow effect and it is particularly relevant that, as pointed out by Ffowcs-Williams and Hawkings, the Reynolds stresses near the blade are dominated by laminar flow perturbations. Turbulent flow is constrained to small regions, mainly in the blade wakes, and the strength of random quadrupoles may be significantly lower. It is thus necessary to examine the dipole-quadrupole relationships for turbulent flow as a separate matter.

2. SOUND GENERATION BY TURBULENT FLOW

There are two basic turbulence sources, external turbulence interacting with the blade and self-generating turbulence. Although in practice these are highly related, they are best treated by different theoretical methods. External turbulence includes that existing in the atmosphere or that shed from other aircraft components and, more importantly, turbulence shed by other blades. Self-generated turbulence is that in the blade boundary layer but this should be further subdivided into the well behaved attached boundary layer and the separated flows near the blade tips and trailing edges. The latter areas are normally associated with increased levels of turbulence.

The generation of sound from a surface in the presence of turbulence was studied by Curle (Reference 18), who developed the following exact equation for the density perturbation at position x :

$$4\pi a_0^2 \rho = \frac{\partial}{\partial t} \int_A \left[\frac{p_0 v_n}{r} \right] dA - \frac{\partial}{\partial x_i} \int_A \left[\frac{p_{ij} n_j}{r} \right] dA + \frac{\partial^2}{\partial x_i \partial x_j} \int_V \left[\frac{T_{ij}}{r} \right] dV \quad (12)$$

where V and A denote volume and surface integrations, p_{ij} is the nine component stress tensor which includes the viscous and internal pressure forces in the fluid, n_j is the component of the outward normal to the surface, v_n is the normal velocity of the surface and $T_{ij} = \rho v_i v_j + p_{ij} - a_0^2 \rho \delta_{ij}$, an acoustic stress tensor incorporating several effects, the most important of which is generally the turbulent stress.

In fact, this equation is a solution to equation (2) and the three terms on the right hand side are monopole (mass), dipole (force) and quadrupole (stress) components.

Although the appropriate form of the equations for the sound radiated by a surface is known, the exact physical mechanisms which generate the sound in the various cases are not clear. For instance, the fluctuating forces on a stationary surface are supposed to radiate sound, but if the surface is indeed stationary then these forces can do no work. In

the case of a stationary surface it appears that the observed force can be regarded as the consequence of some real source of sound. They do not in themselves produce the sound but are convenient for its calculation.

For an infinite plane surface this property of the surface can be shown explicitly using the reflection principle. The rigorous derivation of equation (12) above applies when the observation point x is inside the volume of integration V . If the observation point is outside the volume V then we derive

$$0 = \frac{\partial^2}{\partial x_i \partial x_j} \int_V \left[\frac{T_{ij}}{r} \right] dV - \frac{\partial}{\partial x_i} \int_A \left[\frac{F_{ij} n_i}{r} \right] dA + \frac{\partial}{\partial t} \int_A \left[\frac{p_0 v_n}{r} \right] dA \quad (13)$$

These two relations (12) and (13), may be used together for the case of turbulence above an infinite plane surface. First note that the sound at the observation point is truly given by equation (12) so that if we know the strength of the acoustic stress and the pressure and mass sources on the boundary the sound can be calculated. Furthermore, by letting the volume V extend to infinity the source terms at infinity will become zero and all that is necessary is to integrate the surface terms over the plane boundary alone. But the plane boundary can be simulated by a supposed image turbulence, which reflects the real turbulence in the plane. Furthermore, the image turbulence together with the image fluctuating pressure makes precisely no contribution to the sound at the observation point by virtue of equation (13). Thus equations (12) for V and (13) for an image volume V' can be added together.

Now the normal pressure terms for the real and image cases are equal and opposite. The tangential terms are due only to viscous forces and are negligible and v_n is zero for the rigid boundary. Thus, adding (12) and (13) gives rise to a cancellation of the direct, static, pressure terms so that the sound field at x can be written as:

$$4\pi a_0^2 \rho(x) = \frac{\partial^2}{\partial x_i \partial x_j} \int_{V+V'} \left[\frac{T_{ij}}{r} \right] dV \quad (14)$$

providing the viscous terms can be ignored which is shown to be the case experimentally (see for example, Lighthill, Reference 11).

Equation (14) shows that the total sound field is just the sum of the real and image turbulent radiation. Thus the infinite plane can be regarded simply as a passive reflector of the turbulent sound emission. The fluctuating pressures on the plane are merely a result of the reflection process.

In the case of the finite plane the required image turbulence will not be a simple reflection of the source turbulence. Here it is possible to regard the turbulent field either as reflected and diffracted by the finite plane as the source, or to regard the actual pressure field on the plate as a source. From the physical point of view probably the first explanation is more correct, but from the calculation point of view the second

way of looking at the process is more helpful. The scattering process for a finite plate can result in magnification of the quadrupole field. It is therefore often more convenient to study the sound field due to the pressures, which are basically dipole, and hence of a higher efficiency. This approach retains the largest terms in the acoustic field.

It should be mentioned that a basic theorem of potential theory shows that any field can be constructed from an appropriate assemblage of any order multipoles. Thus the quadrupole field of turbulence can be constructed from the dipole field of the plate. Only for the infinite plate case the integrated dipole strength would be just zero; finite dipole radiation must be expected from a finite plate.

These remarks do have practical significance in noise control, for they suggest that turbulence over extended surfaces will radiate as U^8 (quadrupole), while the same turbulence passing over a small surface will radiate as U^6 (dipole). A reasonable estimate seems to be that sound from turbulence within about a wavelength of the plate edge will be magnified while turbulence over the plate outside this region will simply be reflected.

This has important consequences for the velocity dependence of the radiated sound. For a given frequency, the ratio between the wavelength of the source to that of the radiated sound is simply the ratio of the flow velocity to the speed of sound, i.e., the Mach number. Thus at low speeds the sound wavelength is long, and the whole plate can be radiating as a dipole, while for high speeds the sound wavelength is small and the reflection principle comes into its own. Thus it may be expected that the high speed radiation from a boundary layer on a plate will obey the U^8 law, but the radiation will diverge from this law at low speeds. Similarly it is to be expected that the high frequencies will obey a U^8 law while the low frequencies will correspond more closely to a dipole result.

This also explains why the noise radiation of external turbulence, which has a scale of the order of the chord can be calculated in a dipole model. It is to be expected that the true boundary layer noise, where scale is of the order of the boundary layer thickness, would radiate as a quadrupole down to quite low velocities.

a. Radiation Due to External Turbulence

The first example taken will be radiation from a plate in a turbulent airflow. If the speed is subsonic the acoustic wavelength will be larger than the turbulence scale so that sound from plates of dimensions perhaps up to several times the turbulent scale should be calculable simply from the fluctuating pressures.

The expression for the fluctuating density from a distribution of fluctuating sources can be written as:

$$\rho = \frac{x_i - y_i}{4\pi a_0^3 r^2} \int_A \left[\frac{\partial p_i}{\partial t} \right] dA \quad (15)$$

The total acoustic power is the integral of $a_0^3 \rho^2 / \rho_0$ over the field which is

$$W = \frac{1}{12\pi \rho_0 a_0^3} \int_A \int_{A'} \left[\frac{\partial p}{\partial t}(x) \right] \left[\frac{\partial p}{\partial t}(x') \right] dA dA' \quad (16)$$

Thus we should evaluate the retarded (source) time correlation of the rate of change of pressure on the plate. Now to use this expression we have already had to assume the plate dimension was of the order of the acoustic wavelength. If we now assume it is small compared to the wavelength then the "compact" source assumption can be utilized and the retarded time assumption dropped. Next, one of the integrations over the surface is simply a correlation integral and we can write

$$\int_{A'} \frac{\partial p}{\partial t}(x) \frac{\partial p}{\partial t}(x') dA' = \overline{\frac{\partial p}{\partial t}}^2 A_c \quad (17)$$

where A_c is the correlation area of the pressures. This gives

$$W = \frac{1}{12\pi \rho_0 a_0^3} \int_A \overline{\frac{\partial p}{\partial t}}^2 A_c dA \quad (18)$$

If the blade is in a homogeneous patch of turbulence then the integral simply becomes a multiple by the blade area, A_b . The effects of variation of conditions over the blade span will be studied in Section II.4.

To evaluate equation (18) for the case of impinging turbulence we may take advantage of the results of Kemp and Sears (Reference 14) as simplified by Lawson (Reference 15). This shows that the mean lift per unit span on an airfoil in a sinusoidal gust of frequency ω and magnitude u is

$$L = \frac{\pi \rho_0 c U u}{\left(\frac{\pi \omega c}{U} \right)^{1/2}} \quad (19)$$

where c is the airfoil chord.

To extend this to three dimensional conditions we note that the mean lift in terms of pressure fluctuations is:

$$L = p_{rms} \sqrt{l_c c} \quad \text{per unit span} \quad (20)$$

where l_c is the correlation length in the c direction.

If we also put $\left(\frac{\partial p}{\partial t}\right)^2 = \omega^2 \bar{p}^2$ where ω is a typical frequency, then equation (18) becomes, using the results above

$$W = \frac{1}{12\pi\rho_0 a_0^3} A_c (2A) \frac{\omega^2}{c l_c} \frac{\pi\rho_0 c U^3 u^2}{\omega} \quad (21)$$

The $2A$ arises because both sides of the plate radiate. If we finally put $\omega = U/l$, where l is a typical length and let $A_c = l^2$, $l_c = l$, the final result for the sound power radiated is

$$W = \frac{1}{6} \frac{\rho_0 U^4 u^2 A}{a_0^3} \quad (22)$$

This result is almost identical with that of Sharland (Reference 16) for the same case, except he has a factor $\pi/20$ instead of $1/6$. Somewhat less restrictive assumptions have been made in the present investigation.

b. Boundary Layer Radiation

The same formula can be applied to radiation from the boundary layer pressure fluctuations acting on the plate. It will be recalled that theory indicates the direct quadrupole radiation from the turbulence to be stronger for this case, nevertheless it is of interest to attempt a boundary layer pressure fluctuation calculation.

Equation (18) gives

$$W = \frac{1}{12\pi\rho_0 a_0^3} \int \bar{p}^2 \omega^2 A_c dA \quad (23)$$

Experiments indicate that \bar{p}^2 is of the order that $\bar{p}^2 = 36 \times 10^{-6} q^2$, where q is the dynamic head $(\rho_0 U^2/2)$. However, there is a rather less agreement over the correlation data magnitude.

Values of correlation areas assumed by various authors are given in Table I. There now seems little doubt that the correlation area assumed by Doak was far too large, while that of Lighthill is somewhat too small. These assumptions were based on limited available data sources. Most recent studies of boundary layer pressure fluctuations have broadly agreed with Bull's data (Reference 20). Thus the correlation area can be expressed as $\omega^2 S_c = KU^2$ where the constant K is the range $0.1 < K < 1.0$. Substituting into equation (23) gives the approximate result

$$W \approx \frac{10^{-7} \rho_0 U^6 A}{a_0^3} \quad (24)$$

in agreement with Sharland (Reference 16).

Comparing equation (22) with equation (24) shows that an input turbulence level of as little as 0.001 is sufficient to outweigh the direct radiation of the boundary layer pressure fluctuations. Two assumptions were made in the derivation of equation (18), that the blade was small and the sources compact. The compact source assumption is probably reasonable because the eddy scale is small, but the small blade assumption is not necessarily correct, and it could be more appropriate in this case to calculate the sound as a turbulence reflection. If we crudely assume that the turbulence is similar to that in a jet we can use an empirical model for the radiated jet noise (Reference 11):

$$\frac{W}{W_j} = 3 \times 10^{-5} M^5 \quad (25)$$

relating the mechanical and acoustic powers of the jet. The mechanical power of the plate is roughly $0.05 \rho_0 U^3 A$ and the acoustic output must be quadrupled to allow for reflection. Thus it appears that

$$W = \frac{6 \times 10^{-6} \rho_0 U^8 A}{a_0^5} \quad (26)$$

could be an order of magnitude estimate for the turbulence noise output. Equation (26) shows that the sound due to turbulent radiation will be higher than that due to pressure fluctuations for speeds greater than $M = 0.1$. This offers some confirmation of the small power output of the pressure terms on a large plate. The estimate (26) does not include the effect of plate edges on the sound. The trailing edge turbulence radiation should be enhanced by this effect. On the other hand, the turbulence in the boundary layer has an increased decay time scale compared with a jet, and this would result in a noise radiation somewhat less than the above estimate.

c. Vortex Shedding Noise

Little data are available on the magnitude of lift fluctuations induced by the bound circulation changes which accompany trailing edge vortex shedding. Sharland quotes from unpublished data that fluctuating lift coefficients should be of the numerical order of the $-1/5$ power of the Reynolds number and gives the result for the total radiated power

$$W = \frac{\rho_0 U^6 (Re)^{-0.4} A}{120 \pi a_0^3} \quad (27)$$

3. COMPARISON WITH PREVIOUS EXPERIMENTAL DATA

The classic theories advanced above suggest that broadband noise radiation from propellers will obey a U^6 law when under the action of external turbulence of scale comparable with blade chord, but may show a U^8 dependence (as for jet noise) when under the action of

boundary layer turbulence — at least at moderate and high speeds. Self interaction with separated flows probably comes into an intermediate category.

Sharland performed a key experiment which demonstrated the relative importance of self excited and external turbulence to the radiated noise. He measured the broadband noise radiated by a small plate inserted into the flow of an air jet at positions located in both the laminar flow region close to the nozzle and the fully developed turbulent flow eight diameters downstream. His results, which compare the experimental data with estimates based on equations (22), (24), and (27) (or very similar ones) are presented in Figure 4. The highest levels were obtained in the turbulent flow region and the external turbulence equation (22) is seen to predict the observed levels very accurately.

The laminar flow levels were around 15 dB less and the vortex shedding equation (27) gives a better estimate of the level than does the external turbulence equation (based on the turbulent shear levels surrounding the laminar core), apparently confirming the predominance of vortex shedding in this case. However, the validity of the assumptions used in equation (27) is unclear and it is also important to note that, as shown by Tu (Reference 38) even for a carefully designed nozzle, turbulence levels can reach 1 - 2% in the "laminar cores" of jets. These would be quite sufficient to explain Sharland's laminar flow data and the vortex shedding effect remains open to question. The boundary layer level predicted by equation (24) is practically 20 dB too low but again an appropriate magnitude for (p/q) is not clear.

A further source of data is that of Yudin (Reference 3) who performed experiments with rotating cylindrical loads. This experiment necessarily involves passing each rod through the wake of its predecessor and Yudin's U^6 results therefore verify the dipole model for external turbulence. Yudin claimed that the sound radiated was due to the Karman Vortex Street leaving the rods and used the term "vortex noise" for the phenomenon. However it is impossible to ascertain whether the self excited force fluctuations or the turbulent inflow was in fact responsible for the noise.

4. NOISE RADIATION BY ROTATING RANDOM FORCES

a. Theory

The previous sections have described the background to the present study and in particular demonstrated the analytical techniques for estimating the broad features of noise attributable to turbulent flow processes. It has been shown that provided the scale of turbulent fluctuations is not significantly smaller than the blade chord dimensions it is adequate to calculate the noise radiated by the surface pressures by a dipole model. The next step is to derive a more complete solution for the noise radiated by rotating sources as a basis for a detailed correlation with experimental data to be presented in Section III. The theory outlined below is essentially an extension of that developed by Lowson and Ollerhead for harmonic rotor noise and is in fact a more rigorous development of the analysis performed in Appendix II of Reference 8. The theory has recently been presented in detail by Lowson (Reference 22) and an equivalent approach was also pursued by Ffowcs-Williams and Hawkings (Reference 13).

The original analysis (Reference 8) assumed that the blade airloads could be expanded as a Fourier series, which in turn limited the noise to a periodic signal containing harmonics of the disc rotational frequency f_0 . Cancellations due to symmetry of all blades in the rotor further eliminates all frequencies which are not harmonics of the blade passage frequency Bf_0 . Random noise on the other hand is radiated by blade loads which can occur at any frequency and it is thus necessary to derive the spectrum function of the observed sound. That is, we have to evaluate

$$\hat{p}(f) = \int_{-\infty}^{\infty} p(t) \exp -2\pi i f t \, dt \quad (28)$$

where $p(f)$ is the Generalized Spectrum Function at the observer's position. From Reference (10) the sound due to a fluctuating point force in arbitrary motion may be written

$$p(t) = \left[\frac{x_i - y_i}{(1 - M_r)_0 a_0 r} \frac{\partial}{\partial t} \left\{ \frac{F_i}{4\pi r (1 - M_r)} \right\} \right] \quad (29)$$

With this substitution, equation (28) may be integrated by parts at the source time (ignoring the near field) to yield

$$\hat{p}(f) = \int_{-\infty}^{\infty} \frac{if(x_i - y_i)}{2a_0 r} F_i \exp -2\pi i f(\tau + r/a_0) \, d\tau \quad (30)$$

The thrust and drag force components, T and D , are used (see figure 3) together with the far field retarded time approximations of References 10, 12 and 37 which is

$$r = r_1 - \frac{yR}{r_1} \cos \Omega t \quad (31)$$

The random thrust or drag forces are in turn represented by their spectrum functions

$\hat{T}(g)$ and $\hat{D}(g)$ where

$$\hat{T}(g) = \int_{-\infty}^{\infty} T(t) \exp -2\pi g t \, dt \quad (32)$$

and

$$\hat{T}(t) = \int_{-\infty}^{\infty} \hat{T}(g) \exp 2\pi i g t \, dg$$

Substitution of these relationships into equation (30) yields (putting $x/r_1 = \cos \theta$, $y/r_1 = \sin \theta$)

$$\begin{aligned} \hat{p}(f) = & \int_{-\infty}^{\infty} \int_{-\infty}^{\infty} \frac{-if}{2a_0 r_1} \left\{ \hat{T}(g) \cos \theta + \hat{D}(g) \sin \theta \sin \Omega \tau \right\} \\ & \cdot \exp -2\pi i \left\{ (f-g)\tau + \frac{fr_1}{a_0} - \frac{fR}{a_0} \sin \theta \cos \Omega \tau \right\} dg \, d\tau \end{aligned} \quad (33)$$

which is integrated to give a series solution summed over a summation parameter μ :

$$\hat{p}(f) = \frac{if}{2a_0 r_i} \sum_{\mu=-\infty}^{\infty} i^{\mu} \left\{ \hat{T}(f - \mu f_0) \cos \theta - \frac{\mu a_0}{2\pi f R} \hat{D}(f - \mu f_0) \right\} J_{\mu} \left(\frac{2\pi f R}{a_0} \sin \theta \right) \quad (34)$$

where J_{μ} is a Bessel Function of the first kind and order μ . Before proceeding to a discussion of this equation it is of considerable interest to compare it with the equivalent result for harmonic forces from Reference 8. This can be written

$$p_n = \frac{n\Omega i}{4\pi a_0 r_i} \sum_{\mu=-\infty}^{\infty} i^{-\mu} \left\{ T_{n-\mu} \cos \theta - \frac{\mu a_0}{n\Omega R} D_{n-\mu} \right\} J_{\mu} \left(\frac{n\Omega R}{a_0} \sin \theta \right) \quad (35)$$

where p_n is the pressure amplitude of the n -th harmonic, and T_{λ} , D_{λ} are the (complex) amplitudes of the λ -th harmonic of thrust and drag, using the equivalences $f = \frac{n\Omega}{2\pi}$ and $\mu = n - \lambda$. It may be seen that the equations have in fact identical forms, with the harmonic amplitudes and spectrum functions of the blade loads being interchanged. However, a significant difference is that whereas the harmonic component p_n has direct practical value, the spectrum function \hat{p} has no direct physical meaning and the power spectral density $w(f)$ of the observed sound must be calculated.

To do so it is convenient to rewrite equation (34) in the form

$$\hat{p}(f) = \frac{f}{2a_0 r_i} \sum_{\mu=-\infty}^{\infty} \hat{F}(f - \mu f_0) G_{\mu}(R, f) \quad (36)$$

where it is assumed that the thrust and drag terms are simply components of the same normal force term F , where

$$\hat{T} = \hat{F} \cos \alpha' \quad ; \quad \hat{D} = \hat{F} \sin \alpha' \quad (37)$$

α' being a physical blade pitch angle. The normal force F is in turn defined in terms of a load per unit blade length L such that $F = \int L(\eta) d\eta$, where the limits of integration are for the moment omitted. The "acoustic transfer function" $G_{\mu}(R, f)$ is defined as

$$G_{\mu}(R, f) = \left\{ \cos \alpha' \cos \theta - \frac{\mu a_0 \sin \alpha'}{2\pi f R} \right\} J_{\mu} \left(\frac{2\pi f R \sin \theta}{a_0} \right) \quad (38)$$

The equation for the observed PSD is

$$w(f) = \lim_{T \rightarrow \infty} \frac{1}{T} \int_{\eta} \int_{\eta'} \hat{p}(\eta, f) \hat{p}^*(\eta', f) d\eta d\eta' \quad (39)$$

where η and η' are independent spanwise coordinates and \hat{p}^* is a complex conjugate of \hat{p} . Upon making the appropriate substitutions and putting $\eta' = \eta + \zeta$, equation (39) can be rewritten

$$w(f) = \lim_{T \rightarrow \infty} \frac{1}{T} \int_{\eta} \int_{\eta'} \frac{f^2}{4a_0^2 r_1^2} \sum_{\mu} \sum_{\nu} \hat{L}(\eta, f - \mu f_0) \hat{L}^*(\eta', f - \nu f_0) \cdot G_{\mu}(\eta, f) G_{\nu}(\eta', f) d\eta d\eta' \quad (40)$$

If it is now assumed that the cross terms in the summation cancel, which implies that frequency components separated by the increment f_0 are statistically independent*, and that G_{μ} and G_{ν} vary little over a typical dimension ζ , then equation (40) becomes

$$w(f) = \frac{f^2}{4a_0^2 r_1^2} \int_{\eta} \int_{\zeta} \sum_{\mu=-\infty}^{\infty} w_L'(\eta, \zeta, f - \mu f_0) |G_{\mu}(\eta, f)|^2 d\zeta d\eta \quad (41)$$

where w_L' is the cross power spectral density of the spanwise blade loading at positions η and $\eta + \zeta$. Finally, the ζ integration is performed to give

$$w(f) = \frac{f^2}{4a_0^2 r_1^2} \int_{\eta} \sum_{\mu=-\infty}^{\infty} w_L(\eta, f - \mu f_0) l_{\eta}(f - \mu f_0) |G_{\mu}(\eta, f)|^2 d\eta \quad (42)$$

where w_L is the power spectral density of the spanwise blade loading at position η and frequency $f - \mu f_0$ and l_{η} is a spanwise correlation length in the vicinity of η within which the fluctuation at frequency $f - \mu f_0$ may be regarded as phase coherent.

* This is true for stationary signals.

The modulus squared of the "acoustic transfer function" is

$$\left| G_{\mu}(\eta, f) \right|^2 = - \left\{ \cos \theta \cos \alpha - \frac{p_0 a_0}{2\pi f \eta} \sin \alpha \right\}^2 J_{\mu}^2 \left(\frac{2\pi f \eta \sin \theta}{a_0} \right) \quad (43)$$

A further step may be taken by defining the blade loading function $w_L(f)$ in terms of the surface pressure spectrum $w_p(f)$ so that

$$w_L(f) \approx w_p(f) l_c c$$

where c is the blade chord and l_c is a chordwise correlation length. As noted previously, if $l_c \ll c$ the problem is more properly treated by a quadrupole analysis so that the above approximation is only true for fairly large l_c . However, it does allow some account to be taken of the chordwise decorrelation at moderately high frequencies by writing equation (42) as follows

$$w(f) \approx \frac{f^2}{4a_0^2 r_1^2} \int_{\eta} \sum_{\mu=-\infty}^{\infty} w_p(\eta, f - \mu f_0) A_c(\eta, f - \mu f_0) \left| G_{\mu}(\eta, f) \right|^2 c d\eta \quad (44)$$

b. Discussion of Results

The dipole radiation by the random airloads acting on a propeller blade is completely defined by equation (44), and solutions may be obtained if the spanwise distributions of the power spectral density of the pressure fluctuations $w_p(\eta, f)$ and their spatial correlation $A_c(\eta, f)$ are known. Before proceeding to a discussion of computational problems, however, it is as well to examine the result in some detail in order to understand the basic features of the noise radiation.

Ignoring for the moment the summation over the parameter μ we see that the acoustic transfer function G bears a close resemblance to an equivalent component in the Gutin equation for the radiation by steady thrust and drag forces which may be written

$$p_n = \frac{n f F}{a_0 r_1} \left(\cos \theta \cos \alpha - \frac{a_0 \sin \alpha}{2\pi f_0 \eta} \right) J_n \left(\frac{2\pi f_0 \eta \sin \theta}{a_0} \right) \quad (45)$$

where p_n is the pressure amplitude of the n -th harmonic of rotational noise. F is again a "normal" force whose components $F \cos \alpha$ and $F \sin \alpha$ are total thrust and drag forces respectively. In this steady load case, the basic features of the directivity pattern are controlled by the term

$$\cos \theta \cos \alpha - \frac{a_0 \sin \alpha}{2\pi f_0 \eta}$$

which exhibits two lobes with a null occurring at some angle ahead of the propeller plane (unless the second term is greater than $\cos \alpha$). The Bessel function J_n is zero for zero argument so that theoretically no harmonic noise is radiated along the propeller axis. Also, in the Gutin equation for a subsonic propeller, the argument is always less than the order and so the function never reaches its first peak which occurs when the argument is slightly greater than the order.

On the other hand, in equation (43), μ can be any positive or negative integer so that the argument of the Bessel function can exceed the order by any margin. In this situation, as θ increases from 0 to π , the Bessel function can follow many oscillations about zero so that the radiation pattern for any μ can exhibit many lobes. This is shown in figure 5 taken from Reference 8, for various argument to order ratios. When many of these μ "modes" are added together the superposition of the various patterns smooths out the directivity profile to a fairly smooth function.

Two other important properties of the Bessel functions which allow considerable computational simplification are: (i) that for any given (non-zero) order, their values are insignificant at small arguments before a fairly sharp rise to their first peak, and (ii) that for any argument, the envelope of their peak values remain relatively constant with change in order up to a "cut-off" order. These features are shown in Figure 3 in which $10 \log J_{mB}^2 (mB M \sin \theta)$ is plotted against order (mB), for various arguments. Thus the significant range of the summation parameter μ in equation (44) is confined to limits approximately equal to the Bessel function argument, i.e., $\mu = \pm \frac{2\pi f \eta \sin \theta}{a_0}$.

From a physical point of view, these facts indicate that the noise spectrum at frequency f is generated by blade pressure energy spread over a range of frequencies between $f \pm f_0 M \sin \theta$ where M is the rotational Mach number of the blade coordinate η ; i.e. $M = 2\pi\eta/a_0$. This is entirely due to the Doppler effect which causes a modulation of the frequencies observed from a rotating source. Thus, as the observer moves away from the propeller axis, the observed frequency spectrum is broadened due to rotation. Conversely, on the propeller axis, there is no Doppler effect and the μ summation disappears. This fact is most important from an experimental standpoint since it shows that acoustic spectrum measured on the axis is generated entirely by the fluctuating loads on the blade and is simply related to their integrated spectrum.

c. Computation

At the outset of this program it was hoped to make experimental measurements of some of the properties of w_p and A_c to provide a basis for the numerical evaluation of equation (44). Attempts to do this will be described in Section III, but their success was somewhat limited and it has been necessary to further simplify the theoretical result. To do this, the concept adopted by Gutin and other investigators, that acoustically effective blade loads can be concentrated at a single point on the blade, is used to eliminate the spanwise integration. It was shown in Reference 8, that this procedure gives satisfactory results for harmonic blade loadings and the same arguments apply to the present case. Also, an optimum

loading station appears to be at 0.8 of the radius. After this radial integration, equation (44) becomes

$$w(f) = \frac{f^2}{4a_0^2 r_1^2} \sum_{\mu=-\infty}^{\infty} w_p(R, f-\mu f_0) A_c(R, f-\mu f_0) \left| G_{\mu}(R, f) \right|^2 A_b \quad (46)$$

where A_b is the blade surface area. On the assumption that the pressure fluctuations on different blades are totally uncorrelated with each other, this is simply the total area of all blades.* Although not specifically identified as such, w_p and A_c are "effective values" appropriate to the concentrated source assumption.

The main problem associated with the practical use of equation (46), is now that of calculating the Bessel functions, particularly those of high order and high argument. Even using a high speed recursion method, machine computation is lengthy and difficult and to make the analysis tractable for limited computer facilities, a Bessel function approximation has been employed in many of the calculations performed in this study. It is found that the value of $J_{\mu}^2(\mu) = 0.195\mu^{-0.66}$ and the assumption adopted is that

$$\begin{aligned} J_{\mu}^2(z) &\approx J_{\mu}^2(\mu) && \text{for } \mu < z \\ &= 0 && \text{otherwise} \end{aligned} \quad (47)$$

This approximation is felt to be very useful for this particular application and should result in very small errors for a large saving in computer time. For $\mu = 0$, either the exact value or the approximation $J_0(z) = e^{-0.3z^2}$ has been used for small z .

* but see Section IV.1.

SECTION III

EXPERIMENTAL PROGRAM

1. OBJECTIVES

Previously reported measurements of propeller noise (References 23 to 26, for example) have either been directed towards a general description of the noise field in terms of overall sound level or have been restricted in analysis detail by the use of relatively broad filter bandwidths (compared to the harmonic separation). This has precluded a separation of the harmonic and broadband noise components of propeller noise spectra except in the region of the first few harmonics of the blade passage frequency and has resulted in a general subdivision of propeller noise characteristics into "rotational" and "vortex" components, the latter being generally assumed to comprise all the energy in the region of the Strouhal frequency. It is obvious that such lack of detail can lead to misinterpretations of the origins of sound generation, which, as previously discussed, can be associated with the particular nature of fluid medium disturbance. In the case of propellers, these disturbances arise from the movement of the blades through the medium which creates direct and viscous shear force conditions in the region of each blade and in the wake.

The analytical representation of these effects in propeller noise theories has been somewhat limited by a lack of knowledge of the unsteady aerodynamics, except in low harmonic cases where cyclic loads can be predicted with reasonable accuracy such as the helicopter rotor case. In considering the basic areas of ignorance in the preceding theories, it is apparent for example that the effects of wake turbulence and blade impingement rely completely on some knowledge of the turbulence intensities and profile geometries in relation to blade parameters. Further, the use of such information is based on a simplified Sears function which is more appropriate to sinusoidal gusts of scale length approximating to a blade chord. Consequently, to justify the usage of such expressions, and indeed, to provide a basic input to the subsequent noise theories based on them, it is apparent that some preliminary experimental studies should be conducted along the lines of a verification analysis. While the form of such an experimental study may take various complexities into consideration, the basic technique derived for the present program was based on an emphasis of interest in broadband noise phenomena and therefore concentrated on the effects of turbulence and wake geometry. A wind tunnel test program was devised which would allow a detailed examination of the wake geometry and in particular, the turbulence intensities within the wake field of a simple airfoil section blade with different blade tip shapes. Wake geometries have previously been studied in some detail, as for example by Silverstein et al (Reference 27), but defined in terms of the dynamic pressure loss and downwash characteristics. In the present study the objectives were to briefly check the Silverstein relationships and to derive a similar relationship for the turbulence magnitudes in terms of streamwise direction, which is of course, pertinent to the propeller blade separation and wake impingement problem.

As an obvious follow-up to this study, an additional blade was mounted in the wind tunnel, in a tandem arrangement with the previous blade such that it was immersed in that blade's wake. The downstream blade was instrumented with four pressure transducers which were flush mounted on one surface, at the quarter- and mid-chord positions. Pressure measurements were obtained under this impinging wake condition and then with the upstream blade removed such that the instrumented blade was influenced only by the free stream turbulence and its self-generated turbulence.

The further requirements of the experimental program on low speed propeller noise were simply defined by the need for a detailed description of the actual operating blade loading conditions on a propeller, and for a detailed analysis of the radiated noise field. A whirl test program was therefore defined by which blade pressure and noise field measurements would be obtained for a number of propeller configurations and (static) operating rotational speeds. For the blade pressure measurements, five 1/8-inch diameter pressure transducers were installed near the tip of one propeller blade of a four-blade configuration. Data were obtained from these transducers during a preliminary test at zero blade tip angle and at three rotational speeds. These data were not recorded on magnetic tape, but analyzed in one-third octave bands by an on-line analyzer to determine transducer capabilities and extraneous noise levels. Further tests to obtain and record the blade pressure data at higher blade angles were abandoned due to transducer failures. The data acquired during the preliminary tests are presented in this report.

The propeller noise tests consisted of a radiated noise measurement program on propeller configurations comprising 2, 3, 4, and 6 blades, at various blade angle settings and at three rotational speeds. The effect of tip shape was investigated on a 2-blade and 4-blade propeller. As is shown in Figure 7, the standard tips were formed by rotating the airfoil section about its chord line, the swept tip consisted of a 60° sweep of the leading edge with thickness tapered to retain an approximate 12% t/c ratio over the section. The "trapezoidal" tip was formed by a 15° taper of the leading edge and 25° taper of the trailing edge, with corresponding thickness change as in the case of the swept tip. These profiles were chosen to allow an investigation of the influence of tip vortex geometry on noise generation. Such applications of swept tip to helicopter rotors has reportedly resulted in noise reductions of the order of 5 dB on overall sound pressure and has been attributed to the more rapid diffusion of the tip vortices with resultant lowering of the peak velocities of the vortex. Whether these effects are more significant to the self-induced blade loading or to vortex impingement on succeeding blades has not been clarified in previous studies and the present test program was directed towards such a clarification. The following subsections describe the primary results obtained from each of the experimental tasks and include typical examples of the acquired data. A more complete compilation of the experimental data is presented in Appendix II. A detailed description of the test facilities and measurement techniques is presented in Appendix I.

2. TEST BLADE GEOMETRIES AND PROPELLER DESIGN

The choice of a propeller design suitable for the present study was based on the need for a relatively simple blade geometry which would allow examination of particular design parameters in the noise analysis. The basic configuration employed in the test program therefore consisted of a multi-blade hub with a set of six blades, each blade having low twist and a symmetrical airfoil section with constant thickness and chord over its span. A NACA 0012 section was selected for the study blades because of the considerable amount of basic aerodynamic and noise data already available on this type of airfoil as employed in helicopter rotors. While not truly representative of propeller blades, the relative simplicity of the design was considered to be beneficial to a study of noise generation basics. A diameter of 4 feet was chosen to allow tip velocities in the range of $0.2 \leq M_t \leq 0.5$ to be examined within an acceptable r.p.m. range, and a suitable blade twist rate was chosen which would allow a reasonable range of blade angles to be operated without stall or reverse flow conditions occurring over the blade span. These conditions were examined by a Goldstein-Lock blade element analysis, using section lift and drag coefficients derived from hover performance measurements of a NACA 0012 blade rotor (Reference 28).

The effect of blade tip geometry on the noise generation process was examined by the application of interchangeable tips to the propeller blades. The tip geometries are shown in figure 7. These blade tips were made of cast epoxy resin with an internal sheet metal reinforcement, and fitted to the propeller blades to form a sparwise section of one chord length. A sufficient quantity of identical blade tips were made to each profile for use on six propeller blades and two wind tunnel blades.

The following propeller configurations were employed in the experimental program:

Propeller diameter	:	4 ft.
Hub diameter	:	8 ins.
Blade numbers	:	2, 3, 4 and 6
Blade section	:	NACA 0012
Blade chord	:	3 ins. (constant)
Blade twist (linear from 0.2R to 1.0R)	:	7.5°
Blade Tips	:	Standard Swept Trapezoidal

Each of these configurations is designated as W(B) (tip shape) (α_t) where B is the number of blades. The tip shape is abbreviated to STD (standard), SW (swept), and TR (trapezoidal). The blade tip angle (α_t) is employed in the designation as it was considered that this value might be more meaningful in noise data comparisons than the usual performance parameter $\beta_{0.75}$. In the present geometries, $\beta_{0.75}$ is 2.67° greater than α_t in all cases. Thus, a W2STD8 is the 2-bladed configuration with standard blade tips and a tip angle setting of 8° .

While the above simple propeller geometries were designed to provide a basic model for the study of aerodynamic and acoustic interdependent parameters, and subsequently to provide an analytical foundation for noise prediction methods, the additional use of a more realistic propeller in the whirl test program was considered necessary to provide a basic test on such derivations. For this purpose, noise measurements were conducted for a 2-blade Sensenich W60LK18 propeller (telescoped to 4 ft. diameter). The geometry of this propeller is illustrated in figure 8, and was designed for operation at "zero" advance ratio conditions at tip speed of $M_t = 0.7$.

The thrust and power estimates for each of the propeller configurations tested are summarized in Table II. Blade loading distribution curves for the model propeller are shown in figure 9.

3. WIND TUNNEL TESTS

The test facilities employed in this program are described in detail in Appendix I. Briefly, the facility was a low-speed wind tunnel with a 10" x 30" cross section and 48" working section length. The inlet to the tunnel was modified by a honeycomb section to reduce the free stream turbulence level to an order of less than 1%. The test program indicated a level of 0.4% at a stream velocity of 150 fps.

The wake turbulence studies were conducted by installing a 6-inch span, non-twisted blade on a cantilever mount at the tunnel wall. The turbulence and mean flow measurements were obtained by traversing a hot wire anemometer probe across the blade wake at various streamwise distances behind the blade. These traverses provided on-line plots of the distribution of overall turbulence intensity and mean flow velocity along specified coordinates in the tunnel arrangement. The test arrangement and coordinate convention used in these studies are described by figure 10. Typical data obtained are shown in figure 11, and a complete summary of all significant data levels is compiled in Appendix II. A one-third octave band spectrum of the wake turbulence is shown in figure 12. This procedure was repeated for each of the blade tip shapes.

a. Wake Turbulence Definitions

An overall description of the turbulence field over various cross sections of the blade wake was derived from the basic data by the formation of contour plots, as shown in figure 13. Of immediate note is the significant difference between the three tip shape results. It is apparent that the trapezoidal tip vortex diffuses more rapidly than that of the other blades, which has been suggested in studies of helicopter rotor noise reduction (for example Reference 29) as an explanation of reduced noise of blades with modified tips. If tip vortex impingement occurs in the propeller case, then a noise reduction effect would also be expected by the use of tapered tips. This is further investigated in the whirl test program.

An extensive analysis of the turbulence intensity measurements was carried out to determine whether an analytical description of the turbulence field could be established in terms of the blade geometry and wake coordinates. While it would be expected that such a description would depend on the mean flow velocity gradients through the shed wake and tip

vortex regions, an adequate description of this could not be obtained from the available data. It was in fact found that the maximum streamwise component of turbulence intensity can be simply related to the maximum mean flow defect, as demonstrated by the collapse of data shown in figure 14. An adequate definition of this relationship has been found to be given by

$$\left(\frac{\tilde{u}}{U_{\infty}} \right)_{\max} = 0.1 \left(1 - \frac{\bar{U}}{U_{\infty}} \right)^{\frac{1}{2}} \quad (48)$$

Reference to the tabulated data in Appendix II shows that the maxima of the \tilde{v} component of turbulence, that is, in the direction normal to the free stream and blade $\frac{1}{4}$ -chord line, are of equal intensity to the streamwise component \tilde{u} . Further comparison of the data obtained in the tip vortex region with that of the shed wake field indicates that the maximum turbulence intensities are of the same order of magnitude at streamwise distances greater than one chord from the blade $\frac{1}{4}$ -chord line.

The above findings therefore allow an estimate to be made of the maximum turbulence intensity at any streamwise section of the blade wake, provided the local maximum mean flow defect is known. For this, the work of Silverstein et al (Reference 27) is invaluable and is compared with the present experimental data. In the Silverstein studies the dynamic pressure loss and downwash angles were examined for a number of airfoils, including a NACA 0012, and the derived definition of the dynamic pressure loss was given as

$$\bar{\eta} = 1 - \frac{\bar{q}}{q_{\infty}} = \frac{2.42 C_{d_o}^{\frac{1}{2}}}{\xi + 0.3} \quad (49)$$

where \bar{q} is the local maximum dynamic pressure and q_{∞} is the free stream value. C_{d_o} is the profile drag coefficient at each blade section and ξ is the distance behind the trailing edge, in chord lengths. In terms of the mean flow velocity, the dynamic pressure loss is obviously

$$\bar{\eta} = 1 - \left(\frac{\bar{U}}{U_{\infty}} \right)^2$$

A comparison of this Silverstein expression with the present data is shown in figure 15 and a close agreement is apparent for a profile drag coefficient of $C_{d_o} = .013$ which corresponds

to the two dimensional coefficient of a NACA 0012 section at a blade angle of 8° ($C_{d_o} = .014$, Reference 28). It can therefore be assumed that the wake defect of the

test blades is accurately represented by the Silverstein relationship, and consequently the maximum turbulence level in the wake can be defined by combination of this expression and the turbulence intensity relationship of equation (48).

The definition of wake and tip vortex dimensions, and the distribution of turbulence over these dimensions, is of course important, and again recourse is made to Silverstein's results. First, the thickness of the shed wake has been defined as

$$\bar{\zeta} = \frac{\text{wake width}}{2 \times \text{chord}} = 0.68 C_{d_o}^{\frac{1}{2}} (\bar{\xi} + 0.15)^{\frac{1}{2}} \quad (50)$$

which is shown in figure 16 to give close agreement to the present experimental data where the shed wake thickness has been taken as the dimension between the points of deviation of the turbulence intensity from the free stream level. The distribution of turbulence intensity across this dimension has been found to differ from that obtained by use of Silverstein's dynamic pressure profile. As the experimental profiles are of greater level than the estimated profiles, the difference can be attributed to the additional effects of mean flow velocity gradient. A separation of effects has not been achieved in the present analysis, and the following description of the wake turbulence distribution has been found to provide a reasonably good agreement over the data range:

$$\left(\frac{\tilde{u}}{U_{\infty}} \right)_{\bar{\zeta}'} = \left(\frac{\tilde{u}}{U_{\infty}} \right)_{\text{max}} \times \left(1 - \left(\frac{\bar{\zeta}'}{\bar{\zeta}} \right)^4 \right)^2 \quad (51)$$

where $\bar{\zeta}'$ is the non-dimensional thickness at the wake coordinate considered.

Thus, for the shed wake, a detailed description of the turbulence intensity can be derived from the above expressions.

Attempts to derive a similar description of the tip vortex turbulence scales in terms of the mean flow defect and streamwise position have not been successful. Here, the approach taken was to assume that the mean flow can be described in terms of the bound circulation and hence the blade lift coefficient, by

$$\frac{\tilde{v}}{U_{\infty}} = \frac{C_L c}{8\pi r_v}$$

By then relating \tilde{v} to the mean flow defect, and describing r_v , the vortex core radius at which maximum defect occurs, in terms of C_L and a streamwise coordinate, the essential information for order of magnitude estimates of turbulence intensity could be derived from equation (48), which is shown in figure 14 to be valid for the tip vortex data. This problem obviously requires a more detailed investigation than that afforded by the present program. A general review of the tip vortex experimental data, as tabulated in Appendix II, indicates that for the standard-tip blade the maximum turbulence intensity is of the same order as that in the shed wake. The maximum measured width of this turbulence region is about twice the shed wake thickness, and the maximum intensity occurs on a radius of about 0.3 times the shed wake thickness.

b. Blade Surface Pressure Measurements

The test arrangement for the blade pressure measurements is illustrated in figure 17. As shown, three pressure transducers were installed in the blade surface, along the quarter chord line, and one mounted at the half chord point. The upstream blade was mounted to a tunnel wall fixture which allowed its vertical position, in a plane two chords distant from the instrumented blade, to be adjusted such that it would present an impinging wake to the instrumented blade or be removed to the tunnel ceiling and present negligible influence on the tunnel free stream turbulence. These settings are referred to as "tandem" and "single" blades, respectively. In each of the tandem blade tests, the upstream blade position was adjusted until maximum pressure response was obtained at the instrumented blade transducers. Due to excessive instrumentation noise at frequencies below 400 Hz, the pressure transducer signals were 1/3 octave band analyzed in the range 400-20,000 Hz, and the overall level calculated from these band levels. Figure 18 presents these overall levels (referred to .0002 microbars) for each of the transducers at each blade angle setting. The measurements shown for negative blade angles represent the fluctuating pressures on the "suction" side of the blade, while those shown for positive angles represent the fluctuating pressures on the "pressure" side. The one-third octave spectra of the signals at zero and negative blade angles are presented in figure 19.

Prior to employing these data in an analysis of the originating fields, it is extremely important to consider the effect of transducer size (diameter) on the measured spectra. While the microphone pressure response may be regarded as linear up to frequencies of the order of 40 kHz, its response to a boundary layer field for example, is restricted to a much lower frequency due to phase cancellation for small eddy dimensions. Many studies of this effect have been reported, and from these the response shown in figure 20 is considered appropriate for the 1/8 inch diameter units employed in the present program. The spectra shown in figure 19 will be in error by such an amount, which indicates that the measured band levels above 4000 Hz are much lower than the actual levels.

The influence of a turbulent boundary layer and impinging turbulence on the surface pressures of an airfoil have been expressed in an analytical form in the preceding discussion of noise generation theory. For the boundary layer case, the commonly employed empiricism

$$p_{rms} \approx .006 q_{\infty}$$

has been used to provide an order of magnitude estimate of the blade pressures. For the case of impinging turbulence, a simplified form of the Sears solution to harmonic gust loading has been adopted for the root mean square oscillatory lift per unit span. As presented, this is a function of the steady lift and a reduced frequency parameter. If pressures are considered, and the turbulence scale is approximated by $l_x = U/f$, where f is the characteristic frequency, the Sears expression reduces to the simple form,

$$p_{rms} = \frac{1}{\sqrt{2}} q_{\infty} \left(\frac{\tilde{u}}{U_{\infty}} \right) \quad (52)$$

for each side of the blade.

First, considering the single blade data in terms of expected boundary layer and free stream turbulence effects, an order of the frequency range at which boundary layer pressures would be expected to be maximum is given by

$$\omega = \frac{0.3 U}{\delta^*}$$

where the displacement thickness δ^* can be taken approximately as 1/8 of the boundary layer thickness δ_b . Substitution of the appropriate tunnel flow velocity ($U = 150$ fps), and taking the 1/2-chord point on the blade, Bies' expression (Reference 21) of the boundary layer thickness

$$\frac{\delta_b}{x} = 0.37 \text{Re}_x^{-0.2} \left[1 + \left(\frac{\text{Re}_x}{6.9 \times 10^7} \right)^2 \right]^{0.1}$$

gives a frequency of 20 kHz for a turbulent boundary layer on an infinite length flat plate. Comparing this with the measured blade pressure spectra would suggest that the high frequency content (at $f = 4000$ Hz) might be, in fact, due to the blade boundary layer. The question as to whether transition to turbulent conditions has occurred on the blade at such low Reynolds Numbers ($\text{Re}_x \approx 10^5$) is not easily answered due to the effects of incident stream turbulence on the transition mechanism. Schlichting (Reference 30) gives a critical Reynolds number of 3.5×10^5 as being a lower bound limit for a stream turbulence level of 0.5% incident on a flat plate edge, but on airfoils at Reynolds numbers of 10^5 to 10^6 , the laminar boundary layer has been known to separate and reattach as a turbulent boundary layer.

Now, examining the pressure levels obtained by measurement with those expected from the simplified equations, the predicted orders are 112 dB for boundary layer and 105 dB for a 0.4% turbulence (reference pressure is .0002 microbar) which are certainly in the range of the measured overall levels on the blades. However, due to the emphasis of the spectra at the higher frequencies and the inherent microphone response errors, it is more instructive to study band levels in the lower frequency regime. Taking the 630 Hz one-third octave band because of its distinct differences in level for the single and tandem blade cases, a comparison can be made of the possible causes of these differences. In this band, the tunnel free stream turbulence was measured to be 24 dB less than the overall level of .004. This would give an estimated blade pressure band level of 81 dB SPL, which is lower than any of the measurements in that band. For the impinging wake case, the overall level of impinging turbulence is given as .030 by the earlier measurements and reference to the spectra measured in the shed wake gives the 630 Hz band level as 19 dB down from the overall. Thus the expected pressure band level for the tandem blade case would be about 102 dB, which agrees closely with the measured data obtained under impinging wake conditions. Examination of the turbulence scale at which this agreement is given shows a typical length of U/f equal to a chord length. It may therefore be postulated that the applicability of the simplified Sears function to the impinging turbulence case is verified for scales of this order. It is interesting to note that if the Strouhal number of 0.1 is used, the typical dimension would become 0.1 chord, which for the present blades is also close to the blade thickness. Further discussion of this is contained in Section IV of the report, where the measured propeller noise spectra are reviewed for analytical representation.

In summary, the simplified Sears function has been applied to the impinging wake experimental data and found to provide a close estimate of the blade surface pressures in the frequency region

$$f \approx U_{\infty} / c$$

where c is the blade chord. The boundary layer expression cannot be verified from the available data due to adverse microphone response characteristics at high frequencies.

4. PROPELLER NOISE MEASUREMENT PROGRAM

a. Procedures

The whirl test facility used in this program was designed specifically for the purpose of testing low speed propellers with minimum extraneous aerodynamic and noise effects. The test stand design is illustrated in figure 21 and comprised a 12-foot high cylinder and strut arrangement which supported a 60 hp hydraulic motor and a horizontal cantilevered drive shaft to the propeller hub. A detailed description of this facility is presented in Appendix I. The design speed range of the system was 1000 to 3150 rpm, which would allow tip speeds of a 4 ft. diameter propeller in the range $0.2 \leq M_t \leq 0.6$.

Unfortunately, severe vibration problems imposed an upper limit of $M_t = 0.4$.

As shown in Table III, noise measurements were obtained for model propeller configurations with 2, 3, 4 and 6 blades at a blade tip angle setting of 8° , and for the two-blade set with tip angle variations from -2° to 16° . In addition, the two- and four-blade configurations were tested with modified tip shapes. A further set of noise data was obtained for a 2-blade, 4 ft. diameter Sensenich W60LK18 propeller. Typical hub-blade assemblies are shown in figure 22.

The main objective of this measurement program was to obtain a detailed definition of the "vortex" noise generated by propellers at low tip speeds and various blade loading conditions. The noise measurements were therefore obtained on a radius of 12 ft. ($r/D = 3$) from the propeller center, and in the forward quadrant only, on a horizontal plane through the propeller axis. For each of the configurations, noise measurements were recorded on magnetic tape for microphone azimuth locations of 0° , 30° , 60° and 90° relative to the forward axis. Additional measurements were made at 10° increments for two of the propeller geometries. Each propeller was tested at rotational speeds of 1070, 1605 and 2140 rpm. During each noise data recording test, an on-line $1/3$ octave band analysis was conducted on each microphone signal to provide immediate information on the general characteristics of the noise field. Examples of these spectra, as obtained on the propeller axis for 2-, 4- and 6-blade cases at $M_t = 0.4$, are shown in figure 23.

The spectrum obtained at the same conditions for the Sensenich propeller is shown in figure 24.

An attempt was made to obtain detailed spectral and cross-spectral blade pressure data by installing five 1/8-inch diameter pressure transducers on the surface of one blade of a four-blade test propeller. Details of the transducer signal transmission arrangements are described in Appendix I. The arrangement of the transducers on the blade surface is shown in figure 25. As a preliminary test of the acquisition system, the propeller blades were set at 0° tip angle and operated at each of the three rotational speeds. The transducer signals were not recorded, but on-line analyzed by a 1/3 octave band spectrometer. The acquired spectra are presented in figure 25 for each of the transducer signals at each test rotational speed. Attempts to obtain further recorded data at different blade loading conditions were unsuccessful due to the failure of the transducer units. The remainder of the test program was concentrated in obtaining radiated noise data for the various propeller cases.

An immediately apparent anomaly in the 1/3 octave spectra, as illustrated in figure 23, is the existence of predominantly high levels at frequencies in the range of 10 kHz and 25 kHz. In some cases this high frequency content dictated the overall measured level and an extensive effort was devoted to detecting the source of these components. At first these high frequencies were suspected to be due to extraneous effects such as an overemphasis in the microphone response characteristics or an excessive noise component of the hydraulic drive system at loaded conditions. A microphone response problem was in fact discovered, and accounted for the 25 kHz component and an overemphasis of the 10 kHz component. However it did not explain the predominantly high amplitude of the 10 kHz component at 2140 rpm. Tests at the lower rotational speed showed that the frequency varied directly with speed, giving a predominant spectral component at 5 kHz in the low speed case. A narrow band analysis of this component (for the high speed case) is shown in figure 27 and indicates discrete frequency characteristics which do not follow a consistent harmonic relationship over the data range and could not be associated with any test rig mechanisms. Hydraulic feed lines were insulated to prevent noise radiation and the motor assembly was checked for improper alignments. These had no influence on the high frequency components. Attention was then focussed on the blade assemblies to determine whether the source was due to a blade defect. Various changes were made with no resultant effect. At this stage in the program it was decided to proceed with the propeller noise measurements and defer a further analysis of the high frequency components to a later phase when additional reduced data would be available.

b. Noise Data Analysis

A typical set of the acquired noise recordings was selected for preliminary detailed spectrum analysis. These data were reduced by narrow (constant) bandwidth analysis and are shown in figure 28 for the 2-blade propeller cases, at $M_t = 0.4$, with six different blade angle settings. The bandwidth used in these cases was 25 Hz, which is approximately one-third of the blade passage frequency. A corresponding spectrum obtained for the Sensenich propeller at the $M_t = 0.4$ condition is shown in figure 29.

It is obvious from these spectra that the characteristic spectral distributions given by the broader 1/3 octave band analysis may be entirely due to harmonic content, rather than the usually assumed random "vortex" noise. To separate the harmonic and broadband components in each test record, a narrow band analysis is obviously necessary. However, the magnitude of such a task in terms of analysis time precluded the further use of constant bandwidth method for the entire data quantity. Recourse was therefore made to a 1% bandwidth analysis for the remainder of the data records. The capability of 1% bandwidth reduction to resolve up to fifty harmonics of a periodic signal was considered adequate for present purposes. However, the capability of resolving the random noise content of the data is restricted and an examination of the inherent limitations was conducted. First, the theoretical limitation was determined by deriving the ratio of peak (rms) level to filter crossover level (+3 dB) using the known filter shape characteristics. Second, a record with known harmonic and signal-to-noise content was analyzed by the 1% bandwidth method. (The signal was first formed digitally, digital-to-analog converted, and evaluated by a very narrow bandwidth analysis). It was found that these methods provided essentially the same results, and a criterion for broadband noise evaluation in a harmonic record was developed and applied to each of the 1% analyzed data obtained from the propeller noise records. Briefly, this criterion consists of a definition of the minimum signal-to-base level ratio of the analyzer, as a function of harmonic number. Only data levels which were within this ratio (relative to the measured harmonic level) were considered to be valid measurements of the random noise content of the propeller noise record. This procedure was applied to every 1% bandwidth spectrum obtained in the present program.

Typical examples of 1% bandwidth spectra are shown in figure 30 for the on-axis noise of the 3-, 4- and 6-bladed test propellers at $M = 0.4$. To aid in the task of interpretive study of the data, the noise spectral characteristics were categorized as harmonic and broadband noise content, and tabulations of the data levels of each component were compiled, as presented in Appendix II. The harmonic content was obtained directly from the 1% bandwidth spectra. The broadband content was also obtained from the 1% analysis, within the limitations described above, and converted to 1/3 octave band levels by a bandwidth correction factor of

$$\Delta \text{ (dB)} = 10 \log \left(\frac{\Delta f_1}{\Delta f_2} \right) = 12.5 \text{ dB}$$

where Δf_1 is the bandwidth of a 1/3 octave (23.1% f) and Δf_2 is the effective bandwidth of the analyzer (1.3% f).

c. Discussion of Test Results

This discussion covers the main features of the data acquired during the propeller noise measurement program and of the characteristics apparent in the narrow band analyzed data. A brief discussion is given of some characteristics of the spectra which are, at the present time, essentially unexplained. In these, the significance was considered to be outside the scope of the present study and are included here as points of interest to further investigations of propeller noise generation.

(1) High Frequency Noise Content (5 kHz to 20 kHz)

The following characteristics of the high frequency noise have been determined by examination of all test data:

- (a) The effect is apparent in most records obtained for the test propeller, but is not apparent in the Sensenich propeller data.
- (b) The center frequency varies linearly with rotational speed, from 5 kHz at $M_t = 0.2$ to 10 kHz at $M_t = 0.4$.
- (c) The effect consists of a number of discrete frequency components, as shown by the 1% bandwidth spectrum in figure 27, which do not appear to follow a consistent harmonic relationship over the entire data range. These frequencies could not be associated with any test rig mechanisms.
- (d) The amplitude of these noise components varies with blade number, blade tip angle, rotational speed and blade tip shape, as shown in figures 31, (a) to (c). In particular, the variance with blade tip angle is of significance and suggests the origin might be related to a localized blade tip effect which is strongest at low blade tip angles and diminishes with increased angle. At zero tip angle the noise component is not distinguishable in the 1% bandwidth spectra. The 16° tip angle case can be regarded as a tip stall condition.
- (e) The directivity of the noise is of the form shown in figure 31 (a), with a maximum on the propeller axis and minimum in the plane of the propeller.

While the above observations suggest that the high frequency noise components were generated by the test propeller rather than by extraneous sources, the fact that the effect was not observed in the Sensenich propeller cases, and cannot be found in any other reported propeller or helicopter noise data, leads to the conclusion that the mechanism is related only to the particular test propeller design used in the present program. A more detailed examination of the possible origins of the effect has therefore been omitted from the scope of the current studies.

(2) Wind Gust Effects:

Another problem encountered in the data analyses and interpretive studies was due to a variance of the noise level over the period of the noise record. In some cases this variance could be attributed to wind gust effects although precaution had been taken to avoid such conditions. A measure of this gust effect on the 2-blade and 6-blade propellers was obtained

by taking a time history of the sound level in each $1/3$ octave band and noting the increase in level which occurred between the steady and gust parts of the history. As shown in figure 32, the increase occurs over a selective frequency band in the region of relatively high order harmonics. A visual display of the noise signals on an oscilloscope indicated that the change was distinctly related to the harmonic content. In fact, the noise sounded very much like helicopter blade "slap" when the gusts occurred. Again, the immediate problem was to eliminate such effects from the data employed in the interpretive study and the above observations are only presented here as points of interest. Under zero wind conditions, the lower order harmonics were observed to fluctuate rapidly and while the overall effect was not distinctly noticeable in the auditory signature, the effect on the narrow band analysis was a major point of concern. By repeated analysis of a number of data cases it was established that the broadband content of the signal was relatively steady under the zero wind conditions, but was influenced by gusts to about the same degree as the harmonic content. All analysis data employed in the interpretive program was free from such effects.

d. Propeller Noise Characteristics

The most significant feature of the narrow band spectra obtained from the static test program is the extent of the harmonic components present. Although the relative amplitudes of harmonics have been known to decay at a slower rate than that predicted by Gutin theory, and have been explained in principle by Lawson and Ollerhead (Reference 8) and others for the case of harmonically loaded rotors of helicopters, the extension of the propeller noise harmonics at almost constant amplitudes to an order of thirty or forty has not been previously debated in any detail. The well known categorization of propeller noise into "rotational" and "vortex" components may therefore be questioned at this time. In most of the original studies of propeller noise, conducted many years ago when sophisticated analysis equipment was not available, the usual approach to this categorization was based on a resolution of the first four harmonics only and regarding the remainder of the spectrum (in $1/3$ octave or octave bands) as the vortex noise component. Comparison of the $1/3$ octave spectra of figures 23 and 24 with the narrow band spectra clearly illustrates the misinterpretation which may result from such categorization. A further division of the harmonic content into 'rotational' and 'unsteady' components can be made, based on the theoretical analyses of the problem. The "rotational" noise is defined as that harmonic noise content which results from the steady loads on the rotating blades as defined by Gutin theory, while the "unsteady" noise originates from the harmonic content of the unsteady blade load conditions. As is pointed out later, the mechanisms by which these harmonic loads originate on propeller blades are not clearly understood, and consequently recourse is made to the acoustic data to provide some knowledge of the loading amplitudes and harmonic range. Similarly, the origins of the broadband noise can be regarded as the random content of the unsteady blade loading, and may be best understood by examination of the acoustic data with the aid of the theoretical expressions given in Section II. As is explained in the derivation of the propeller noise theory, the sound measured at any point in the radiation field is a complex summation of contributions from the various steady and unsteady blade loading terms. The sound measured in a narrow frequency band, centered

on a harmonic of the blade passage frequency, contains contributions from a wide range of frequencies in the blade loading spectrum, except when the sound is measured on the propeller axis. This exception provides a relatively simple solution to the whole complex problem of understanding the unsteady loading terms. On the axis, the "steady load" noise terms are zero, and the noise measured in a narrow frequency band is the result of the unsteady blade loadings in that narrow band only. This applies equally to the harmonic and broadband noise content. It is therefore clear that an interpretation of the propeller noise data is best made by reference to the "on-axis" spectra. To further aid the interpretation, the broadband and harmonic content of the narrow band spectra have been extracted from the analysis data and are now discussed separately.

(1) Broadband Noise

The random noise content, which is the main topic of study in the present program is presented in spectrum form, in figures 33 to 36, for each of the propeller configurations examined. (These are presented from the tabulated data in Appendix II.) Taking first a general review of the data by comparison of the "overall" levels calculated from the band levels, it is shown in figure 37 that the directivity of the noise is such that the highest levels occur near the propeller axis, which agrees with the findings of all other studies of "vortex" noise. The dependency of the noise levels on blade velocity,

however, suggests a V^4 relationship rather than the expected sixth power law for dipole sources. While this would suggest a monopole type source no physical justification for such an assumption can be made at this time. A detailed and thorough reexamination of the basic noise records and the analyzed spectra was therefore conducted and a possible source of error in the data has been attributed to extraneous test rig noise at the lowest speed condition only. This comment is made with some reservation as the test rig was carefully designed to preclude such effects and a detailed study of the rig noise was carried out prior to commencement of the propeller test program. In certain data cases obtained at $M_t = 0.2$, the basic noise records were recognized as being significantly defective and

were immediately omitted from the interpretive analysis. Reference to the blade pressure measurements obtained in the propeller test program provides a further clue to the actual velocity dependence. As shown in figure 38, the overall mean square pressure calculated from the data over the frequency band 400 Hz to 20 kHz for each of the propeller speeds

clearly indicated a U^4 trend which, according to theory, provides a U^6 law for the radiated noise. On these basic findings, it has been concluded that the broadband data obtained at the lowest propeller speed is erroneous and that the general interpretation of the data should be referred to the higher speed cases which contain a clear definition of the propeller-generated broadband noise. The dependency of the noise level on blade loading conditions is illustrated in figures 37(b) and (d). In figure 37(b) the effect of blade number is shown for the cases in which the test propeller was changed only by the addition of blades. It is seen that, with the exception of the 6-blade case, this dependency is of the form,

$$p^2 \sim B^{-2}$$

which can, of course, be a combination of thrust and blade area effects. The data shown in figure 37(d) illustrates the thrust loading effect as obtained by operating the 2-bladed test propeller at various tip angle settings from $\alpha_t = 0^\circ$ to 16° . Here, the dependency is not immediately obvious. As discussed in the next section, this can probably be attributed to the increasing significance of wake impingement at low thrust coefficients. From the available data the dependency can be approximated as

$$p^2 \sim C_T^2$$

with the understanding that a divergence occurs at very low thrust coefficients.

In combining these results, the dependency of C_T on blade number (i.e., $C_T \sim \sqrt{B}$) is used. Thus

$$p^2 \sim C_T^\alpha B^\beta$$

becomes $\sim C_T^2 B^\beta$ (from the fixed B result)

and $\sim B^{\beta+1}$ (by substitution of $C_T \sim \sqrt{B}$)

$\sim B^{-2}$ (from variable B (and C_T) result)

Thus the combined result for the broadband noise dependency is given by $\alpha = 2$, $\beta = -3$, i.e.,

$$p^2 \sim C_T^2 B^{-3} \quad (53)$$

for the test propellers with constant area per blade. A closer examination of the dependency of the blade area effects is conducted in Section IV, where a complete empirical analysis is presented.

The spectral features of the broadband noise are distinctly similar in all cases, with the spectral maxima occurring at frequencies directly proportional to the blade tip velocity. It would therefore appear appropriate to define a "universal" shape factor for the spectral distribution of the broadband noise and to relate the center frequency to some scale length by the well established Strouhal number dependency. This is also further discussed in the next section.

The effect of blade tip shape on the broadband noise spectra can be examined by comparison of the data tabulated in Appendix II. In the 2-blade configurations, the tip shape had no apparent influence on the spectral levels. Some differences of noise data are noticeable in the 4-blade propeller test results. These differences are summarized as follows:

- The swept-tip data shows an increase of the order of 3 dB for the on-axis noise, and 4 to 5 dB for azimuths of 30° and 60° (relative to the standard-tip noise data).
- The trapezoidal-tip data shows no change in the on-axis noise levels, but a 2 to 3 dB reduction is apparent at other azimuthal stations (again relative to the standard-tip noise data).

(2) Harmonic Noise

As already noted, the significance of the harmonic noise content in the measured spectra extends to much higher orders than would be previously expected, and again a discussion of the general characteristics of the data is best made by reference to the on-axis data which should, in theory, contain only the unsteady loading contributions at corresponding harmonics. A clear indication of the general form of the spectral envelopes is given by the narrow band analyses of figures 28 to 30. In particular, figures 28(a) to (f) for the two-blade propeller cases indicate that the envelope of the lower order harmonics varies in form from case to case, but the harmonic decay rate and the harmonic order at which the decay commences is relatively uniform for these cases. In fact, by plotting the harmonic levels against harmonic number (m), as shown in figures 39 to 40, the characteristic envelope of most of the data cases can be represented by a constant level (independent of harmonic number) up to a transition point, and for higher orders by

$$p_{mB}^2 = p_0^2 (mB)^{-k}$$

where p_0^2 is the envelope maximum and k is a decay exponent. The variance of k with thrust coefficient and blade tip velocity is shown in figure 41. It is apparent that although some dependency on these parameters exists, the differences in the present data range are negligible in terms of the overall noise signature.

Of greatest significance to the propeller noise problem is, of course, the maximum level of the harmonic envelope and its relationship to design and operating parameters. A full discussion of this is contained in the following section where empirical relationships are derived as a basis for the noise prediction theory. In the present context of general observations, the characteristics shown in figure 42 are typical of the trends over the complete data range. The directivity of the data is generally such that the maximum harmonic level in the forward hemisphere occurs near the axis. This is obviously complicated by the steady (Gutin) load components at off-axis positions. A consistent dependence on blade number is not apparent, except that, as in the broadband noise data, the six-blade case level tends to be higher than the general trend. It is therefore assumed that, with the latter exception noted, the harmonic envelope level is independent of blade number (B) in cases where the only change in the propeller is the addition of identical blades. From figure 42(d) the variation with C_T is notable, except at very low C_T , as:

$$p_0^2 \sim C_T^2 \quad (\text{for } B = 2)$$

The above observations can be interrelated through the $C_T \sim \sqrt{B}$ dependence (as in the broadband noise discussion) to give

$$p_0^2 \sim C_T^2 / B \quad (54)$$

for the harmonic envelope level.

Further examination of blade number and solidity dependence is presented later. The velocity dependence of the harmonic data has been found to be U^6 in almost all cases, as is to be expected.

An assessment of the influence of blade tip shape on the harmonic noise components has not been possible in the available data, due to the large fluctuation of the lower order harmonics during a record history.

SECTION IV

CORRELATION OF THEORY AND EXPERIMENT

In this section the analytical and experimental results presented in Sections II and III are employed to determine the dependencies of the rotating source characteristics upon the propeller geometry and performance parameters. The experimental measurements have made it clear that both harmonic and random components of the noise are of the same order of magnitude to very high frequencies and it is clearly necessary to consider both components in this analysis. To do so it is assumed that the two are indeed separable and the observed acoustic spectra reflect the combination of discrete frequency spikes and continuously distributed random energy. This is convenient from both analytical and physical points of view but it would be equally valid to regard this as the radiation from a randomly modulated harmonic source, i.e. one whose spectrum is not an ideal set of spikes but a series of narrow bands of noise. For present purposes, the harmonic and broadband components are examined separately.

1. BROADBAND NOISE RADIATION

The two unknowns in equation (46) are $w_p(f)$, the power spectral density of the random differential pressure fluctuations acting on the blades, and A_c , their correlation area.

Both quantities are "effective" values which relate to the concentrated loads assumption. Some information about the magnitude of the surface pressure fluctuations can be obtained from the measured data presented in figure 26. Unfortunately, its applicability is restricted for two reasons: Firstly, the spectra are defined in 1/3 octave bandwidths which are inadequate to resolve the harmonic and broadband components except at very low frequencies; and secondly, because of finite transducer size, measurement errors may be expected to increase fairly rapidly at frequencies above about 4000 Hz.

Thus the main source of guidance must be the noise measurements themselves, and detailed analysis of all available records obtained for the $\theta = 0^\circ$ (axial) location suggests that the broadband spectrum level rises from low frequencies and decays at high frequencies at a rate of about 9 dB for octave (the corresponding rates for 1/3 octave band levels being +12 and -6 dB per octave, respectively). An appropriate function which exhibits this characteristic is:

$$w(f) \sim \frac{f^3}{(f_c^2 + f^2)^3} \quad (55)$$

The center frequency f_c , at which the spectrum level peaks, may be expected to vary with speed according to the Strouhal relationship

$$f_c = N_S U/d \quad (56)$$

where U is a typical velocity and d is a typical blade dimension related to its turbulence generating characteristics. The projected thickness of the blade (i.e. a frontal thickness corrected for angle of attack) is frequently used for this purpose, but in the absence of firm experimental support for this choice there seems little point for the moment in using anything more elaborate than the chord dimension c . The spectrum shape defined above was fitted to each set of measured data to obtain the approximate values for f_c listed in Table IV and figure 43 shows a collapse of the non-dimensional frequency f_c/U_t plotted against the blade thrust coefficient C_{T_b} . The plot shows a slight trend toward lower frequencies as C_{T_b} (and whence angle of attack) is increased but the data scatter is rather high. The average value of the Strouhal Number ($N_S = f_c c/U_t$) is 0.85.

The acoustic spectrum measured on the axis is the product of the transfer function (itself proportional to frequency squared) and the effective blade loading spectrum. The effective loading spectrum thus has a spectrum proportional to

$$\frac{f}{(f_c^2 + f^2)^3} \quad (57)$$

which in turn is a product of the effective mean square pressure spectrum and the frequency dependence of the correlation area. Without measurements of one or the other of these quantities we must resort to hypothesis to discriminate between them. In this choice we may be guided by the well established laws for jet flows and turbulent boundary layers that typical correlation lengths vary inversely as frequency. Thus for the propeller case we may assume that, for high frequencies at least, the correlation area A_c is inversely proportional to the square of frequency. However, A_c cannot grow in size indefinitely with a reduction in frequency since it must be limited by the physical dimensions of the blade. The spanwise correlation length is also limited in effect by the fact that although the total blade area was introduced in equation (46) to represent the spanwise integration, the inboard blade sections will be very ineffective acoustically because of the U^6 law. Indeed, since this law suggests that the outer 35% of the blade generates 95% of the noise, it is more appropriate to use an "effective" blade area A_0 in equation (46) which is around 40% of the total blade area.

Thus at low frequencies the correlation area will be independent of frequency. At intermediate frequencies an inverse frequency (f^{-1}) dependence may be anticipated. Mainly for convenience of calculation the following formula for the correlation area has been assumed:

$$A_c = A_0 / 1 + (f/f_c)^2 \quad (58)$$

which leaves a pressure squared spectrum of the form

$$w_p(f) = \overline{p^2} \frac{2 f_c^2 f}{(f_c^2 + f^2)^2} \quad (59)$$

Here the normalizing constant of $2f_c$ has been introduced to ensure that the spectrum integrates over frequency to unity. $\overline{p^2}$ is thus the effective mean square differential pressure acting on the blade.

The convenience of the above formula may be seen by substituting them into equation (46) and performing the integration for the mean square acoustic pressure on the axis

$$\overline{p^2}_{\theta=0} = \int_0^{\infty} w_p(f) df$$

to yield

$$\overline{p^2}_{\theta=0} = \frac{A_0 A_b N_S^2 U_t^2 p^2}{8 c^2 r_1^2 a_0^2} \quad (60)$$

As confirmed experimentally in Section III, the mean square surface pressure, $\overline{p^2}$, is proportional to U_t^4 and can thus be written in the form

$$\overline{p^2} = (p_{q_t})^2 \left(\frac{1}{2} \rho_0 U_t^2 \right)^2$$

Consequently, equation (60) can be written as

$$\overline{p^2} = \frac{K U_t^6 A_b}{r_1^2} \quad (61)$$

where K may be expected to be a function of the particular flow conditions. Hubbard (Reference 4) collapsed propeller vortex noise data and found K to be 4.5×10^{-11} for a distance of 300 ft. However, numerous investigators (References 5, 7 and 31) have found that for helicopter rotors at least, K is proportional to the blade thrust coefficient C_{T_b} ,

implying that blade load fluctuations are proportional to mean thrust. Attempts to collapse the data of Section III according to the same laws left a high degree of scatter and a search was made for a more appropriate function. This yielded the result

$$\overline{p^2} \sim \frac{C_{T_b}^2}{B} \cdot \frac{U_t^6 A_b}{r_1^2} \quad (62)$$

where B is the number of blades. The data collapse is shown in figure 44 as a plot of

$OASPL_B - 60 \log \left(\frac{U_t}{100} \right) - 10 \log A_b$ against C_{T_b} / \sqrt{B} and although the scatter

is still fairly high this is the best achieved. The low speed data were omitted from this collapse for reasons discussed in Section III. It should be noted that only data for blade pitch angles

of 8° and above are included in these plots. The lower pitch data have been omitted because of the uncertainty regarding the thrust coefficients at low angles of attack. Also, the data depart from the thrust-squared dependency at these low angles as shown by the data presented in Section III, figure 37. This effect was also demonstrated by Widnall (Reference 31), who collapsed helicopter noise data against blade thrust coefficient to show a distinct levelling-out and increase of noise level for blade thrust coefficients less than about 0.2. This is attributed to the interaction between blades and the wakes from preceding blades and the fact that at low incidence angles the pressure fluctuations are probably more dependent upon drag coefficient than thrust coefficient.

Based on the line fitted through the experimental points in figure 44, and using an "effective" blade area of $0.4 A_0$, it is found that

$$(P/q_i)^2 A_0/c^2 = \frac{4 \times 10^{-4}}{B} (C_{T_b})^2 \quad (63)$$

This relationship is probably valid for $C_T/\sqrt{B} > 0.1$, underestimating the pressure fluctuation at lower values for reasons mentioned above.

2. HARMONIC NOISE RADIATION

It is apparent from the results presented in Section III that the problems of broadband radiation may perhaps be of academic interest from the standpoint of quiet aircraft design since in practically all configurations, the discrete components of the harmonic noise were of equal importance in the spectrum to very high frequencies. At low frequencies, the relative subjective importance of harmonic and broadband noise radiation is a function of the critical bandwidth of the hearing system and ideally the two components should be analyzed independently using critical filter bandwidths. The dimensions of the critical bands at low frequencies are open to question (Reference 32); however, there is little doubt that harmonic noise is predominant in that region anyway. At higher frequencies, when the critical bandwidth is greater than the fundamental blade passage frequency (i.e. the interharmonic spacing), it is appropriate to measure both components with a bandwidth equal to the blade passage frequency. Using this criterion it is found that the harmonic noise exceeds the broadband noise at frequencies up to the region of f_c and remains of the same order at higher frequencies.

This is totally inconsistent with the Gutin analysis, which, for blade tip Mach numbers of only 0.4, predicts a rapid roll-off of harmonic level with frequency, and of course, no radiation along the axis. The fact that the axially radiated noise exhibited as much harmonic noise as the off-axis noise is a clear indication of the existence of harmonic airloads acting on the blades. The noise radiation by these loads can be treated analytically using equation (35), but again the problem arises of how to estimate the magnitude of the loads.

Since no narrow band analyses of the blade surface pressures were made, the best clue to this is again the axially radiated noise signature. A detailed examination of the 1% analyses revealed that up to 50 or 60 individual harmonics of the blade passage frequency could

frequently be identified and that, on average, the harmonic levels did not decrease until mB exceeded 30 to 40. Harmonics higher than this decayed at rates between 6 and 12 dB per octave with the higher rates corresponding to the higher speeds. In fact the average value, namely 9 dB per octave, is consistent with decay rates observed for helicopters. Remembering that the dipole sound radiates as frequency squared, the corresponding effective airload harmonics decay at $mB^{-2.5}$. However, unlike the helicopter cases studied in Reference 8, the harmonics level off at low frequency.

On average then, the acoustic harmonics correspond to a spectrum function of the form

$$\overline{p_n^2} = p_1^2 / 1 + (n/n_c)^3 \quad (64)$$

where n is a harmonic number based on the disc frequency. Note that only the values $n = mB$ exist for any propeller. The critical value n_c , which is found to be about 36, on average, marks the frequency at which the spectrum rolls off to a slope of -9 dB per octave. Equation (35), for harmonic radiation, can be written for the axial case as

$$\overline{p_n^2} = \frac{n^2 f_0^2}{4 a_0^2 r_1^2} T_n^2 \quad (65)$$

where T_n is the rms value of the n -th harmonic thrust fluctuation. Thus, from equation (64), T_n^2 must have the form

$$T_n^2 = \frac{T_1^2}{n^2 \left\{ 1 + (n/n_c)^3 \right\}} \quad (66)$$

where T_1 is the value for the first harmonic. Frequencies are always proportional to the disc frequency ($f_0 = U_f / 2 \pi R$), so that equation (65) can be written in the form

$$\overline{p^2} = K U_f^6 C_T^2 A \quad (67)$$

That is, harmonic noise should be proportional to disc area, rather than blade area.

Experimental levels for the axially radiated harmonic noise were obtained as the average low frequency level in each case and normalized by subtracting the term $60 \log U_f$ (since A is constant for the propellers studied). Again, substantial scatter was encountered when this level was plotted against C_T , and in analogy with the broadband result, C_T / \sqrt{B} yielded a better collapse. This is shown in figure 45, where the low speed cases have this time been retained (see Section III).

The line (through the data points) which is proportional to C_T^2/B gives the result

$$\frac{T_1}{T_0} = \frac{.04}{B} \quad (68)$$

Thus the amplitude of the fluctuating loads relative to the steady thrust T_0 appears to decrease with blade number.

3. THE ORIGINS OF THE FLUCTUATING AIRLOADS

Equations (63) and (68) give the magnitudes of the effective harmonic and fluctuating airloads which act upon the blades. Both are proportional to the ratio of the steady forces divided by the square root of the number of blades. However, the harmonic loads are proportional to the total disc area whereas the random loads vary as the total blade area. This is because the frequencies of the random fluctuations are dependent on the blade chord dimension and the harmonic frequencies are related to the propeller diameter (for given tip speeds). At high frequencies the empirical spectral shapes adopted for the two components converge (on f^{-3}) so that there is a constant (decibel) difference between the two. This difference can be calculated from the results of the previous section to be

$$SPL_H - SPL_B = 1 + 10 \log_{10} \sigma + 30 \log_{10} \left(\frac{n_c}{n} \cdot \frac{f}{f_c} \right) - 10 \log_{10} \frac{\Delta f}{f_c} \quad (69)$$

where σ is the propeller solidity and Δf is the bandwidth with which the random level is measured. Using the Strouhal relationship for f_c , remembering that $f = n f_0$ and that for equivalence of the two component levels $\Delta f = f_0$, and putting $n_c = 36$ gives the result

$$SPL_H - SPL_B = 10 \log_{10} \left(\frac{\sigma c^2}{R^2} \right) + 33 \quad (70)$$

for $f \gg f_c$, $n \gg n_c$. Thus for the typical values $\sigma = c/R = 0.1$ the harmonic noise exceeds the broadband noise by 3 dB at high frequencies.

This result, however, is based upon the empirical evidence of a limited quantity of data which has been constrained to fit the requirements of formal acoustic theory. It must be recognized that experimentally, the division between harmonic and broadband energy is not a clear one and slightly different interpretations of the boundaries could produce very different end results. All the measured spectra showed similar characteristics and particularly a gradual merging of the harmonic and broadband spectra. The empirical harmonic spectrum shape adopted is based on those harmonic levels which could be distinguished from the random background. This process becomes increasingly error prone at higher frequencies and there is a risk of mistaking random level fluctuations for harmonic

spikes. On the other hand, most data were obtained from constant percentage bandwidth analysis where, for equal power spectra, the harmonic levels fall off at 3 dB per octave relative to random energy with increasing frequency so that mistaken identity would have resulted in different frequency exponents in the two spectrum formulas.

Also, the fact that the two components behave similarly at higher frequencies is not surprising since it is to be expected that the harmonic and random pressure fluctuations have related origins, origins which are of course identical from the viewpoint that the observed spectra are indeed series of narrowband components whose center frequencies are harmonically related. This will be discussed later. Attention will firstly be confined to the broadband component.

a. Random Pressure Fluctuations

Equation (63) provides an estimate of the product $(P/q_t) A_0/c^2$, where P is an effective rms differential pressure amplitude. For a 4-blade propeller operating at a blade thrust coefficient of 0.3 this yields

$$(P/q_t)^2 A_0/c^2 = 0.9 \times 10^{-5} \quad (71)$$

The propeller blade surface pressure measurements presented in Section III show that for the 4-blade, zero angle of attack case, the rms surface pressure fluctuation, P_s , was of the order 0.012q (both quantities measured at the 85% radial station). The acoustic data clearly show a reduction of level for finite pitch angles and on the basis of the two-blade results, it may be assumed that at a blade thrust coefficient of approximately 0.3, the levels would be some 5 dB less. Thus we may estimate that for $C_{T_b} = 0.3$, $P_s/q \approx .007$. Remembering that

the differential pressure, P , will be nearly twice the surface pressure (in the frequency range of interest) and referring pressures to the tip dynamic pressure q_t , we obtain

$$P/q_t \approx 0.009 \quad \text{from the surface pressure measurements.}$$

This may be compared with a value derived from the acoustic data as follows. The constant A_0 is the correlation area at the center frequency f_c where it may be assumed that the chordwise correlation length l_c is of the order of the chord. The lateral correlation length is probably somewhat less than this, say $0.3 c$, so that $A_0/c^2 = 0.3$. Thus, for 4 blades and $C_{T_b} = 0.3$, equation (71) indicates that

$$P/q_t \approx 0.0055 \quad \text{to explain the observed noise}$$

This is a little less than the value derived above and suggests that the measured surface pressure fluctuations were not typical of the entire outboard region of the blade, but were perhaps representative of the tip region only. However, in the light of the various assumptions made, it is obviously not possible to place a great deal of confidence in this statement and it should perhaps be remarked that the two values are in good agreement.

The two results do however provide an indication of the likely range of the fluctuating pressure magnitude, suggesting that the random noise could equally well emanate from small regions of high level pressure disturbance or larger regions of smaller pressure fluctuations.

The turbulent boundary layer would of course be extended over a large region of the blade and could be expected to exert pressures of the order $P_s/q \approx 0.01$ or more on the blade surface. On the other hand, the turbulence scale is small with correlation lengths typically rather less than the blade thickness so that $(P/q_s)^2 A_0/c^2$ is unlikely to exceed 10^{-6} for the boundary layer case. At the same time it must be admitted that very little is known about the behavior of propeller and rotor boundary layers and such phenomena as oscillating transition points and separated flows could very easily add a further 10 dB to this value. Thus although the turbulent boundary layer is unlikely to be a major contributor to propeller broadband noise radiation, it cannot be ruled out entirely.

To give the same result as Sharland's expression for vortex shedding noise at a Reynolds Number of 10^6 , equation (60) would require a value for $(P/q)^2 A_0/c^2$ of 0.2×10^{-4} , which is in the middle of the range given by equation (63) for practical blade thrust coefficients. If Sharland's equation is realistic, then vortex shedding is a likely source of measured random noise radiation.*

Equation (19), which is a modified form of the Sears function describing airfoil response to fluctuating inflow velocities can be rewritten in the form

$$(P/q) = \sqrt{2} \, u/U$$

where u is the rms velocity fluctuation in the crossflow direction. Assuming a correlation area of $0.3 c^2$, this result shows that flow turbulence levels of only 0.1% would be sufficient to explain typical broadband noise levels. Data presented in Section III shows that levels well in excess of 1% are encountered in the shed and trailing airfoil wakes which certainly explains the sharp increase of noise radiation observed at low thrust coefficients where direct blade/wake impingement occurs. Even when impingement does not occur, it is to be expected that turbulence levels as low as 0.1% will extend for considerable distance beyond the measurable wake boundaries, and cause significant noise radiation, especially in the static thrust case.

In summary, it would seem that the attached turbulent boundary layer, although a possible contributor to broadband noise radiation, is the least likely of the sources considered. Separated flows near the blade extremities are far more likely to be responsible for the observed random acoustic energy. The vortex shedding mechanism appears to fit the observed data, but the basis for the calculations are unverified.* Stream turbulence,

* See later comments in Section V.3.e.

is also a likely source on the basis of the studies performed. On the basis of Sears' function, extremely small turbulence levels would account for the noise radiation and the wind tunnel experiments substantiate a correlation between measured surface pressure fluctuations and upstream turbulence levels.

The reason why the relative pressure fluctuations should diminish as the number of blades is increased is not clear, but does lend further support to the conclusion that stream turbulence may be a predominant source of noise. This is because both the boundary layer and vortex shedding processes should be unaffected by blade number. On the other hand, upstream turbulence levels will be highly dependent upon the propeller configuration; an increased blade number, for example, means a reduced blade-to-blade spacing and a corresponding increase in turbulence scale. This in turn could imply a trend toward less efficient, higher frequency radiation. The fact that the harmonic noise measurements yield the same blade number trend also points toward a dependency on gross propeller geometry.

b. Harmonic Pressure Fluctuations

The existence of periodic airloads on an axial flow propeller is difficult to explain in the absence of flow disturbance or other interference effects. However, that these loads exist, there is little doubt, both from the results of the present study and other measurements of propeller and rotor noise. Although the Gutin theory predicts the first few harmonics of "rotational" noise reasonably accurately for high tip speeds and positions immediately behind the disc plane where the steady source terms peak, it badly underestimates harmonic levels in all other situations. Helicopter blades were thought to suffer from high harmonic airloads because of forward flight asymmetry, but a study of experimental data (e.g. References 33 and 36) shows that the loads are equally great in hover conditions. Lowson and Ollerhead showed that good correlation could be obtained with helicopter main rotor data if the harmonic airloads were assumed equal to the steady forces divided by the 2.5-th power of the harmonic number. For $B = 4$, equation (68) gives, for the high frequencies when $n \gg n_c$

$$\frac{T_n}{T_0} = \frac{4.3}{n^{2.5}} \quad (72)$$

which is 12.5 dB greater than the helicopter result. At lower frequencies of course the levels are substantially lower.

In the present tests every effort was made to ensure that the propeller was free from aerodynamic interference and the possibility that the harmonic noise is caused by periodic disturbances of the inflow must be discounted. Three possible sources suggest themselves: The first is that the wake from each blade oscillates in some periodic manner causing periodic angle of attack variation on the following blade. This seems unlikely. The second is that the blades are vibrating in one or several possible modes causing sympathetic airload fluctuations. This is a strong possibility since very small vibration amplitudes could cause the pressure fluctuations responsible for the noise. The third possibility is that

blade-to-blade correlation of the fluctuating pressures causes selective amplification of random energy at multiples of the blade passage frequency. This phenomenon would explain directly the observed narrow band characteristics of the radiated noise. If the random pressure fluctuations are indeed largely attributable to upstream flow disturbances caused by preceding blades, then a strong interblade coupling must be expected.

A final word may be addressed at the significant effect of wind gusts on both harmonic and broadband noise levels. Gust velocities of just a few feet per second were sufficient to increase levels in certain regions of the spectrum by 10 dB and more. This strongly suggests that wake impingements or instabilities play a major role in the noise generation process. The effect of such velocity perturbations could have only a very minor effect on the "self induced" pressure fluctuations due to boundary layers and vortex shedding, whereas slight movements of incoming vortices could result in major changes to the externally induced pressures. This would of course be especially true if the disturbance made the difference between impingement or non-impingement of a vortex wake.

4. PREDICTION OF PROPELLER NOISE RADIATION

The empirically derived loading functions (58), (59), (63), (66) and (68), have been used to compute the noise radiation patterns according to the theoretical results (46) and (35) using the computational approximations discussed in Section II.4.c. The computed spectra, both broadband and harmonic, are compared with the experimental results in figures 33 through 40. With a small number of exceptions, the agreement is considered to be acceptable and sufficient to allow the methods to be used for propeller noise tradeoff studies with some confidence provided the limitation of the analysis are recognized.

These limitations are of course concerned with the range of validity of the empirical loading functions (59) and (66). This can only be determined by experimental validation and the authors would certainly not recommend unwarranted use above tip Mach Numbers of say 0.5 to 0.6. However, the most serious practical restriction is the unknown effect of axial velocity. The present data, like most available propeller noise measurements, were obtained in static thrust conditions where the inflow velocities are relatively low. It is considered that most evidence examined supports the contention that in this static case at least the stream turbulence deposited by the blades themselves is largely responsible for both harmonic and broadband noise radiation. In forward flight, the entire flow pattern is radically changed and significant acoustic changes are likely to result.

However, since the vortex shedding and boundary layer mechanisms could also be responsible for substantial broadband noise radiation it is unlikely that the random component would be markedly reduced. On the other hand, the sharply increased axial flow velocities will practically eliminate blade-to-blade wake interactions, considerably reducing harmonic noise caused by flow disturbances. Only if blade vibration is significant would the higher harmonic noise levels remain high. From a practical standpoint of course the broadband noise will maintain significant spectrum levels at mid to high frequencies and

the steady blade forces would continue to radiate the lower harmonics at angles away from the axis. Along the axis of rotation, however, the lower harmonic radiation could be sharply reduced relative to static thrust conditions and this would encompass a frequency range of critical importance to the aural detection problem, at least for low flying aircraft.

These are questions which must be answered by future research. For the present, the following recommendations are made relative to the problem of propeller noise prediction:

- (a) That the methods described be used for calculating the noise of static propellers in the tip speed range $M = 0.2$ to 0.5 . Their applicability for propellers with higher tip speeds requires experimental verification.
- (b) That the methods described be used with the same tip-speed restrictions for forward flight configurations on the understanding that levels might be overestimated, especially for the harmonic components and especially near the propeller axis. The acoustic effects of forward speed must be accounted for if necessary (see the next Section).

Generalized theoretical results have been condensed into a convenient form for manual calculation in Appendix III. Graphs and charts are provided, together with complete instructions for their use, which will provide results rapidly and to within 2 dB of the accuracy obtainable from the numerical methods described previously.

5. EFFECTS OF FORWARD SPEED

The theoretical results derived in Section II apply to the case of a static propeller. In forward flight, two effects modify the radiated noise. The first, an aerodynamic one, is caused by the change of propeller operating conditions which changes the thrust-to-torque ratio and the flow pattern through the disc. As discussed previously, the detailed effects of the flow changes cannot be predicted and further experimental work is necessary to resolve this question. The gross effects of the modified T/D ratio is, of course, easily accounted for. The second effect is an acoustic one and is a further result of the Doppler effect which causes an amplification of forward radiated sound and a change of frequency heard by a stationary observer. The amplification can be calculated by substituting the term $r_1 (1 - M_0 \cos \theta)$ for the hub to observer distance r_1 , wherever it appears in the acoustic equations. The Mach Number, M_0 , is the velocity with which the propeller moves along its axis of rotation and θ is the angle between this axis and the observer, at the source time τ . The source time now takes on added significance because during the time it takes the sound to reach the observer, the propeller itself has moved forward a distance $\Delta r_1 = r_1 / \sigma_0$.

The distance transformation can be seen by reference to the well known results of Garrick and Watkins (Reference 34), who showed that for a propeller, the moving source version of the Gutin equation is

$$|C_n| = \left[\frac{n \Omega}{2\pi a_0 s} \left\{ T_0 \left(M_0 + \frac{x'}{s} \right) \frac{1}{\beta^2} - \frac{D_0}{M} \right\} J_n \left(\frac{n M y}{s} \right) \right] \quad (73)$$

where $s = r_1 - M_0 x$; $x' = x - M_0 r_1$; $\beta^2 = 1 - M_0^2$

These substitutions give the result

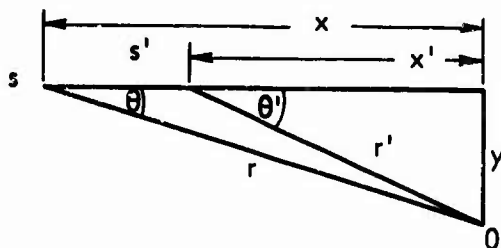
$$|C_n| = \left[\frac{n \Omega}{2\pi a_0 (r_1 - M_0 x)} \left\{ \frac{x T_0}{r_1 - M_0 x} - \frac{D_0}{M} \right\} J_n \left(\frac{n M y}{r_1 - M_0 x} \right) \right] \quad (74)$$

Putting $x/r = \cos \theta$ and $y/r = \sin \theta$, the Gutin equation (73) can be written

$$|C_n| = \left[\frac{n \Omega}{2\pi c_0 r_1} \left\{ \frac{x T_0}{r_1} - \frac{D_0}{M} \right\} J_n \left(\frac{n M y}{r_1} \right) \right] \quad (75)$$

It may be seen that equation (74) is identical to (75), with r_1 replaced by $r_1 - M_0 x/r_1$.

The square brackets indicate evaluation at the source time. Thus, if primes are used to denote quantities evaluated at the observer time, (so that r' and θ' are the source-to-observer coordinates at time t), the source coordinates r and θ can be readily calculated from the sketch below, which shows the source positions s' and s corresponding to the observer and source times.



If Δt is the time of transmission along s_0 , then

$$a_0^2 \Delta t^2 = x^2 + y^2$$

or

$$a_0^2 \Delta t^2 = (x' + M_0 \Delta t)^2 + y^2$$

whence

$$\Delta t = \frac{M_0 x' + \sqrt{x'^2 + y'^2 (1 - M_0^2)}}{a_0 (1 - M_0^2)} \quad (76)$$

$$\theta = \tan^{-1} \frac{(1 - M_0^2) \tan \theta'}{1 + M_0 \sqrt{1 + (1 - M_0^2) \tan^2 \theta'}} \quad (77)$$

and

$$r = r' \cos \theta' \frac{M_0 + \sqrt{1 + (1 - M_0^2) \tan^2 \theta'}}{1 - M_0^2} \quad (78)$$

Equations (77) and (78) are the "retarded coordinates" which must be used to calculate the sound field relative to the instantaneous source position.

It should be noted that when θ is small, i.e., for locations near the axis, equation (78) gives

$$r \approx \frac{r'}{1 - M_0}$$

which almost exactly cancels the Doppler amplification factor accounted for by multiplying r_1 by $(1 - M_0 \cos \theta)$. Thus, to a first approximation the sound field relative to the instantaneous source position is equal to the static field. This is shown in figure 46(a) which shows the computed effect of axial Mach Number up to 0.3. On the positive x axis, the effect is of course zero, whereas the maximum changes may be observed in the plane of rotation. The rotational Mach Number in this example is 0.5 and the overall random noise level is plotted. This figure demonstrates the magnitude of the acoustic (Doppler) effect only and the additional change caused by realistic modifications to the thrust to torque ratio may be found in figure 46(b), where the blade pitch angle has been varied to maintain the same normal force (the slight level reduction on the forward axis is due to a reduction in the thrust component). Again the effects on overall levels are small, illustrating the relatively insignificant role of the torque component which is negligible except at positions near to the disc plane.

In summary, it seems that for low forward speeds, it will normally be sufficiently accurate, for practical purposes, to calculate the sound field relative to the instantaneous position of a moving propeller using a static acoustic analysis, but using the thrust and torque loads which occur in forward flight.

6. DESIGN REQUIREMENTS FOR A QUIET PROPELLER

The harmonic radiation is given by the proportionality

$$\overline{p_H^2} \sim \frac{f_0^2 T_0^2}{a_0^2 r_1^2 B}$$

The spectrum level which controls the subjective attributes of the sound is proportional to $\overline{p_H^2}/f_0$. Therefore, for a given propeller thrust it is necessary to minimize the ratio f_0/B where $f_0 = U_t/2\pi R$.

The broadband radiation can be defined

$$\begin{aligned} \overline{p_B^2} &= \frac{A_0 A_b}{a_0^2 r_1^2} \frac{N_S}{c^2} \rho_0^2 U_t^4 (P/q)^2 \\ &\sim U_t^2/B A_b \quad \text{for a given thrust} \end{aligned}$$

Thus to minimize the total acoustic radiation it is necessary to minimize the tip speed U_t and maximize the radius R , the blade area A_b , and the number of blades B . However, these steps all result in a reduction of the disc and blade thrust coefficients and, as we have seen, can only be reduced to a certain critical level before an increase in noise results due to direct wake impingement. A tentative lower limit for C_{T_b} is between $0.07\sqrt{B}$ and $0.1\sqrt{B}$.

The operating Reynolds number range of low-speed, quiet propeller designs will tend to be in the critical range of 10^5 to 10^6 , where boundary layer instability effects may be the cause of the predominant noise signature. To achieve the full benefit of noise reduction by tip speed reduction, it may be necessary to devote attention to detailed blade design, with emphasis on boundary layer transition characteristics* and sensitivity to turbulent inflow and gust fields.

* See Addendum to Section V.

SECTION V

CONCLUSIONS AND RECOMMENDATIONS

A combined theoretical and experimental study has been performed with the objective of deriving a more basic understanding of the random noise generating mechanisms of propellers operating at low tip speeds. This involved the application of rotating source theory to the random force case, the experimental measurement of both source and radiation parameters required for the application and verification of the theory and the development of simplified procedures which may be used in tradeoff studies to minimize propeller noise. The many findings of the study are listed below under various subheadings and are followed by a number of recommendations for future research.

1. THEORETICAL ANALYSIS

- a. Theoretical expressions describing the noise radiation by rotating random sources have been programmed for computer solution: These allow a complete description of the spectral and directional characteristics of the random noise field surrounding a propeller in terms of the random forces acting on the blade.
- b. The equations which describe random and harmonic radiation are very similar and so therefore are their basic parametric dependencies. For example, all source frequencies in the range $f(1 - M \sin \theta) < f_0 < f(1 + M \sin \theta)$, where M is the rotational Mach number and θ is the angle from the axis of rotation, contribute to sound observed at the frequency f . Thus, rotation has no acoustic effect on axially radiated noise ($\theta = 0$).
- c. Noise radiation along the axis of rotation is completely controlled by the unsteady blade loads. Measurements at this location are thus extremely important to an understanding of propeller noise mechanisms.
- d. Random noise originates from a variety of turbulent phenomena. It is shown that turbulence itself generates the noise; the blade merely acts as a reflecting surface. However, provided the turbulence scale is not small compared with the chord dimensions, it is appropriate to treat the blade as a dipole source.
- e. The acoustic theory for random loads, like that for harmonically fluctuating loads, can be as rigorous as the source definition will allow. Again, the major practical problem is that of describing the source in terms of surface pressure spectra and correlation areas.

2. EXPERIMENTS

- a. Wake turbulence and blade surface pressure fluctuations were measured in a low speed wind tunnel at velocities of 150 ft. per second. The tunnel turbulence level was 0.4%. Measurements were made on single and tandem blades to investigate the effects of stream turbulence on the fluctuating pressure levels.
- b. Sears' function appears to provide a reasonable estimate of the fluctuating pressure levels resulting from incoming flow disturbances. Fluctuations which might be attributable to the boundary layer could not be identified due to predominance of stream turbulence induced levels and transducer roll-off at high frequencies.

- c. Turbulence intensities in the wake, both the sheet wake behind the blade and the trailing tip vortex regions can be related to the mean flow defect by the relationship

$$\frac{u}{U_{\infty}} = 0.1 \sqrt{1 - \frac{U}{U_{\infty}}}$$

- d. Three different blade tip shapes were studied experimentally: a standard "square" tip, a 60° swept tip, and a trapezoidal tip. The tip vortex behind the trapezoidal tip diffuses more rapidly than those of either standard or swept tip.
- e. Measurements of blade surface pressure fluctuation were also made with five transducers installed in a propeller blade. However, the planned program could not be completed due to transducer failure.
- f. Free field propeller noise measurements were made in a forward quadrant for tip speeds in the range $M = 0.2$ to $M = 0.4$. Tests at higher speeds were prevented by rig vibration. Sound recordings were spectrum analyzed and it was found necessary to resort to narrow band analysis to discriminate between random and harmonic noise at all frequencies. As many as 50 or more harmonics of the blade passage frequency could frequently be identified.
- g. At the higher frequencies it is difficult to separate the harmonic and random components from the measured noise and indeed it could be equally correct to consider the spectrum as a sum of harmonically related narrow bands of noise. For the purposes of analysis and prediction it has been assumed that the two can be separated and that the pure harmonics are superimposed on a background of random noise.
- h. Harmonic noise levels were observed to vary as the sixth power of velocity confirming the validity of the dipole analysis. An apparent departure of the random noise from this law at the lowest speed was attributed to ambient noise interference.

- i. Noise levels increased at low inflow velocity, high blade angle and high blade number conditions. These can be attributed to wake interaction or local blade stall effects, and impose practical limits on the noise reduction which may be achieved through changes in gross configuration features.
- j. Changes in propeller blade tip shape produced insignificant effect on the harmonic and broadband content of the noise spectra, in the frequency range of main interest.
- k. The noise of the test propeller and the commercial (Sensenich) propeller was extremely sensitive to small wind gusts, with level increases of as much as 10 dB occurring in the mid frequency range. Analysis of the gust effects indicated a definite frequency selectivity of the noise increases.
- l. The specially built research propeller exhibited a very high frequency noise component which in many cases dominated the overall sound pressure level (2 - 20,000 Hz) at field positions near the propeller axis. This component was found to be sensitive to blade tip speed, tip angle and tip shape, and followed a Strouhal frequency scaling.

3. CORRELATION OF THEORY AND EXPERIMENT

- a. The axially radiated random noise peaks at a center frequency of approximately $f_c = 0.85 U_t/c$, where U_t is the propeller tip speed and c is the chord. A slight tendency for this frequency to diminish with increased angle of attack could not be regarded as statistically significant. The power spectral density of the axial noise rises and falls about the center frequency at asymptotic rates of 9 dB per octave.
- b. Axial harmonic levels were found to remain approximately constant for the first few harmonics, rolling off at rates between 6 and 12 dB per octave at higher frequencies. An average formula for the observed spectral form is

$$\overline{p_{mB}^2} = \overline{p_1^2} \left\{ 1 + \left(\frac{mB}{36} \right)^3 \right\}^{-1}$$

The effective blade loads responsible for this noise vary as $\overline{p_{mB}^2} (mB)^{-2}$. At high frequencies this has the same form as the result previously obtained for helicopter noise. However, the present results indicated levels which, at high frequencies, are 12.5 dB greater than those given by the previous formula. These penetrate the frequency range usually assigned to random vortex noise.

- c. Both harmonically and randomly fluctuating loads appear to decrease, relative to the steady forces, inversely as the square root of the number of blades.

- d. Several possible sources of noise generation have been examined, but a clear separation of these into order of significance has not been possible from the available data. The operating Reynolds number range, based on chord, of the test propellers and of full-scale quiet propeller designs, falls in the range 10^5 to 10^6 which suggests that the noise sources may be associated with the instability of the boundary layer — and hence differ from conventional-propeller noise mechanisms. The possible sources in this critical Reynolds number range are:
- (i) an oscillating laminar separation;
 - (ii) large areas of unstable laminar boundary layer;
 - (iii) stream turbulence.

The latter effect is well known in transitional boundary layer studies, where large fluctuating velocity fields have been induced by (controlled) turbulence inflow. Its relevance to propeller noise has not been previously considered.

- e. Although Sharland's expressions for the vortex shedding process provide the correct levels and frequencies, recent independent experimental results by Davis and Foley (unpublished -- communicated by M.V. Lawson) show levels of fluctuation at least 20 dB below Sharland's experiments, in a very low turbulence flow. The latter work suggests that trailing-edge "vortex noise", in the generally accepted sense, is insignificant.
- f. It has not been possible to explain the origin of the harmonically varying blade forces although it has been concluded that they are most probably the result of blade/wake interaction effects and blade-to-blade pressure correlations. Again the sensitivity of the local blade boundary layer in the critical Reynolds Number domain may account for the significance of such external influences in the noise generation process. The fluctuating levels are exceedingly small and it is also possible that blade vibration plays some part in this mechanism.

4. PREDICTION

- a. Generalized source functions have been defined as a basis for theoretical noise calculations. These show reasonable agreement with the experimental results for both harmonic and random components.
- b. Propeller noise prediction procedures are presented which allow hand computation with the aid of a number of charts of both harmonic and random noise radiation. These are believed to be valid for tip speeds between $M = 0.2$ and $M = 0.5$ or 0.6 and for blade thrust coefficients in excess of $0.1 \sqrt{B}$. At lower thrust coefficients they are likely to underestimate the radiated noise.
- c. The steady force terms (Gutin) have little influence on the noise of low speed propellers except for the lowest harmonics at large angles from the shaft axis.

- d. Axial motion at moderate speeds has little effect on the calculated noise relative to the instantaneous position of the source. The static predictions should be sufficiently accurate for axial Mach numbers at least up to 0.3. However, a major unknown exists with regard to the effect of forward speed on the fluctuating blade forces. If these are dependent upon the wake turbulence, substantial noise reductions, both harmonic and broadband, could result in forward flight when the axial flow is significantly higher.

5. NOISE CONTROL

- (a) The results of the present study indicate that, to minimize propeller noise, the tip speed should be reduced and the blade area, radius and number of blades increased within limits imposed by a lower blade thrust coefficient of approximately

$$C_{T_b} = 0.1 \sqrt{B}.$$

- (b) Low speed propellers with tip region Reynolds numbers in the critical (transition) range will require detailed study of their (noise) sensitivity to inflow turbulence and discrete gust fields.
- (c) See Addendum to this Section.

6. RECOMMENDATIONS

The present study has provided further insight into the "vortex-noise" problems associated with low speed propellers, and has clearly indicated areas where existing knowledge is inadequate. When the Gutin-type noise content is reduced to achieve a quiet propeller, other noise sources become predominate and differ in origin from those previously studied for conventional propellers. It is therefore essential to study these sources in more detail in order to establish more definitive guidelines for optimum propeller noise reduction. The immediate problem is one of unsteady aerodynamics and can be studied effectively by the use of acoustic theory, which allows blade load information to be extracted from noise measurements.

There are three main areas of study which require detailed attention; namely, the influence of transitional Reynolds number effects, the effects of atmospheric gusts, and the high frequency tip noise origins. The first two of these may be interrelated in the critical Reynolds number region of operation, but the tip noise seems to have a distinctly different, and as yet unexplained, origin.

Studies of the transitional Reynolds number effects should be aimed towards two objectives. The first of these is the understanding of the source mechanism details and dependencies, which can be examined by use of acoustic measurements on the axis of propeller systems with various modified (e.g. tripped) boundary layers. The present study has shown that high frequency surface pressure measurements are feasible, and although an investigation is required of the reasons for the transducer failures, their usage in future investigations of propeller noise sources should be pursued, as the resulting information on spatial and temporal aspects of the blade loadings would be extremely valuable. The second objective is the selection of blade airfoil profiles which allow noise control in quiet propeller designs. This

is probably a long-term objective as experimentation on such effects is more laborious. However, the need for a guideline to detailed blade design is well established and the findings of the present study offer a new line of approach to the problem.

The very high frequency "tip-noise" noted in the present study, and in other unpublished data, has possibly not been identified in conventional-propeller noise spectra due to the cut-off of the analysis frequency range of interest. On a Strouhal scaling basis, this noise component would be maximized at 1000 Hz for a quiet propeller of 1 ft tip chord operating at a tip Mach number of 0.1, and could therefore dominate the subjective noise signature. It is clearly of considerable importance to further isolate and examine this potential noise problem and to establish methods for its control and possible elimination. Such investigations would be related to tip geometry.

A most important question related to the application of the present results to quiet propeller design studies is that of the effects of axial motion on the unsteady blade loads. This is best answered by flight test and a modest program could be pursued to measure the noise radiated by a single propeller on a whirl stand, under static operation on an aircraft and in flight. In each case the axially radiated noise is of prime importance. In flight this could be obtained by flying the aircraft toward a tower mounted microphone or by supporting a microphone in front of a propeller on a twin engine aircraft. Both methods should be investigated.

In the meantime it is considered necessary to validate or refine the prediction procedures presented herein through application to the noise of a variety of propeller designs. The data upon which they are based were of necessity limited and additional verification is required to improve the confidence with which they may be used.

7. ADDENDUM

The original concept of the present study program was directed towards an understanding of the expected broadband noise sources. The findings of the study, however, have pointed towards other source mechanisms which may control the extensive harmonic range and the broadband noise exhibited by the low speed propellers. In particular, the whole concept of transitional boundary layer problems was not expected and hence not closely examined in the present experimental studies. To provide some additional basis for the concept, a simple experimental test was set up subsequent to the original writing of this report. This test and the results are described in Appendix IV. Briefly, the experiment was conducted by taking noise measurements on the axis of a small (model) propeller over a range of rotational speeds. The measurements comprised 1/3 octave band spectra of the noise of the basic (unmodified) propeller, a propeller modified by "roughing" the leading edge of the blades, and a propeller modified by building a very small ridge along the upper surface span near the leading edge. The objective was to trip, and hence stabilize, the boundary layer. The results indicated that reductions of up to 5 dBA were obtained by the modified blades, relative to the unmodified propeller noise level.

This experiment tends to confirm the belief that the "unsteady-load" noise is related to transition instabilities.

REFERENCES

1. Gutin, L., "On the Sound Field of a Rotating Propeller," *Physiks Zeitschrift der Sowjetunion*, Band A Heft 1 (1936), Translated as NACA TM-1195, October 1948.
2. Stowell, E. Z. and Deming, A. T., "Vortex Noise from Rotating Cylindrical Rods," NACA TN 519.
3. Yudin, E. Y., "On the Vortex Sound from Rotating Rods," NACA TM 1136.
4. Hubbard, H. H., "Propeller Noise Charts for Transport Airplanes," NACA TN 2968, June 1953.
5. Schlegel, R. G., King, R. J. and Mull, H. R., "Helicopter Rotor Noise Generation and Propagation," USAAVLABS Tech. Report 66-4, U. S. Army Aviation Materiel Laboratories, Fort Eustis, Virginia, October 1966.
6. Goddard, J. O. and Stuckey, T. J., "Investigation and Prediction of Helicopter Rotor Noise," *J. Sound Vib.* Vol. 4, No. 3.
7. Davidson, I. M. and Hargest, T. J., "Helicopter Noise," *J. Roy. Aeronautical Society*, Vol. 69, No. 653, pp. 325-336, May 1965.
8. Lowson, M. V. and Ollerhead, J. B., "Studies of Helicopter Rotor Noise," USAAVLABS TR68-60, 1968.
9. Loewy, R. G. and Sutton, L. R., "A Theory for Predicting the Rotational Noise of Lifting Rotors in Forward Flight Including a Comparison with Experiment," *J. Sound* Vol. 4, No. 3, pp. 305-349, November 1966.
10. Lowson, M. V., "The Sound Field for Singularities in Motion," *Proc. Roy. Soc. (London) A*, Vol. 286, pp. 559-572, August 1965.
11. Lighthill, M. J., "Sound Generated Aerodynamically, Bakerian Lecture 1961", *Proc. Roy. Soc. (London) A*, Vol. 267, pp. 147-182, 1962.
12. Lowson, M. V., "Thoughts on Broad Band Noise Radiation by a Helicopter," Wyle Laboratories Report WR 68-20, December 1968.
13. Frowcs Williams, J. E. and Hawkins, D. L., "Theory Relating to the Noise of Rotating Machinery," *J. Sound Vib.*, Vol. 10, No. 1, pp. 10-21, July 1969.

14. Kemp, N. H., and Sears, W. R., "The Unsteady Forces Due to Viscous Wakes in Turbomachinery," *J. Aero. Sc.*, July 1955.
15. Lowson, M. V., "Theoretical Analysis of Compressor Noise," *J. Acoust. Soc. Amer.*, Vol. 47, No. 1 (Pt. 2), pp. 371-385, January 1970. (see also NASA CR 1287).
16. Sharland, J. J., "Sources of Noise in Axial Flow Fans," *J. Sound Vib.*, Vol. 1, No. 3, pp. 302-322, 1964.
17. Doak, P. E., "Acoustic Radiation from a Turbulent Fluid Containing Foreign Bodies," *Proc. Roy. Soc. (London)*, Vol. 254 A.
18. Curle, N., "The Influence of Solid Boundaries on Aerodynamic Sound," *Proc. Roy. Soc.* A231, 1955.
19. Bull, M. K., Willis, J. L., "Some Results of Experimental Investigations of the Surface Pressure Field Due to a Turbulent Boundary Layer," *Univ. Southampton AASU199*, 1961.
20. Bull, M. K., "Properties of the Fluctuating Wall Pressure Field of a Turbulent Boundary Layer," *AGARD Report 455*, April 1963.
21. Bies, D. A., "A Review of Flight and Wind Tunnel Measurements of Boundary Layer Pressure Fluctuations and Induced Response," *NASA CR-626*, October 1966.
22. Lowson, M. V., "Rotor Noise Radiation in Non-Uniform Flow," Paper D2 Proceedings of a Symposium on Aerodynamic Noise, Loughborough University, September 1970.
23. Hubbard, H. H. and Lassiter, L., "Sound from a Two-Blade Propeller at Supersonic Tip Speeds," *NACA Report 1079*.
24. Hicks, C. W. and Hubbard, H. H., "Comparison of Sound Emission from Two-Blade, Four-Blade and Seven-Blade Propellers," *NACA Tech. Note 1354*, July 1947.
25. Roberts, J. P. and Beranek, L. L., "Experiments in External Noise Reduction of a Small Pusher-Type Amphibian Airplane," *NACA TN 2727*, 1952.
26. Hubbard, H. H., "Sound from Dual-Rotating and Multiple Single-Rotating Propellers," *NACA TN 1654*, 1943.

27. Silverstein, A., Katzoff, S., and Bullivant, W. K., "Downwash and Wake Behind Plain and Flapped Airfoils," NACA R651, 1939.
28. Carpenter, P. J., "Lift and Profile Drag Characteristics of a NACA 0012 Airfoil Section as Derived from Measured Helicopter Rotor Hovering Performance," NACA TN 4357, 1958.
29. Spivey, W. A., and Morehouse, "New Insights in the Design of Swept Tip Rotor Blades," 26th Forum of Am. Hel. Soc., 1970.
30. Schlichting, H., Boundary Layer Theory, McGraw Hill (6th ed.), 1968.
31. Widnall, S. E., "A Correlation of Vortex Noise Data from Helicopter Main Rotors," J. Aircraft, Vol. 6, No. 3, pp. 279-281, May-June 1969.
32. Ollerhead, J. B., "Helicopter Aural Detectability," Wyle Laboratories Report 71-3, for USAAVLABS, 1971.
33. Scheiman, J., "A Tabulation of Helicopter Rotor-Blade Differential Pressures, Stresses, and Motions, as Measured In-Flight," NASA TM-X-952, National Aeronautics and Space Administration, Washington, D.C., March 1964.
34. Garrick, I. E. and Watkins, C. E., "A Theoretical Study of the Effect of Forward Speed on the Free Space Sound-Pressure Field Around Propellers," NACA Report 1198, 1954.
35. Dommash, D. O., "Elements of Propeller and Helicopter Aerodynamics," Pitman, 1953.
36. Burpo, F. B., and Lynn, R. R., "Measurement of Dynamic Airloads on a Full Scale Semi-Rigid Rotor," Bell Helicopter Company, TCREC Technical Report 62-42, U. S. Army Transportation Research Command, Fort Eustis, Virginia, December 1962.
37. Lowson, M. V., "Basic Mechanism of Noise Generation by Helicopters," V/STOL Aircraft and Ground Effect Mechanisms," J. Sound Vib., Vol. 3, Pt. 3, pp. 454-466, 1966.
38. Tu, B. J., "Experimental Investigation of Turbulent Velocities in a Subsonic Circular Jet," Wyle Laboratories WR 70-2, February 1970.

TABLES OF CORRELATION COEFFICIENTS FOR THE CORRELATION COEFFICIENT

Sample Size	10	20	30	40	50	60	70	80	90	100
10	0.95	0.90	0.85	0.80	0.75	0.70	0.65	0.60	0.55	0.50
20	0.90	0.85	0.80	0.75	0.70	0.65	0.60	0.55	0.50	0.45
30	0.85	0.80	0.75	0.70	0.65	0.60	0.55	0.50	0.45	0.40
40	0.80	0.75	0.70	0.65	0.60	0.55	0.50	0.45	0.40	0.35
50	0.75	0.70	0.65	0.60	0.55	0.50	0.45	0.40	0.35	0.30
60	0.70	0.65	0.60	0.55	0.50	0.45	0.40	0.35	0.30	0.25
70	0.65	0.60	0.55	0.50	0.45	0.40	0.35	0.30	0.25	0.20
80	0.60	0.55	0.50	0.45	0.40	0.35	0.30	0.25	0.20	0.15
90	0.55	0.50	0.45	0.40	0.35	0.30	0.25	0.20	0.15	0.10
100	0.50	0.45	0.40	0.35	0.30	0.25	0.20	0.15	0.10	0.05

TABLES

TABLES OF CORRELATION COEFFICIENTS

Sample Size	10	20	30	40	50	60	70	80	90	100
10	0.95	0.90	0.85	0.80	0.75	0.70	0.65	0.60	0.55	0.50
20	0.90	0.85	0.80	0.75	0.70	0.65	0.60	0.55	0.50	0.45
30	0.85	0.80	0.75	0.70	0.65	0.60	0.55	0.50	0.45	0.40
40	0.80	0.75	0.70	0.65	0.60	0.55	0.50	0.45	0.40	0.35
50	0.75	0.70	0.65	0.60	0.55	0.50	0.45	0.40	0.35	0.30
60	0.70	0.65	0.60	0.55	0.50	0.45	0.40	0.35	0.30	0.25
70	0.65	0.60	0.55	0.50	0.45	0.40	0.35	0.30	0.25	0.20
80	0.60	0.55	0.50	0.45	0.40	0.35	0.30	0.25	0.20	0.15
90	0.55	0.50	0.45	0.40	0.35	0.30	0.25	0.20	0.15	0.10
100	0.50	0.45	0.40	0.35	0.30	0.25	0.20	0.15	0.10	0.05

TABLE I
PRESSURE CORRELATION AREAS
IN A TURBULENT BOUNDARY LAYER

Source	S_c	δ^*	$\omega^2 S_c$
Doak (Reference 17)	$144.00 \delta^{*2}$	$0.016 U/\omega$	$63.000 U^2$
Lighthill (Ref 11)	$4.40 \delta^{*2}$	$0.050 U/\omega$	$0.011 U^2$
Bull and Willis (Ref 19)	$1.78 \delta^{*2}$		
Sharland (Ref 16)			$0.500 U^2$
Bull (Reference 20)	$15.00 \delta^{*2}$	$0.300 U/\omega$	$0.135 U^2$

TABLE II
ESTIMATED PERFORMANCE OF TEST PROPELLERS

Propeller Type	C_T	C_T/σ	$M_t = 0.2$		$M_t = 0.3$		$M_t = 0.4$	
			T (lb)	SHP	T (lb)	SHP	T (lb)	SHP
W6 STD 8	.0285	.144	22	1.00	49	3.3	85	7.8
W4 STD 8	.023	.174	18	0.70	40	2.4	71	5.6
W3 STD 8	.0194	.195	15	0.50	33	1.8	58	4.4
W2 STD 8	.015	.225	11	0.40	26	1.3	45	3.0
W2 STD 16	.0315	.477	24	1.00	52	3.2	93	7.7
W2 STD 12	.023	.348	17	0.70	38	2.4	68	5.6
W2 STD 4	.0074	.113	6	---	13	---	26	---
W2 STD 0	.0012	.022	--	---	2	---	4	---
W60 LK 18 (Sensenich)	.0203	---	16	0.65	35	2.2	63	5.2

TABLE III
PROPELLER CONFIGURATIONS TESTED
IN NOISE MEASUREMENT PROGRAM

Tip Angle	Blade Number (B)			
α_t	2	3	4	6
16	X			
12	X			
8	X Δ \diamond	X	X Δ \diamond	X
4	X			
0	X			
-2	X			
Sensenich W60 LK 18 (B = 2, D = 4 ft)				

X = With Standard Blade Tips

Δ = With Swept Blade Tips

\diamond = With Trapezoidal Blade Tips

Configurations denoted by W (B) (tip shape) (α_t)

TABLE IV

MEASURED CENTER FREQUENCIES FOR BROADBAND NOISE ($\theta = 0^\circ$)

PROPELLER CASE	TIP SPEED (ft/sec)	FREQUENCY f_c (Hz)	$N_S = f_c c / U_t$
W ₂ STD 8	224	850	0.66
	336	1100	0.82
	356		
	391	1300	0.83
	419	1350	0.80
	448	1500	0.84
W ₂ STD 12	224	900	1.00
	336	1000	0.75
	448	1400	0.78
W ₂ STD 16	224	750	0.84
	336	800	0.60
	448	1250	0.80
W ₃ STD 8	224	760	0.83
	336	1400	1.04
	448	1600	0.89
W ₄ STD 8	224	720	0.8
	336	1400	1.04
	448	1500	0.88
W ₆ STD 8	224	1100	1.23
	336	1300	0.96
	448	1700	0.95
SENSENICH	224	550	1.03
	336	810	0.99
	448	1050	0.97

FIGURES

66a

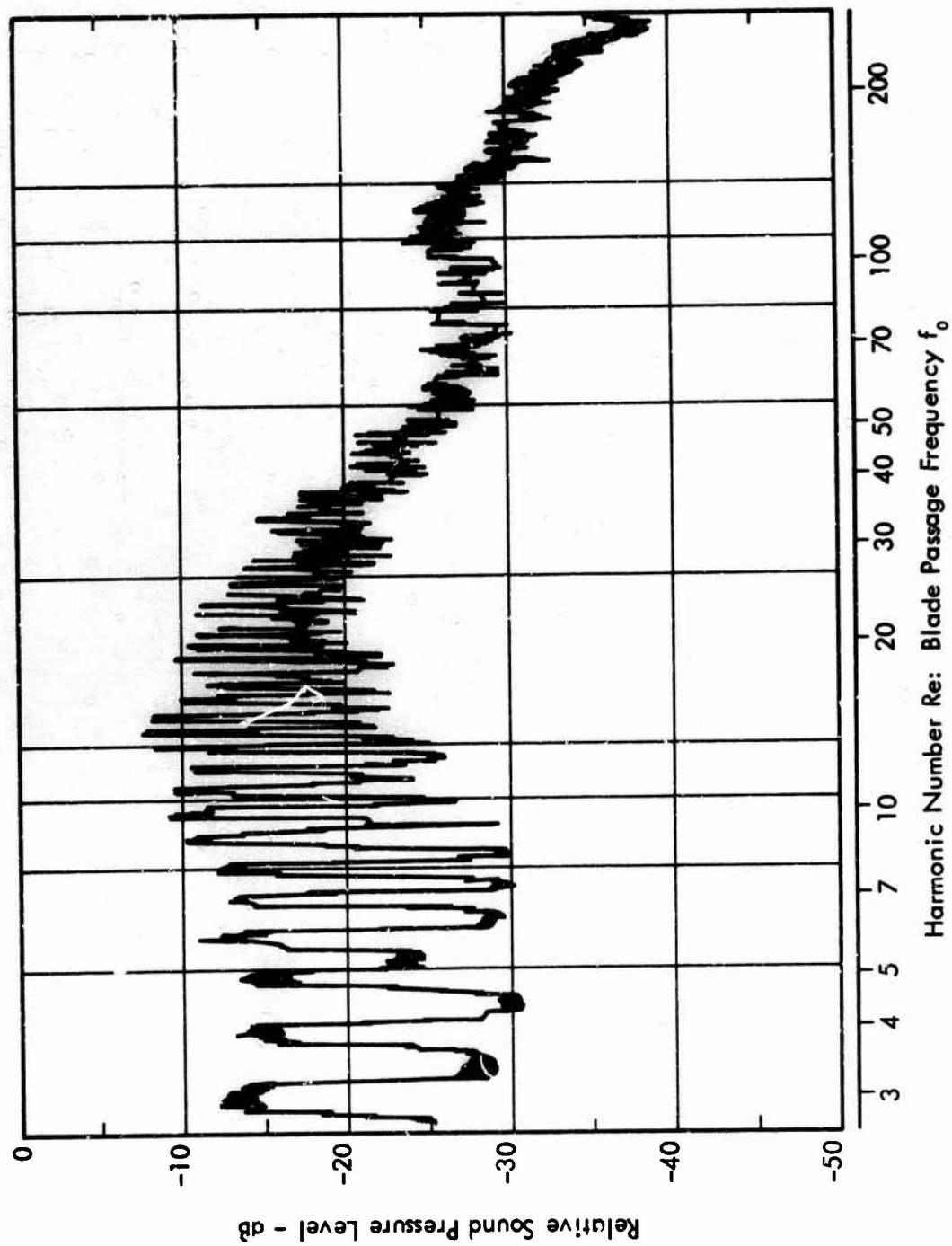


Figure 1. Narrow Band Analysis of Propeller Noise - Bandwidth $\sim f_0/10$

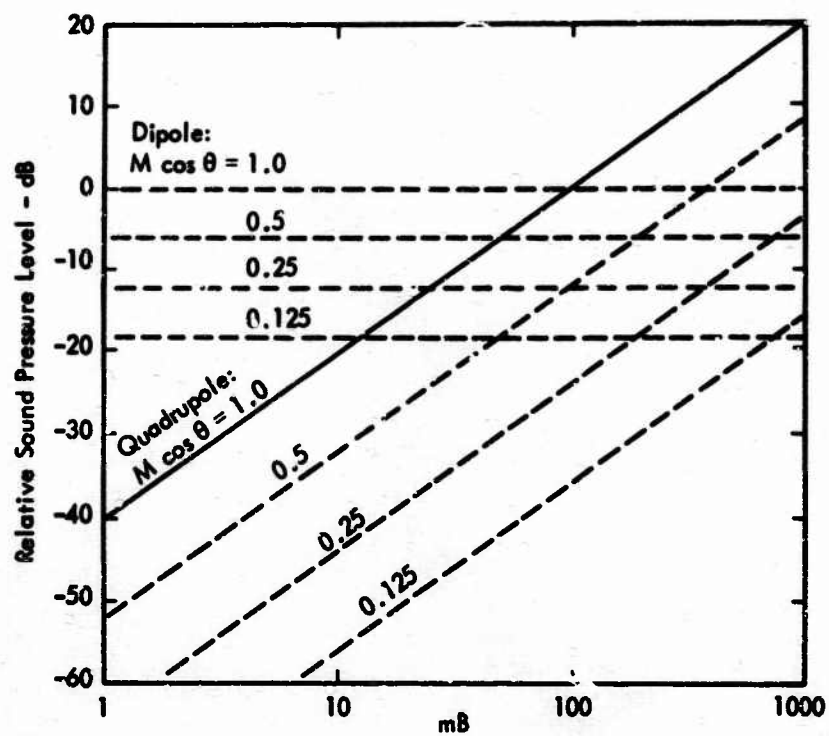


Figure 2. Relative Contributions from Steady Dipole and Quadrupole Sources

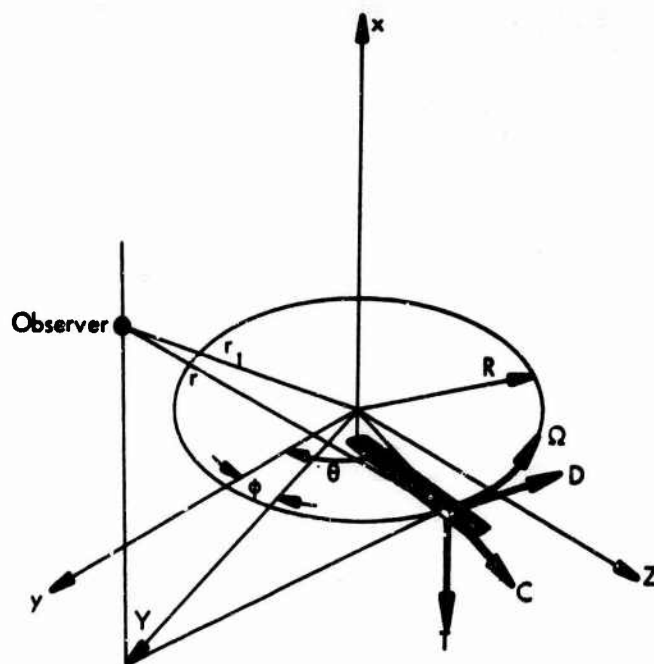


Figure 3. Coordinate System for Propeller Noise Analysis

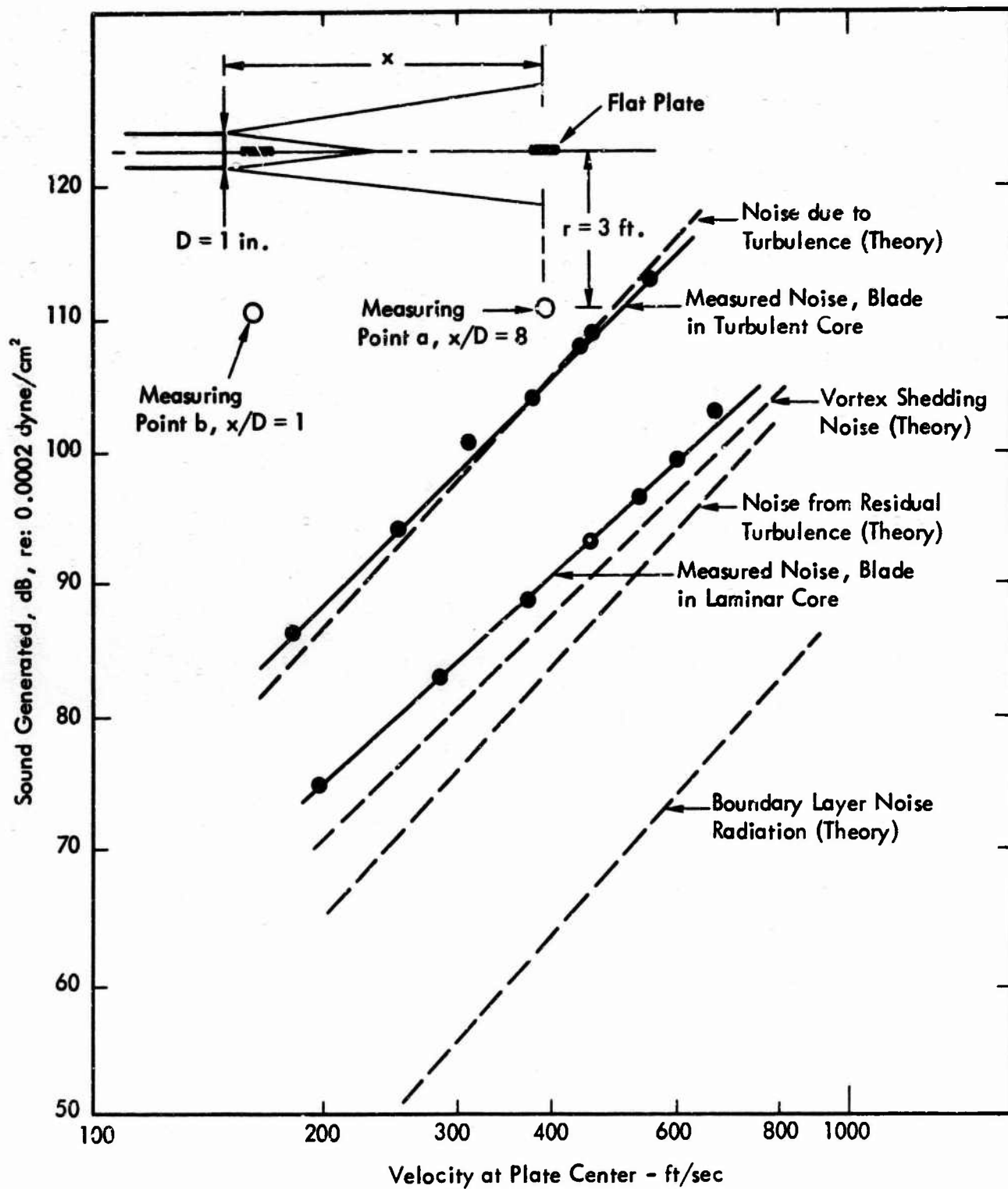


Figure 4. Noise Radiated from a Plate in a Turbulent Airstream (after Sharland, Reference 16)

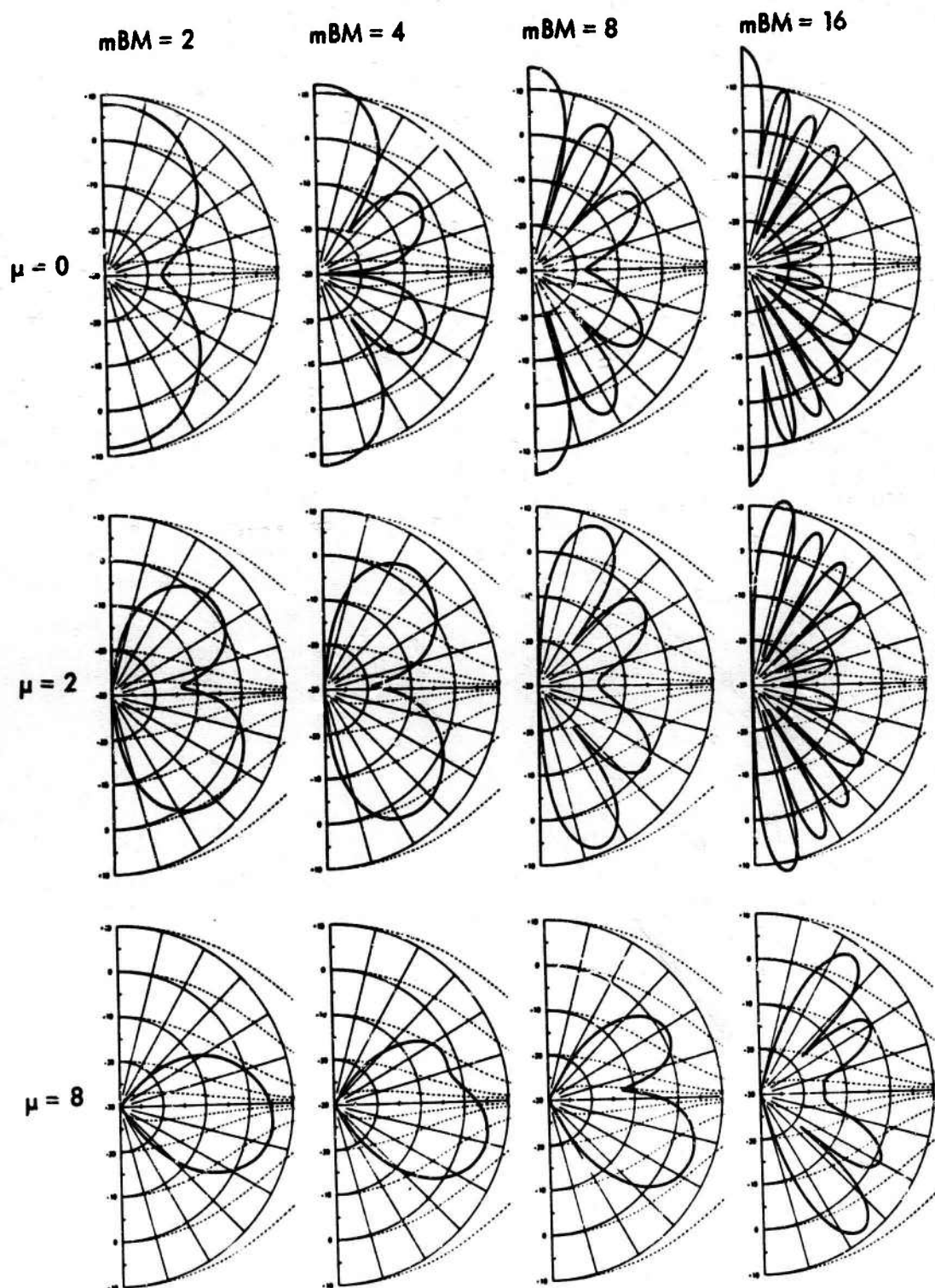


Figure 5. Directionality Patterns for Combined Load in Any One Harmonic (From Reference 8)

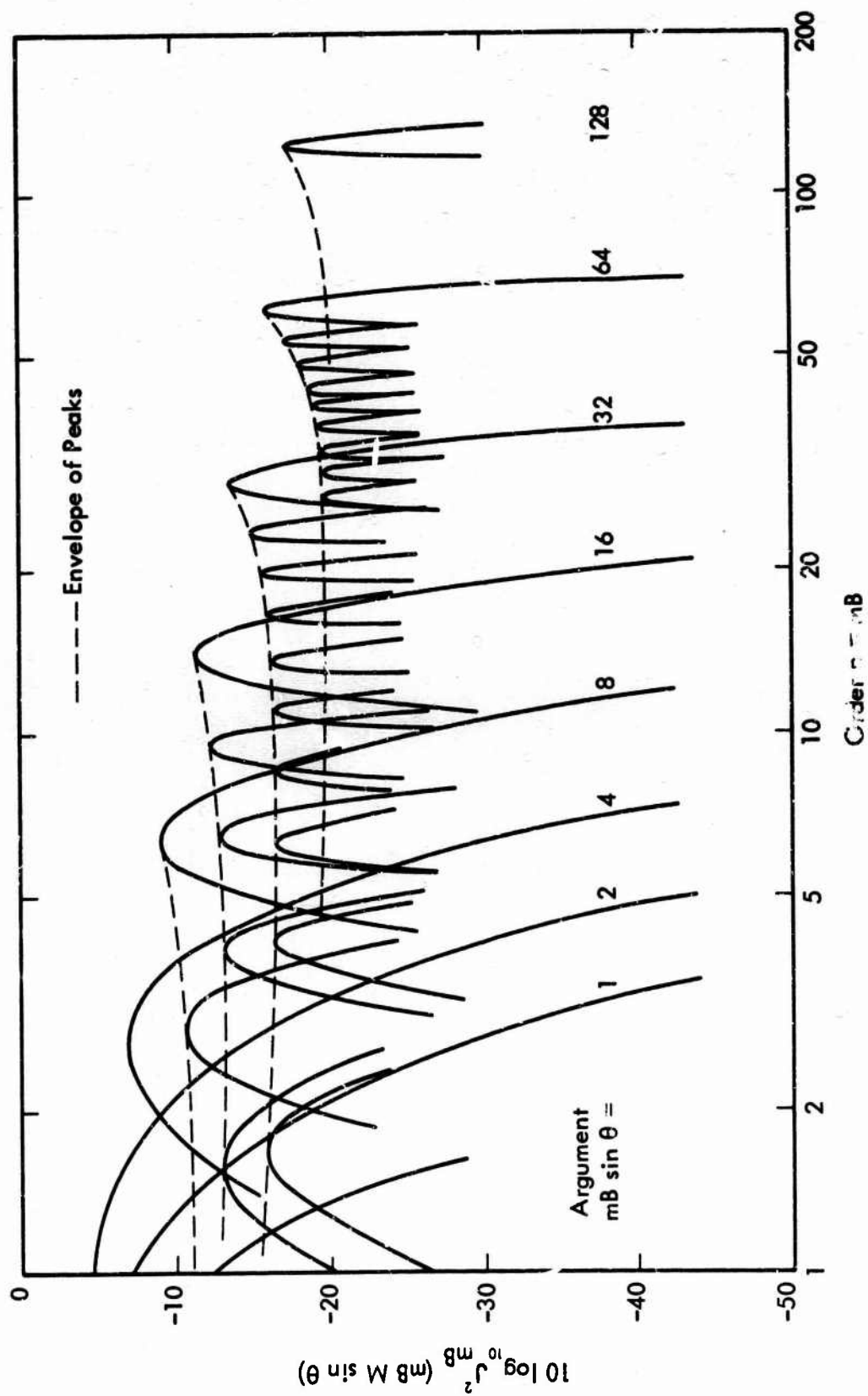


Figure 6. The Variation of $10 \log_{10} J^2_{mB} (mB M \sin \theta)$ with Order and Argument Showing Cut-Off Effect

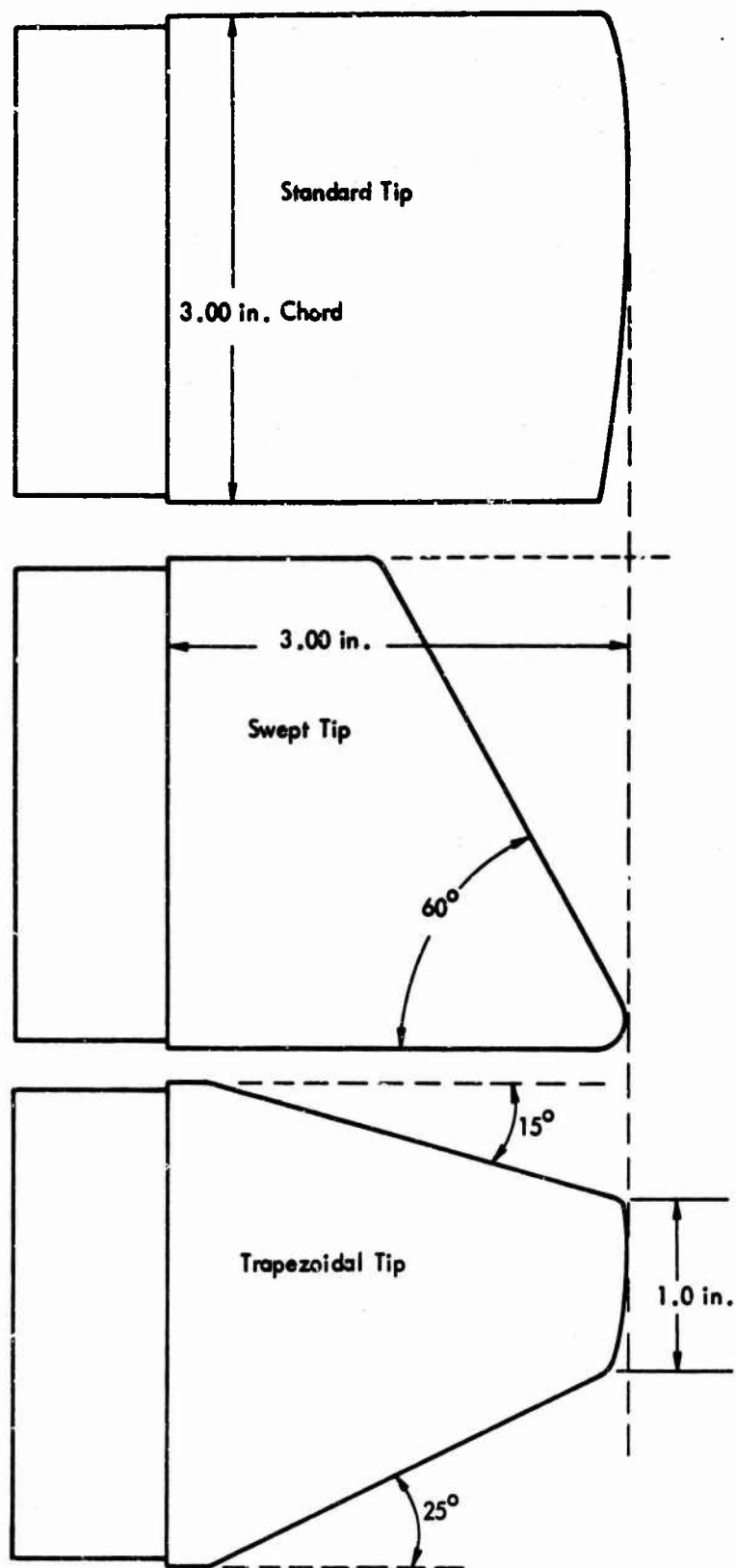
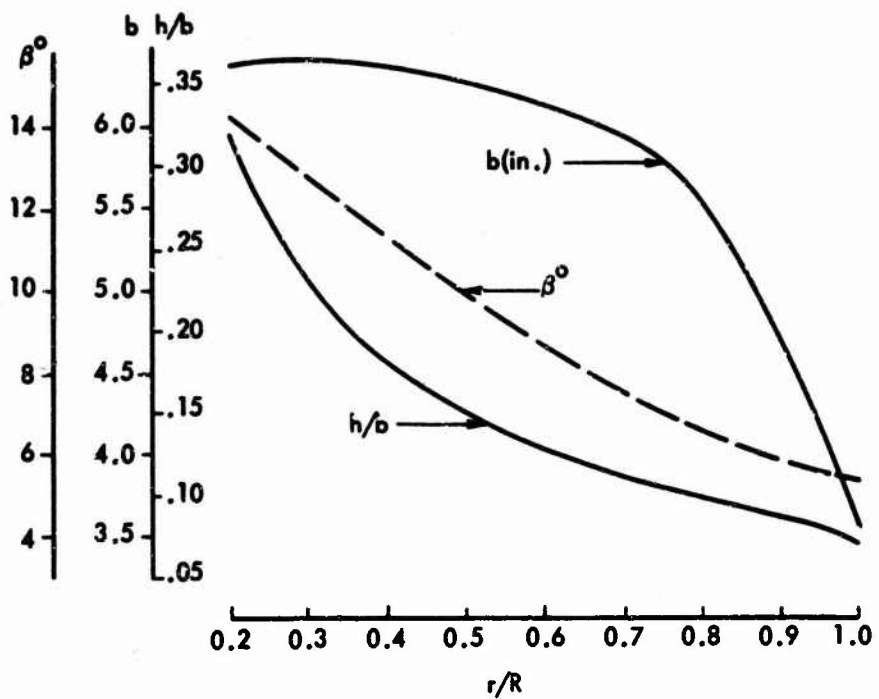


Figure 7. Propeller Tip Geometries Employed in Test Program



b is Blade Chord, β is Section Blade Angle, h/b is Thickness/Chord

Figure 8. Sensenich W60LK 18 Propeller Configuration

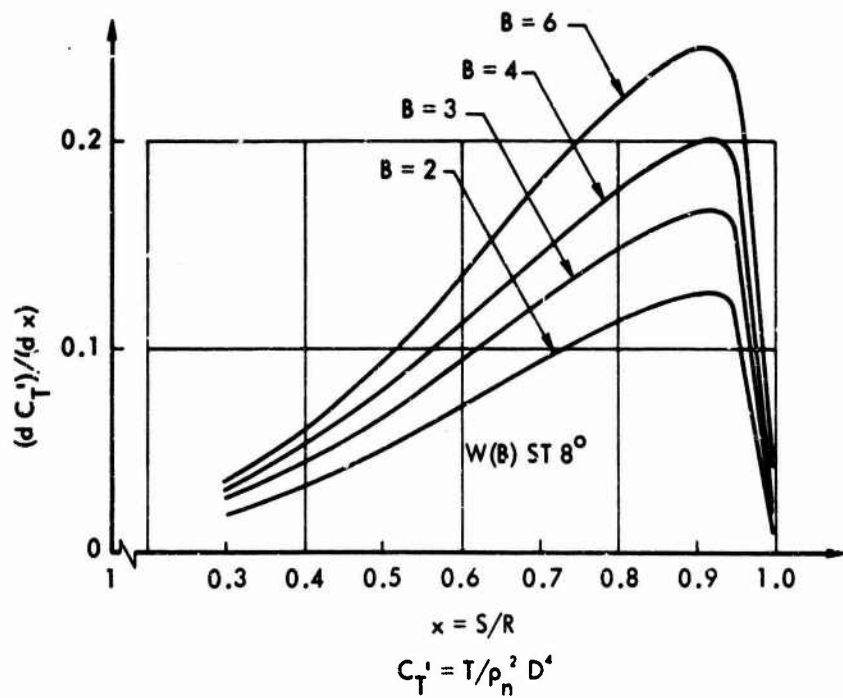


Figure 9. Thrust Grading on Whirl Test Propellers

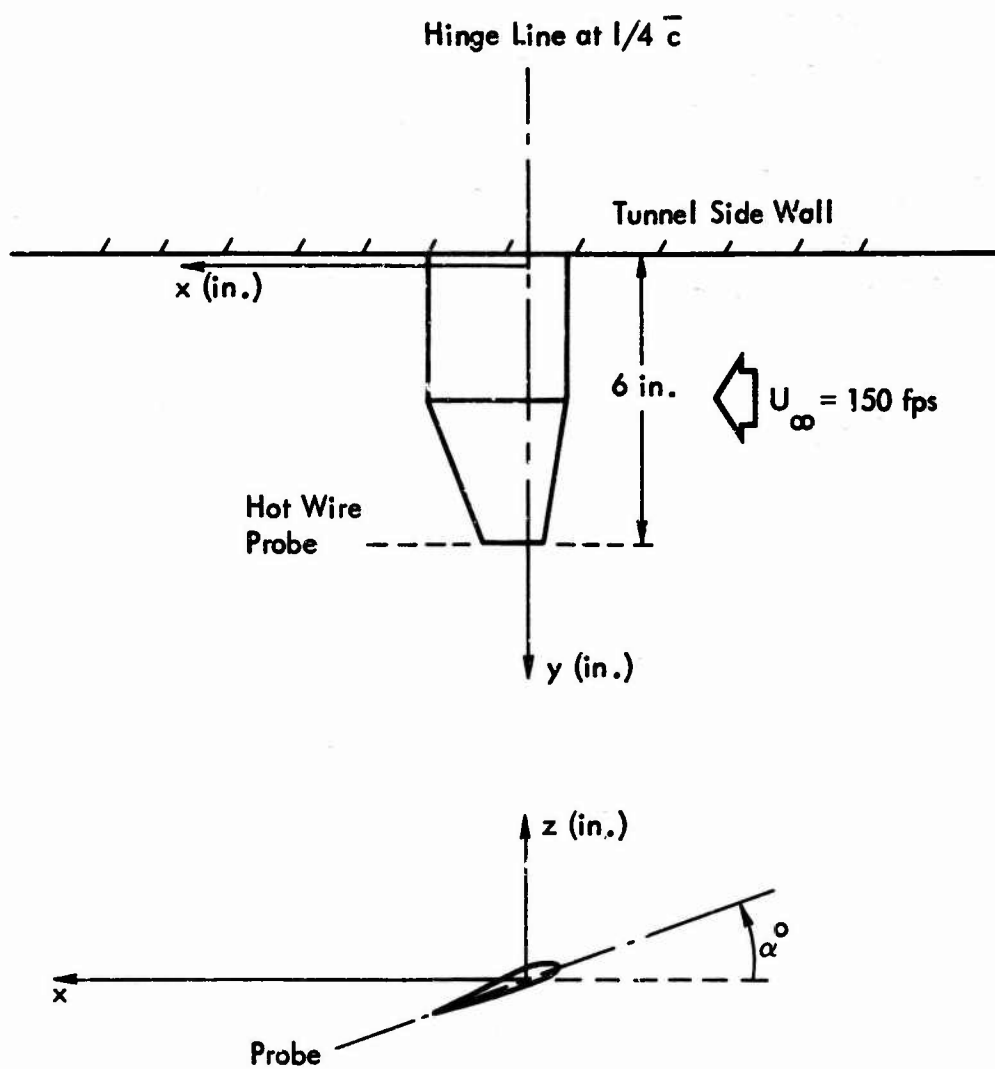


Figure 10. Coordinate Convention for Wake Turbulence Measurements

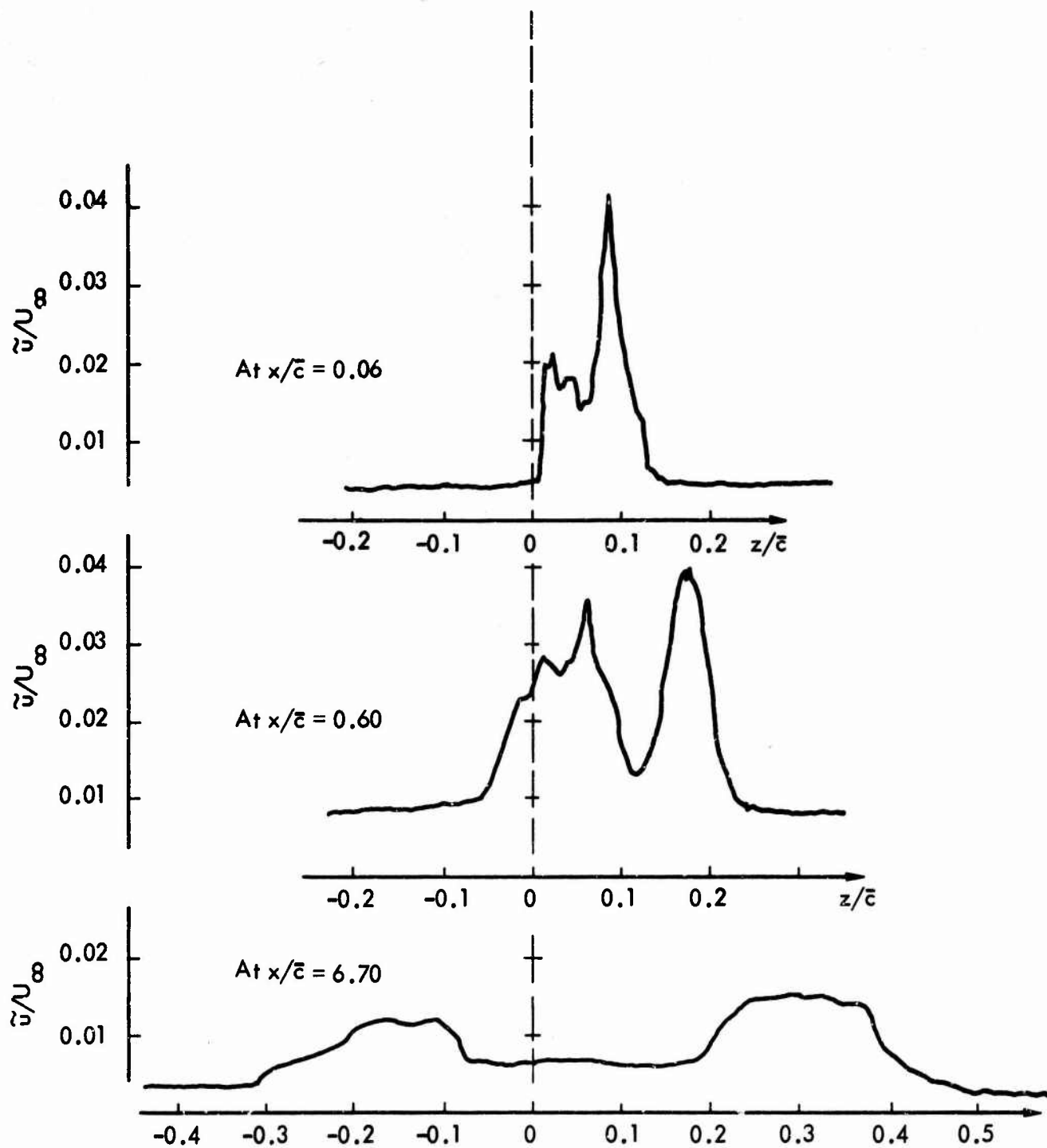


Figure 11. Turbulence Intensity at Tip Vortex of Tunnel Blade
 $(\alpha = 8^\circ, \bar{c} = 3.0 \text{ in.}, \text{ Standard Tip Shape, } U_\infty = 150 \text{ fps})$

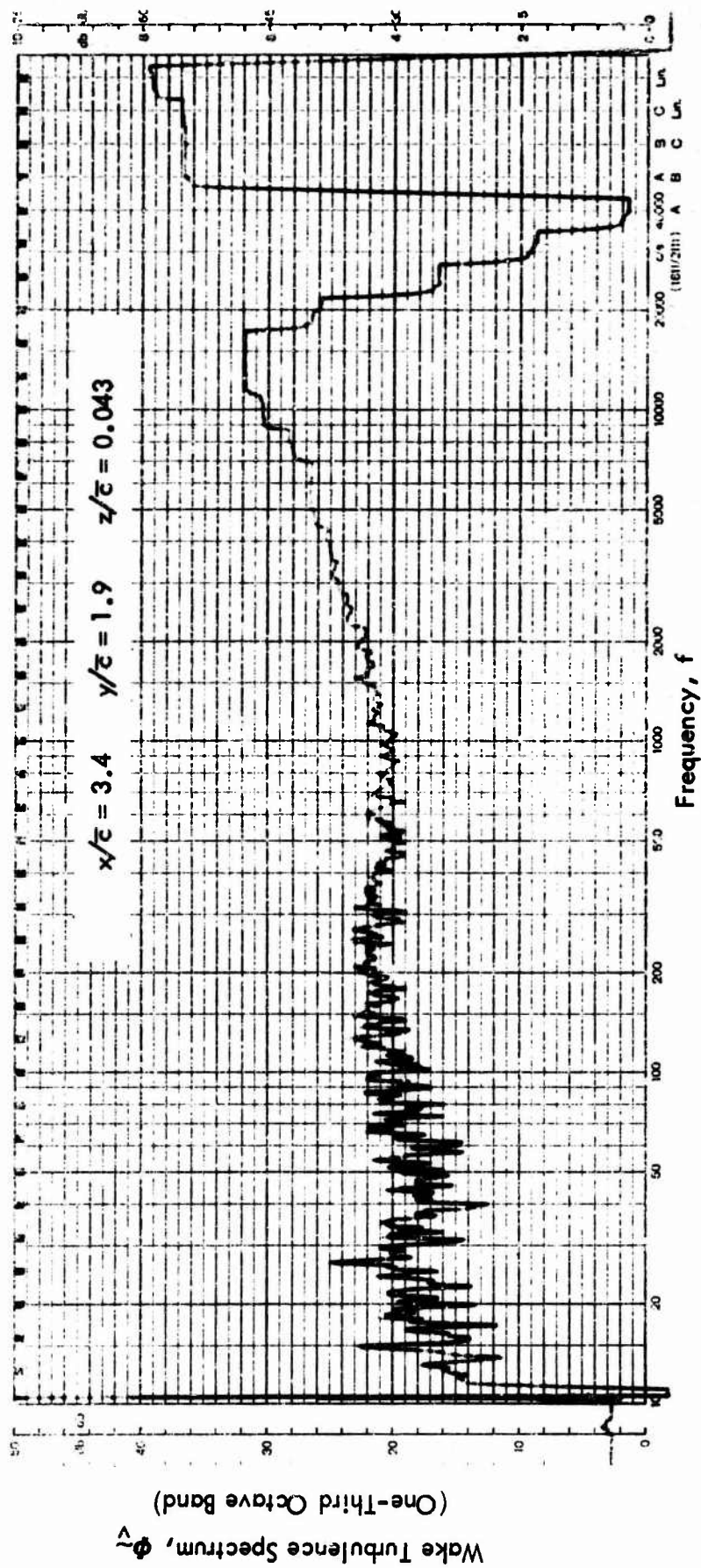
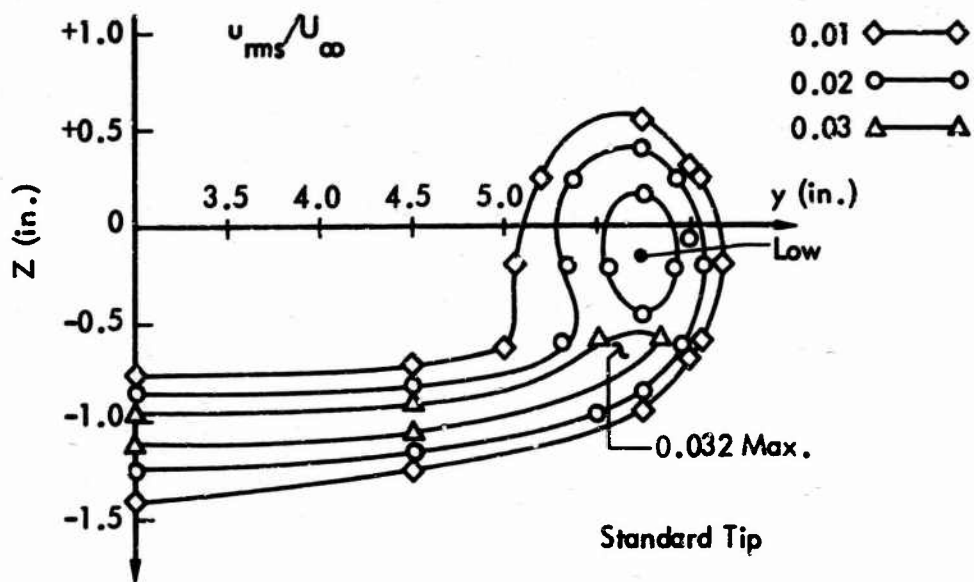
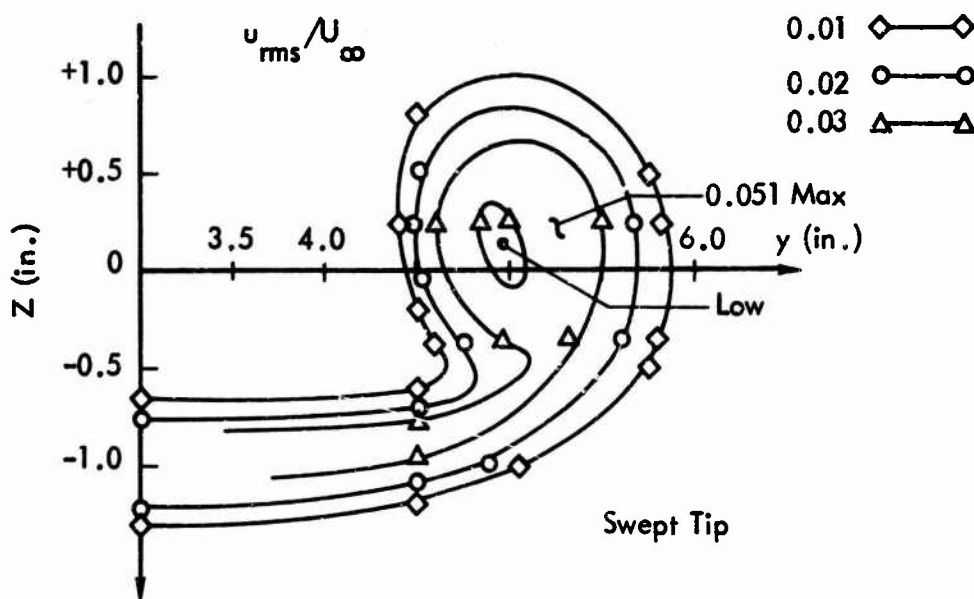


Figure 12. One-Third Octave Band Spectrum of Wind Tunnel Blade Wake3 Turbulence



(a) Standard Tip, $x = 10.25$ in.



(b) Swept Tip, $x = 10.25$ in.

Figure 13. Turbulence Intensity Contours in Wake of Wind Tunnel Blades
($U_{\infty} = 150$ f.p.s., Blade Chord = 3 in., Blade Length = 6 in.)

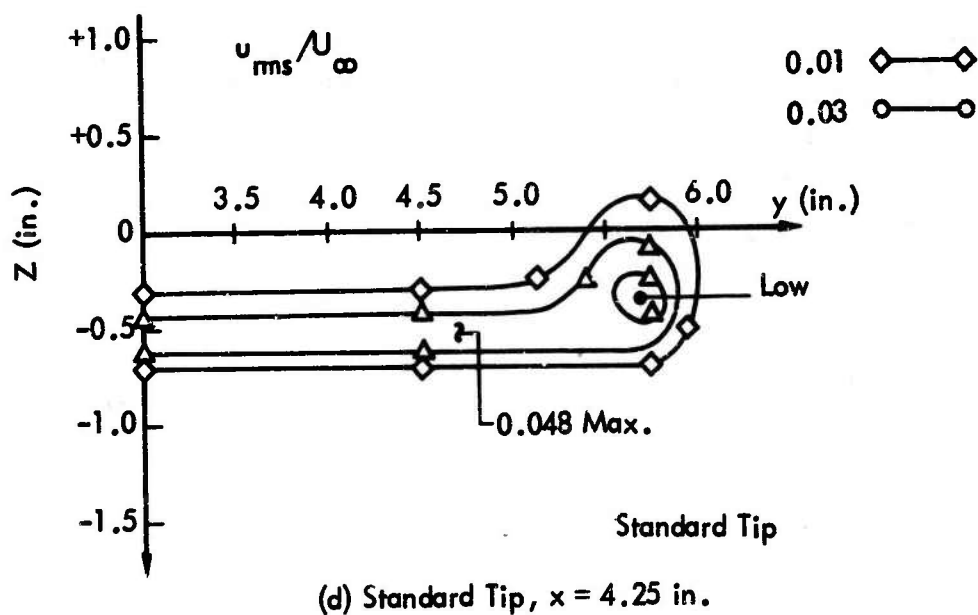
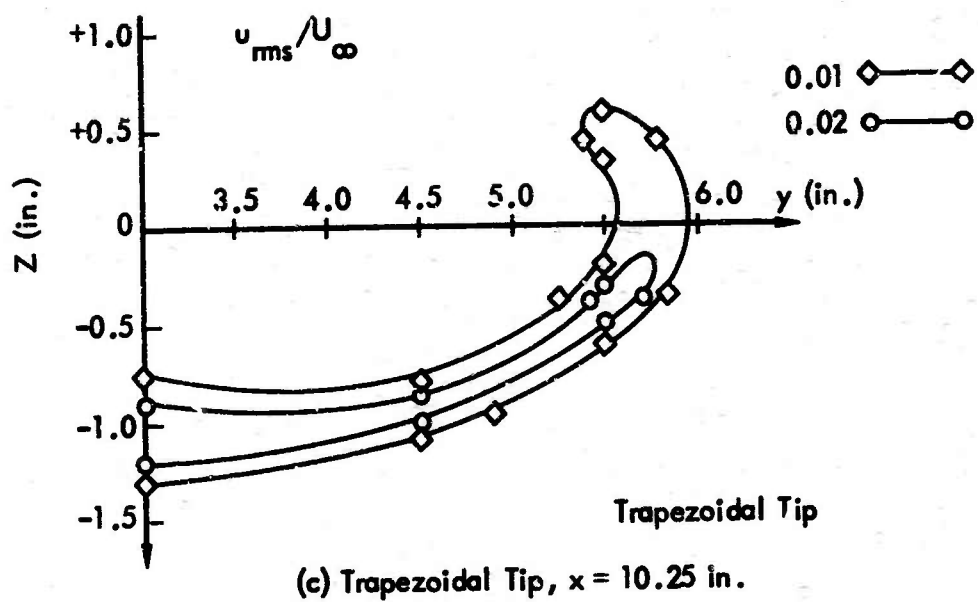
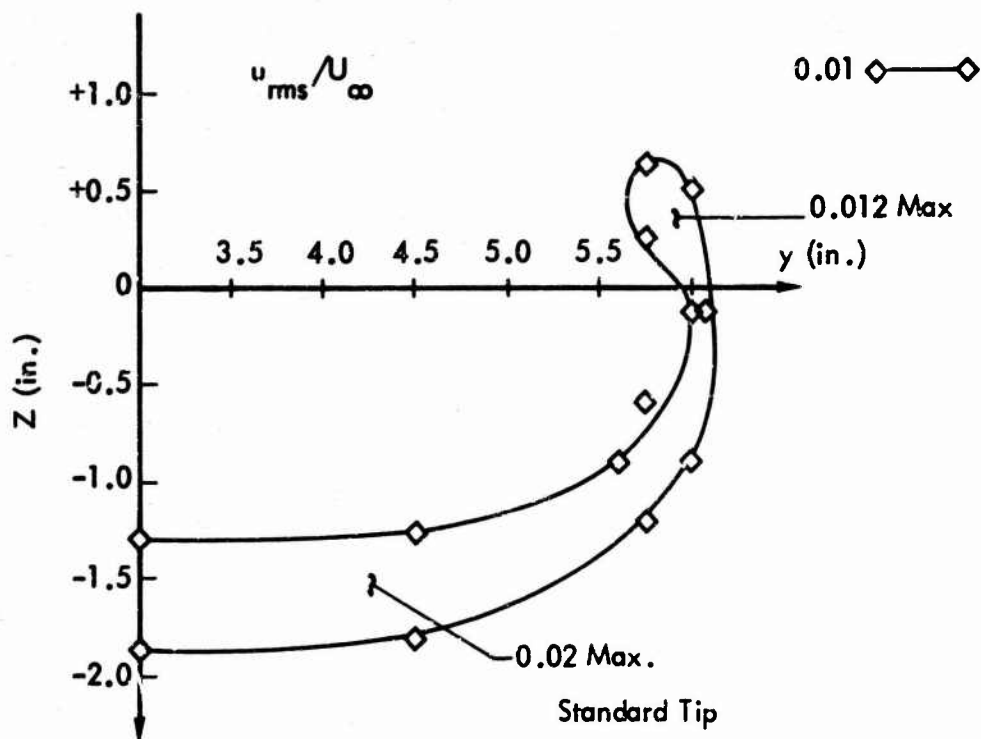


Figure 13. (Continued)



(e) Standard Tip, $x = 22.25$ in.

Figure 13. (Concluded)

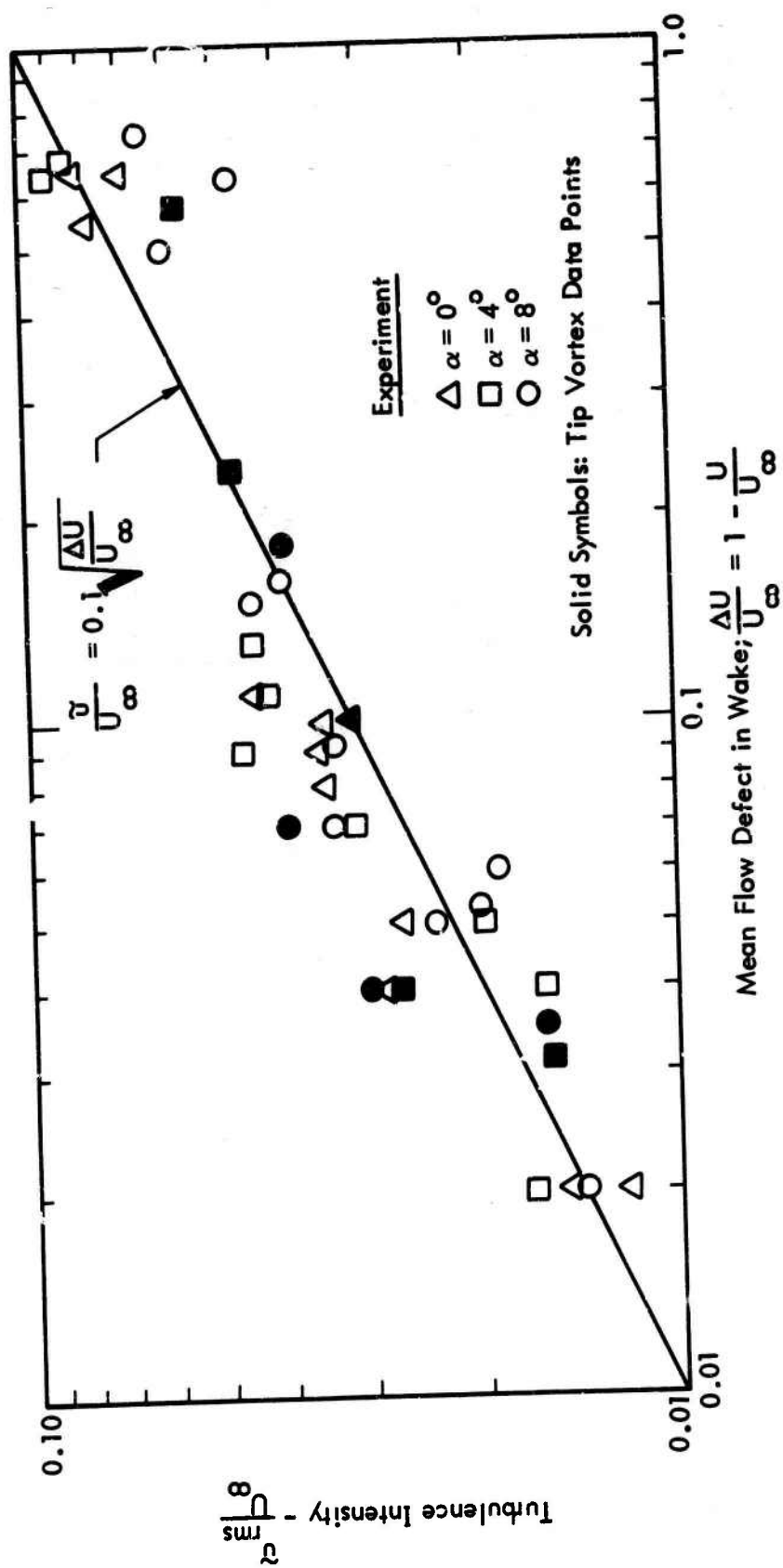


Figure 14. Variation of Maximum Turbulence Intensity in Wake with Respect to Maximum Mean Flow Defect

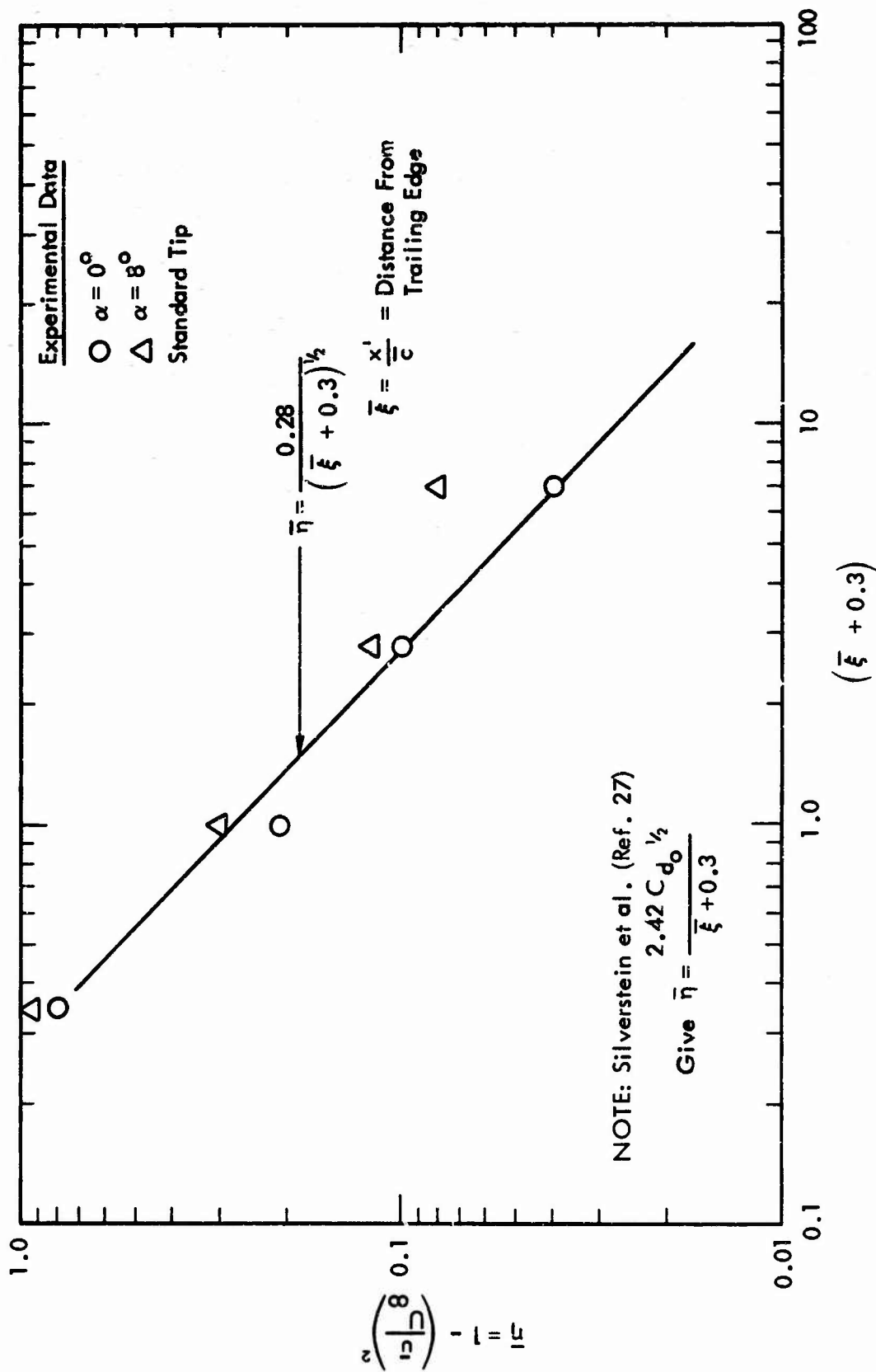


Figure 15. Relationship Between Mean Flow Defect and Distance from Trailing Edge of Blade

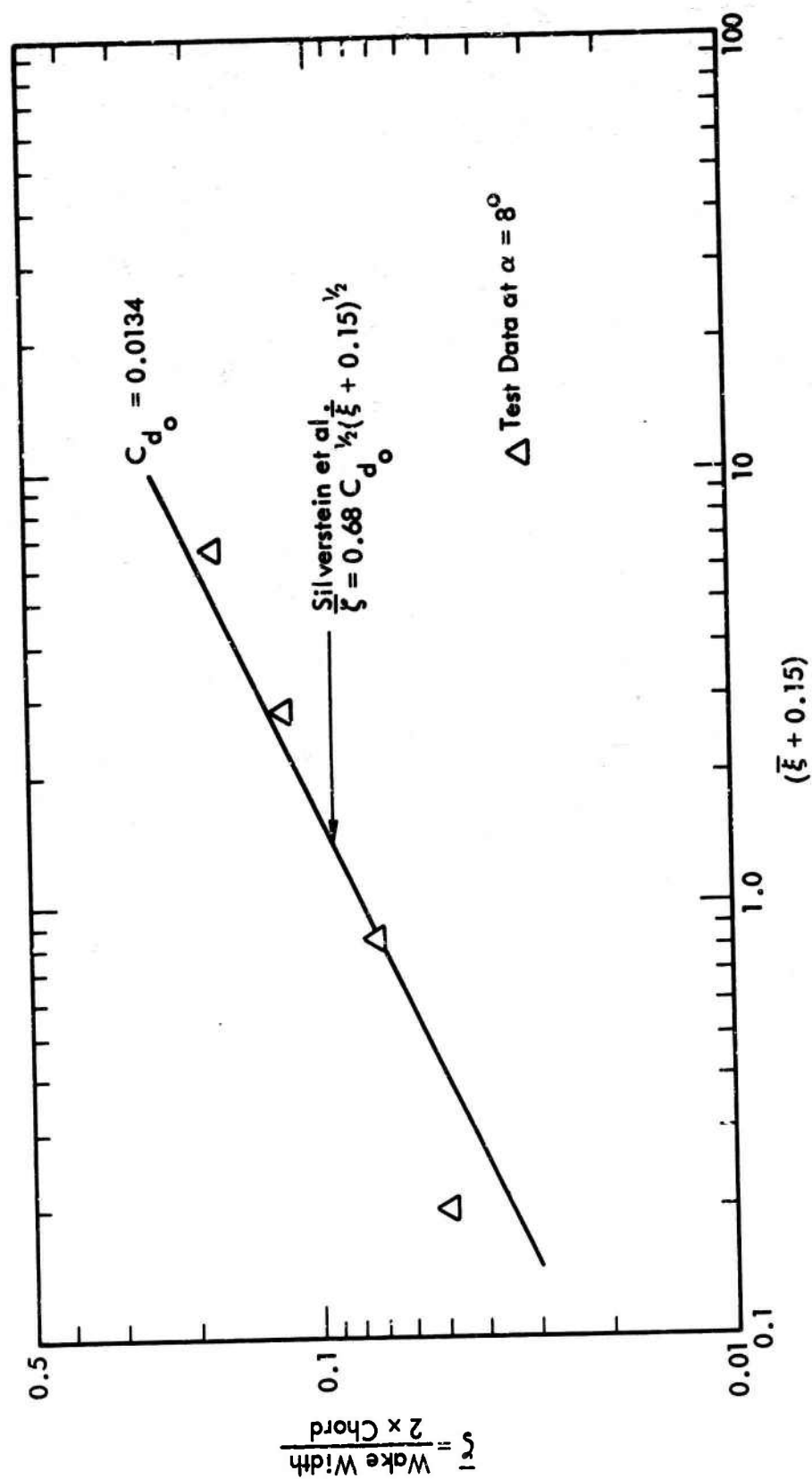
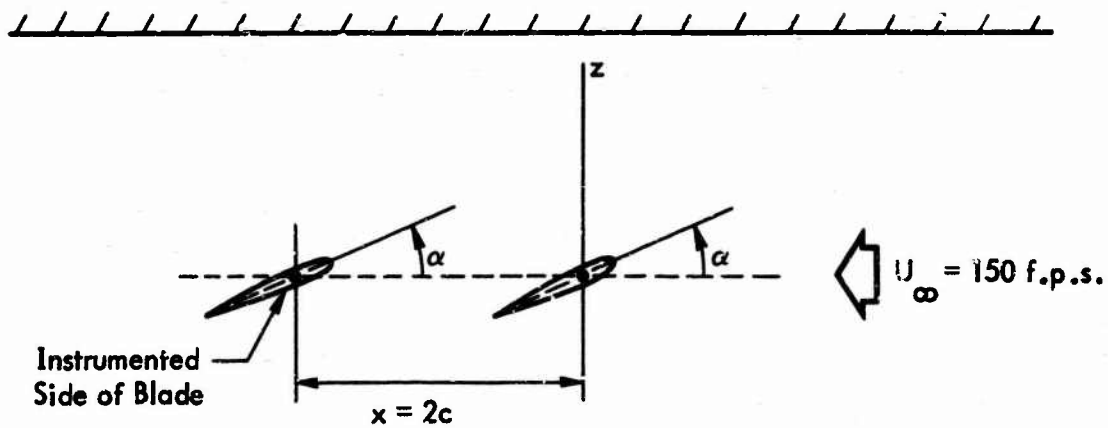
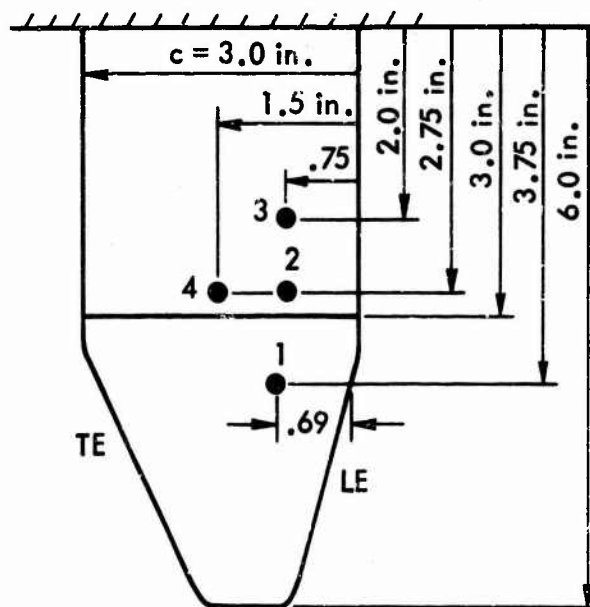


Figure 16. Comparison of Wake Dimensions with Silverstein Theory

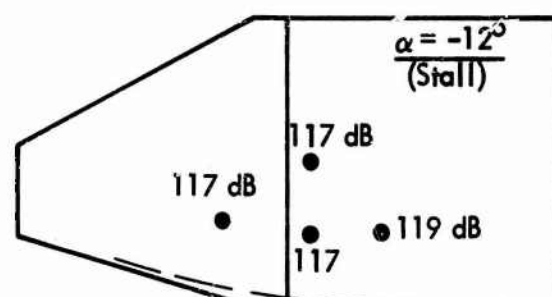
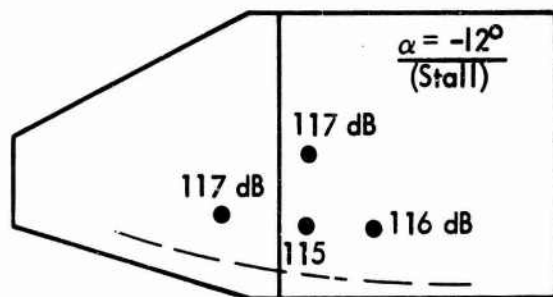
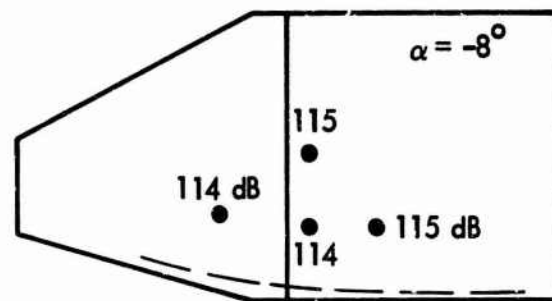
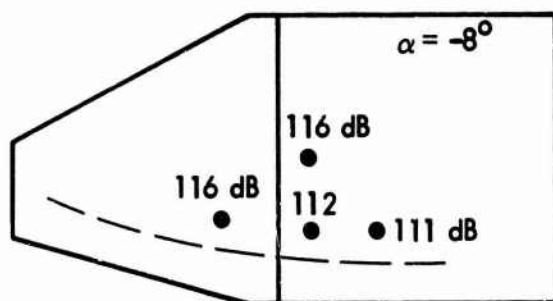
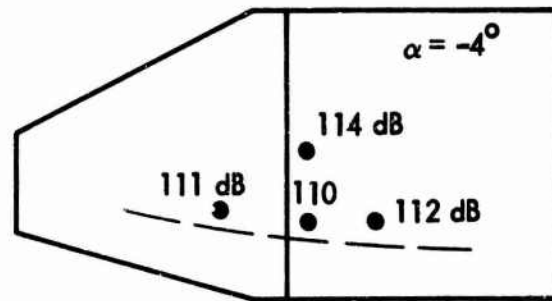
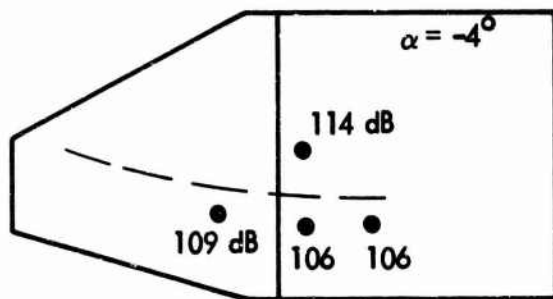
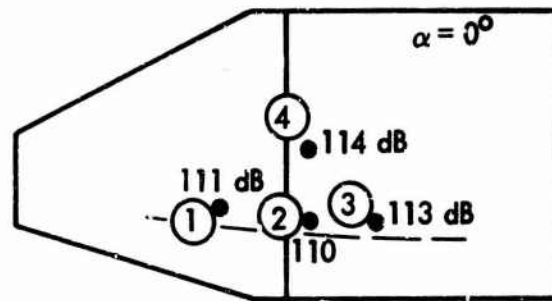
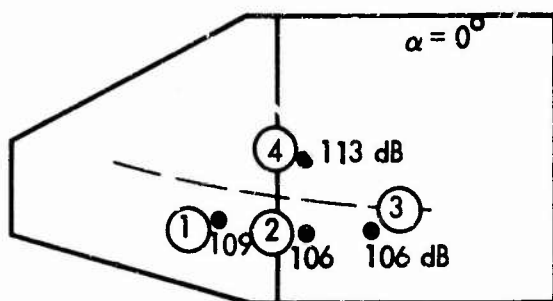


(a) Blade Locations in Wind Tunnel



(b) Positions of Pressure Transducers on Blade

Figure 17. Arrangement of Tandem Blades in Wind Tunnel

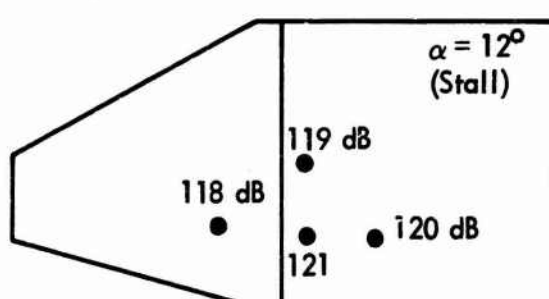
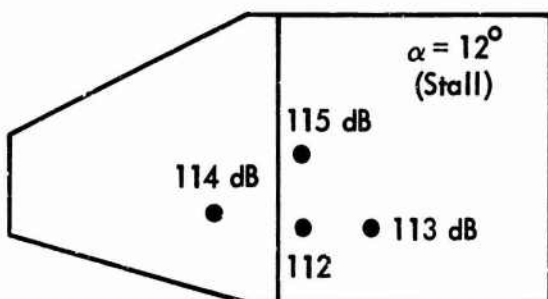
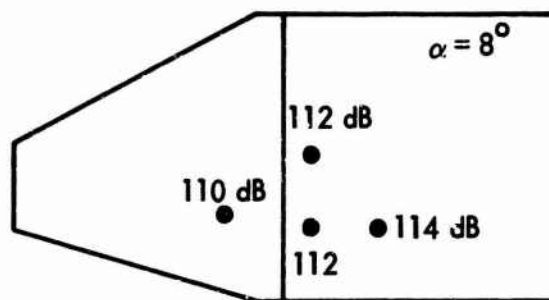
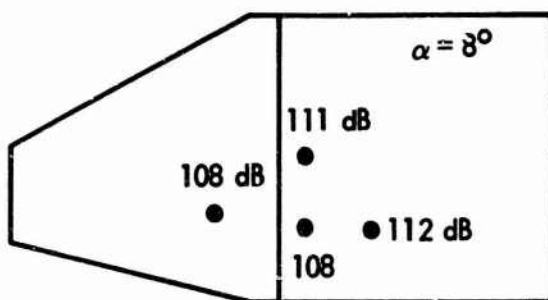
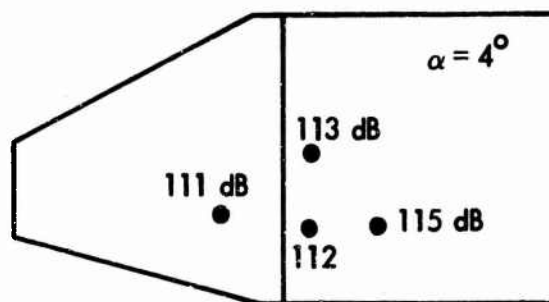
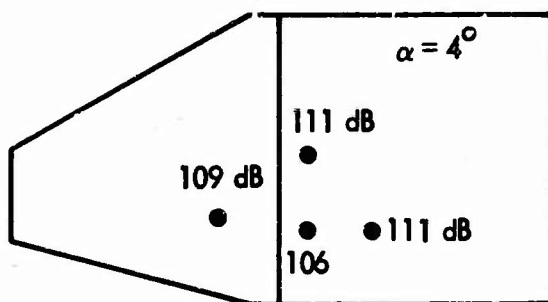


(a) Single Blades

(b) Tandem Blades

NOTE: $0.006 q_\infty = 111.6 \text{ dB}$

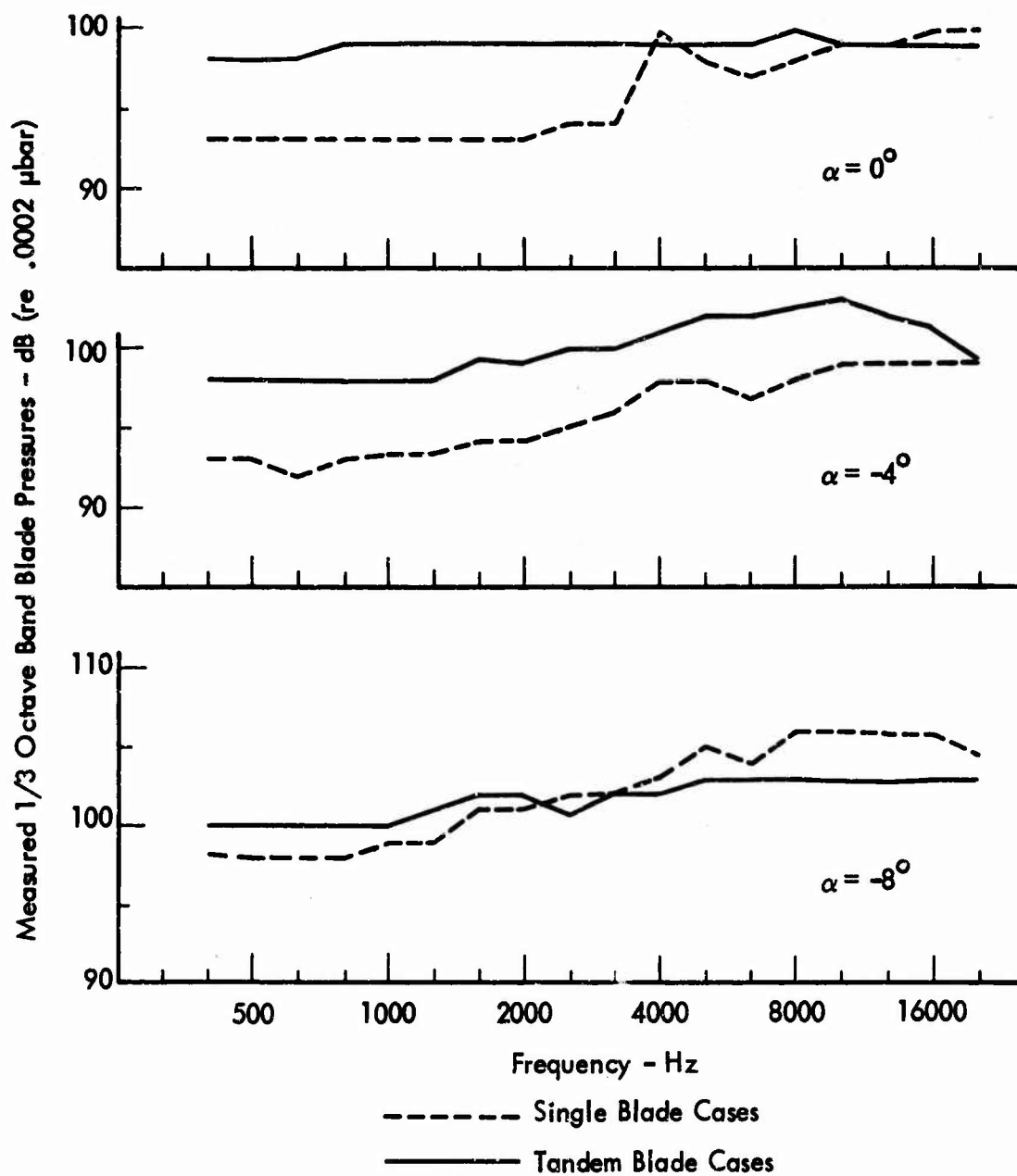
Figure 18. Measured Surface Pressures on Wind Tunnel Blades
(dB re: $.0002 \mu\text{bar}$ in 400-2000 Hz Band)



(c) Single Blade

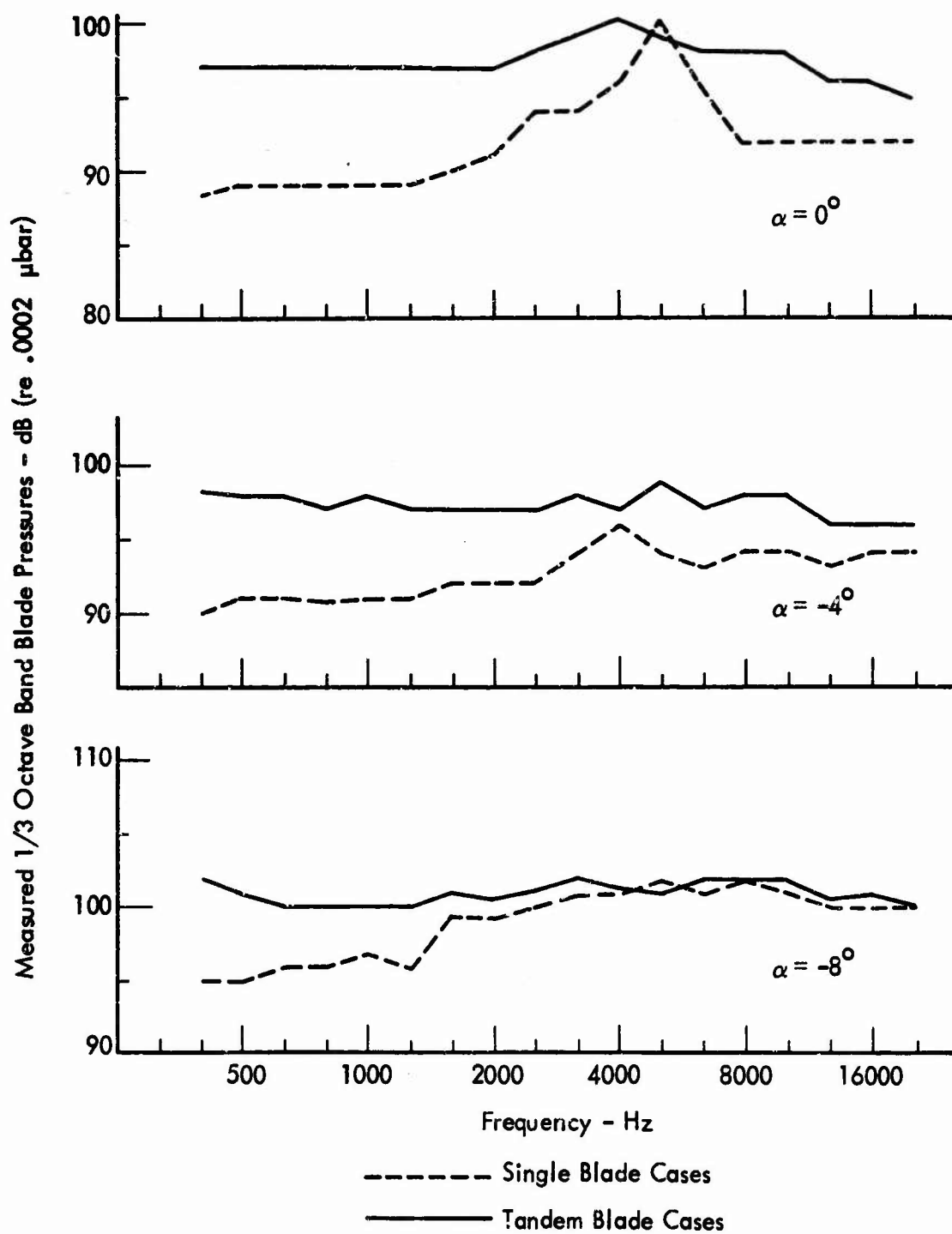
(d) Tandem Blades

Figure 18. (Concluded)



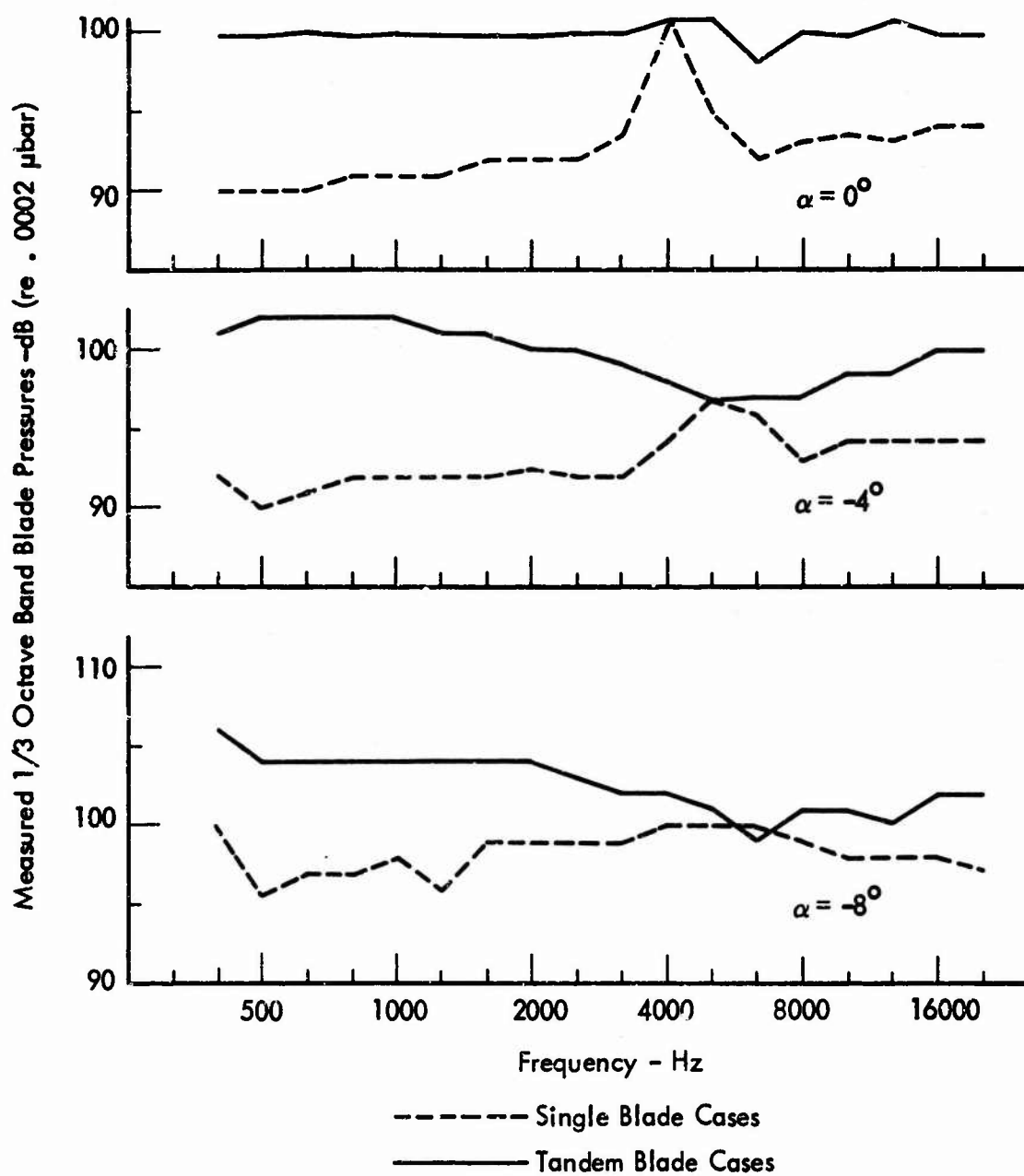
(a) Transducer # 1

Figure 19. One-Third Octave Band Spectra of Wind Tunnel Blade Surface Pressures, Measured for Single and Tandem Blade Arrangements



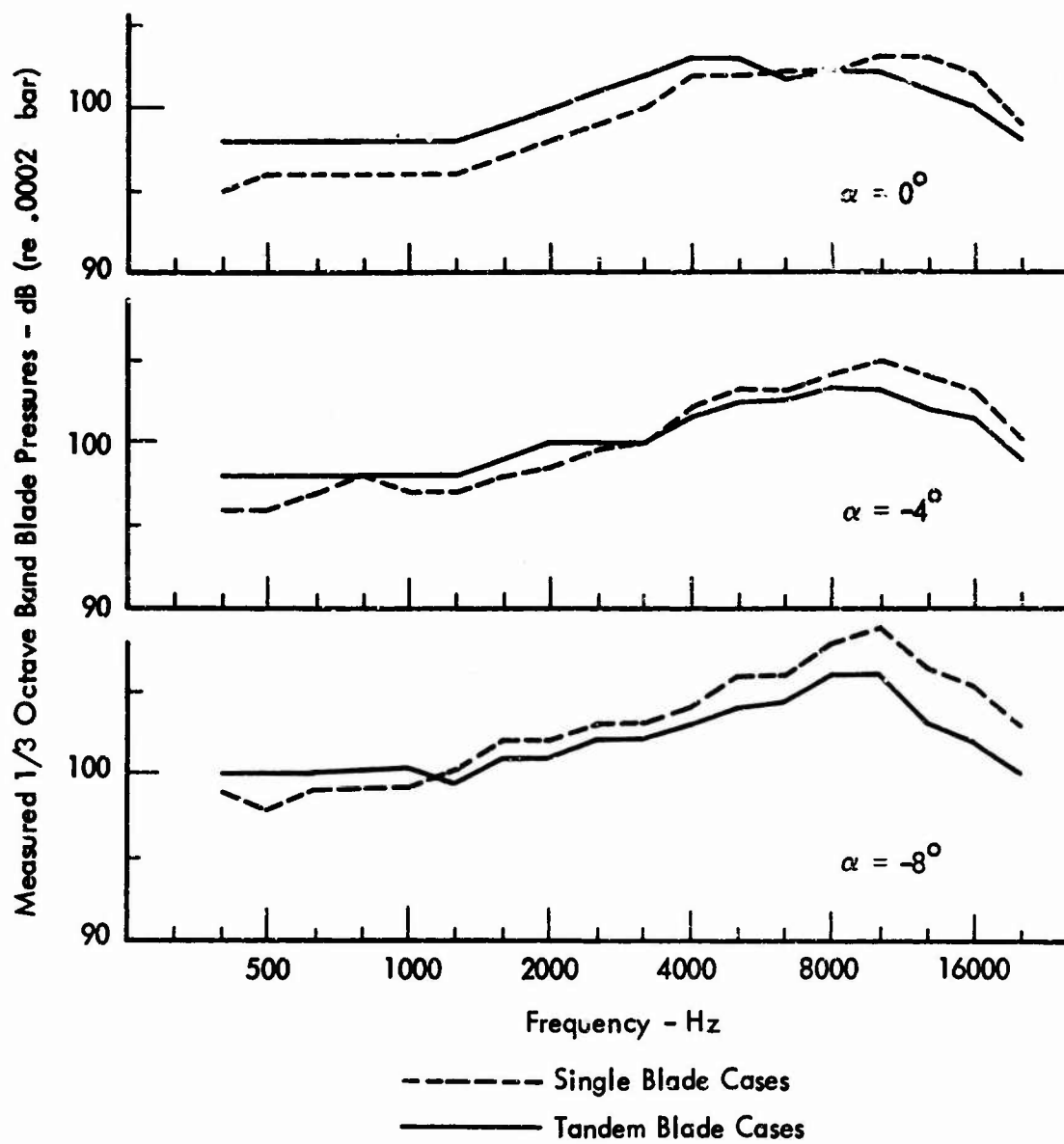
(b) Transducer # 2

Figure 19. (Continued)



(c) Transducer # 3

Figure 19. (Continued)



(d) Transducer # 4

Figure 19. (Concluded)

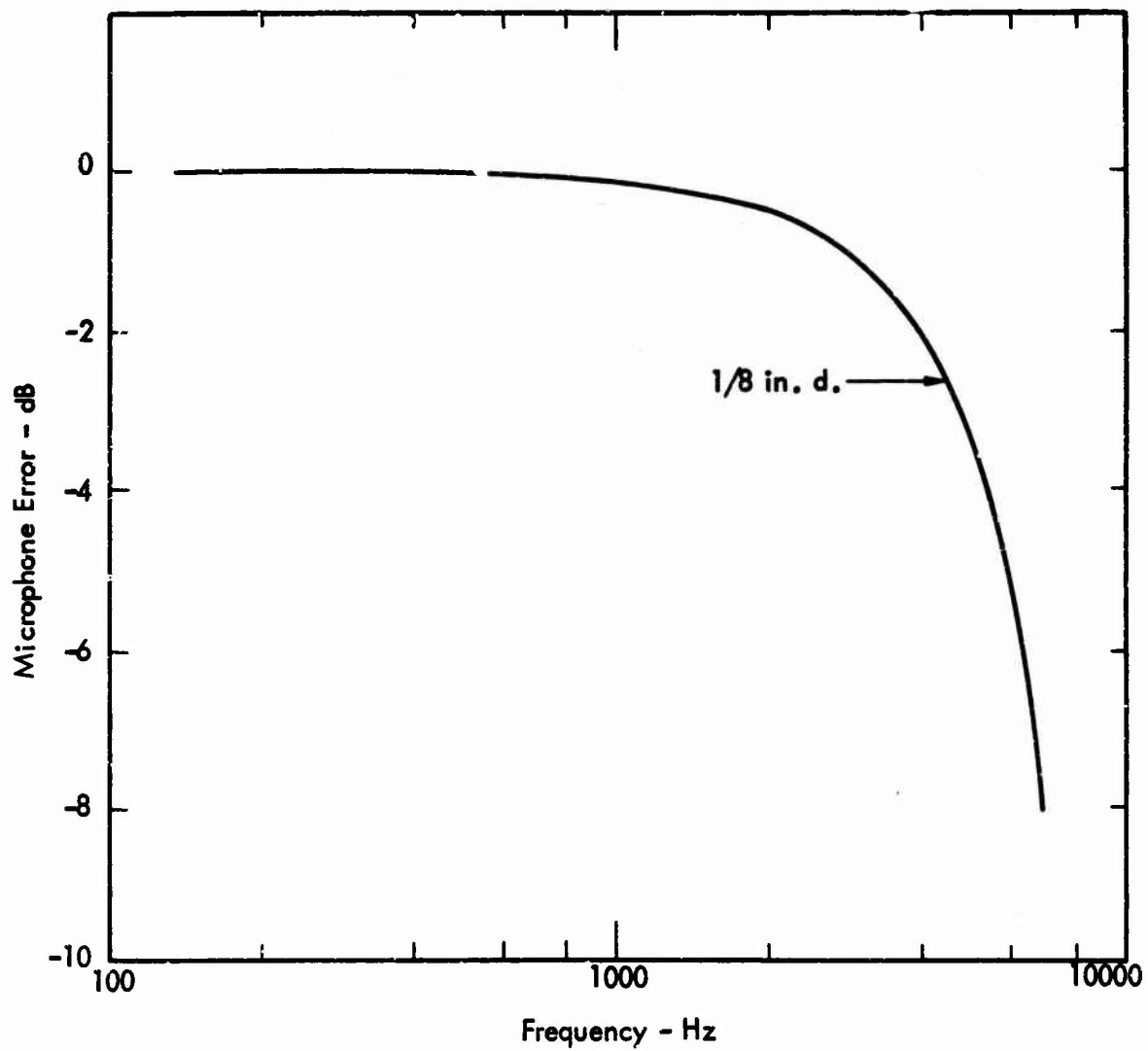
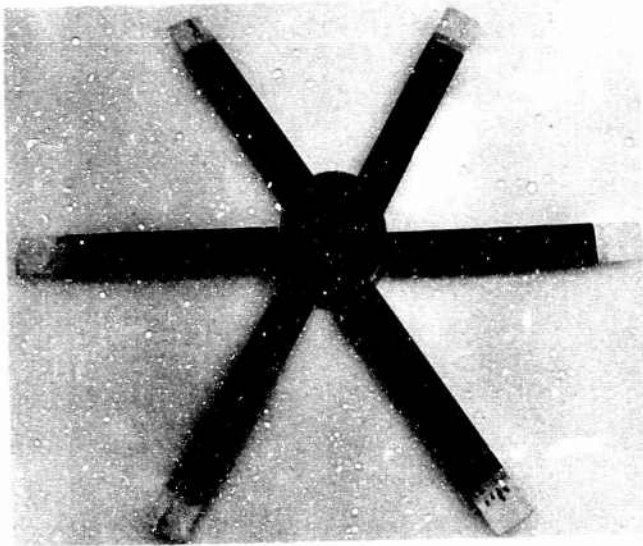


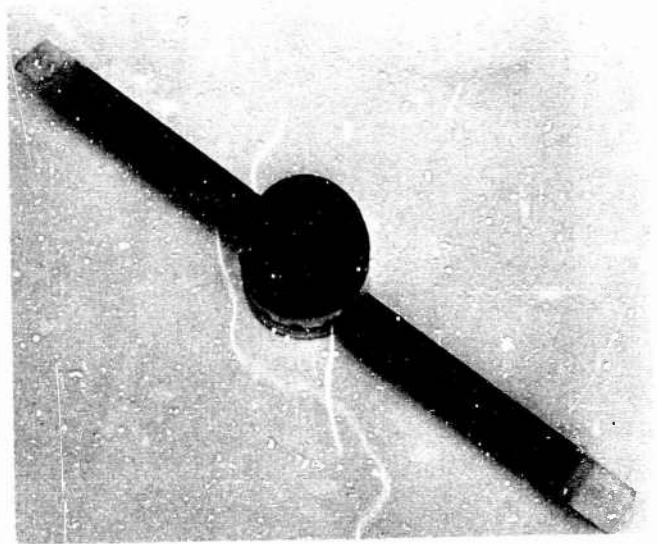
Figure 20. Measurement Error of 1/8-Inch Diameter Pressure Transducers



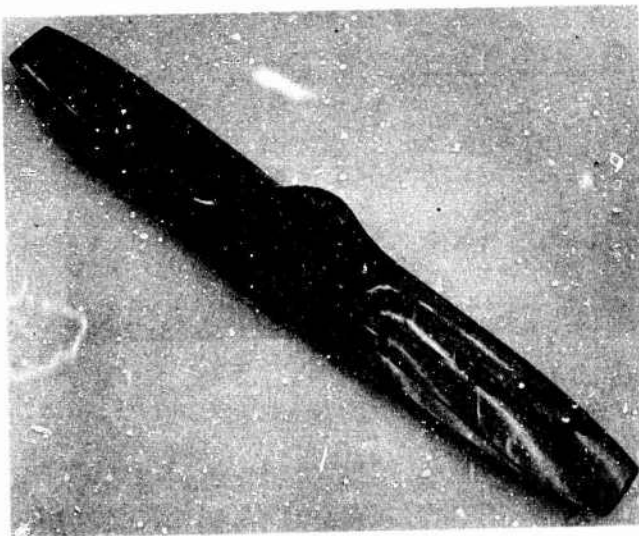
Figure 21. Propeller Whirl Test Facility



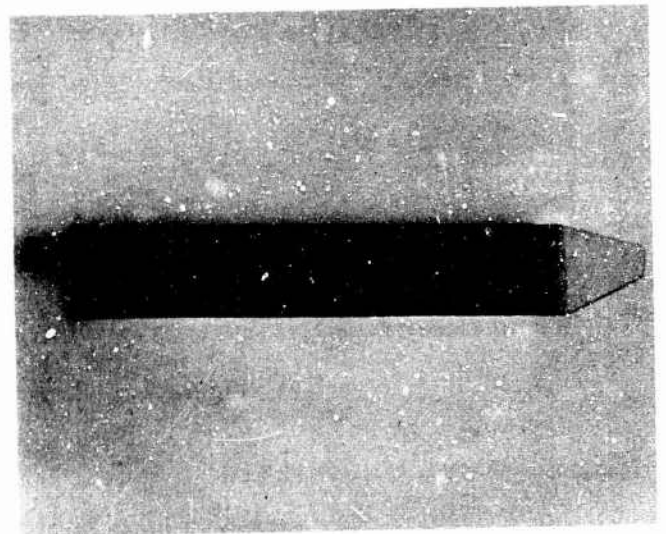
(a) 6 Blade Propeller



(b) 2 Blade Propeller



(c) Sensenich Propeller



(d) Propeller Blade with
Trapezoidal Blade Tip

Figure 22. Propeller Configurations

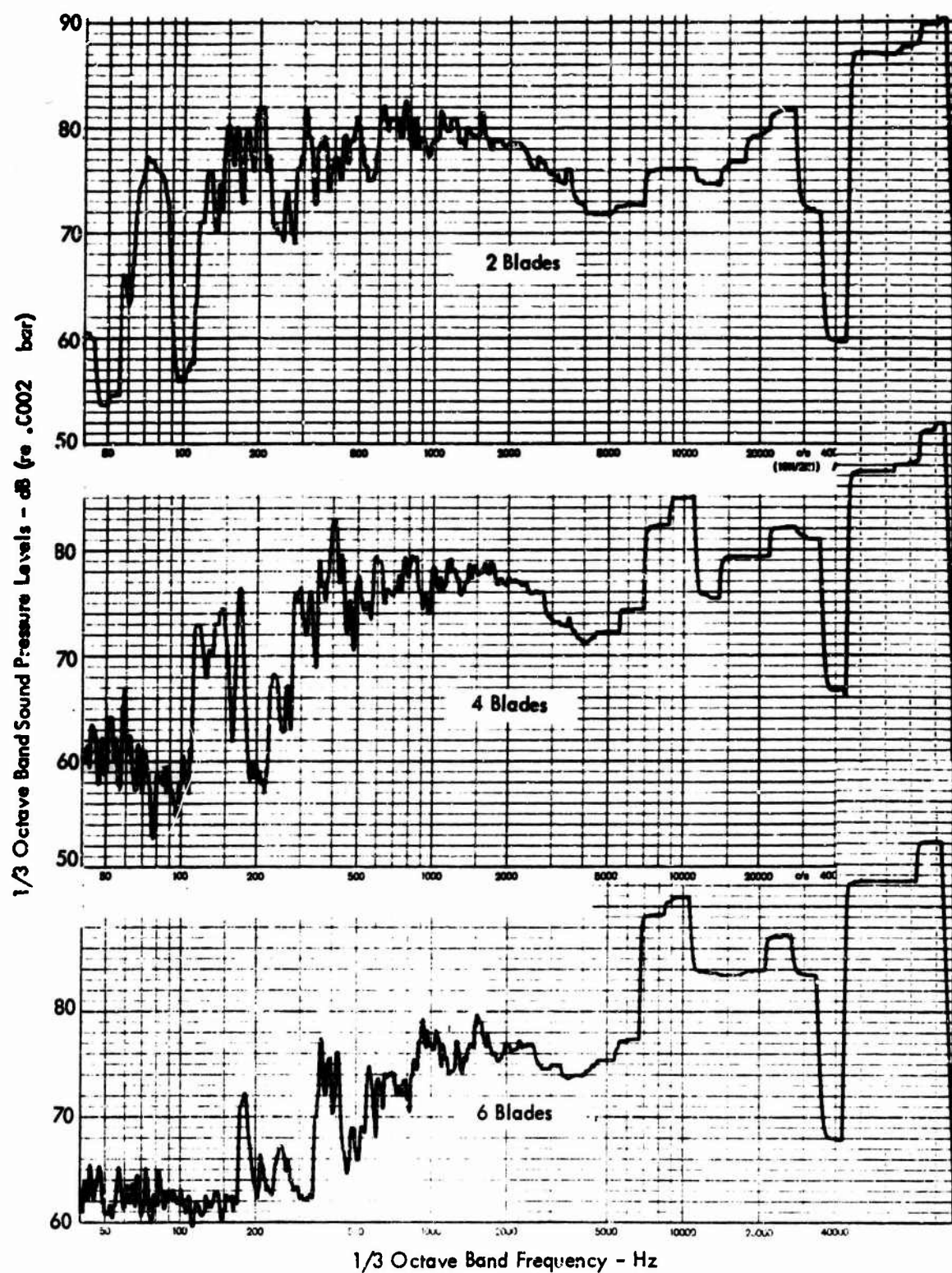


Figure 23. On-Axis One Third Octave Band Noise Spectra of Test Propellers
 $M_t = 0.4$, $D = 4$ ft., $r/D = 3$, $B = 2, 4, 6$

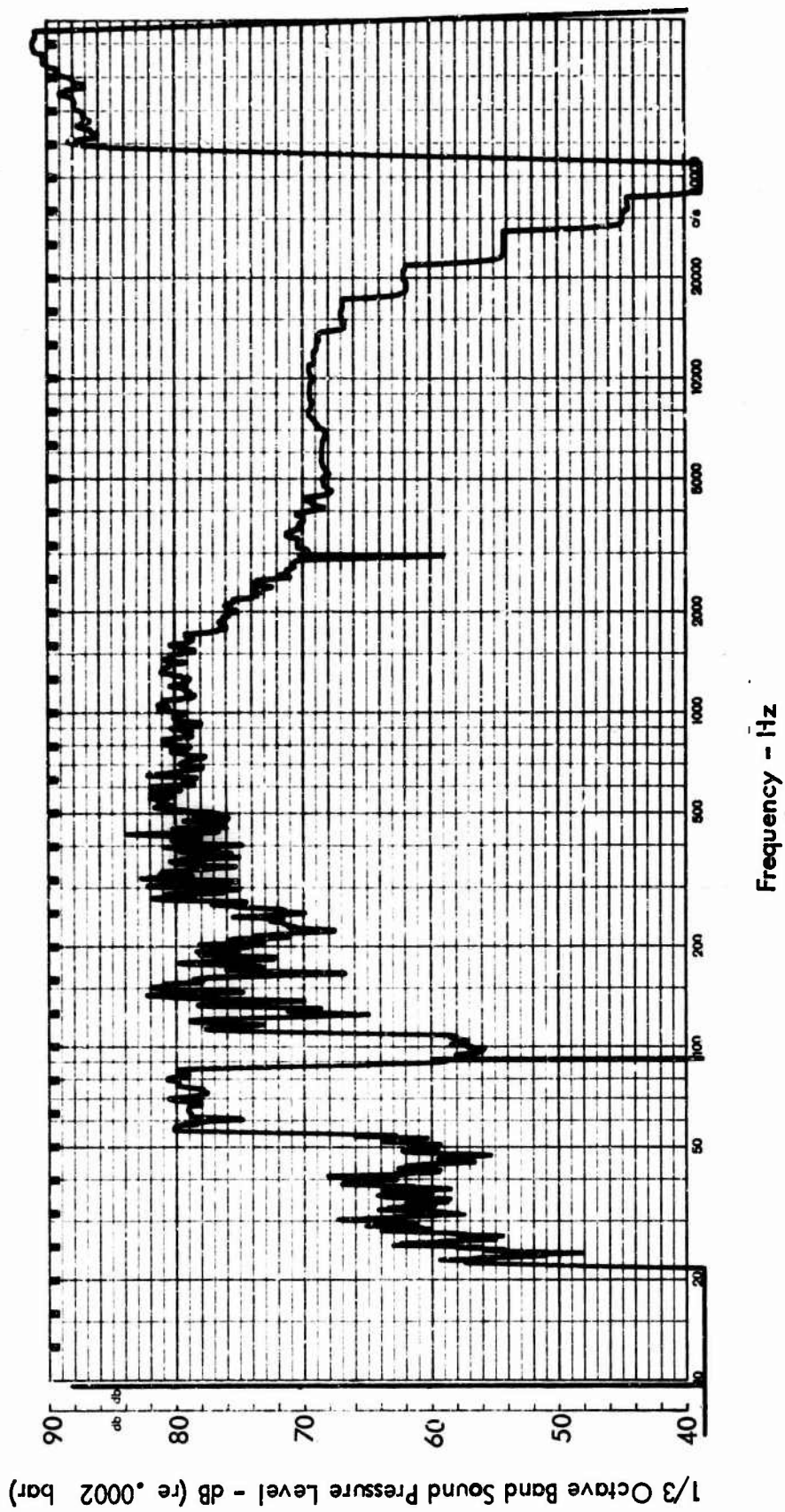


Figure 24. One Third Octave Band Spectrum of Sensenich Propeller Noise
 $M_t = 0.4$, $D = 4$ ft., $r/D = 3$, $B = 2$, $\theta = 0^\circ$ (on axis)

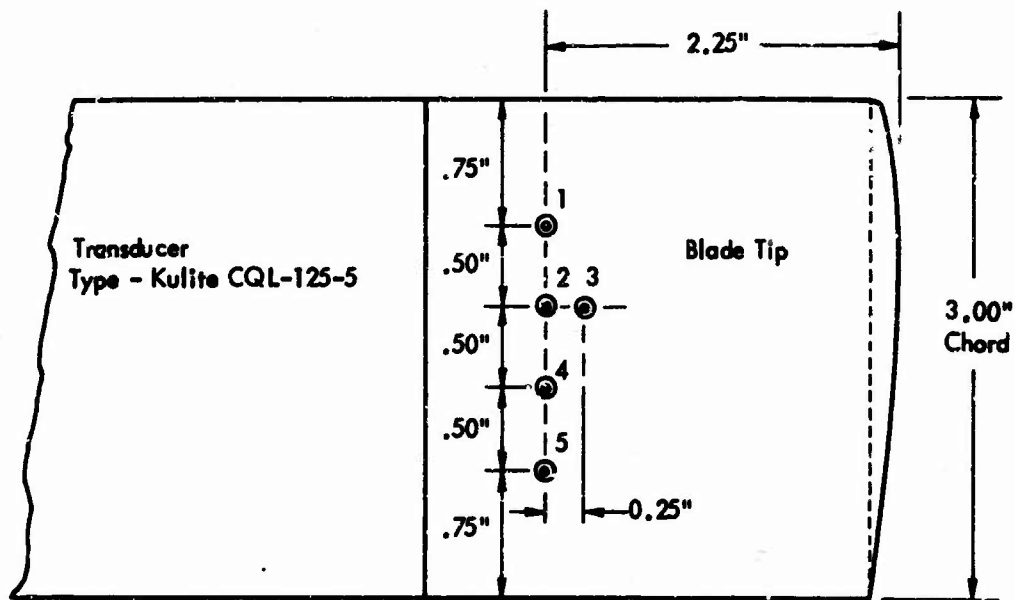
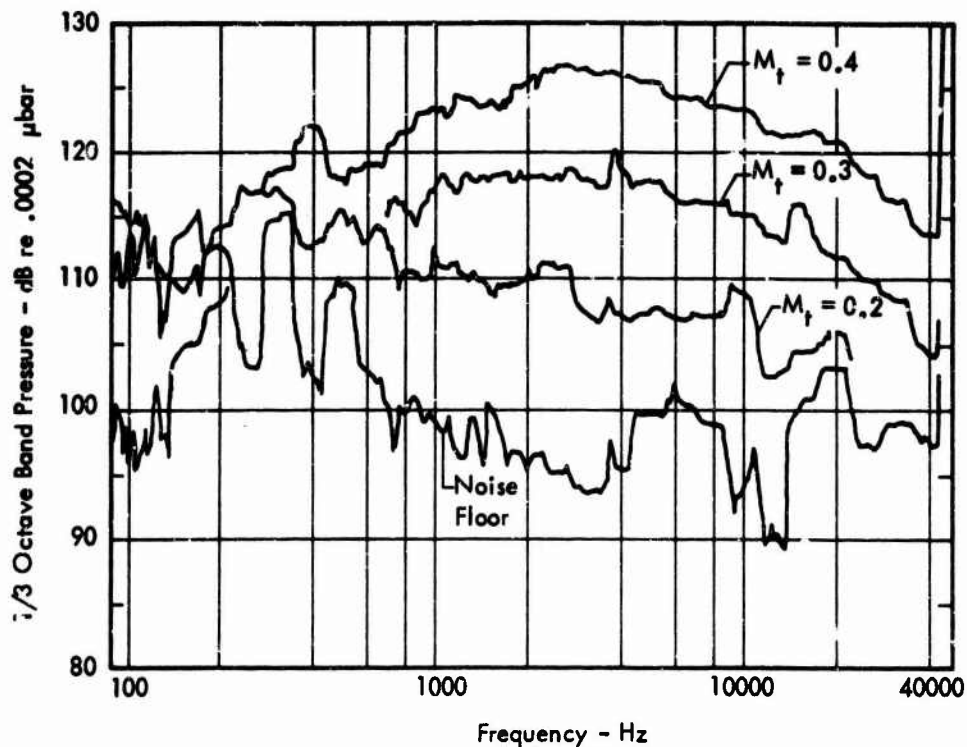
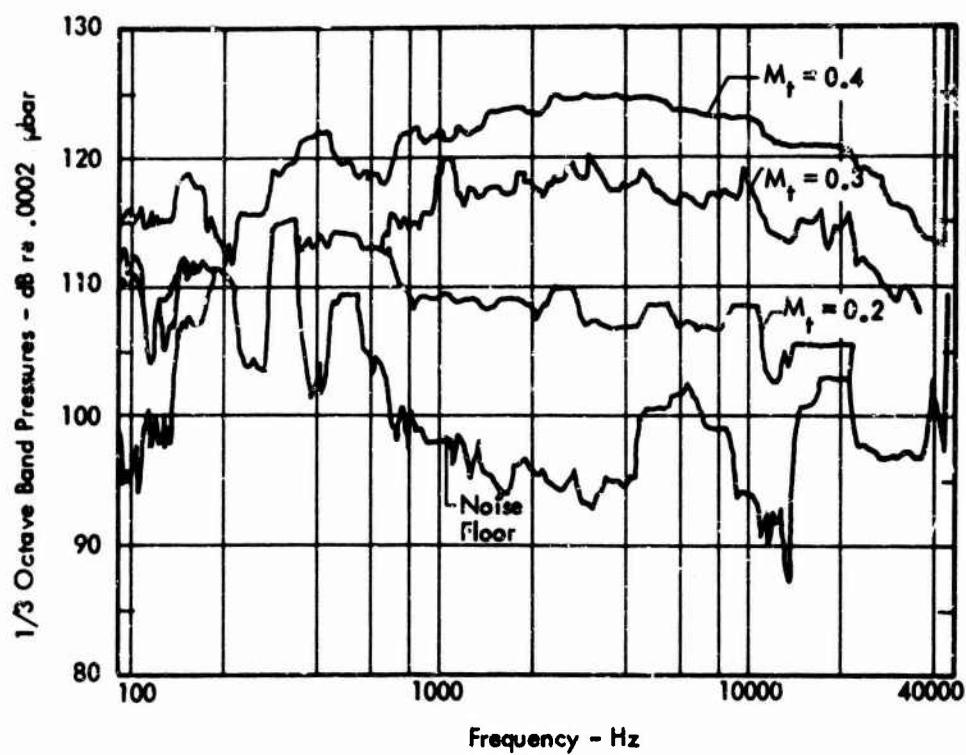


Figure 25. Installation of Pressure Transducers on Propeller Blade

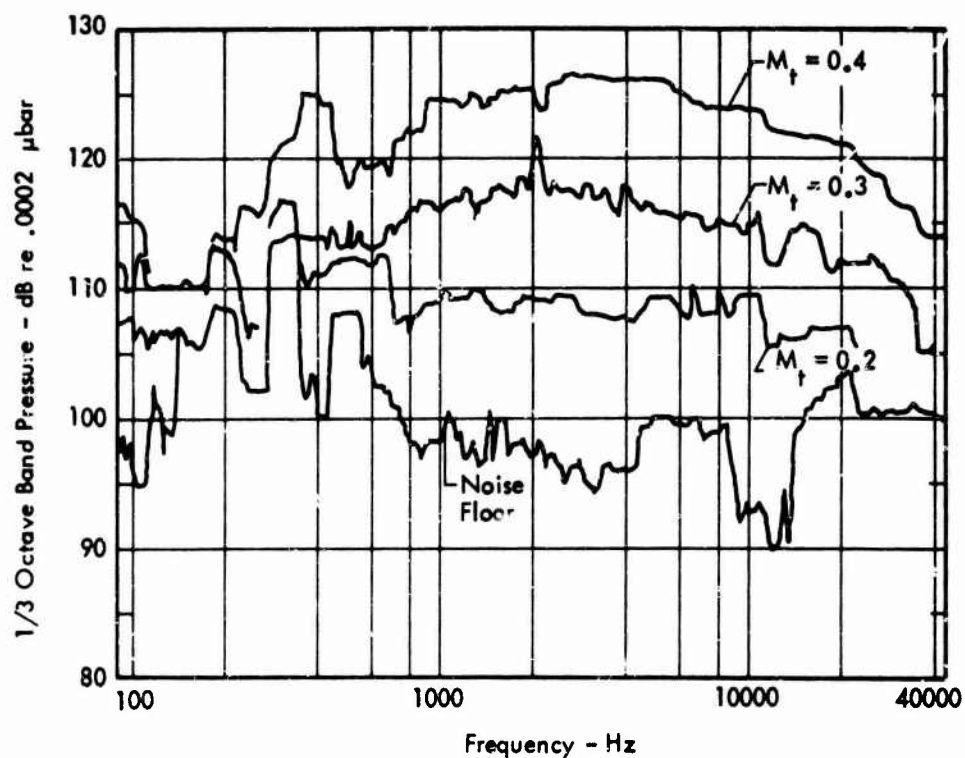


(a) Transducer No. 1

Figure 26. One Third Octave Spectra of Measured Propeller Blade Pressures

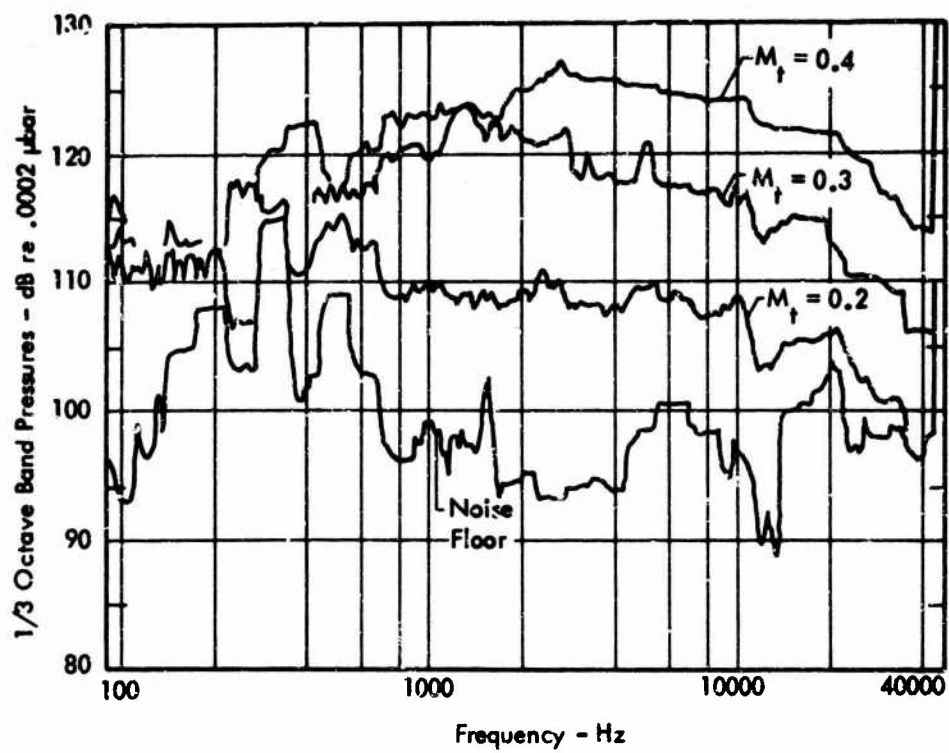


(b) Transducer No. 2

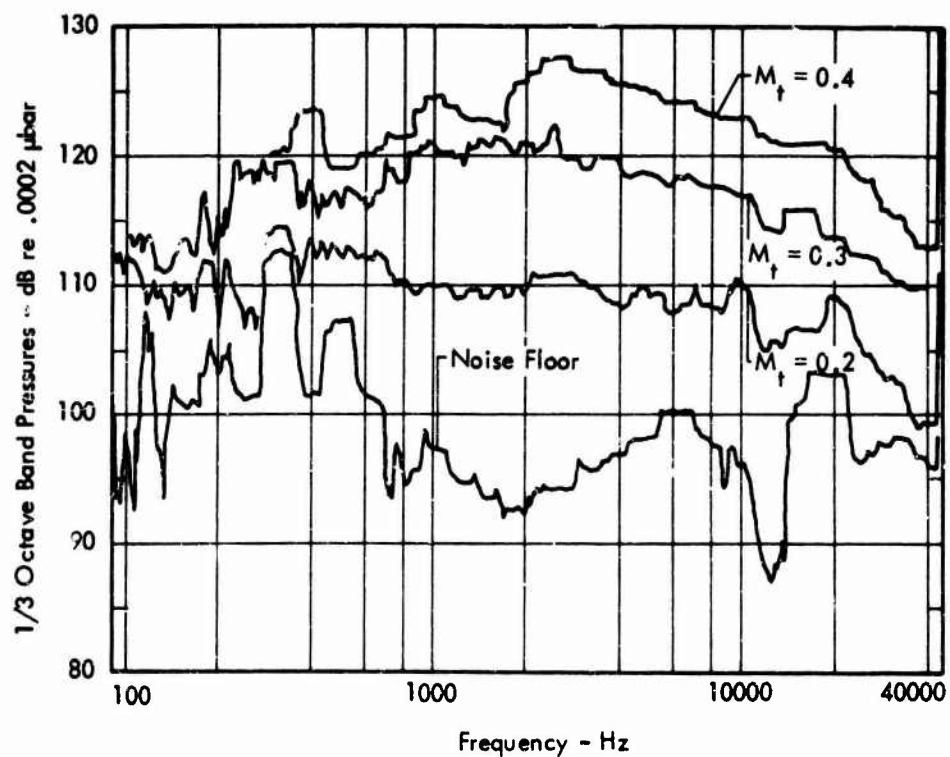


(c) Transducer No. 3

Figure 26. (Continued)



(d) Transducer No. 4



(e) Transducer No. 5

Figure 26. (Concluded)

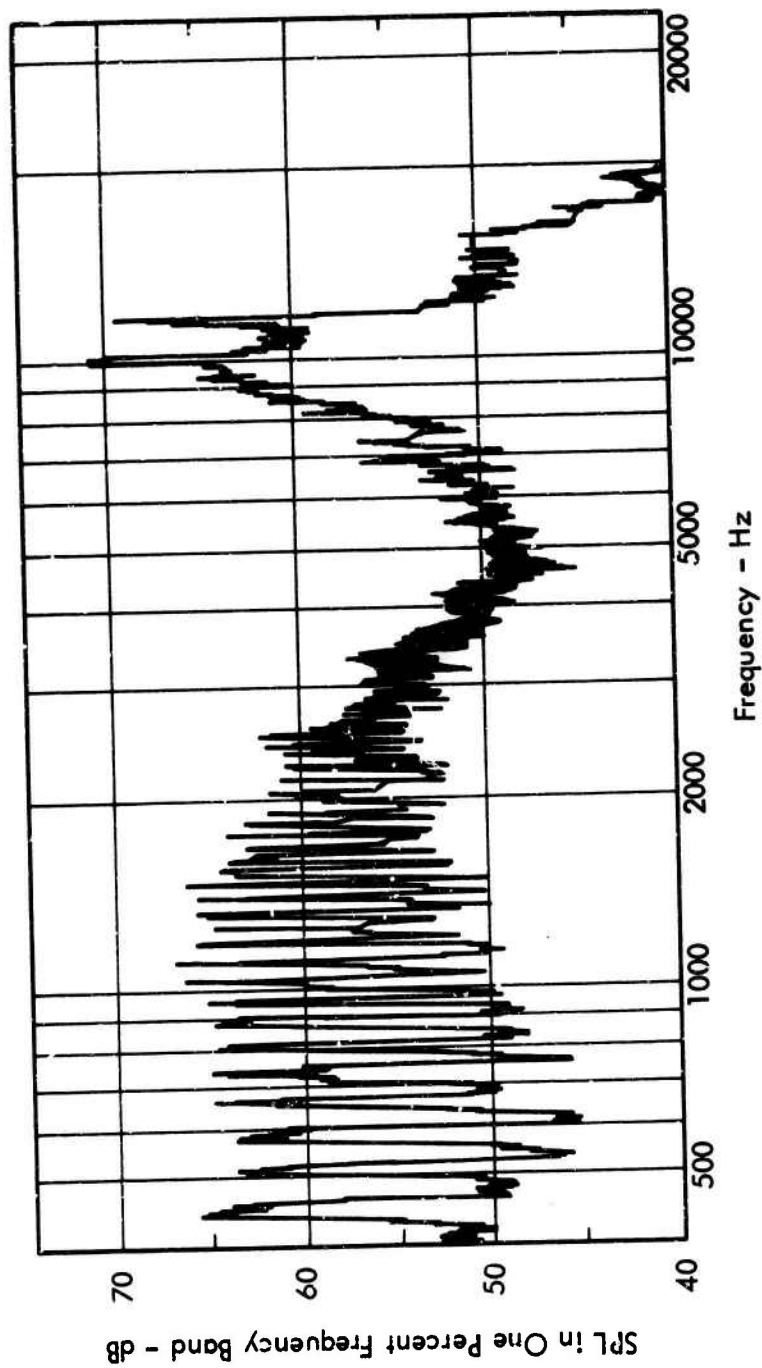
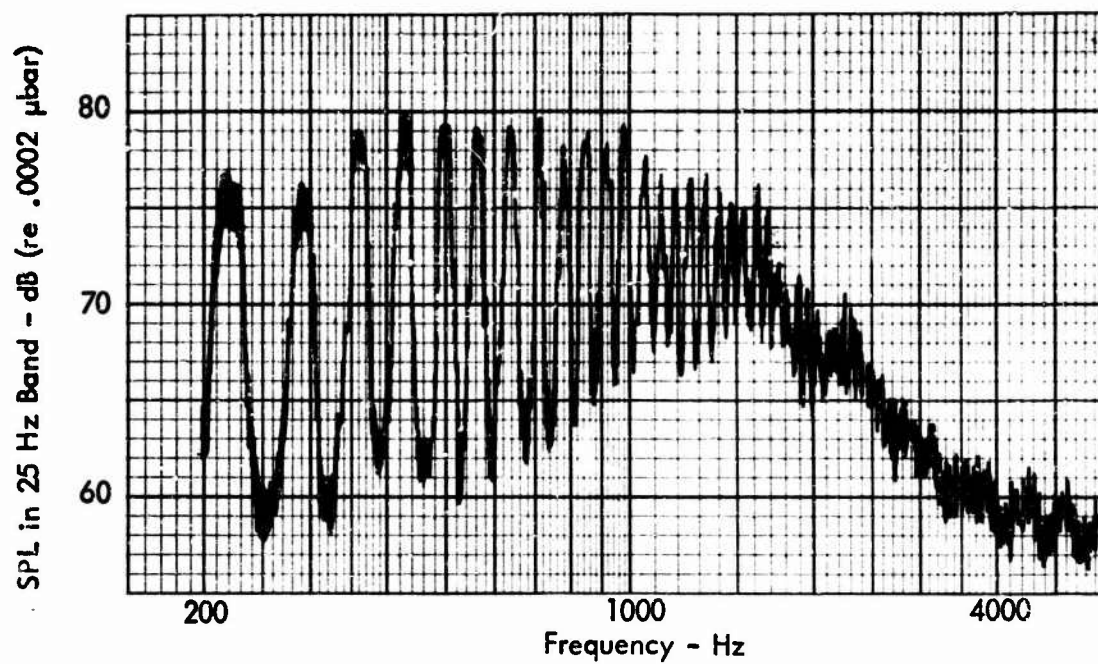
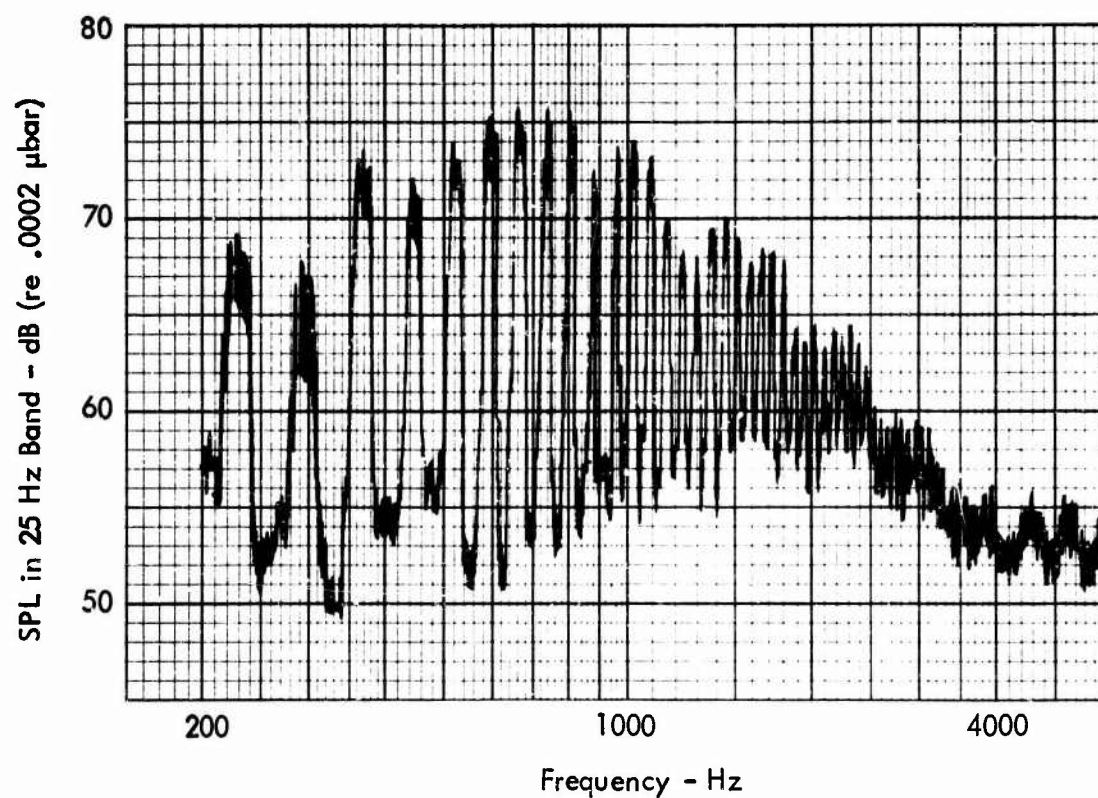


Figure 27. Narrow Band Spectrum of High Frequency Noise Content



(a) $\alpha_T = 16^\circ$, $C_T = 0.032$



(b) $\alpha_T = 12^\circ$, $C_T = 0.023$

Figure 28. Narrow Bandwidth (25 Hz) Spectra of Test Propeller Noise at Various Tip Angle Settings. $M_i = 0.4$, $B = 2$, $\theta = 0^\circ$, $\alpha_T = 16^\circ, 12^\circ, 8^\circ, 4^\circ, 0^\circ, -2^\circ$ †

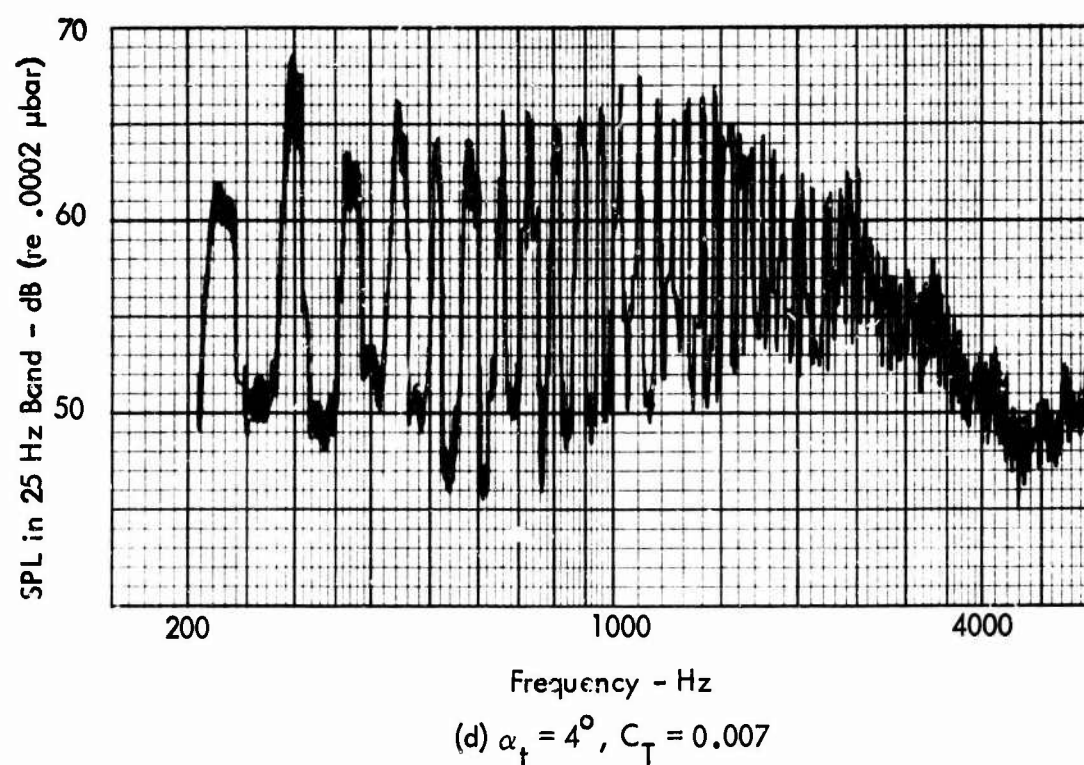
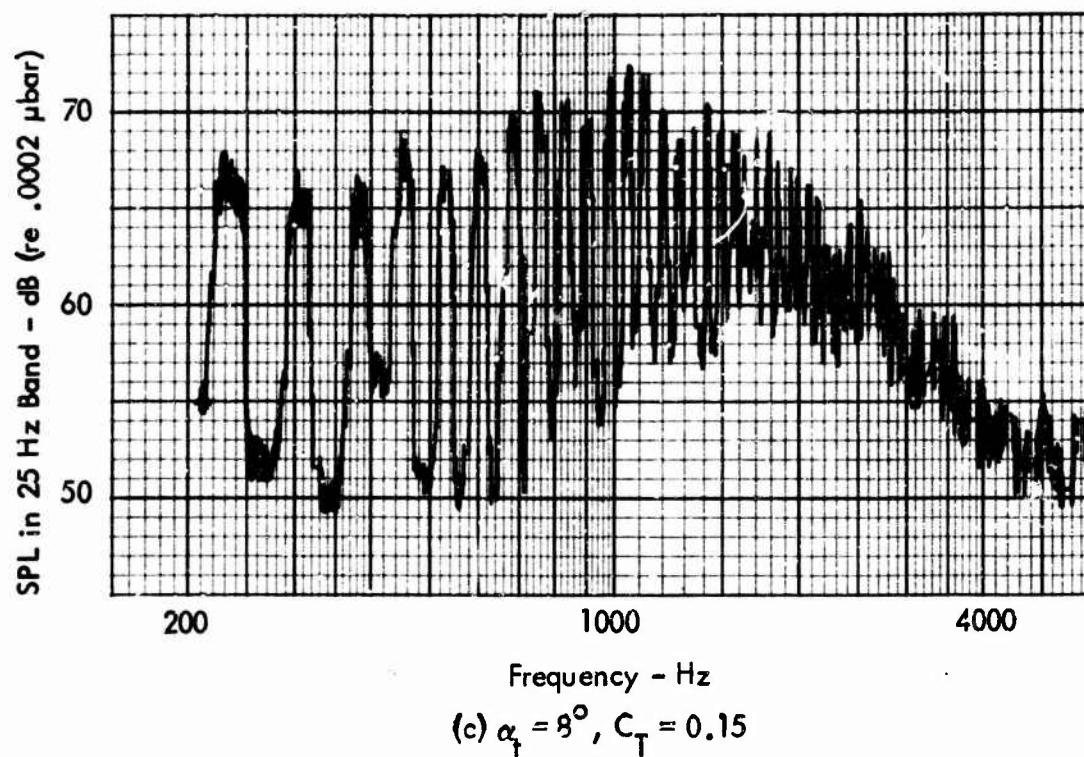
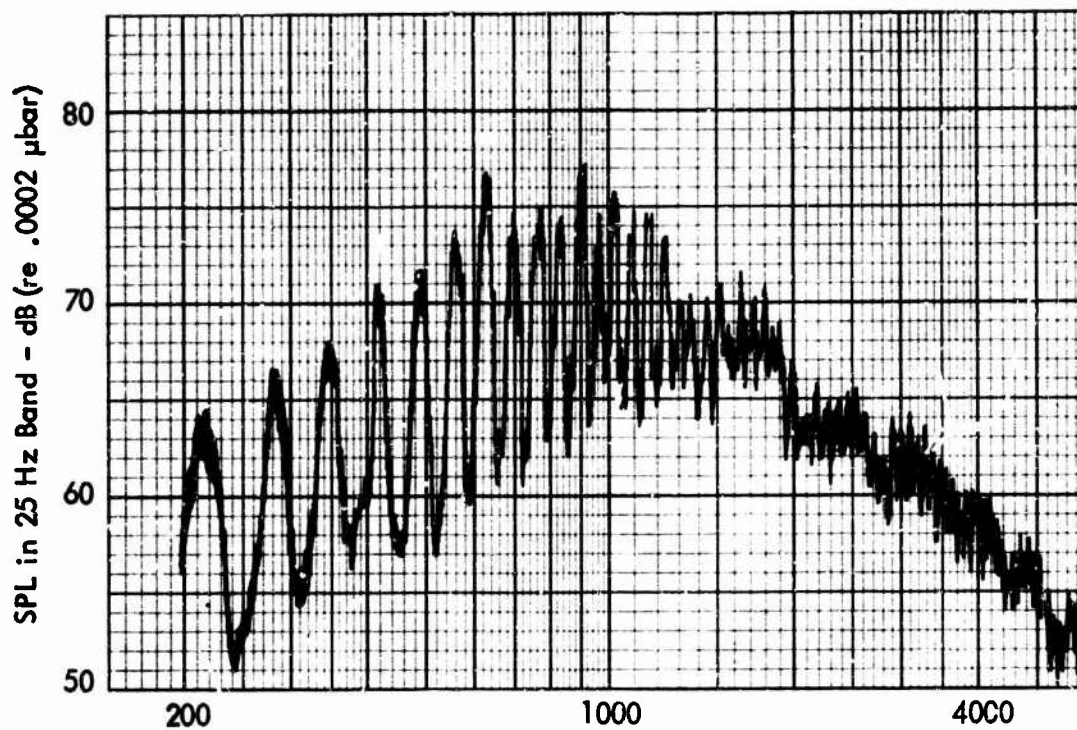
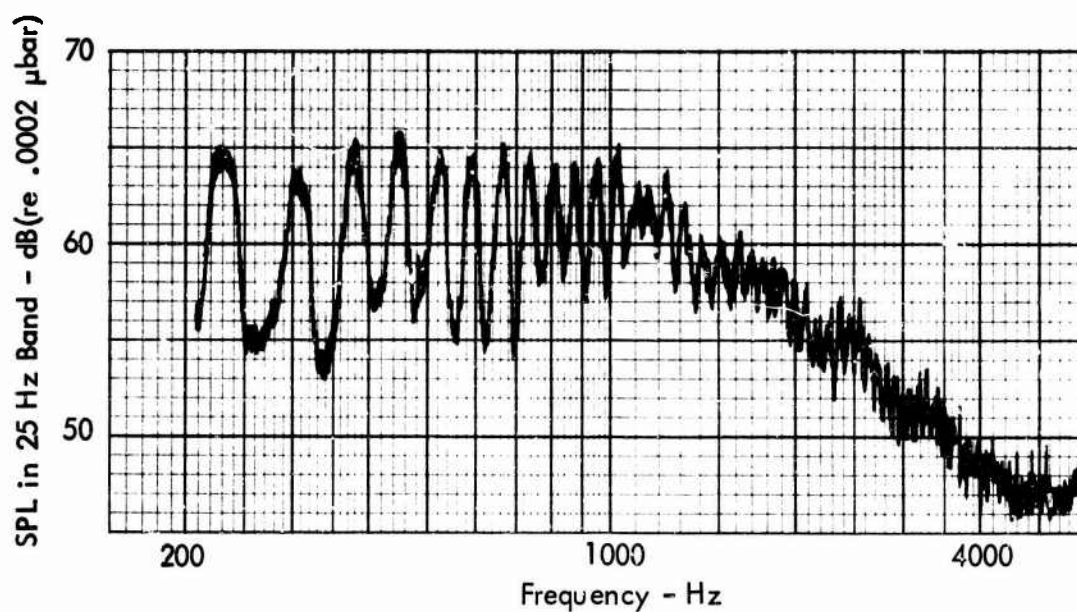


Figure 28. (Continued)



(e) $\alpha_t = 0^\circ$, $C_T = 0.001$



(f) $\alpha_t = -2^\circ$, $C_T = (0)$

Figure 28. (Concluded)

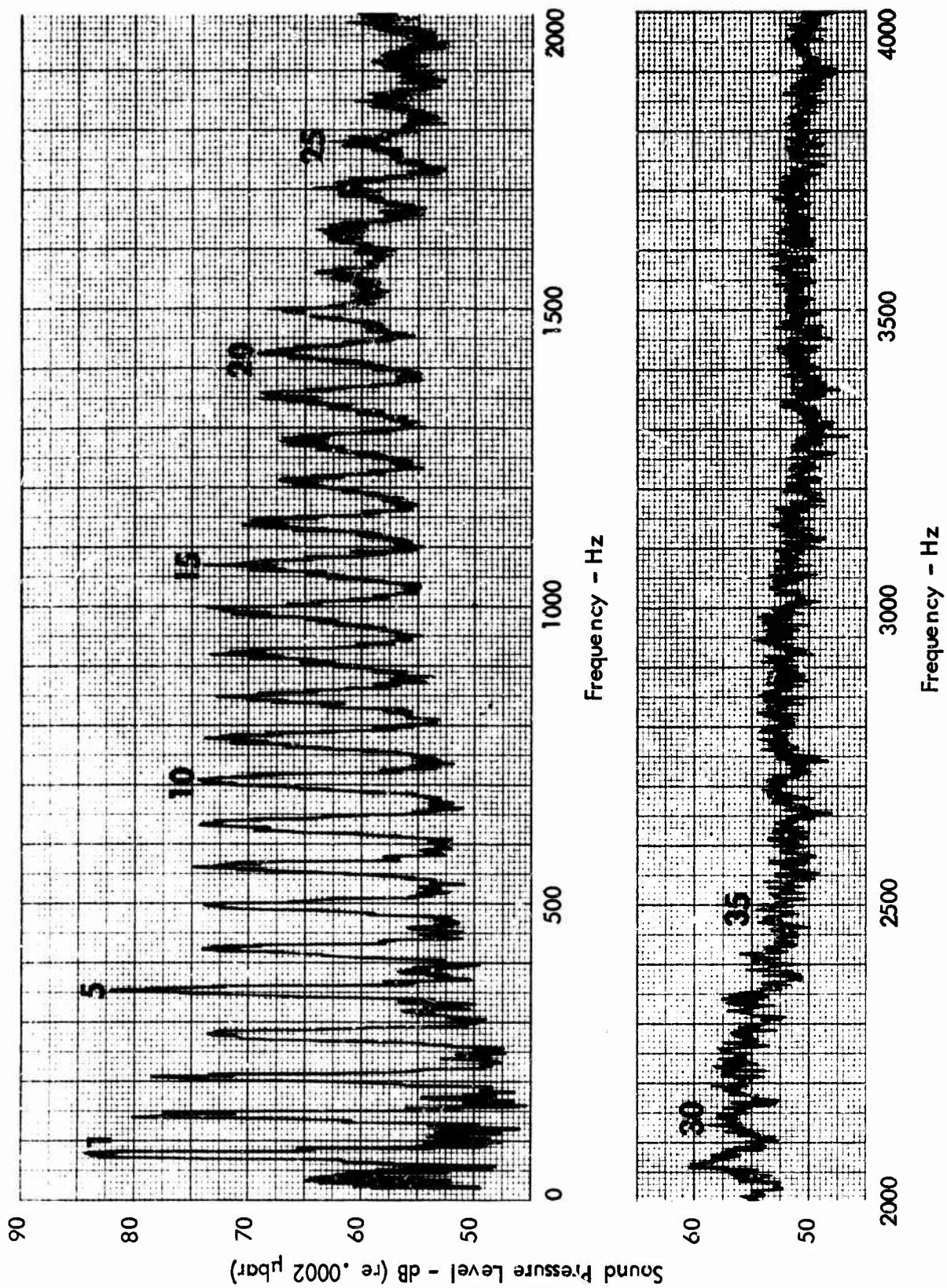
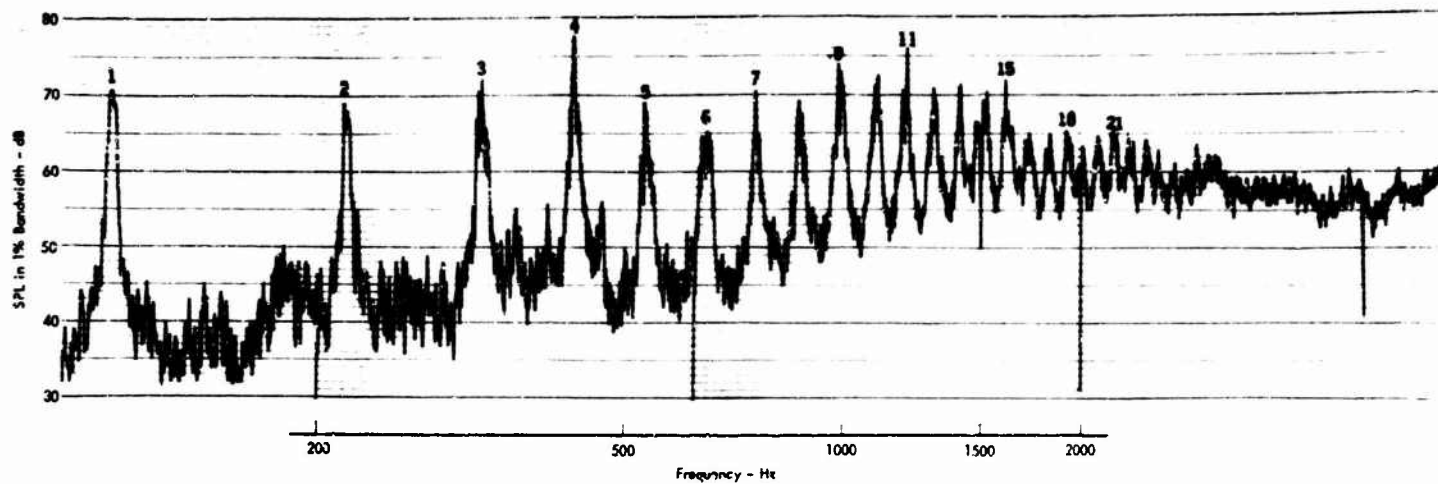
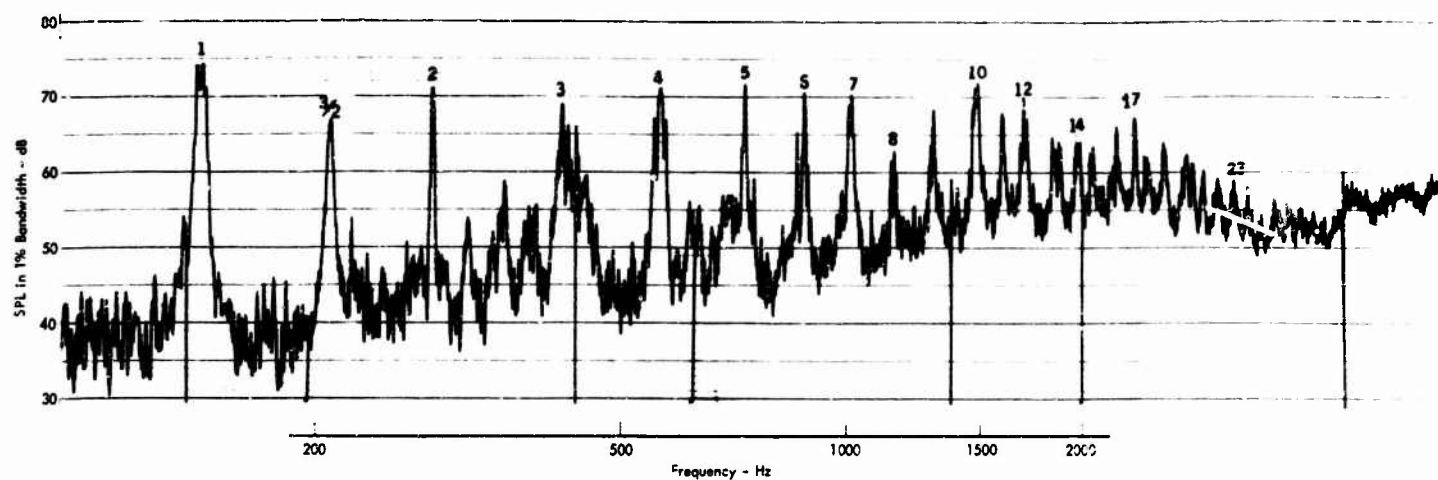


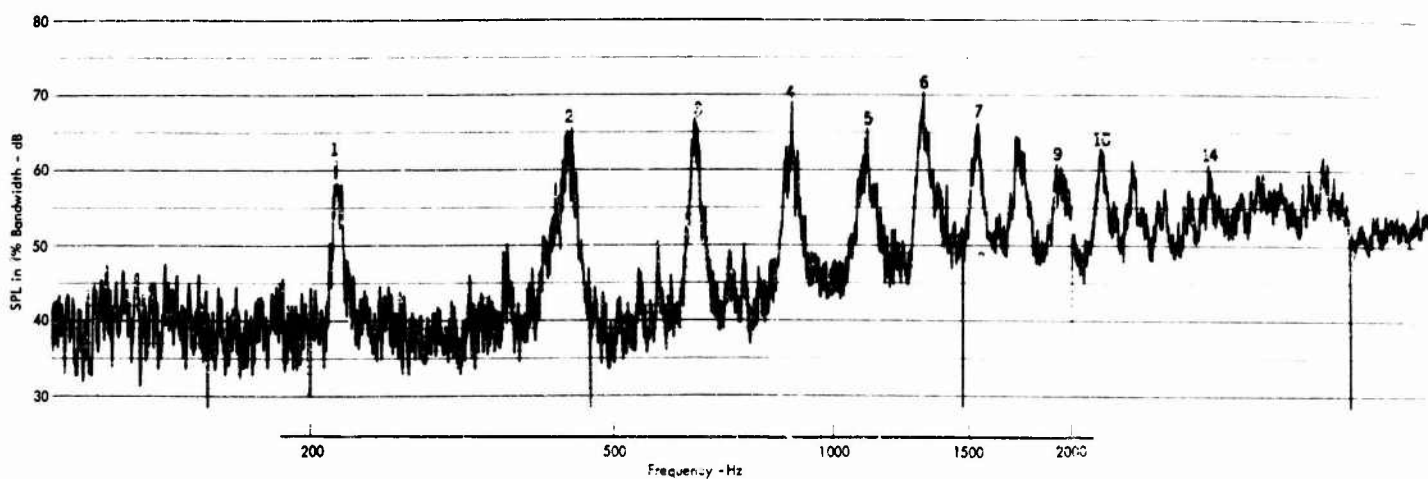
Figure 29. Narrow Band (25 Hz) Spectrum of Sensenich Propeller Noise
 $M_t = 0.4$, $D = 4$ ft., $r/D = 3$, $B = 2$, $\theta = 0^\circ$ (on-axis)



(a) Blade Number = 3



(b) Blade Number = 4



(c) Blade Number = 6

Figure 30. One Percent Bandwidth Spectra of Test Propeller Noise
 $M_t = 0.4$, $D = 4$ ft, $r/D = 3$, $\theta = 0$, $B = 3, 4, 6$

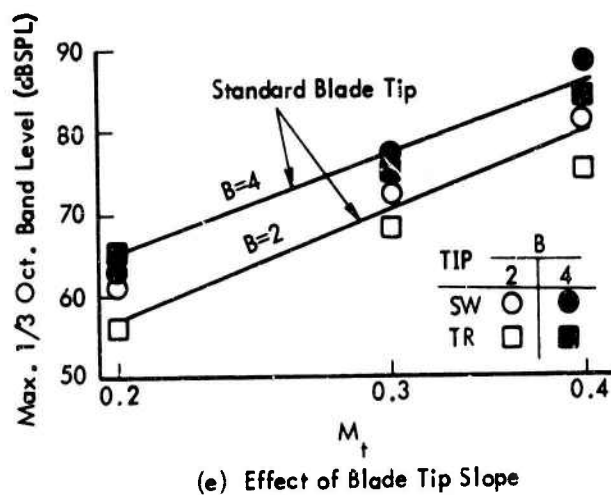
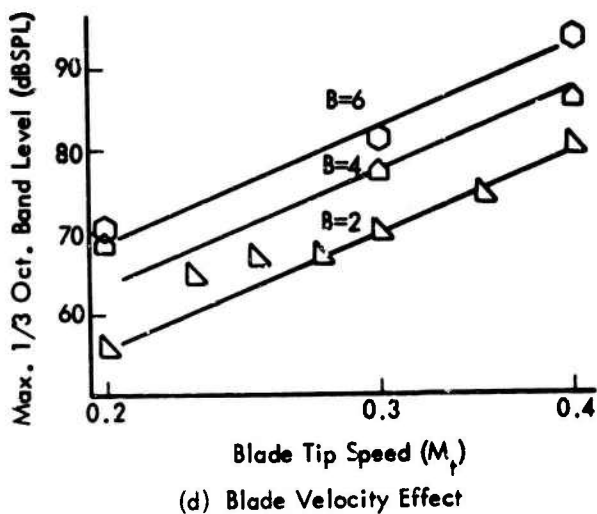
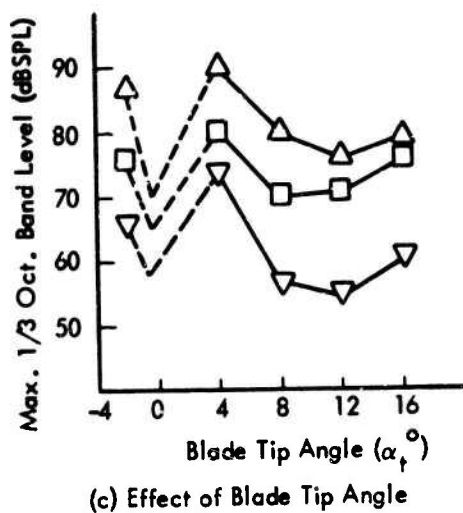
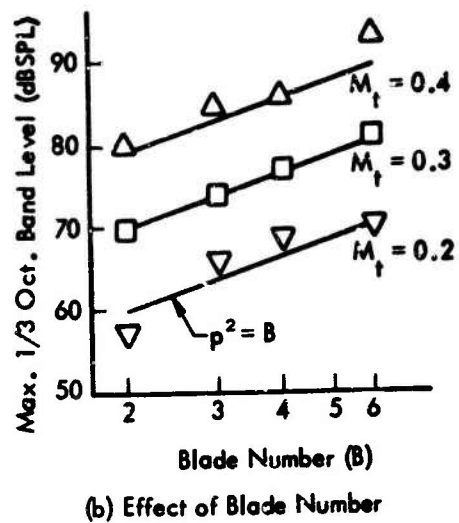
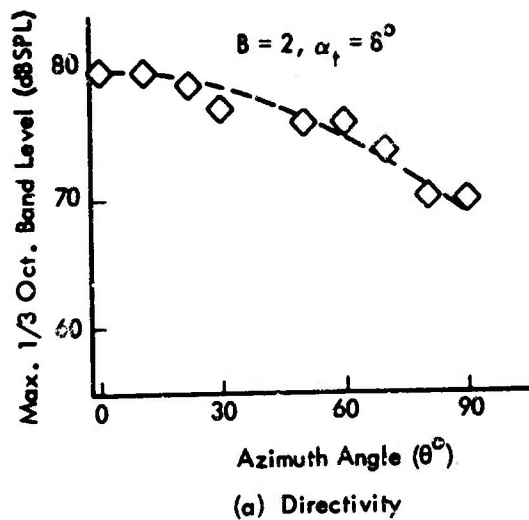


Figure 31. Variation of High Frequency Noise Level with Propeller Geometry

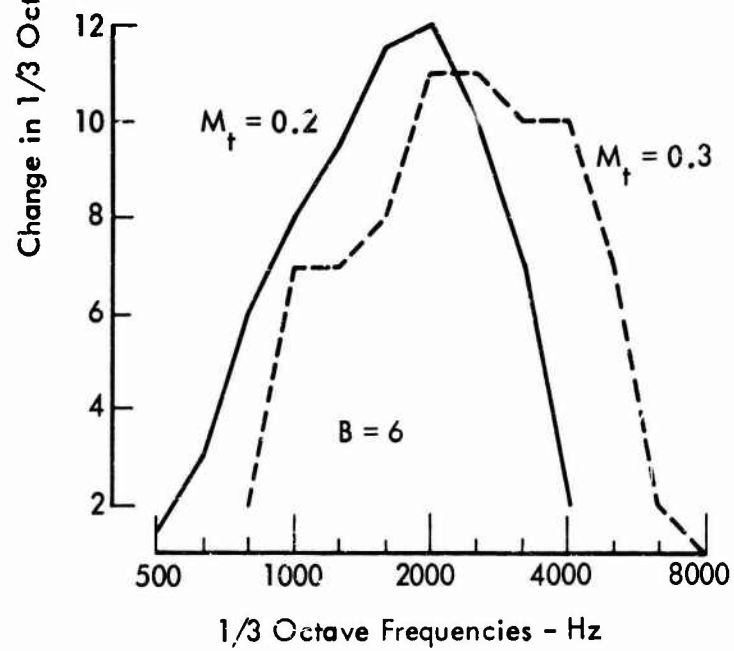
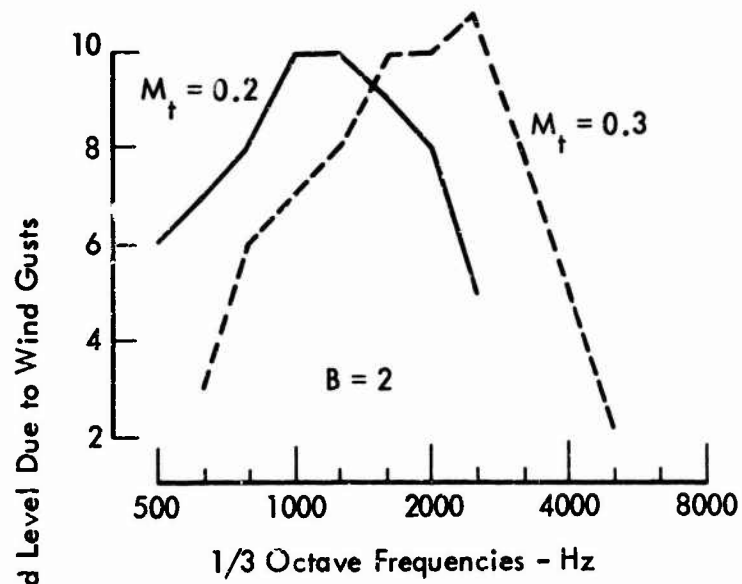


Figure 32. Effect of Wind Gusts on Propeller Noise Analyzed in 1/3 Octave Bands

Measured

$M_t = 0.4$ Δ

$M_t = 0.3$ \square

Theory

—

- - -

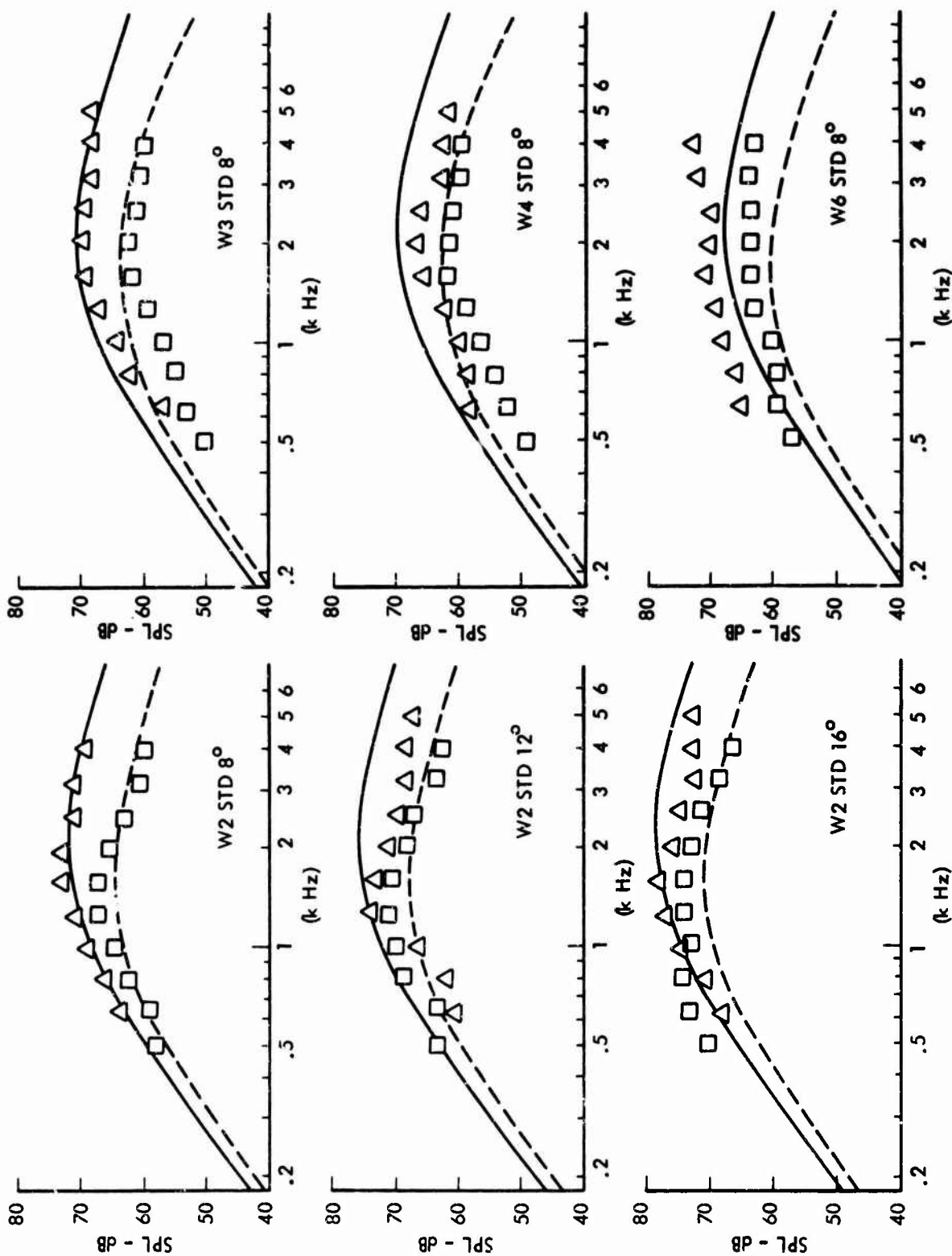


Figure 33. One Third Octave Broadband Noise Levels at $\theta = 0^\circ$ (on-axis)

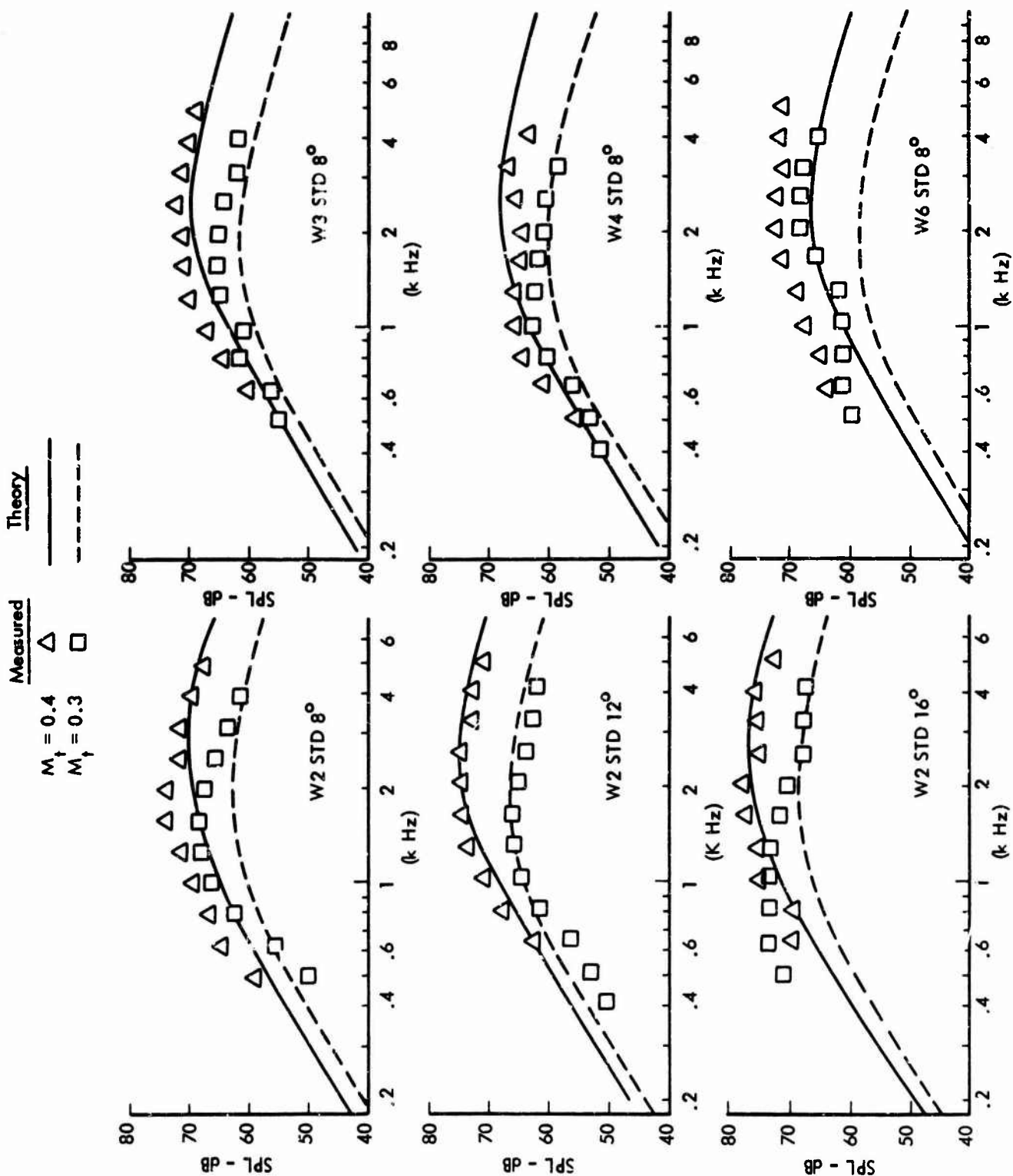


Figure 34. One Third Octave Broadband Noise Levels at $\theta = 30^\circ$ (relative to axis)

Theory

Measured

$M_t = 0.4$

Δ

$M_t = 0.3$

\square

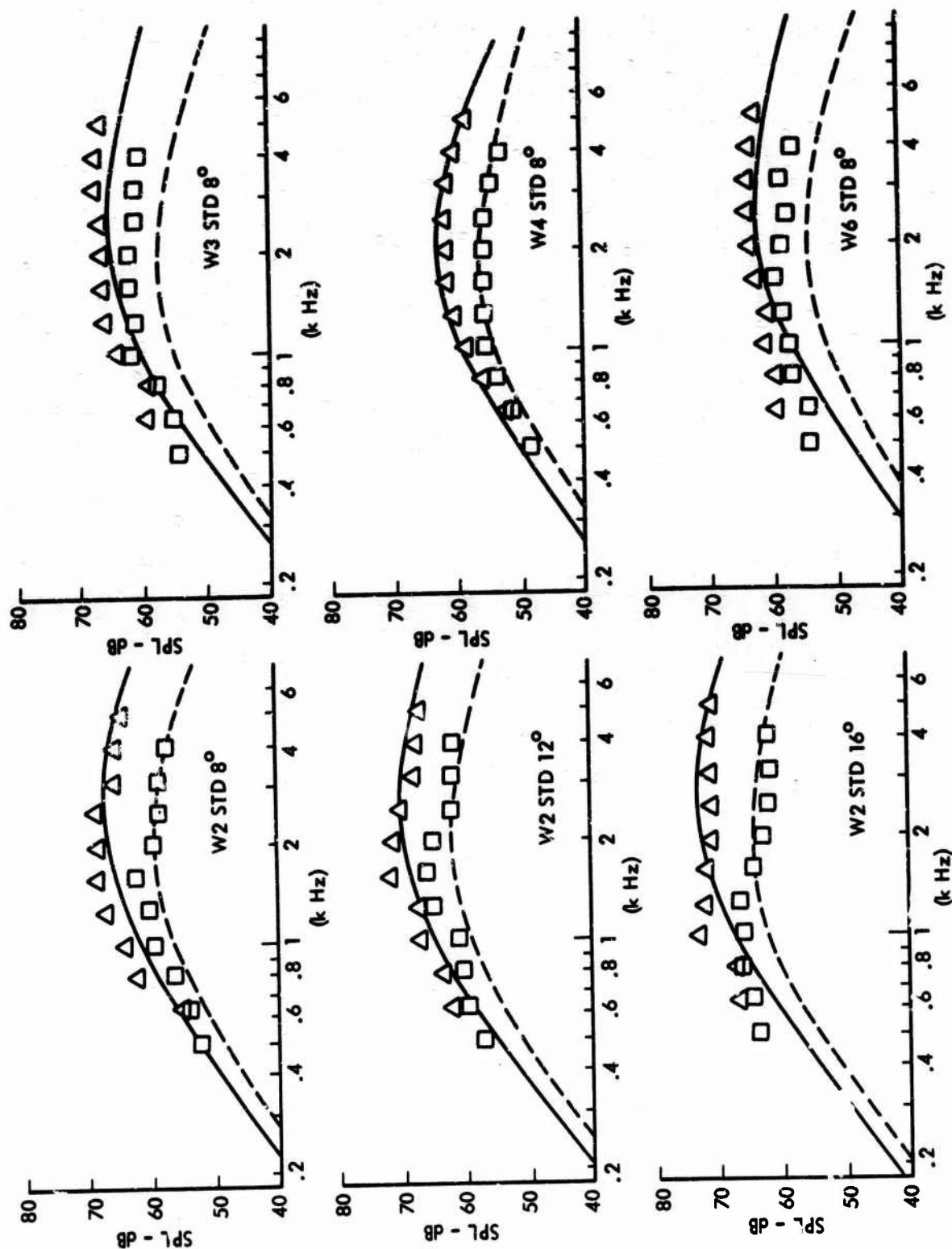


Figure 35. One Third Octave Broadband Noise Levels at $\theta = 60^\circ$ (relative to axis)

	Measured	Theory
$M_t = 0.4$	\triangle	—
$M_t = 0.3$	\square	- - -

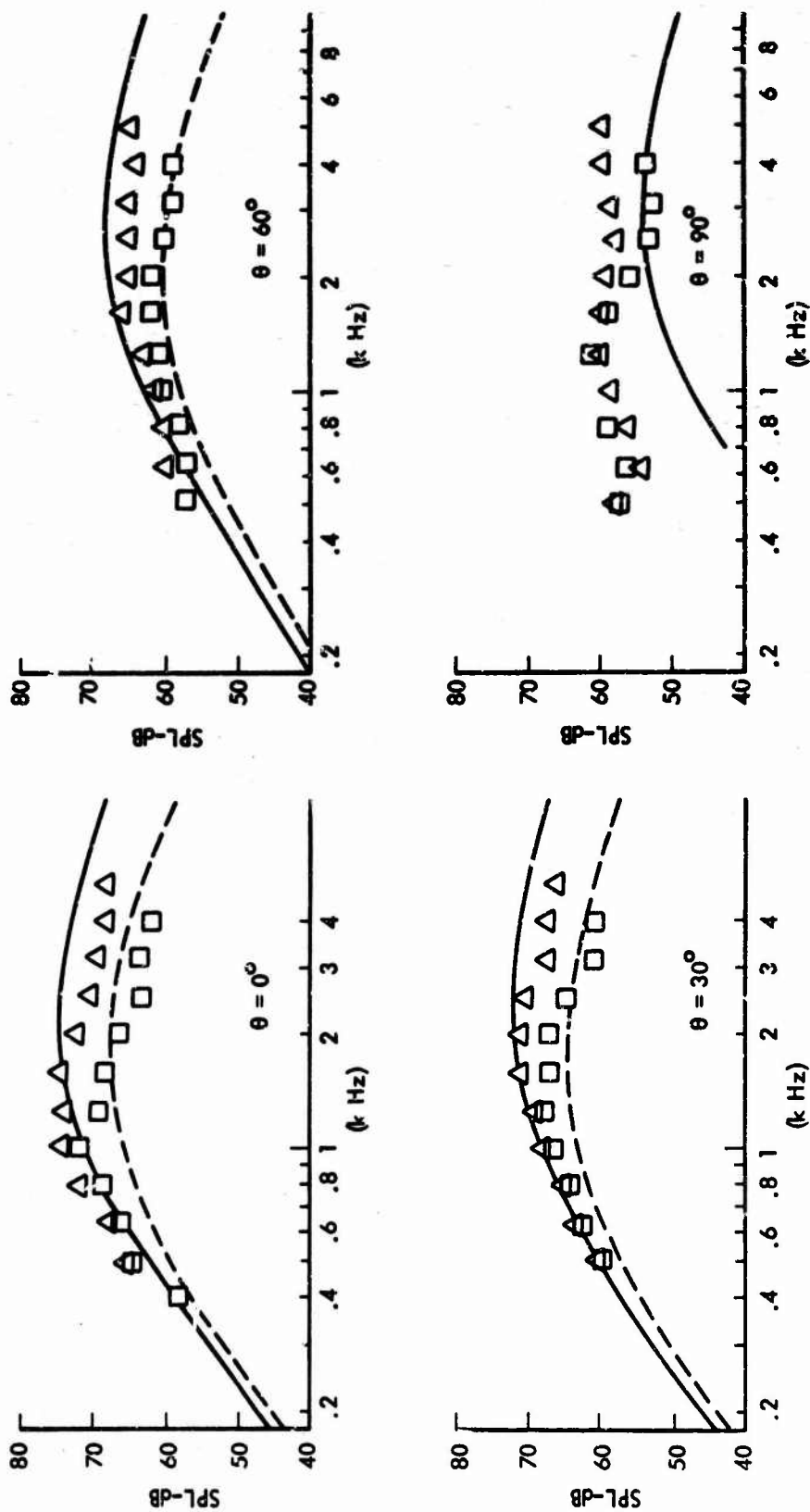
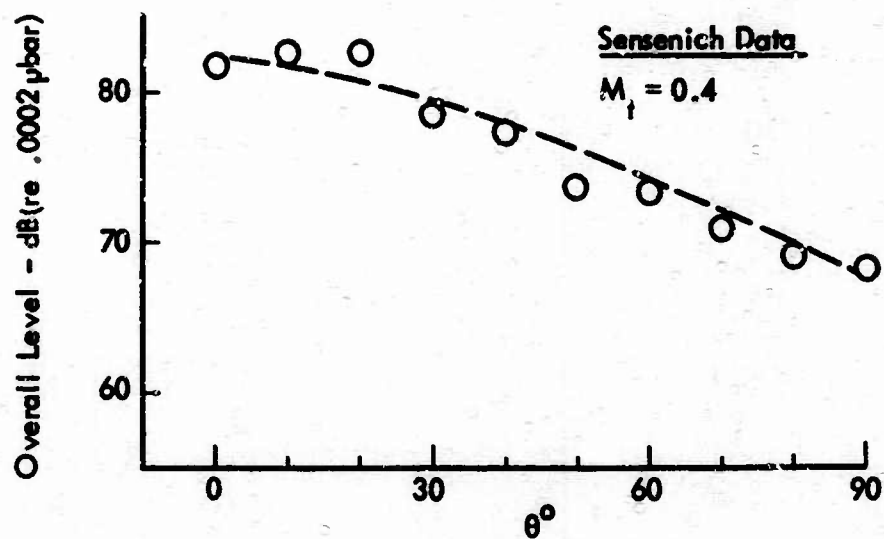
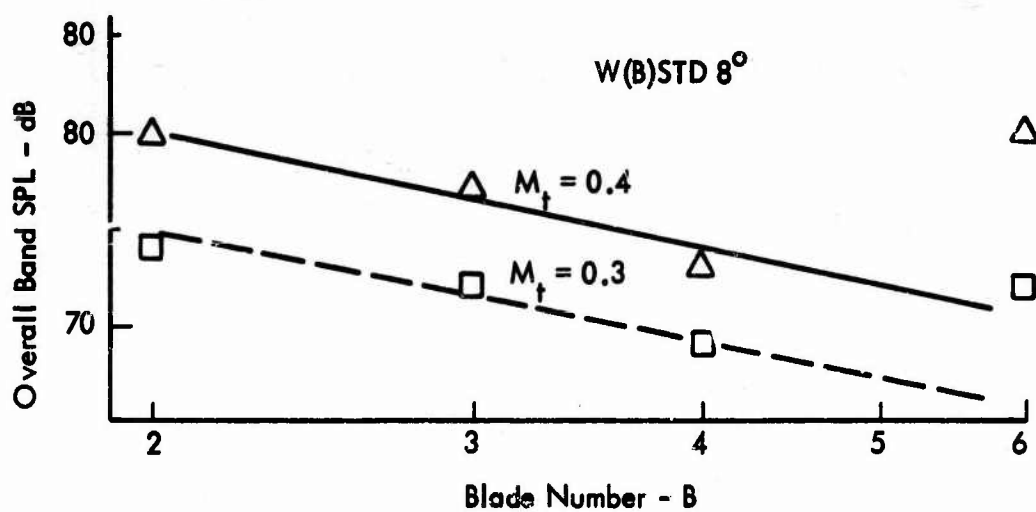


Figure 36. One Third Octave Broadband Noise Levels of Sensenich Propeller

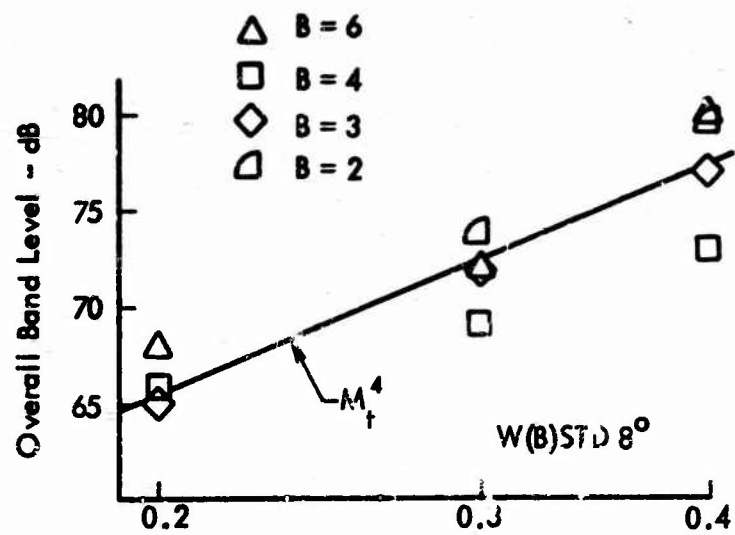


(a) Directivity of Broadband Noise

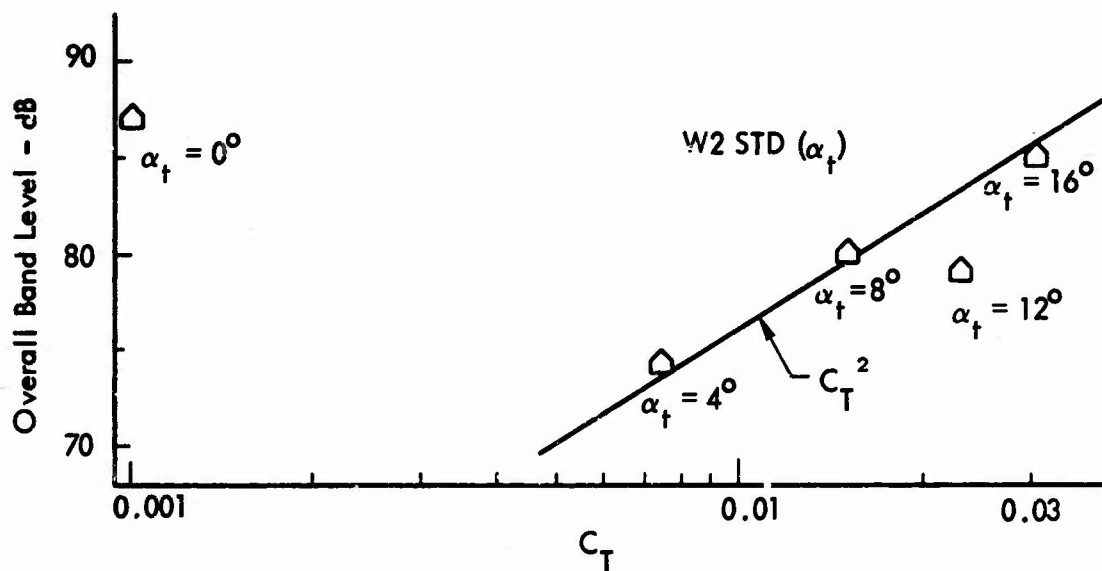


(b) Effect of Blade Number on Broadband Noise

Figure 37. Characteristics of Measured Broadband Noise Content



(c) Velocity Dependence of Measured broadband Levels



(d) C_T Dependence of Measured Broadband Levels
($B = 2$, $M_t = 0.4$, α_f varied)

Figure 37. (Concluded)

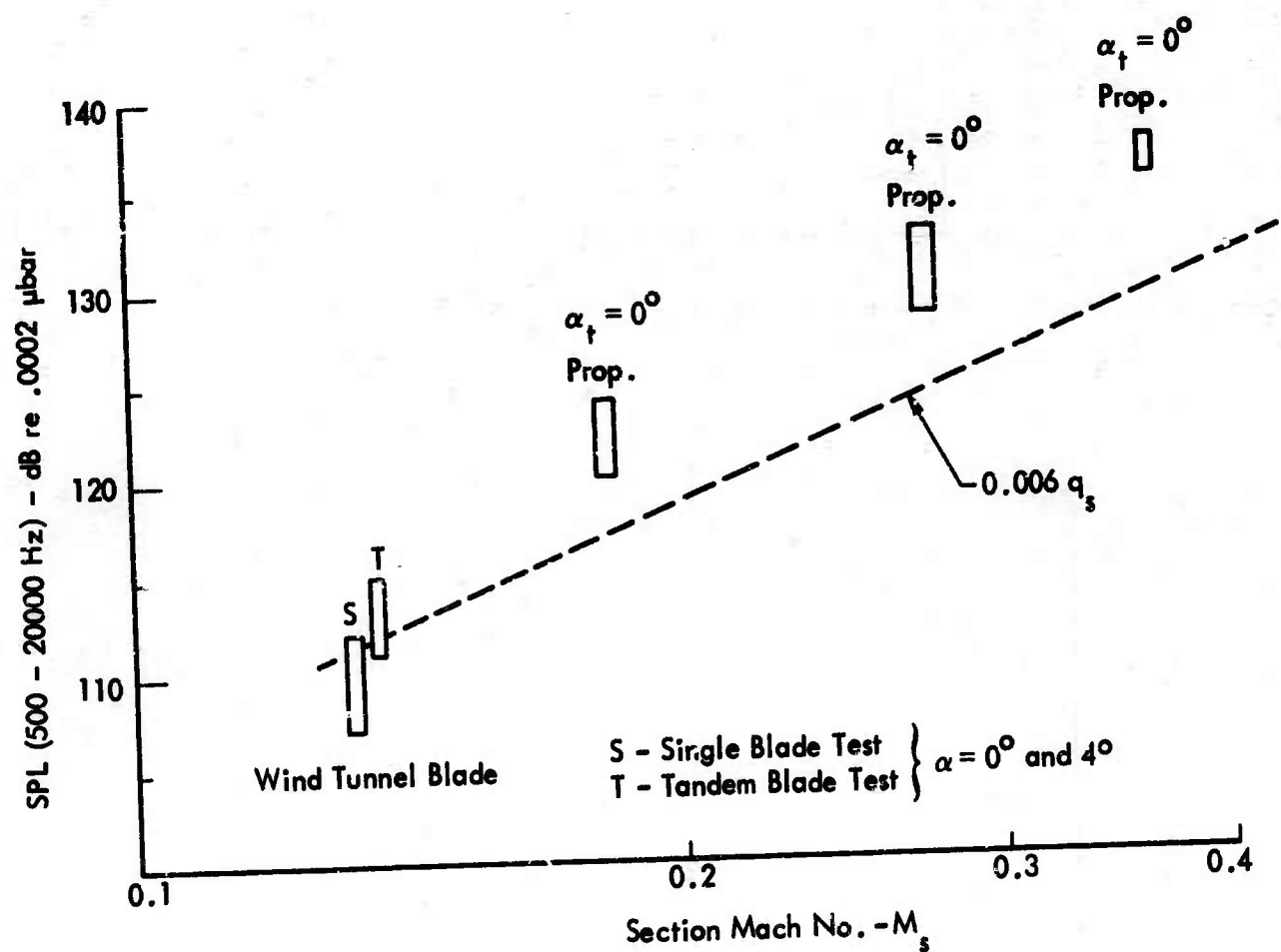


Figure 38. Variation of Measured Blade Surface Pressures with Velocity

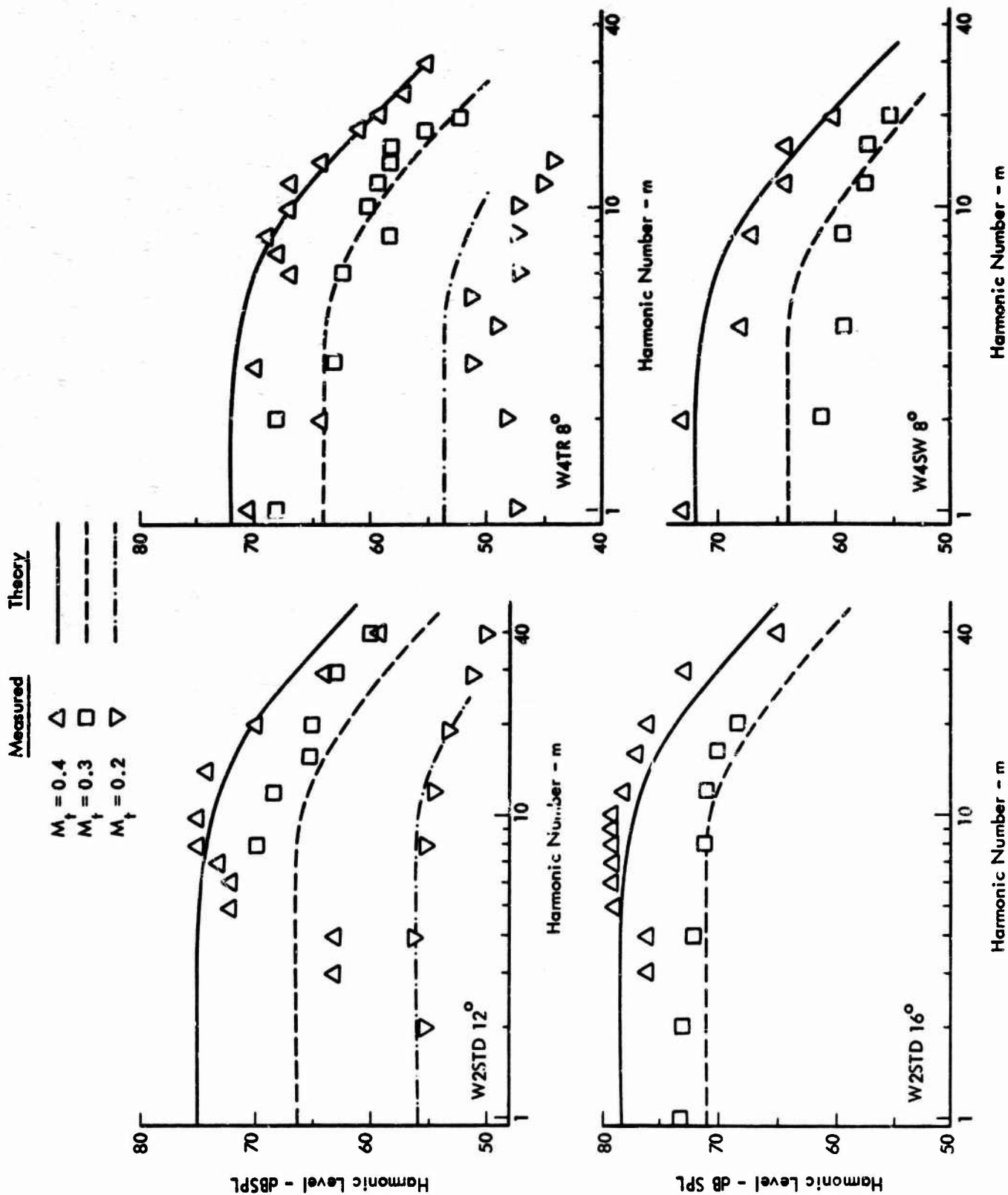


Figure 39. Harmonic Levels of Test Propeller Noise Spectra (on-axis)

Measured Theory

$M_t = 0.4$
 $M_t = 0.3$
 $M_t = 0.2$

—
 - - -
 - · - · -

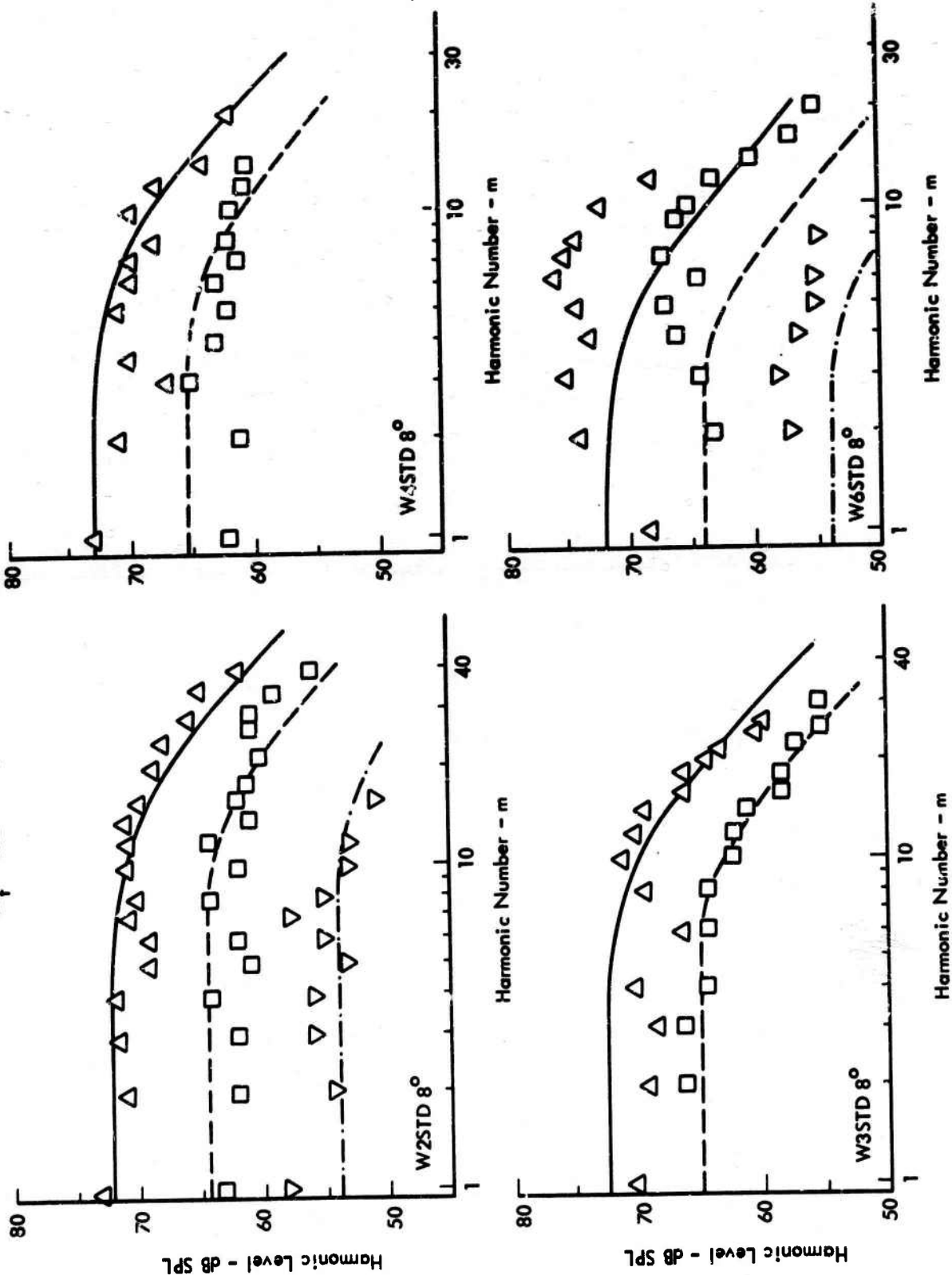
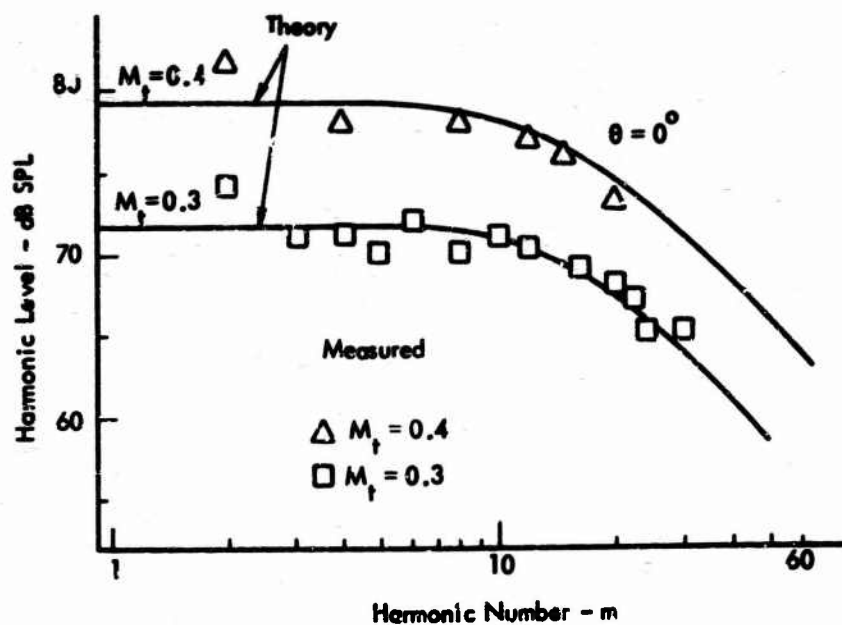
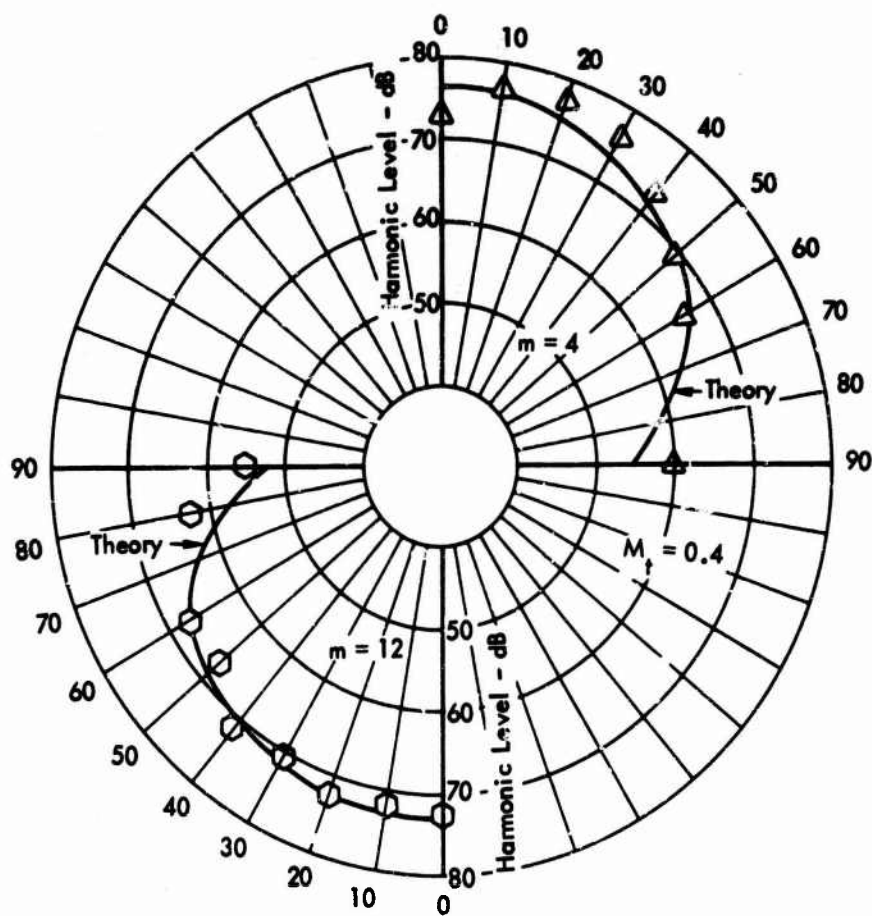


Figure 39. (Concluded)

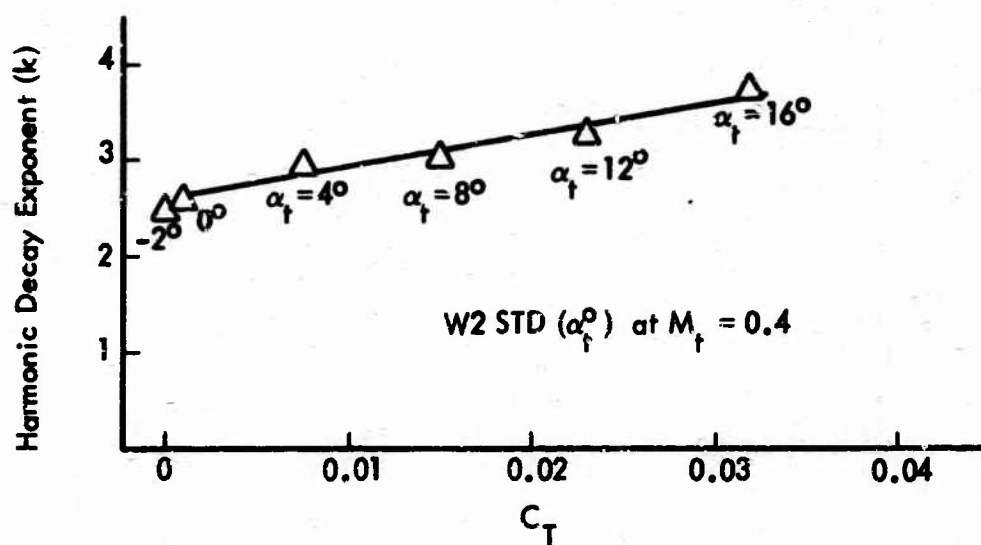


(a) Harmonic Level vs. Harmonic Number

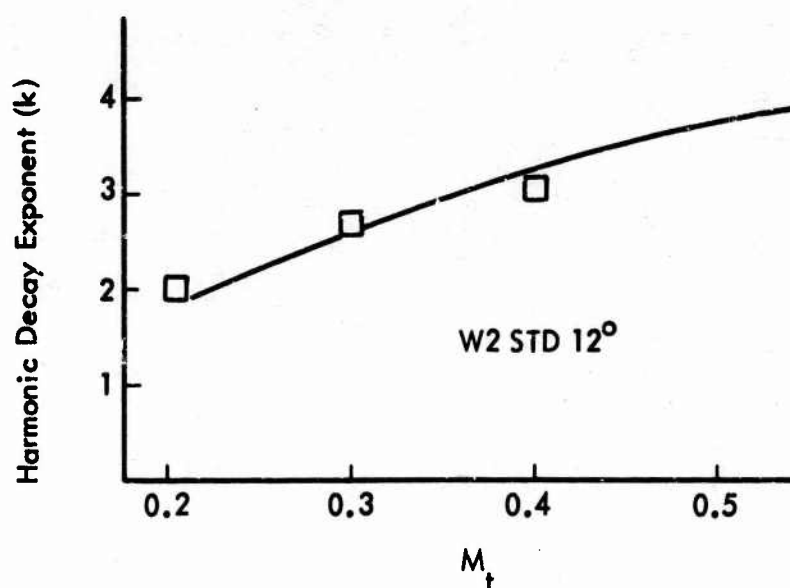


(b) Directivity of $m = 4$ and $m = 12$ Harmonics

Figure 40. Harmonic Content of Sensenich Propeller Noise

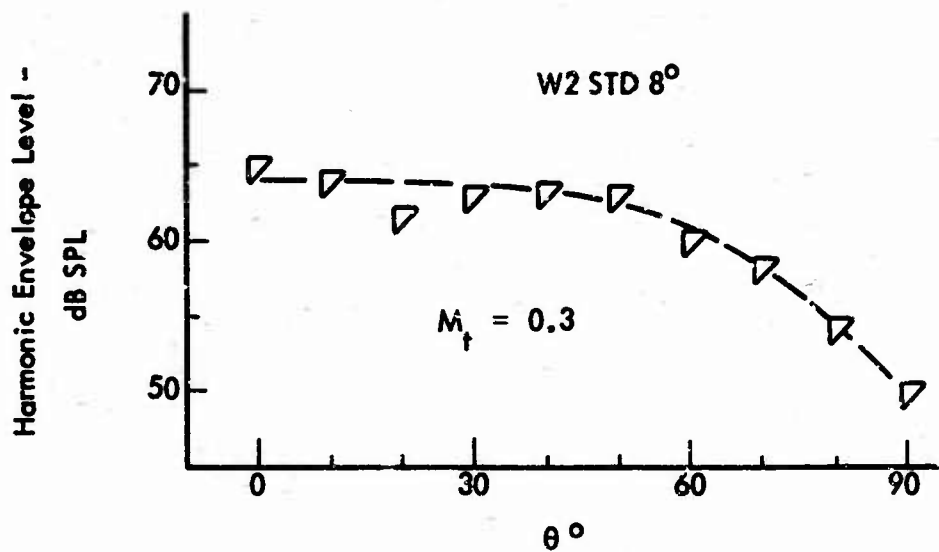


(a) Variance with C_T

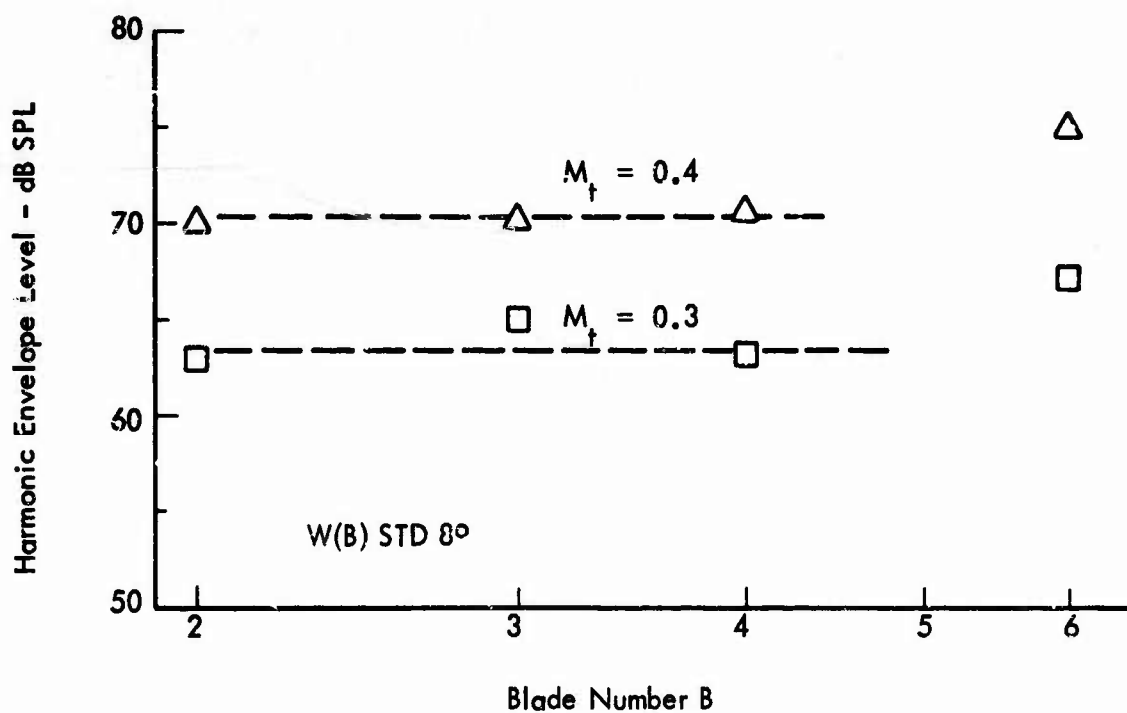


(b) Variance with Blade Tip Speed

Figure 41. Variation of Harmonic Decay Rate with C_T and M_t

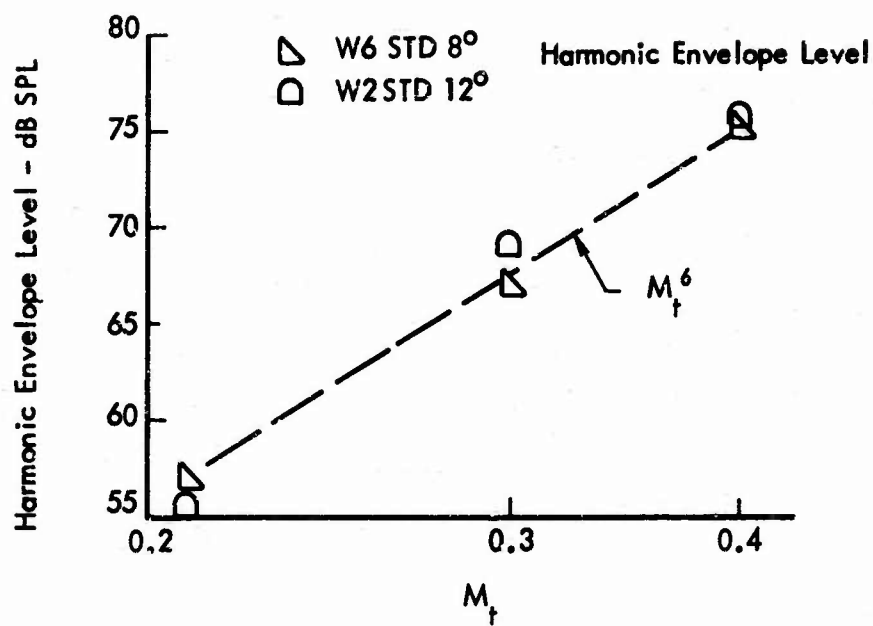


(a) Directivity of Harmonic Noise

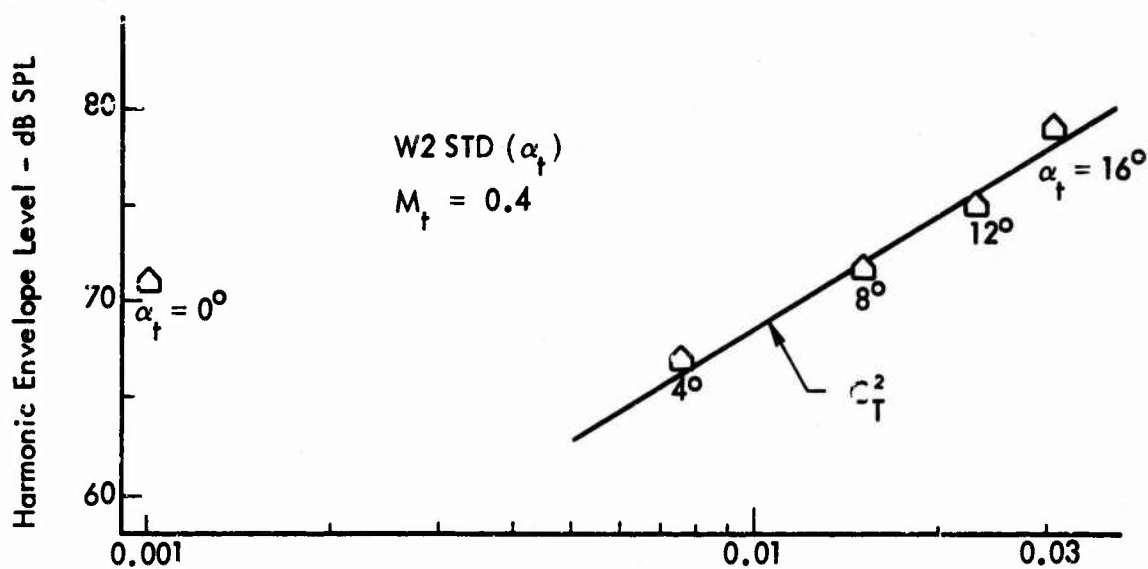


(b) Effect of Blade Number on Harmonic Noise

Figure 42. Characteristics of Measured Harmonic Noise Content



(c) Velocity Dependence of Measured Harmonic Levels



(d) C_T Dependence of Measured Harmonic Levels

Figure 42. (Concluded)

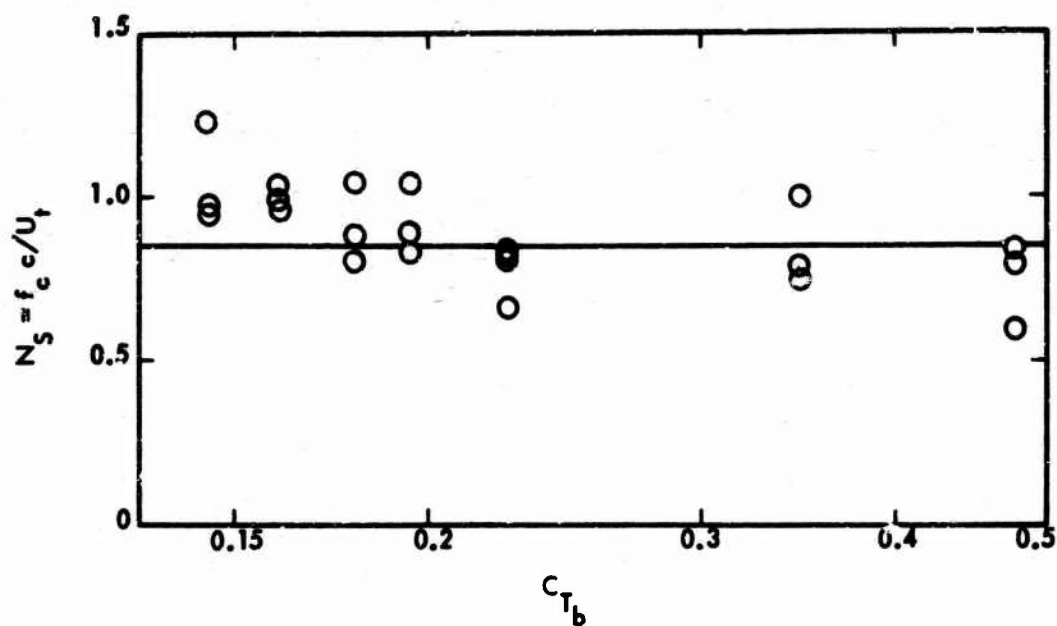


Figure 43. Strouhal Number for Axially Radiated Broadband Noise

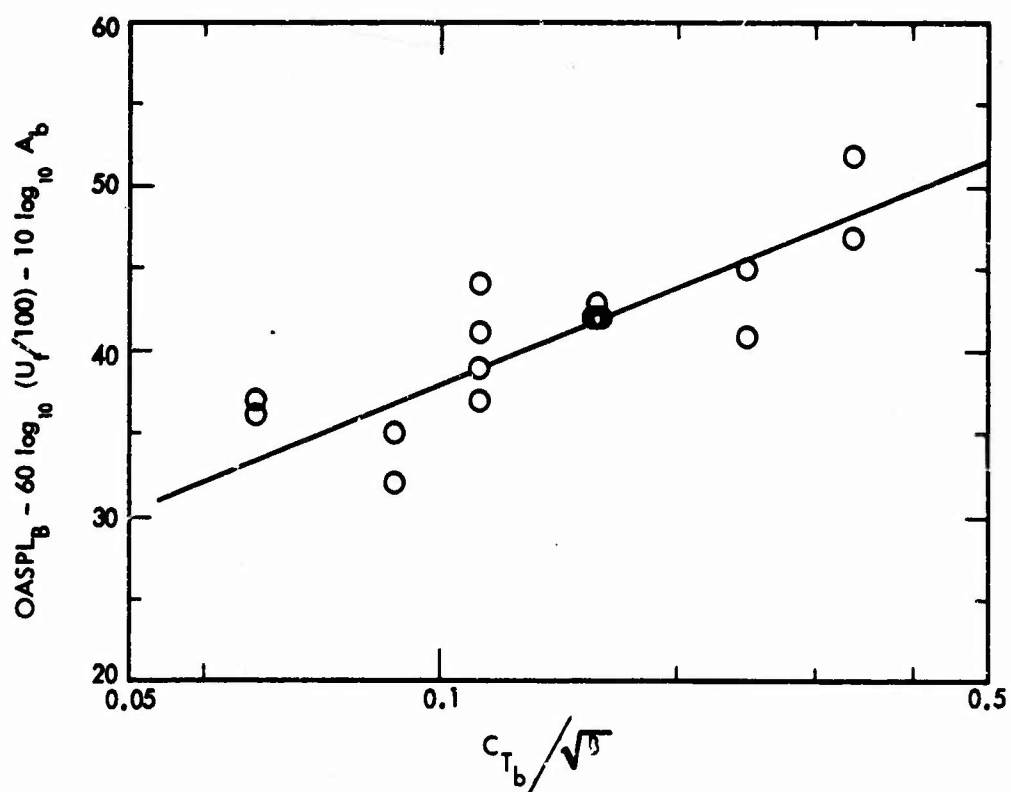


Figure 44. Dependence of Broadband Noise Radiation upon Blade Thrust Coefficient and Number of Blades

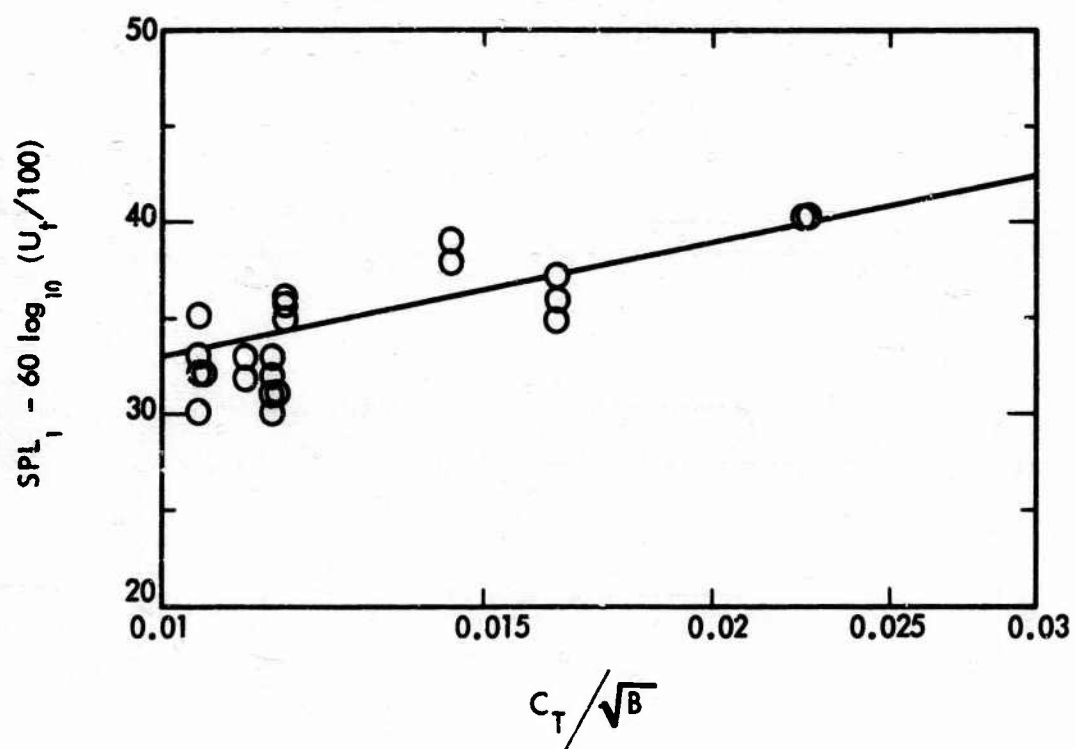


Figure 45. Dependence of Low Harmonic On-Axis Levels upon Disc Thrust Coefficient and Blade Number

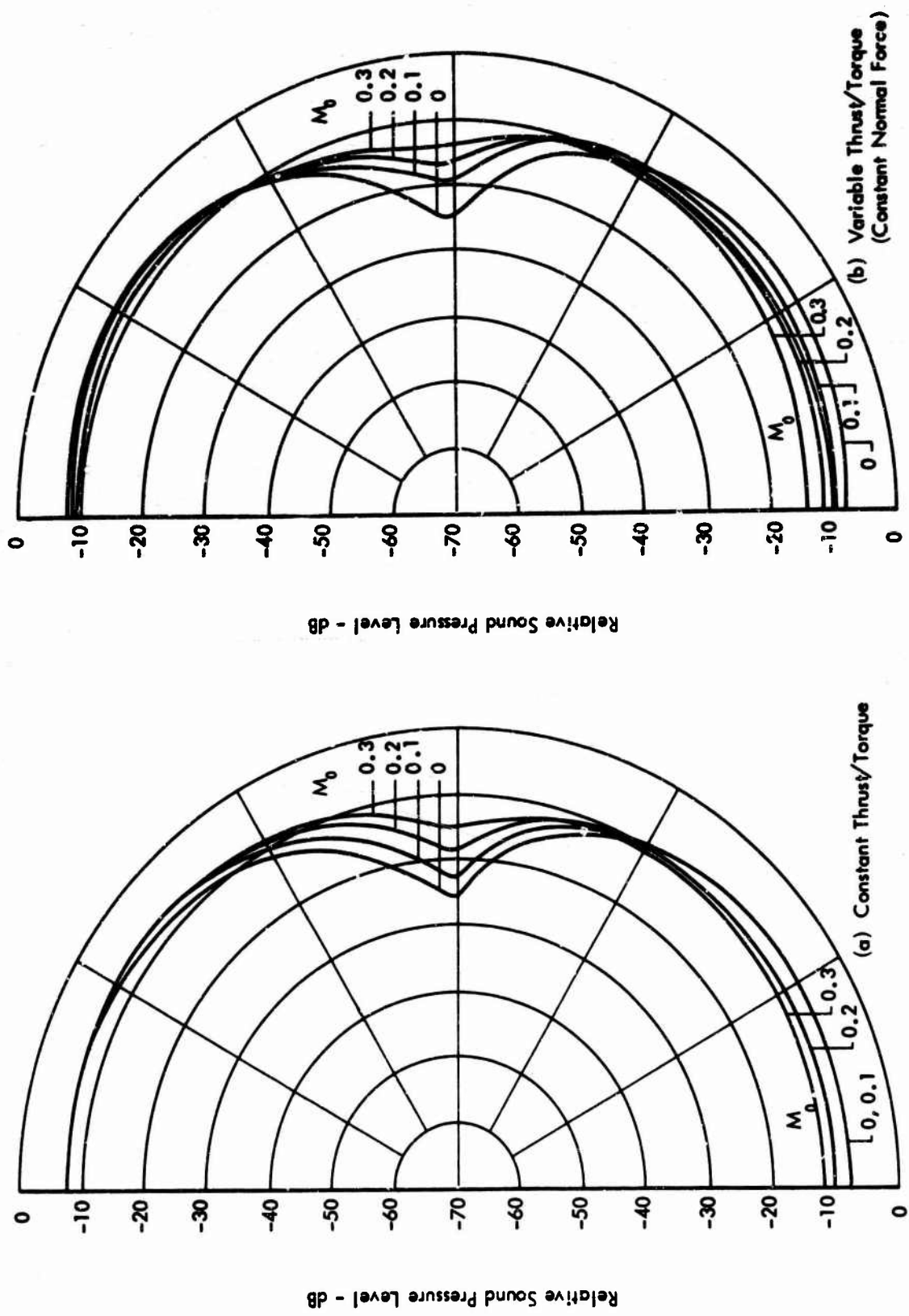


Figure 46. Computed Effect of Forward Speed on Overall Broadband Noise Relative to Instantaneous Position of Propeller

APPENDIX I

122a

APPENDIX I

DESCRIPTION OF THE EXPERIMENTS

SECTION I

INTRODUCTION

A description of the test programs for an experimental investigation of propeller vortex noise is presented in this Appendix. The experimental program encompassed both the aerodynamic and acoustic aspects of the vortex noise generation process. The source mechanisms of vortex noise generation are aerodynamic in origin and a clear understanding of the cause and effect chain of the noise generation process requires an analysis of both aerodynamic and acoustic properties of propeller operation. For this reason, the experimental program involved two studies (1) a wind tunnel study to define the aerodynamic properties of both self-induced and incident-field vorticity and their relative contribution to the random blade loading distributions and, (2) a free-field propeller study to define the acoustic properties of the propeller noise field, and the correlation of the noise field with the random blade loading. A description of the Wind Tunnel Test Program is presented in Section II and a description of the Free-Field Propeller Test Program is presented in Section III.

SECTION II

WIND TUNNEL TEST PROGRAM

1.0 INTRODUCTION

The present section is a description of the test program for the wind tunnel study. The purpose of the wind tunnel test program was to study the unsteady aerodynamic flow fields associated with propeller blades to determine their relative importance as noise source mechanisms. It is well known that various unsteady flow environments result from the passage of viscous flow over airfoil shapes. However, the unsteady loading to the surface of propeller blades has not been studied in light of the present program objectives. Therefore, a systematic experiment has been conducted to examine, in detail, the potential sources of unsteady aerodynamic loads which may result in vortex noise generation. It was felt that these sources could be identified best using stationary blades in a low speed, low turbulence, wind tunnel. Through a systematic variation of blade configurations and blade arrangements, it was anticipated that independent evaluation of the source terms could be made with the result that the dominating mechanisms could be defined. To measure the unsteady loading on the blades, both chordwise and spanwise microphone arrays were used. However, because of the low dynamic pressure associated with the tunnel airflow, measurable effects of test conditions were detected only on the downstream blade for the condition where the downstream blade was in the wake of the upstream blade. Thus, in an attempt to more clearly define the sources of unsteady loading, hot wire studies were performed. Both the trailing edge shed vorticity and the tip vortex were defined from hot wire surveys to establish trends due to the effects of variations in tip shape and blade angle of attack.

This section is subdivided into various sub-section - each of which presents a discussion of various aspects of the test program. Section 2.0 contains a description of the test apparatus and instrumentation. The test procedure and test conditions which were investigated are presented in Section 3.0.

2.0 TEST APPARATUS AND INSTRUMENTATION

2.1 Wind Tunnel Facility

The wind tunnel facility is a low speed wind tunnel having a 10 in. by 32 in. test section and currently capable of operating at speeds slightly above 150 ft per second. The tunnel was designed for low noise and low turbulence operation with an inlet contraction ratio of 16:1. Modifications have been made to the facility for the purposes of the present test. The primary modification consisted of rearranging the tunnel in the aerodynamic laboratory such that the inlet, test section, and blower are acoustically isolated by wall areas. The present tunnel arrangement is shown in Figure I-1.

Calibration studies of the tunnel airstream to assess the mean and fluctuating velocity profiles in the test section were performed. Initial runs revealed a turbulence intensity of 1.5 percent of the free stream velocity for a single screen in the tunnel inlet. The application of a honeycomb section consisting of plastic soda straws 1/4 inch in diameter and 9 inches in length reduced the turbulence intensity to 0.48 percent with only one ft per second reduction in mean airspeed. Thus, it is felt that the tunnel flow was adequate for the present study of propeller vortex noise. New wind tunnel walls were designed to provide the necessary fixtures for the models. Following the installation of these walls, additional calibration runs were performed and these data indicated no detectable change in the tunnel flow characteristics.

2.2 Wind Tunnel Models

The wind tunnel models consisted of three-dimensional propeller blade segments. The present research propeller design was based on a NACA-0012 airfoil section. For the wind tunnel tests, a constant chord, zero twist blade was used. Because of blockage effects in the wind tunnel, it was desirable to maintain a minimum blade thickness and consequently, minimum chord length. However, the model blade had to be sufficiently thick to contain the surface mounted microphones. Taking these factors into consideration a blade with a 3-inch chord was selected. Also, in view of blockage effects on lift and drag (which are related to the overall aerodynamic flow field of the blade) it was decided to test the blades across the short side of the test section. Thus, the three-dimensional blades were approximately 6 inches in span. The blades used in the wind tunnel tests were the same scale and basic design as those used subsequently in the free-field acoustic tests, but without twist or taper.

Both single blade and double, tandem, blade arrangements were investigated. Except for the tip shapes, all blades were zero twist, constant airfoil section (NACA 0012) designs.

A summary of configurations tested are as follows:

- Single Blade, Three-Dimensional Configuration
 - Angle of attack variations
 - Blade tip variations
- Double Blade, Three-Dimensional Configuration
 - Angle of attack variations
 - Blade tip variations
 - Longitudinal and transverse separation variations to simulate effective propeller configurations (x, y)

The arrangement of the blades in the wind tunnel test section is shown in Figure I-2 and I-3.

Blade tip variations consisted of the following geometries:

- Standard tip which is formed by rotating the NACA-0012 airfoil section about the chord line located at the end of the constant chord portion of the blade
- Swept tip with a 60-degree aft swept leading edge
- Trapezoidal tip with a 15° leading edge taper and a 25° trailing edge taper

Schematics of these configurations are presented in Figure 1-4. The notation used to identify model configurations is given in the main text (Figure 17).

2.3 Instrumentation for Data Acquisition

Instrumentation for the acquisition of test data consisted of microphones, signal conditioning equipment, and analog data recording equipment. The microphones were positioned in both the chordwise and spanwise directions as shown in Figure 17 of the main text. Also, their positions relative to the tunnel sidewalls were held constant. For the tandem configuration, instrumentation was located only in the aft blade. The purpose of the microphones were to record, in both the chordwise and spanwise directions, the fluctuating pressure environment induced on the blade. The microphones used for the test are Kulite-ultra-miniature microphones Type CQL-125-5S. The Kulite microphone diaphragm diameter was 0.125 inch, and they are manufactured using a monolithic integrated Wheatstone bridge directly formed on a silicon diaphragm. The CQL-125-5S has an input impedance of approximately 1000 ohms and may be excited with a 5 volt AC or DC power supply. At a rated pressure of 5 psi they have a sensitivity of 7 millivolts/volt (or 35 mv/psi). During the experiments, the reference pressure was sealed and remained at a constant pressure. The natural frequency of the microphones is about 100K Hz, giving a flat dynamic response to about 25K Hz. These instruments have been used with excellent success in previous experiments of a similar nature conducted by Wyle. The signal conditioning electronics were standard instrumentation components for the microphones used.

In addition to the microphone instrumentation, surveys of the tunnel airstream and blade wakes were taken with hot-wire instrumentation. These data were used to define both the mean flow and turbulent properties of the tunnel flow and the blade trailing edge shed vortex and the tip vortex and helped to define critical conditions at which the flow fields from upstream blades interact with trailing blades. The hot-wire instrumentation consisted of the following components.

- Thermo-Systems, Inc., Model 1054A constant temperature hot-wire anemometers with linearizers. These anemometers gave a linear voltage response with the speed range of the tunnel. Manufacturer specifications indicate that the frequency response of the Model 1054 anemometers are flat from D.C. to 200K Hz.

- Hot-wire probes with both single wire and X wire probe elements. A single straight wire was used to measure the streamwise velocity component; whereas, a pair of wires in the form of an "X" was used to measure cross-stream components. These probes were constructed at Wyle. The wire elements are 0.00015 inch-diameter tungsten with an effective length of 0.04 inches. The wires were electroplated with copper before they were mounted on the probes with soft solder.

Instrumentation for data reduction is discussed in the following section.

2.4 Instrumentation for Data Reduction

The analog instrumentation for on-line data reduction consisted of the following:

- A Bruel and Kjaer Type 2112 Audio Frequency Spectrometer. The B and K spectrometer provided one-third octave spectra and overall sound pressure level parameters.
- A Bruel and Kjaer Type 2305 Graphic Level Recorder. The B and K Level Recorder provided plots of the one-third octave spectra and overall sound pressure levels.
- A Ballantine Model 320 true rms voltmeter. The rms voltmeter was employed for measuring the turbulent intensities over a frequency range from 5 Hz to 25K Hz.
- A F.L. Mosely Model 135C plotter. The Mosely X-Y plotter provided analog records of mean and turbulent velocity variations in both normal and spanwise directions.

3.0 TEST PROCEDURE AND CONDITIONS

Because of the importance of defining and minimizing free-stream disturbances prior to conducting the model propeller blade tests, the tests were conducted in two phases. Phase I was a calibration of the wind tunnel facility to assess the mean- and turbulent-flow properties of the tunnel air stream and to experiment with modifications to the facility to arrive at symmetrical mean-flow profiles and minimum air-stream turbulent intensity. Phase II consisted of the parametric propeller blade tests to assess the various source mechanisms which may contribute to propeller vortex noise generation. These tests will be discussed separately.

Phase I - Wind Tunnel Calibration - Preliminary experiments have been conducted to assess the mean- and turbulent-flow properties of the tunnel airstream using temporary side walls in the test section. Following the fabrication and installation of the side walls which were used for the present study, a thorough calibration of the test section was performed. Surveys of mean- and turbulent-velocity were taken in both the longitudinal and spanwise directions for the region to be occupied by the model propeller blades. Efforts were made through tunnel inlet modifications to arrive at tunnel configurations which would give optimum flow conditions (i.e., smooth, symmetrical mean flow profiles and minimum velocity turbulence levels).

Phase II - Model Propeller Blade Tests - The procedure for the model propeller blade test was designed to facilitate an independent evaluation of the various source mechanisms which may contribute to propeller vortex noise generation. The source of pressure fluctuations which may induce unsteady loads on propeller blades are identified as follows:

- Boundary Layer Turbulence
- Trailing Edge Shed Vorticity (Near-Wake)
- Trailing Tip Vortex (Near-Wake)
- Turbulent Wake (Far-Wake)

To provide for independent evaluation, the following tests were planned and the pressure fluctuation sources which exist are identified.

- Single Three-Dimensional Blade
 - Boundary Layer Pressure Fluctuations
 - Near-Wake - Trailing Edge Shed Vorticity
 - Near-Wake - Tip Vortex
- Double Three-Dimensional Blades Positioned in an Offset Tandem Arrangement
 - Boundary Layer Pressure Fluctuations
 - Near-Wake - Trailing Edge Shed Vorticity
 - Near-Wake - Tip Vortex
 - Turbulent Wake - (Far-Wake)

To assist in the interpretation of the fluctuating pressure data and to provide further insight into the sources of unsteady blade loading, a comprehensive hot wire study was performed. The hot wire study consisted of both spanwise and normal traverses relative to the blade surface for various fixed longitudinal locations. A typical arrangement showing the hot-wire probe and a single blade configuration is presented in Figure I-3.

The wind tunnel test phase also involved a study of the effects of both aerodynamic and geometric parameters on the unsteady flow field. These variables consisted of the following:

1. Tip Shape - Three different tip shapes were examined - standard tip, 60-degree swept tip, and trapezoidal tip.
2. Blade Angle - Four blade angles to simulate a range of loading conditions were examined.
3. Blade Orientation (double 3-D configuration only) - Three horizontal relative positions of the downstream blade were examined to simulate a range of relative flow fields representative of actual propeller blade conditions (simulation of combined RPM, free-stream velocity, and blade number effect).
4. Free-Stream Velocity - The wind tunnel test simulated relatively low speed operating conditions. Thus, studies at only one free-stream condition ($U_{\infty} = 150 \text{ ft/sec}$) were performed.

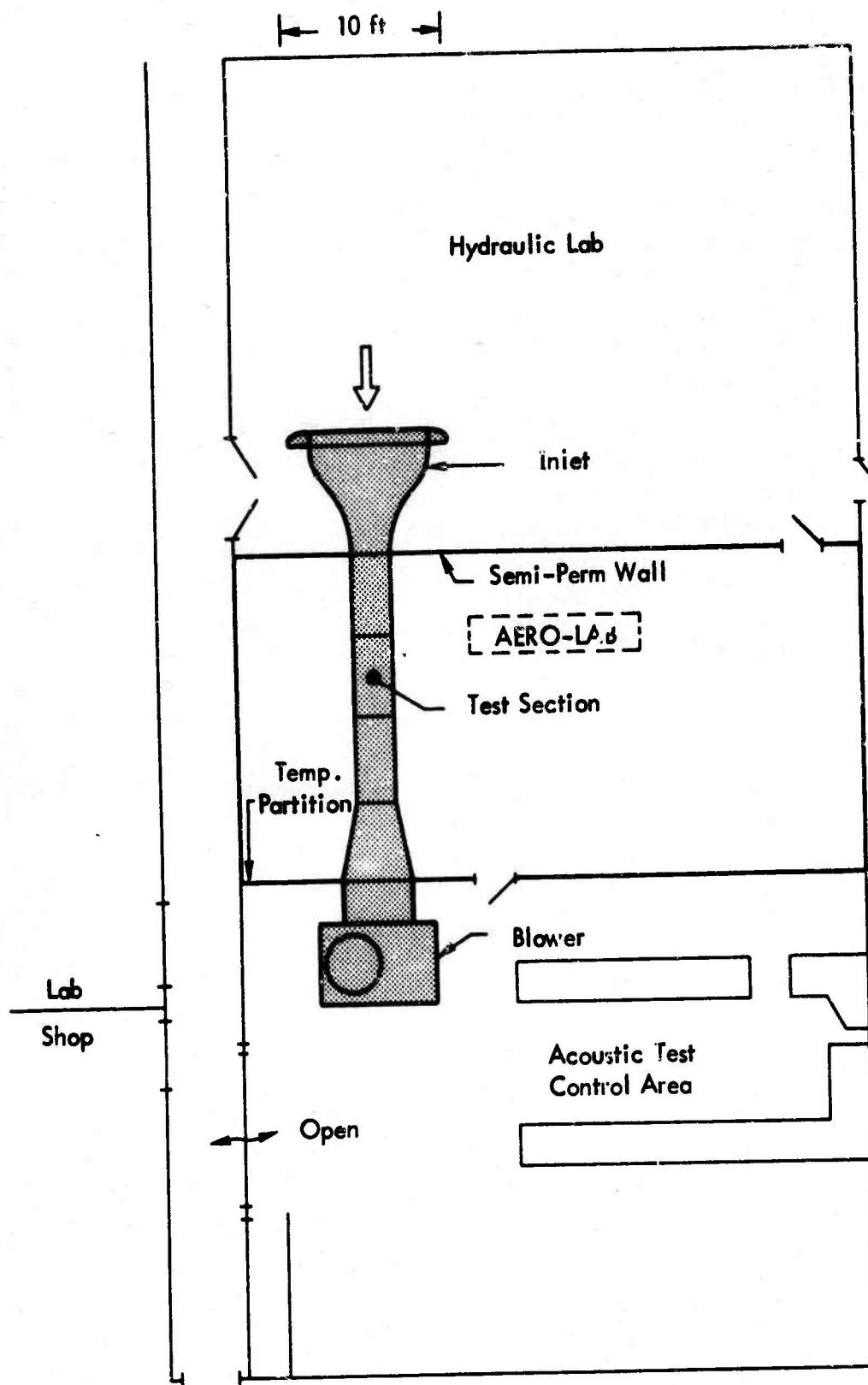


Figure 1-1. Arrangement of the Wind Tunnel in the Aerodynamic Laboratory

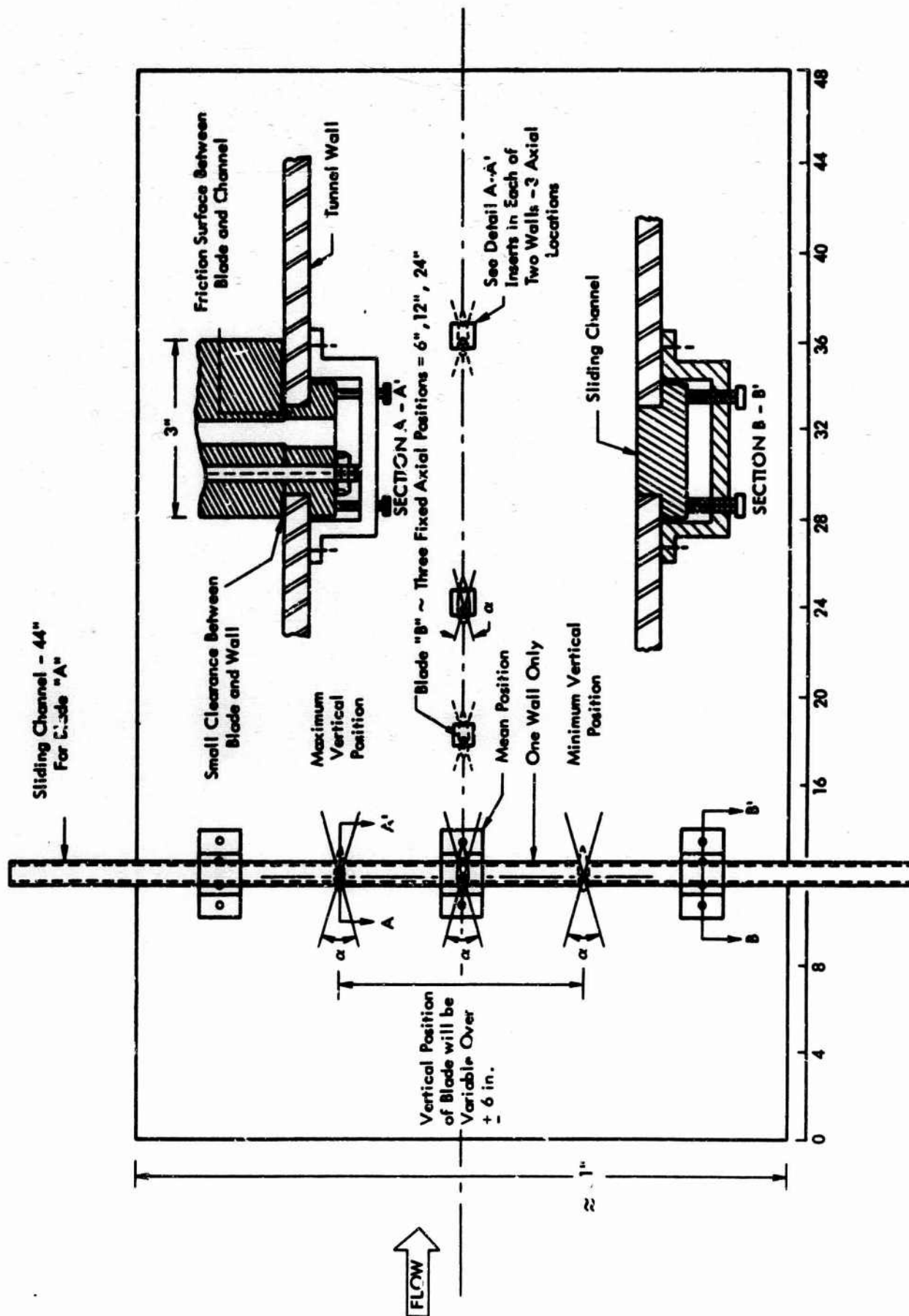


Figure 1-2. Schematic of the Wind Tunnel Model Installation

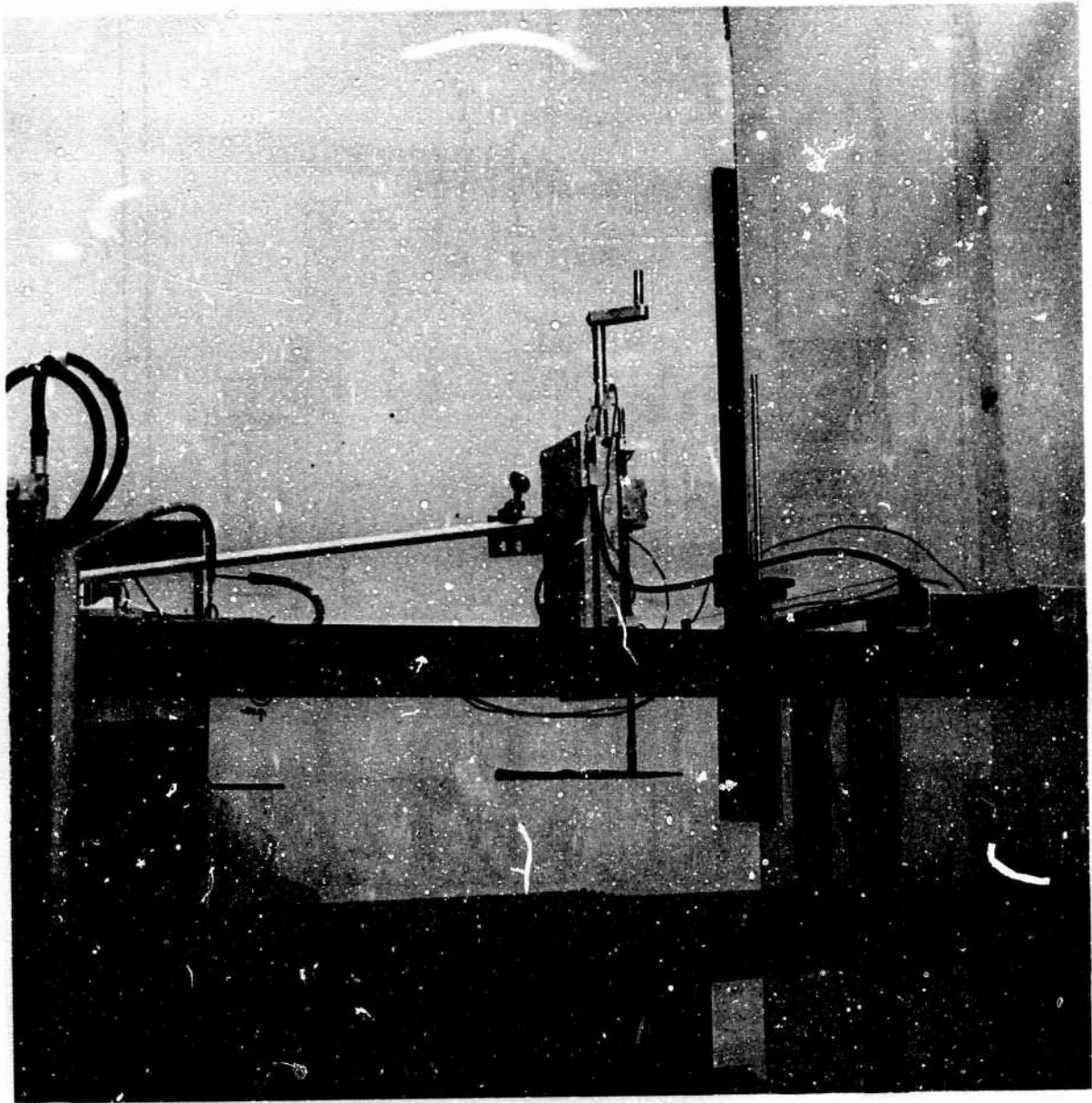


Figure I-3. Photograph of the Wind Tunnel Model Installation showing a Typical Propeller Blade and the Hot-Wire Probe

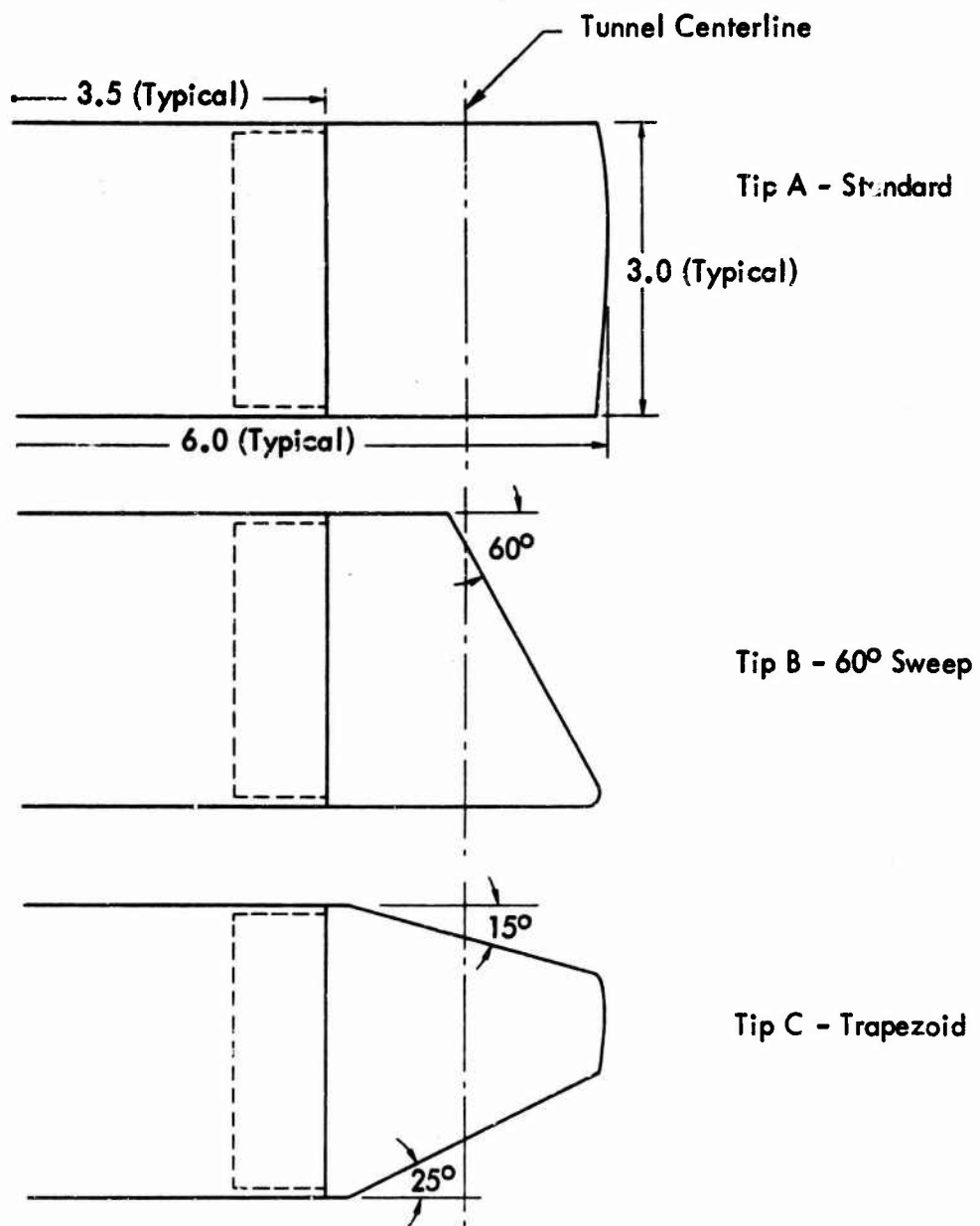


Figure I-4. Plan View of Wind Tunnel Blade Configurations,
Airfoil Section - NACA 0012

SECTION III

FREE-FIELD PROPELLER TEST PROGRAM

1.0 INTRODUCTION

Free-field tests were conducted using various 4-foot diameter propeller configurations to measure the noise field radiated by the propeller and the pressure fluctuations acting on the propeller blades. The objectives of these tests were to obtain data which could be used for direct correlation of the noise field with the aerodynamic and geometric parameters of the propeller operation, direct correlation of the fluctuating loads with the noise field (as required by the theory), and direct correlation of the fluctuating loads with the aerodynamic and geometric parameters. The tests were conducted in the absence of free-stream flow; however, it was felt that the important aero-acoustic properties of propeller noise sources and their relationship to the noise field could be identified using the test stand data together with the wind tunnel test results (as discussed in Section II). A brief summary of the test apparatus and the test procedure and conditions is presented in following sections.

2.0 TEST APPARATUS AND INSTRUMENTATION

2.1 Free-Field Propeller Test Facility

A photograph of the final design of the propeller test facility is shown in Figure I-5. This facility was located in the hazardous test area at Wyle-Huntsville. The test apparatus consisted of a test stand with the propeller drive axis positioned approximately 12 feet above ground level. The following test requirements contributed to the selection of this final design.

- The primary object of the propeller test facility was to provide propeller rotation over an rpm range up to 3150 rpm so that free-field acoustic measurements could be obtained in a plane passing through the axis of propeller rotation. Thus, a cantilevered drive system was selected so that acoustic measurements could be taken at a constant height above the ground and over an angle range (relative to the axis of rotation) from 0 to near 180 degrees.
- To preclude interference between the propeller airstream and the test stand structure, a small-diameter, cantilevered drive assembly was required. The drive assembly positioned the propeller at 1.5 diameter (6 feet) from the test stand support structure. This separation distance between the propeller and facility structure proved to be adequate for the tests.

- Accurate variable rpm control was required over a rotational speed range from 1000 to 3150 rpm. This was achieved using a 74.5 hp hydraulic drive motor.

The development of the facility — its design fabrication, assembly, and check-out — represented a major milestone in the overall research program. The test facility was relatively complex in design since the nature of the test objectives required that the facility be designed to perform several functions simultaneously. In certain areas, the test objectives resulted in conflicting design requirements and, as a result, the final design was the result of a trade-off between facility requirements so that each test objective could be realized. The various components of the facility are discussed in the following sub-sections.

2.1.1 Test Stand

The test stand consisted of (1) a massive reinforced concrete pad and (2) a steel support structure for the motor drive assembly, as shown in Figure I-6. The concrete pad was 10 x 10 feet square and 12 inches thick. The pad was reinforced with 8-inch I-beams strategically located so that the test stand could be welded to the pad structure. The test stand consisted of a 20-inch diameter, schedule 40 steel pipe with 8-inch I-beam braces. A 1-inch steel plate was used to tie the assembly together at the top of the structure, and steel legs, which were welded to the top plate, provided a means of attaching the motor drive assembly to the test stand.

The main support pipe for the test stand was filled with sand to dampen the structure and thus minimize the noise radiation from the structure. Also, 2-inch thick horse-hair batts were taped to the test stand to minimize the reflected noise. The ground surface beneath the propeller was covered with horse-hair batts to minimize ground reflected noise.

2.1.2 Motor Drive Assembly

The motor drive assembly consisted of (1) a hydraulic drive motor, (2) a drive shaft assembly, (3) thrust sensor, and (4) drive housing. The hydraulic motor was a Dennison Model MIC-052-21 vane type motor capable of 74.5 horsepower at a maximum rotational speed of 3600 rpm and maximum pressure of 2500 psia. The output torque was 52.07 in.-lb/100 psi. The hydraulic flow rate for the motor was 1.416 gpm/100 rpm. The drive shaft assembly consisted of two, in-line, shafts. The main drive shaft was supported in the cantilevered housing with a roller bearing with an inner movable race at the propeller end and a thrust bearing at the motor end of the cantilevered housing. Axial loads from the main drive were transmitted through a four-leg thrust sensor. The interconnecting drive shaft was supported on two pillow-block bearings and provided the necessary interconnection between the drive motor and the main drive shaft. Dodge para-flex couplings were used at the interconnections of the drive assembly. The drive shaft assembly was hollow to allow for instrumentation

leads from the propeller-mounted microphones. The slip-ring assembly was connected to the interconnecting drive shaft between the two pillow-block supports (see Figure I-7).

The drive housing consisted of an 8-inch, schedule 80 steel pipe which was cantilevered from an 18-inch, schedule 40 steel pipe which housed the motor and interconnecting drive components. The cantilevered housing was braced with triangular webs and bolted to the larger motor housing. Steel lugs, welded to the motor housing mated with similar lugs on the test stand and steel bolts were used to hold the two assemblies together.

2.2 Propellers

Two basic propeller systems were tested: (1) a variable geometry propeller system designed by Wyle Laboratories, and (2) a fixed geometry Sensenich propeller. The variable geometry propeller was designed to facilitate a range of configurations and test conditions as follows:

- Propeller Diameter — 4 feet
- Blade Number — 2, 3, 4, 6
- Tip Shape — Standard, Swept, Trapezoidal
- Tip Angle — Continuously Variable
- Blade Chord — 3 inches
- Blade Section — NACA 0012
- Blade Twist — 7.5°
- Blade Coning Angle — 1°

A schematic of a typical propeller blade (with standard tip) is shown in Figure I-8. A series of photographs, showing the 2, 4, and 6 blade configurations, blades with various tip shapes, and the disassembled hub are presented in Figures I-9 through I-13. The hub was 8 inches in diameter and was fabricated of aluminum. The blades were steel with a hollow core and the blade tips were aluminum reinforced plastic.

The fixed geometry propeller was a 2-blade, 4-foot diameter Sensenich W 60 LK 18 propeller. The Sensenich propeller was constructed of laminated wood with an aluminum adapter for mating the propeller to the motor drive assembly (see Figure I-14).

2.3 Instrumentation

Instrumentation for the free-field propeller tests consisted of (1) free-field microphones and signal conditioning electronics for measuring the noise radiated by the propellers, and (2) blade mounted microphones and signal conditioning electronics for measuring the fluctuating pressures on the propeller blades. For the free-field measurements, the instrumentation system consisted of the following components:

- B & K Type 4134 Microphone with protective grid
- Standard B & K Electronics for Signal Conditioning
- Ampex Two-Channel Tape Recorder

The microphone was supported on a 12-foot pole with a tripod base which was manually moved to various locations for the required directivity measurements.

The blade-mounted microphones were Kulite CQL-125-5S ultra-miniature pressure sensors having 0.125" diaphragms. The Kulite microphones were manufactured using a monolithic integrated circuit Wheatstone bridge directly formed on a silicon diaphragm. A sealed reference pressure design was employed for the present test. These microphones have a nominal sensitivity of 1.4 mv/v/psi with a diaphragm natural frequency of approximately 70 K Hz. Excitation voltage is 5 v nominal and 10 v maximum. Standard signal conditioning electronics were employed with the exception that microphone signal output was routed through a slip-ring assembly. A Lebow model 6116-12 slip ring assembly was employed. This assembly provided twelve electronic channels with a low noise floor and a flat frequency response for rotational speeds up to at least 3200 rpm. Also, for certain runs, Burr-Brown Model 3071/25 operational amplifiers were housed in the propeller hub for amplifying the signal prior to transmission through the slip-ring assembly. The amplifier package and the slip-ring assembly are shown in Figure I-12.

Failure of all but two of the blade mounted microphones and failure of the hydraulic pump necessitated termination of the fluctuating pressure tests during the check-out and evaluation phase. Thus, data were not recorded on tape since, during check-out, only a graphic level recorder was in use to monitor and record the output of the blade mounted microphones. Microphone locations are given in the main report.

3.0 TEST PROCEDURE AND CONDITION

The test was conducted in three phases: Phase I was a check-out of the motor drive system for the purpose of evaluating the operational characteristics of the motor drive including the no-load noise radiated by the drive system; Phase II consisted of propeller tests for the purpose of measuring the free-field noise; and, Phase III consisted of propeller tests for the purpose of measuring fluctuating pressures on the propeller blades. These phases will be discussed separately.

Phase I — Facility Check-Out

During the facility check-out phase, a number of problems were discovered which necessitated modifications to the basic design of the propeller test facility. The initial design of the motor drive assembly was found to be inadequate. The interconnecting motor drive shaft experienced a critical speed whirl condition at approximately 2700 rpm. Thus, modifications were made which resulted in the design presented in Figures I-5 through I-7. Also, excessive vibration of the test stand was experienced at rotational speeds above 1600 rpm. An additional structural member was added to reinforce the rear support I-beam of the test stand and this eliminated the vibration problem. Following these modifications, the facility appeared to perform to its original design objectives; however, the maximum speed was limited to 2400 rpm so that all test data could be obtained over the lower speed range prior to performing any high speed tests. Failure of the hydraulic pump which supplied high pressure hydraulic fluid to the drive motor necessitated a termination in the test program prior to beginning the high speed tests.

Phase II — Free-Field Acoustic Tests

A number of configurations were tested for the purpose of measuring the noise radiated by the propellers. Test configurations consisted of the Wyle propeller with 2, 3, 4 and 6 blades, at various blade angle settings and at three rotational speeds. The test conditions are summarized in Table III of the main report. A further set of noise data was obtained for the Sensenich propeller at the same speed settings as for the Wyle propeller.

The procedure for the tests was, for a given configuration and microphone location, the rotational speed was set and microphone data was recorded for two minutes while holding the propeller speed constant. The range of speed settings were examined prior to moving the microphone to a new location.

Phase III — Blade Fluctuating Pressure Measurements

Because of the delicate nature of the microphones, extreme care had to be taken in order to obtain blade fluctuating pressure measurements. During the initial tests of this phase, numerous instrumentation problems were encountered which necessitated a number of trial and error studies which included variations in:

- microphone location in the blades
- microphone signal conditioning equipment, and
- microphone calibration procedures

Fluctuating pressure levels on the blades appeared to be approximately 20 dB lower than anticipated such that the signal was near the noise floor of the instrumentation. Various surveys were performed in an attempt to locate the regions of high unsteady blade loading. This necessitated a number of installation and removal cycles on the microphones and all but two instruments eventually suffered mechanical damage. A limited amount of useful data was obtained in the blade tips; however, these data were recorded only in a single channel sequence such that correlation between channels was not possible. The eventual failure of the hydraulic system necessitated termination of the test before useful microphone data could be obtained.



Figure i-5. Photograph of the Free-Field Propeller Test Facility

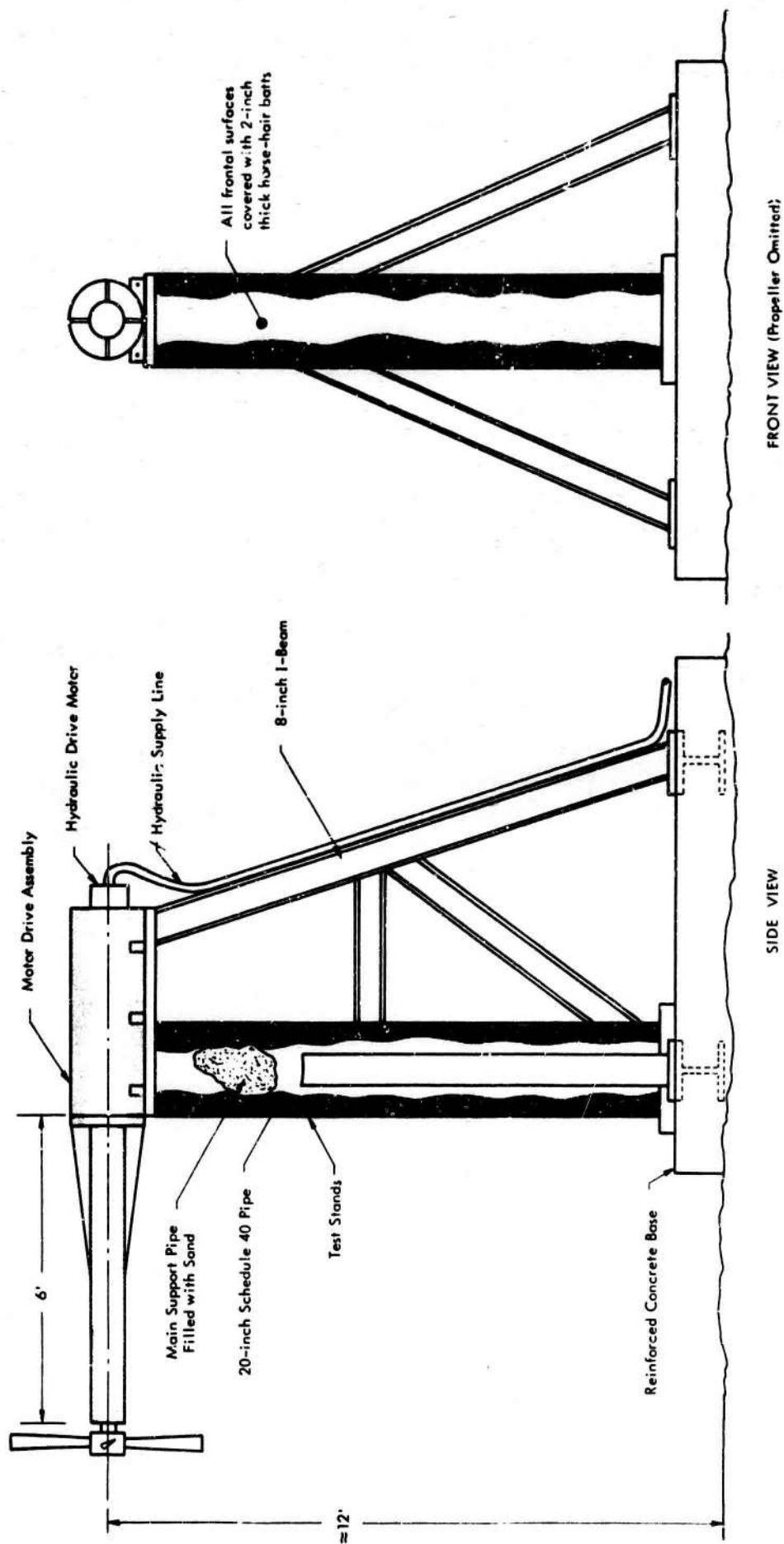


Figure I-6. Schematic of the Free-Field Propeller Test Facility

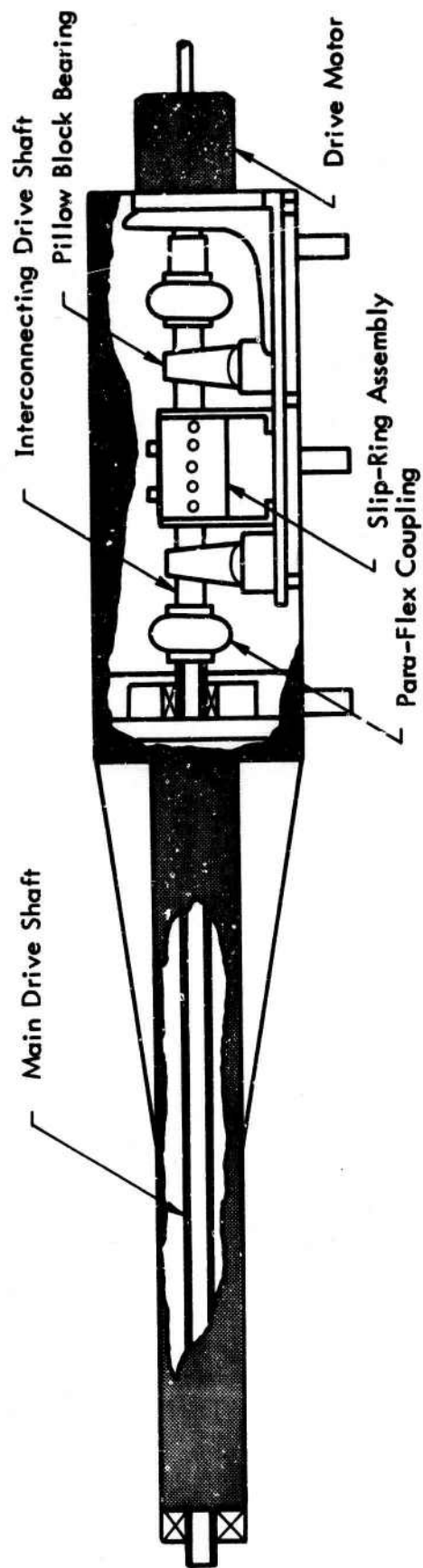


Figure 1-7. Schematic of the Motor Drive Assembly for the Free-Field Propeller Test Facility

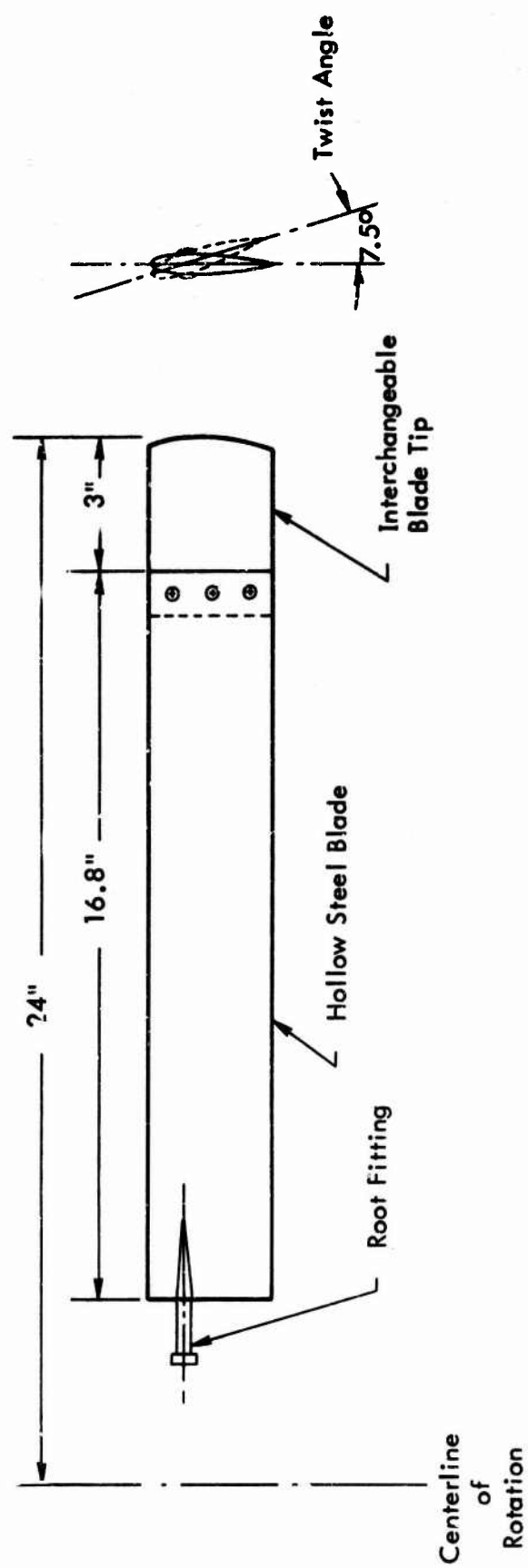


Figure I-8. Details of a Typical Wyle Propeller Blade

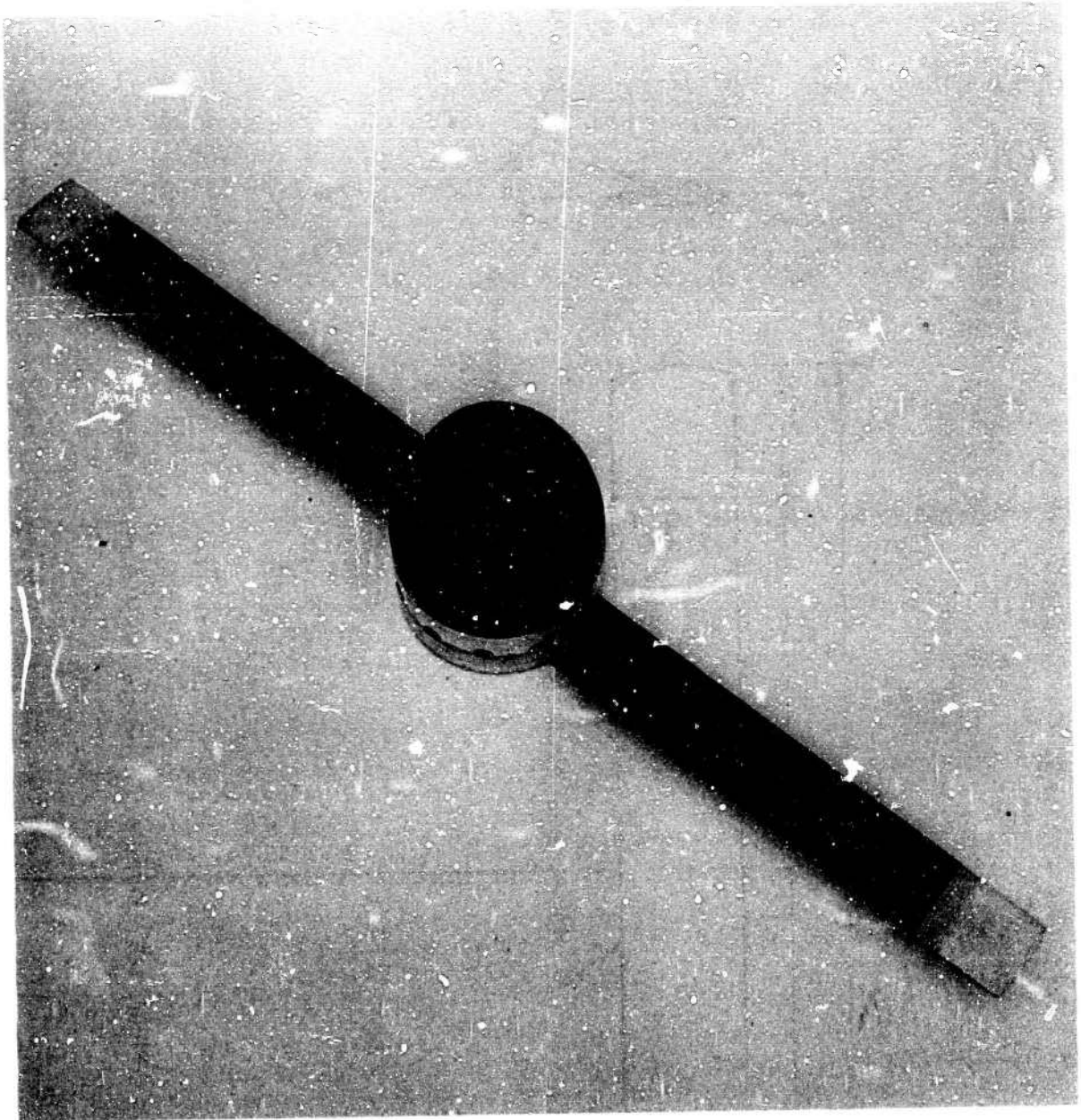


Figure I-9. Photograph of the Wyle 2-Blade Propeller Configuration

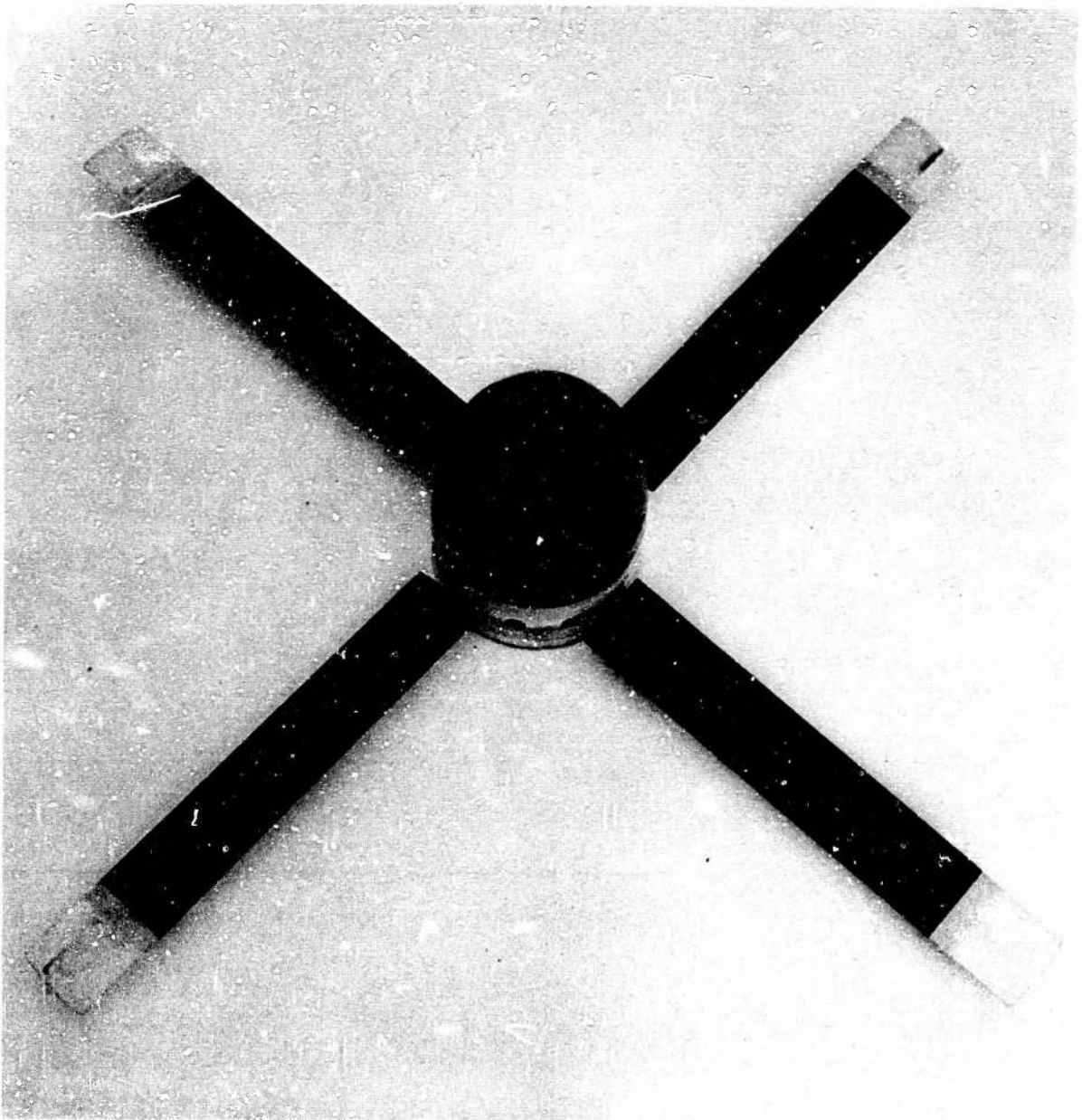


Figure I-10. Photograph of the Wyle 4-Blade Propeller Configuration

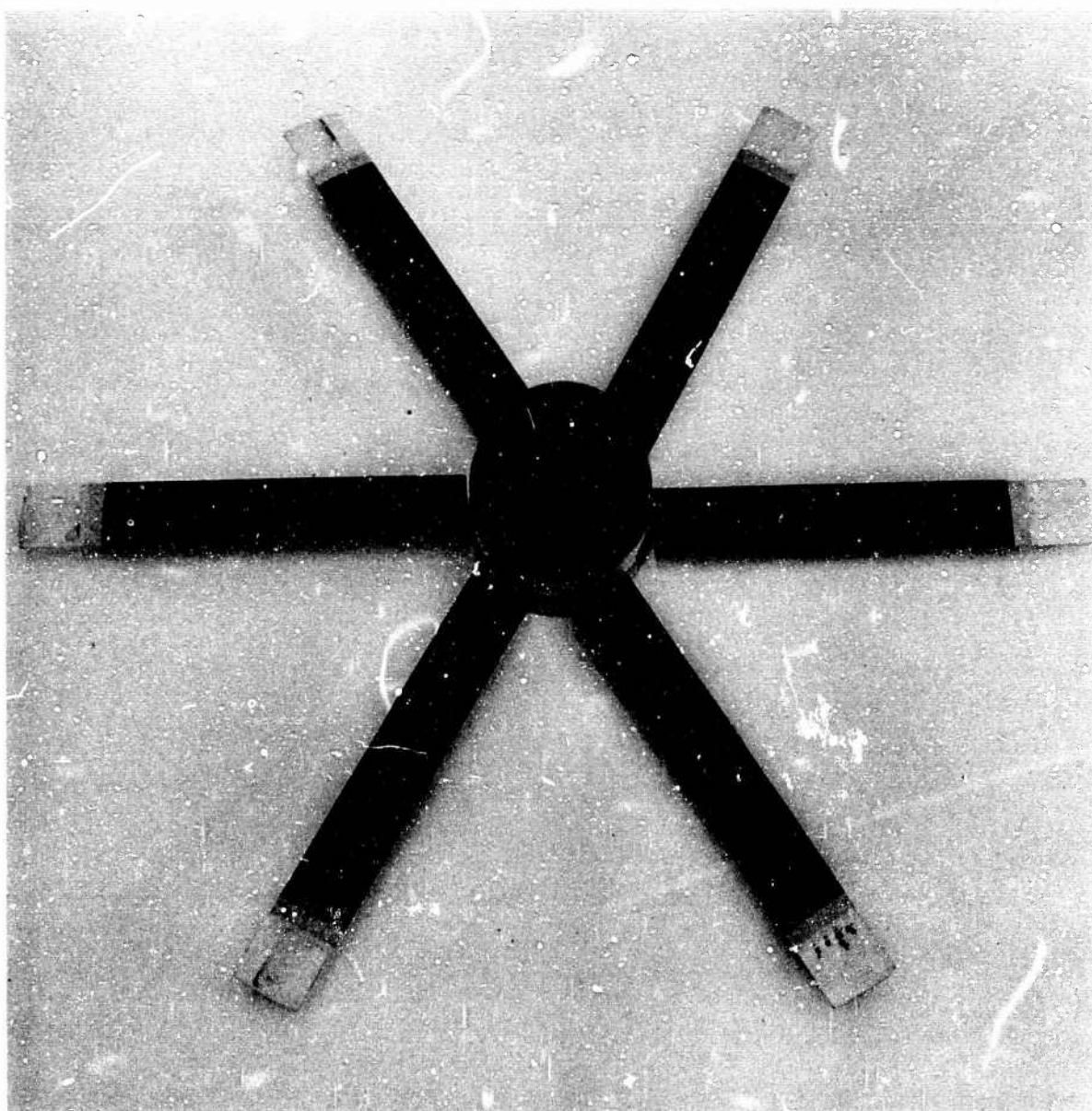


Figure I-11. Photograph of the Wyle 6-Blade Propeller Configuration

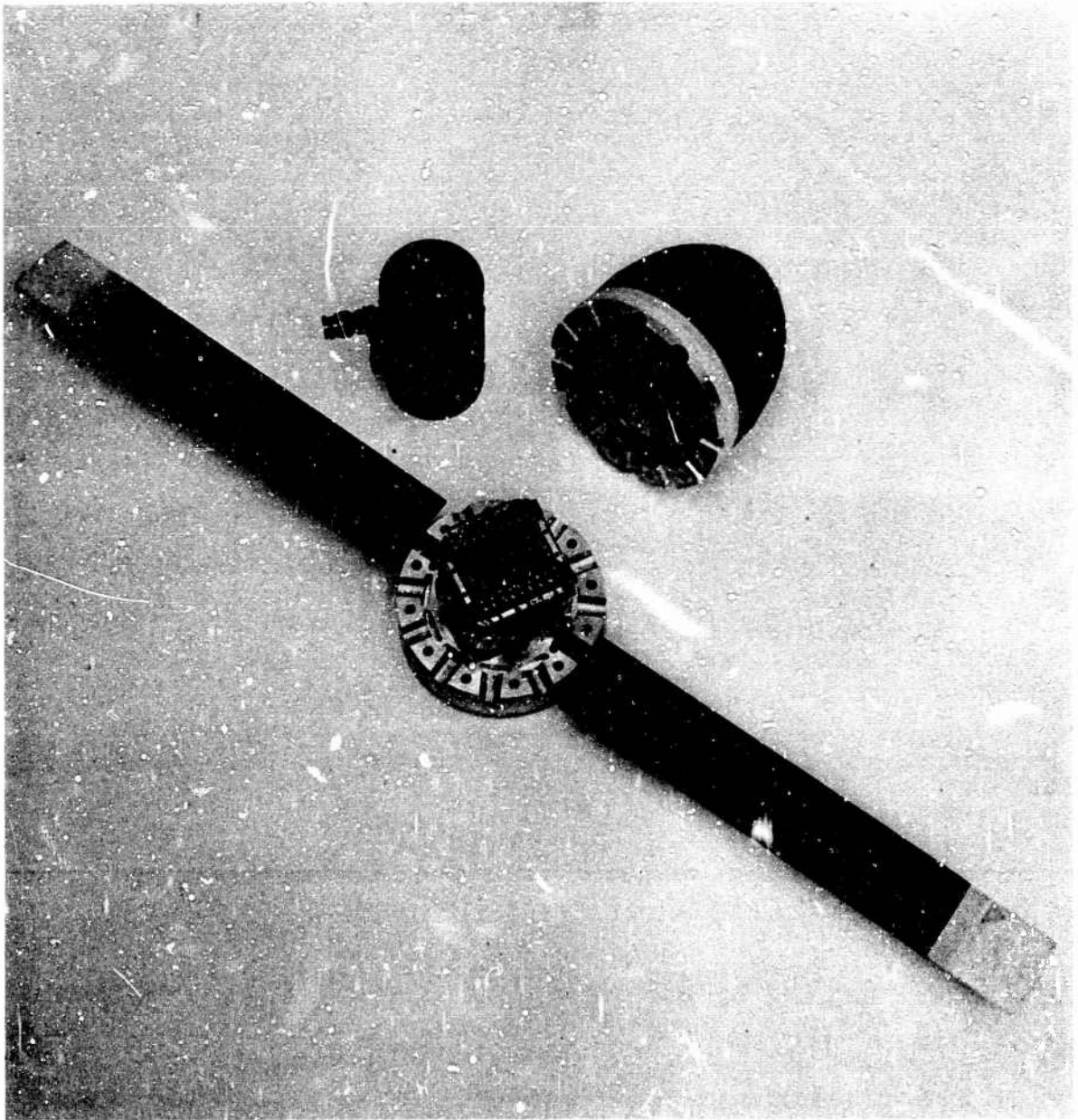


Figure I-12. Photograph of the Wyle 2-Blade Propeller showing the Amplifier Package and Slip-Ring Assembly

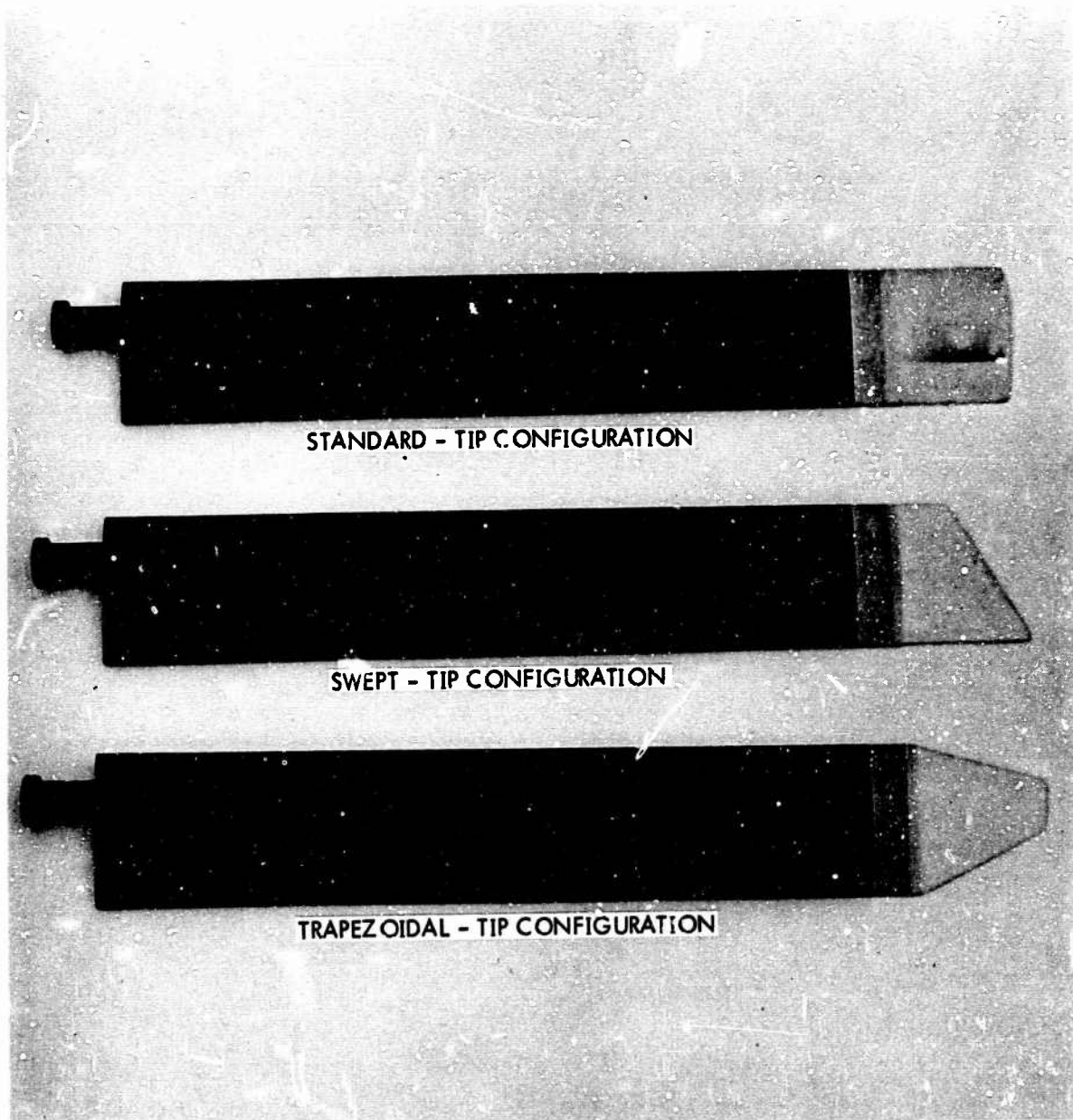


Figure I-13. Photograph of the Wyle Propeller Blades showing the Three Tip Configurations



Figure I-14. Photograph of the Sensenich Propeller

APPENDIX II

EXPERIMENTAL DATA

This Appendix is a compilation of typical basic data samples obtained during the experimental program. Emphasis is given to the tabulation of the propeller noise data in analyzed form, such that the data can be employed for reference in related studies of propeller noise generation. The data presented are categorized as follows:

- Wind Tunnel Test Results
 - Wake Turbulence Surveys
- Propeller Whirl Test Results
 - Broadband Noise Spectra at $M_t = 0.2, 0.3$ and 0.4
 - Harmonic Noise Spectra at $M_t = 0.2, 0.3$ and 0.4

The methods by which the data were obtained, and the appropriate test conditions, are summarized for each data set. Measured spectra of blade surface pressures acquired in the wind tunnel and whirl tests are presented in the main report as Figures 19 and 26, respectively.

WIND TUNNEL TEST RESULTS

Wake Turbulence Surveys

The wake turbulence data shown in Figure II.1 are typical of the direct measurements obtained by automatic scans of a hot wire anemometer probe across the wake of a cantilever mounted blade with a standard blade tip. These measurements were conducted in a wind tunnel of 10" x 30" cross section, at a flow velocity of 150 f.p.s. The free stream turbulence is shown to be of the order of .4%. The data shown represent the streamwise component of the turbulence intensity, defined as \tilde{u}/U_∞ where \tilde{u} is the root mean square value of the fluctuating component of streamwise flow and U_∞ is the free stream mean velocity. These data were obtained at four streamwise stations in the wake of a 3-inch chord, 6-inch semi-span blade of airfoil section approximating to NACA 0012 dimensions, and with a standard blade tip. The blade angle relative to the tunnel axis was incremented from 0° to 12° in steps of 4° in each test.

Similar surveys of \tilde{u}/U_∞ were conducted at one streamwise station in the wake of the blade with a 60° swept tip and with a trapezoidal shaped blade tip. These blade tips replaced the outer 3-inch spanwise section of the previously described blade.

Details of the tip geometries are contained in Figure 7 of the main report. The wind tunnel facility and details of the measurement procedures are described in Appendix I. Characteristic values of the maximum measured turbulence intensities, mean flow variations and wake dimensions are tabulated in the present Appendix as Tables II.1 to II.3. These shed wake and tip vortex data are compiled from the hot wire probe traverse plots at each of the test conditions.

PROPELLER WHIRL TEST RESULTS

Broadband Noise Spectra at $M_t = 0.3$ and 0.4

The broadband noise data compiled in Tables II.4 to II.6 are one-third octave band levels over the frequency range 400-4000 Hz, obtained from 1% bandwidth analysis of the propeller noise recordings and converted for bandwidth by a correction of 13 dB. The noise recordings were obtained on a radius of 12 ft. from the center of each 4 ft. diameter propeller. The azimuthal position of the measurement microphone on this radius is referenced to the propeller forward axis.

The measurement program was conducted at three propeller rotational speeds: 1070, 1605 and 2140 rpm, respectively. Broadband noise data for the lowest speed cases may be influenced by extraneous test-rig noise.

Harmonic Noise Spectra at $M_t = 0.2, 0.3$ and 0.4

The harmonic content of the 1% bandwidth spectra is summarized in Tables II.7 to II.8 for each of the propeller configurations and test conditions described above. Due to the predominant interest in broadband noise during this study, the lower order harmonics have not been analyzed for all test cases. In the region of the propeller axis, the levels of the lower order harmonics were observed to fluctuate by as much as 10 dB during a record history. The levels presented in the tables are considered to be the maxima for each quoted harmonic of the blade passage frequency.

The tabulations are arranged in similar format to the broadband noise data, for each of the propeller geometry variations.

TABLE II.1
MAXIMUM STREAMWISE COMPONENTS OF TURBULENCE INTENSITY
IN WAKE OF WIND TUNNEL TEST BLADE

(Standard Tip Shape)		Inboard Spanwise Distance from Blade Tip (in.)									
Downstream Distance from $\frac{1}{2} c$ x (in.)	Blade Angle α°	3.0				1.5				0.25 *	
		\bar{u}/U_∞	\bar{v}/U_∞	t_w	\bar{w}/U_∞	\bar{u}/U_∞	\bar{v}/U_∞	t_w	\bar{w}/U_∞	\bar{u}/U_∞	t_w
2.44	0	0.071	0.35	0.25	0.080	0.43	0.45	0.45	0.083	0.34	0.25
	4	0.091	0.36	0.25	0.090	0.35	0.25	0.25	0.055	0.42	0.25
	8	0.064	0.25	0.3	0.047	0.38	0.4	0.4	0.04	0.82	0.40
	12	0.050	0.12	0.4	0.04	0.24	0.35	0.35	0.025	1.18	0.50
4.25	0	0.035	0.90	0.5	0.045	0.89	0.55	0.55	0.036	0.91	0.45
	4	0.047	0.91	0.5	0.045	0.87	0.5	0.5	0.049	0.76	0.65
	8	0.045	0.84	0.5	0.048	0.85	0.4	0.4	0.04	0.93	0.85
	12	0.062	0.74	0.6	0.058	0.78	0.5	0.5	0.037	1.13	1.0
10.25	0	0.029	0.96	0.75	0.035	0.92	1.0	1.0	0.027	0.95	0.6
	4	0.031	0.93	0.8	0.035	0.92	0.8	0.8	0.028	0.96	1.35
	8	0.034	0.91	0.8	0.034	0.92	0.6	0.6	0.030	0.96	1.65
	12	0.049	0.87	1.25	0.047	0.92	1.25	1.25	0.032	0.95	1.85
22.25	0	0.015	0.98	0.9	0.015	0.97	0.9	0.9	0.012	0.98	0.85
	4	0.016	0.96	0.8	0.020	0.95	0.75	0.75	0.015	0.97	1.6
	8	0.019	0.94	1.08	0.020	0.95	0.87	0.87	0.016	0.97	2.25
	12	0.026	0.94	1.37	0.026	0.92	1.3	1.3	0.02	0.95	3.0

* Tip Vortex Region chord = 3.0 in., semi span = 6.0 in., NACA 0012 approx.

TABLE II.2
 MAXIMUM STREAMWISE COMPONENTS OF TURBULENCE INTENSITY
 IN WAKE OF SWEEP AND TRAPEZOIDAL TIP BLADES
 (at $x = 10.25$ in.)

Blade Tip Shape	Blade Angle α°	Inboard Spanwise Distance from Blade Tip (in.)							
		3.0				1.5			
		\bar{u}/U_∞	\bar{u}/U_∞	t_w	\bar{u}/U_∞	\bar{u}/U_∞	t_w	\bar{u}/U_∞	t_w
60° Swept	0	0.026	0.96	0.65	0.030	0.97	0.85	0.035	0.95
	4	0.026	0.96	0.77	0.033	0.95	0.80	0.033	0.97
	8	0.029	0.94	0.9	0.025	0.95	0.8	0.051	---
	12	0.04	0.92	1.15	0.039	0.94	1.9	0.012	---
Trape- zoidal	0	0.025	0.94	0.7	0.025	0.96	1.1	0.010	---
	4	0.026	0.94	0.85	0.025	0.95	0.75	0.038	---
	8	0.025	0.94	0.75	0.025	0.94	0.65	0.023	---
	12	0.033	0.92	0.85	0.033	0.94	0.85	0.024	0.97

* Tip Vortex Region

TABLE II.3

MAXIMUM COMPONENTS OF TURBULENCE INTENSITY
IN DIRECTION NORMAL TO BLADE SURFACE

Downstream Distance from $\frac{1}{4} \bar{c}$ x (in.)	Blade Angle α°	Inboard Spanwise Distance from Blade Tip (in.)					
		3.0		1.5		0.25 *	
		\tilde{v}/U_∞	t_w	\tilde{v}/U_∞	t_w	\tilde{v}/U_∞	t_w
10.25	0	0.033	0.8	0.032	1.1	0.017	0.65
	4	0.034	0.9	0.033	0.9	0.031	1.25
	8	0.033	0.7	0.033	0.7	0.033	1.5
	12	0.051	1.15	0.032	0.95	0.039	2.0

* Tip Vortex Region

TABLE II.4

ONE-THIRD OCTAVE BAND LEVELS OF MODEL PROPELLER
BROADBAND NOISE AT 12 FT RADIUS FROM HUB

(Propeller diameter = 4 ft, Blade chord = 0.25 ft,
NACA 0012 section, Linear twist 7.5° from 0.3R to 1.0R)

(a) 2 Blades, Standard Tips, 16° Tip Angle										(W2 STD 16°)			
RPM:		1070				1605				2140			
Angle for Forward Axis (°)		0	30	60	90	0	30	60	90	0	30	60	90
One-Third Octave Band Center Frequencies (Hz)	400	58	59	54	53	--	--	--	--	--	--	--	--
	500	58	60	56	53	70	71	64	61	--	--	--	--
	630	58	61	56	53	73	74	64	61	68	69	66	65
	800	60	61	56	54	74	73	66	60	71	69	67	65
	1000	60	61	56	54	73	73	66	61	75	75	73	69
	1250	60	61	56	54	74	73	66	62	77	75	72	69
	1600	61	61	57	54	74	71	64	62	79	76	72	69
	2000	57	59	56	54	73	70	63	61	76	76	71	70
	2500	56	56	53	53	71	67	62	61	75	74	71	70
	3200	54	55	51	50	68	67	62	61	73	75	71	70
	4000	--	--	--		66	67	62	61	73	75	71	70
5000	--	--	--		--	--	--	--	73	72	71	69	
Overall Band Level		69	70	65	63	82	81	74	71	85	84	80	78

(b) 2 Blades, Standard Tips, 12° Tip Angle													(W2 STD 12°)			
RPM:		1070				1605				2140						
Angle for Forward Axis (°)		0	30	60	90	0	30	60	90	0	30	60	90			
One-Third Octave Band Center Frequencies (Hz)	400	53	50	50	50	--	--	--	--	--	--	--	--			
	500	53	53	50	50	64	52	57	50	--	--	--	--			
	630	55	56	54	52	63	56	60	52	60	62	62	52			
	800	56	56	56	52	69	61	60	53	62	67	64	55			
	1000	59	57	55	51	70	64	61	55	66	70	67	60			
	1250	59	57	54	52	71	65	65	59	73	73	67	60			
	1600	59	58	56	52	71	65	66	58	73	74	72	62			
	2000	56	56	55	51	68	64	65	56	71	74	71	62			
	2500	53	54	52	46	67	63	62	55	69	74	70	61			
	3200	52	53	50	45	63	62	62	54	68	72	68	61			
	4000	--	--	--	--	62	61	62	54	68	72	68	62			
5000	--	--	--	--	--	--	--	--	67	70	67	62				
Overall Band Level		66	65	64	61	78	72	73	65	79	81	78	70			

TABLE II.4 (Continued)

ONE-THIRD OCTAVE BAND LEVELS OF MODEL PROPELLER
BROADBAND NOISE AT 12 FT RADIUS FROM HUB(Propeller diameter = 4 ft, Blade chord = 0.25 ft,
NACA 0012 section, Linear twist 7.5° from 0.3R to 1.0R)

(c) 2 Blades, Standard Tips, 8° Tip Angle										(W2 STD 8°)			
RPM:		1070				1605				2140			
Angle for Forward Axis ($^\circ$)		0	30	60	90	0	30	60	90	0	30	60	90
One-Third Octave Band Center Frequencies (Hz)	400					--	--	--	--	--	--	--	--
	500					58	50	52	50	--	--	--	--
	630					59	55	55	53	64	60	57	64
	800					63	62	56	54	66	63	64	66
	1000					65	66	60	58	69	68	66	69
	1250	(NO DATA)				67	68	60	59	71	71	69	70
	1600					67	68	62	54	73	73	70	71
	2000					66	67	60	56	73	73	70	71
	2500					63	65	58	54	71	71	70	70
	3200					61	63	58	53	71	71	67	69
	4000					60	61	57	50	69	69	67	69
	5000					--	--	--	--	67	67	66	67
Overall Band Level						74	75	70	66	80	80	78	79

(d) 3 Blades, Standard Tips, 8° Tip Angle										(W3 STD 8°)			
RPM:		1070				1605				2140			
Angle for Forward Axis ($^\circ$)		0	30	60	90	0	30	60	90	0	30	60	90
One-Third Octave Band Center Frequencies (Hz)	400	51	52	49	46	--	--	--	--	--	--	--	--
	500	52	53	50	47	50	55	55	50	--	--	--	--
	630	54	55	52	47	53	56	55	50	57	60	59	55
	800	54	56	54	49	55	61	58	52	62	64	59	55
	1000	55	57	54	48	57	61	62	55	64	67	64	60
	1250	57	58	55	48	59	65	61	57	67	70	66	60
	1600	57	59	55	50	62	65	62	57	69	71	66	60
	2000	56	58	55	49	62	65	62	57	69	71	66	60
	2500	54	55	52	48	61	64	61	57	69	72	66	60
	3200	54	55	53	48	60	62	61	57	68	72	67	60
	4000	--	--	--	--	60	62	61	56	68	70	67	60
	5000	--	--	--	--	--	--	--	--	68	69	66	59
Overall Band Level		65	66	63	58	72	73	70	66	77	79	75	69

TABLE II.4 (Continued)

ONE-THIRD OCTAVE BAND LEVELS OF MODEL PROPELLER
BROADBAND NOISE AT 12 FT RADIUS FROM HUB

(Propeller diameter = 4 ft, Blade chord = 0.25 ft,
NACA 0012 section, Linear twist 7.5° from 0.3R to 1.0R)

(e) 4 Blades, Standard Tips, 8° Tip Angle										(W4 STD 8°)			
RPM:		1070				1605				2140			
Angle for Forward Axis (°)		0	30	60	90	0	30	60	90	0	30	60	90
One-Third Octave Band Center Frequencies (Hz)	400	55	45	48	46	--	--	--	--	--	--	--	--
	500	55	48	50	48	50	51	48	50	--	--	--	--
	630	54	50	51	50	52	53	52	54	58	55	52	58
	800	58	53	54	52	54	55	55	54	58	61	56	58
	1000	59	55	54	52	56	60	56	55	60	64	58	58
	1250	57	55	54	52	59	62	56	56	62	65	61	59
	1600	59	55	53	52	62	62	56	57	66	65	63	59
	2000	55	54	52	52	62	61	56	56	67	64	63	59
	2500	51	54	51	48	61	60	56	53	66	64	63	58
	3200	51	52	50	48	60	60	55	52	63	65	62	58
	4000	--	--	--	--	60	58	53	51	63	66	60	58
5000	--	--	--	--	--	--	--	--	62	63	58	57	
Overall Band Level		66	63	62	60	69	69	66	64	73	73	71	68

(f) 6 Blades, Standard Tips, 8° Tip Angle										(W6 STD 8°)				
RPM:		1070				1605				2140				
Angle for Forward Axis (°)		0	30	60	90	0	30	60	90	0	30	60	90	
One-Third Octave Band Center Frequencies (Hz)	400	--				--	--	--	--	--	--	--	--	
	500	--				57	59	56	58	--	--	--	--	
	630	56				59	61	56	58	65	64	60	58	
	800	56				59	61	57	58	66	65	60	59	
	1000	58				60	61	57	56	68	67	61	60	
	1250	60	(NO DATA)				63	61	58	58	69	68	61	61
	1600	61	(NO DATA)				63	65	60	58	71	71	63	62
	2000	60				63	68	58	57	70	72	63	62	
	2500	59				63	68	57	55	70	72	64	60	
	3200	57				64	67	58	55	72	71	64	61	
	4000	--				63	65	56	54	73	71	63	61	
5000	--				--	--	--	--	71	71	63	60		
Overall! Band Level		68				72	75	68	67	79	79	71	70	

TABLE II.4 (Continued)

ONE-THIRD OCTAVE BAND LEVELS OF MODEL PROPELLER
BROADBAND NOISE AT 12 FT RADIUS FROM HUB

(Propeller diameter = 4 ft, Blade chord = 0.25 ft,
NACA 0012 section, Linear twist 7.5° from 0.3R to 1.0R)

(g) 4 Blades, Swept Tips, 8° Tip Angle												(W4 SW 8°)			
RPM:		1070				1605				2140					
Angle for Forward Axis (°)		0	30	60	90	0	30	60	90	0	30	60	90		
One-Third Octave Band Center Frequencies (Hz)	400					--	--	--	--	--	--	--	--		
	500					54	53	53	50	--	--	--	--		
	630					55	56	53	50	63	60	58	58		
	800					58	58	56	53	64	62	61	59		
	1000					60	62	58	54	66	65	64	60		
	1250					63	64	59	55	68	67	65	60		
	1600	(NO DATA)				64	64	62	55	70	69	66	61		
	2000					64	64	60	55	70	69	66	60		
	2500					64	64	60	55	70	69	67	60		
	3200					64	64	61	55	70	69	67	61		
	4000					62	60	59	51	68	66	64	58		
5000					--	--	--	--	66	63	62	56			
Overall Band Level						71				78					

(h) 4 Blades, Trapezoidal Tips, 8° Tip Angle										(W4 TR 8°)			
RPM:		1070				1605				2140			
Angle for Forward Axis (°)		0	30	60	90	0	30	60	90	0	30	60	90
One-Third Octave Band Center Frequencies (Hz)	400					--	--	--	--	--	--	--	--
	500					50	48	47	--	--	--	--	--
	630					53	50	50	--	57	55	56	52
	800					54	52	51	49	58	59	59	55
	1000					57	55	53	51	61	62	60	58
	1250	(NO DATA)				60	58	56	52	63	63	60	59
	1600					63	59	58	53	65	64	61	58
	2000					62	59	59	54	66	64	61	56
	2500					62	59	58	54	66	64	61	56
	3200					61	59	58	53	66	64	60	56
	4000					--	--	--	--	65	62	58	53
5000					--	--	--	--	--	--	--	--	
Overall Band Level						69				74			

TABLE II.4 (Concluded)

ONE-THIRD OCTAVE BAND LEVELS OF MODEL PROPELLER
BROADBAND NOISE AT 12 FT RADIUS FROM HUB

(Propeller diameter = 4 ft, Blade chord = 0.25 ft,
NACA 0012 section, Linear twist 7.5° from 0.3R to 1.0R)

(i) 2 Blades, Trapezoidal Tips, 8° Tip Angle										(W2 TR 8°)			
RPM:		1070				1605				2140			
Angle for Forward Axis ($^\circ$)		0	30	60	90	0	30	60	90	0	30	60	90
One-Third Octave Band Center Frequencies (Hz)	400					--	--	--	--	--	--	--	--
	500					57	54	50	50	60	58	57	57
	630					58	56	54	50	63	60	60	60
	800					61	61	56	53	67	62	60	60
	1000					63	55	59	58	69	67	67	62
	1250					66	68	61	58	71	70	69	69
	1600	(NO DATA)				67	67	61	59	73	73	70	69
	2000					65	67	62	55	72	73	70	67
	2500					64	66	61	55	71	70	70	67
	3200					61	62	60	52	69	70	69	67
	4000					60	60	57	51	69	69	67	67
	5000					--	--	--	--	--	--	--	--
Overall Band Level						74	74	70	67	79	80	77	--

TABLE II.5

ONE-THIRD OCTAVE BAND LEVELS OF SENSENICH
PROPELLER BROADBAND NOISE AT 12 FT RADIUS

(Propeller diameter = 4 ft)

Sensenich W60 LK 18													
RPM:		1070				1605				2140			
Angle for Forward Axis (°)		0	30	60	90	0	30	60	90	0	30	60	90
One-Third Octave Band Center Frequencies (Hz)	400	57	50	45	45	58	--	--	--	--	--	--	--
	500	59	50	45	45	64	60	57	57	65	60	--	--
	630	61	56	54	48	56	62	57	56	67	63	60	54
	800	62	57	55	50	68	64	58	59	72	65	60	56
	1000	61	57	56	50	72	66	60	59	74	67	61	58
	1250	58	57	55	48	69	67	61	61	74	69	63	60
	1600	57	57	54	46	68	67	62	59	75	71	66	60
	2000	53	54	50	45	66	67	62	56	72	71	65	59
	2500	50	45	48	43	63	65	60	53	70	70	65	58
	3200	45	45	45	40	63	61	59	53	69	67	65	59
	4000	--	--	--	--	62	61	59	54	68	67	64	60
	5000	--	--	--	--	--	--	--	--	68	66	65	60
Overall Band Level		68	65	62	57	78	75	70	67	82	78	73	68

TABLE II.6

ONE-THIRD OCTAVE BAND LEVELS OF MODEL PROPELLER
BROADBAND NOISE ON AXIS AT 12 FT RADIUS FROM HUB

(Propeller diameter = 4 ft, Blade chord = 0.25 ft,
NACA 0012 section, Linear twist 7.5° from 0.3R to 1.0R)

Low Blade Angle Cases

RPM:		1070			1605			2140		
Blade Tip Angle ($^\circ$)		4	0	-2	4	0	-2	4	0	-2
One-Third Octave Band Center Frequencies (Hz)	400	57	61	--	--	64	57	--	66	61
	500	59	61	53	--	66	58	--	68	63
	630	61	62	53	--	68	59	--	69	64
	800	62	64	54	--	70	61	64	72	66
	1000	63	67	54	--	71	62	64	76	69
	1250	65	67	55	--	73	63	63	77	69
	1600	68	68	55	--	74	62	68	80	69
	2000	68	65	54	--	73	61	67	80	67
	2500	68	64	53	--	70	58	69	78	66
	3200	61	59	53	--	68	56	66	77	65
	4000	54	52	--	--	68	--	64	75	64
	5000	52	50	--	--	64	--	64	73	--
Overall Band Level		74	75	62	--	82	70	75	87	77

TABLE II.7

**HARMONIC LEVELS OF MODEL PROPELLER NOISE
SPECTRA AT 12 FT RADIUS FROM HUB**

(Propeller diameter = 4 ft, Blade chord = 0.25 ft,
NACA 0012 section, Linear twist 7.5° from 0.3R to 1.0R)

(a) 2 Blades, Standard Tips, 16° Tip Angle										(W2 STD 16°)			
RPM:		1070				1605				2140			
Angle from Forward Axis ($^\circ$)		0	30	60	90	0	30	60	90	0	30	60	90
Harmonic Number (Hz)	1	64	--	--	--	73	--	--	--	--	--	--	--
	2	61	60	54	45	73	--	--	--	--	--	--	--
	4	60	58	53	56	72	70	65	--	76	76	73	67
	8	53	56	55	50	71	65	66	48	79	70	70	67
	12	53	58	52	50	71	64	60	N	78	74	74	N
	16	54	55	50	N	70	65	60	N	77	72	68	N
	20	N	N	N	N	68	N	60	N	76	71	68	N
	30	N	N	N	N	N	N	N	N	67	66	64	N
	40	N	N	N	N	N	N	N	N	65	N	N	N

(b) 2 Blades, Standard Tips, 12° Tip Angle										(W2 STD 12°)			
RPM:		1070				1605				2140			
Angle from Forward Axis ($^\circ$)		0	30	60	90	0	30	60	90	0	30	60	90
Harmonic Number (Hz)	1	--	--	--	--	--	--	--	--	--	--	--	--
	2	55	--	--	--	--	--	--	--	--	--	--	--
	4	56	56	55	43	64	61	54	74				64
	8	55	54	54	45	70	67	57	54	73	74	71	60
	12	54	57	50	44	68	60	59	50	75	74	69	N
	16	54	55	52	N	65	64	57	N	72	73	64	N
	20	53	53	51	N	65	64	59	N	70	69	66	N
	30	51	N	N	N	63	60	N	N	65	63	63	N
	40	50	N	N	N	60	N	N	N	60	N	N	N

N - Not Distinguishable

TABLE II.7 (Continued)

**HARMONIC LEVELS OF MODEL PROPELLER NOISE
SPECTRA AT 12 FT RADIUS FROM HUB**

(Propeller diameter = 4 ft, Blade chord = 0.25 ft,
NACA 0012 section, Linear twist 7.5° from 0.3R to 1.0R)

(c) 2 Blades, Standard Tips, 8° Tip Angle										(W2 STD 8°)			
RPM:		1070				1605				2140			
Angle from Forward Axis (°)		0	30	60	90	0	30	60	90	0	30	60	90
Harmonic Number (Hz)	1	58				63	--	--	--	73	--	--	--
	2	54				62	--	--	--	71	--	--	--
	4	56				64	63	--	--	72	--	--	--
	8	55				64	67	61	54	70	73	68	58
	12	53	(NO DATA)			64	63	59	50	71	72	68	57
	16	51				62	63	57	N	70	71	68	56
	20	N				51	62	58	N	69	70	66	55
	30	N				61	62	58	N	66	66	61	51
	40	N				56	59	N	N	62	62	58	48

(d) 3 Blades, Standard Tip, 8° Tip Angle										(W3 STD 8°)			
RPM:		1070				1605				2140			
Angle from Forward Axis (°)		0	30	60	90	0	30	60	90	0	30	60	90
Harmonic Number (Hz)	1	54	--	--	--	68	--	--	--	70	--	--	--
	2	N	--	--	--	66	--	--	--	69	74	72	--
	4	51	53	52	N	64	65	62	N	70	74	72	N
	8	53	54	53	N	64	61	61	N	69	70	69	N
	12	46	51	50	N	62	60	61	N	70	70	67	N
	16	46	50	48	N	58	61	58	N	66	68	65	N
	20	N	N	N	N	58	60	55	N	64	65	60	N
	30	N	N	N	N	55	N	N	N	59	60	58	N
	40	N	N	N	N	N	N	N	N	N	58	N	N

TABLE II.7 (Continued)

HARMONIC LEVELS OF MODEL PROPELLER NOISE
SPECTRA AT 12 FT RADIUS FROM HUB

(Propeller diameter = 4 ft, Blade chord = 0.25 ft,
NACA 0012 section, Linear twist 7.5° from 0.3R to 1.0R)

(e) 4 Blades, Standard Tips, 8° Tip Angle										(W4 STD 8°)			
RPM:		1070				1605				2140			
Angle from Forward Axis ($^\circ$)		0	30	60	90	0	30	60	90	0	30	60	90
Harmonic Number (Hz)	1	63	--	--	--	62	--	--	--	73	--	--	--
	2	58	--	--	--	61	--	--	--	71	--	--	--
	4	54	--	--	--	63	--	--	--	70	--	--	--
	8	53	54	53	50	61	62	56	51	68	66	63	57
	12	N	52	50	47	61	60	55	50	68	63	62	53
	16	N	49	49	46	60	57	51	N	64	62	64	50
	20	51	48	48	N	57	52	49	N	62	59	63	N
	30	N	N	N	N	N	N	N	N	54	N	N	N
	40	N	N	N	N	N	N	N	N	N	N	N	N

(f) 6 Blades, Standard Tips, 8° Tip Angle										(W6 STD 8°)			
RPM:		1070				1605				2140			
Angle from Forward Axis ($^\circ$)		0	30	60	90	0	30	60	90	0	30	60	90
Harmonic Number (Hz)	1	N	N	N	N	N	N	N	53	68	68	65	N
	2	57	52	52	N	63	60	58	58	73	74	61	N
	4	56	54	52	51	66	63	58	52	73	75	67	63
	8	55	53	51	48	66	63	59	52	74	74	66	61
	12	53	N	N	48	63	63	56	N	68	64	61	56
	16	N	N	N	N	57	N	52	N	65	64	58	51
	20	N	N	N	N	55	N	N	N	N	62	58	N
	30	N	N	N	N	N	N	N	N	N	N	N	N
	40	N	N	N	N	N	N	N	N	N	N	N	N

TABLE II.7 (Continued)

HARMONIC LEVELS OF MODEL PROPELLER NOISE
SPECTRA AT 12 FT RADIUS FROM HUB

(Propeller diameter = 4 ft, Blade chord = 0.25 ft,
NACA 0012 section, Linear twist 7.5° from 0.3R to 1.0R)

(g) 4 Blades, Swept Tips, 8° Tip Angle										(W4 SW 8°)			
RPM:		1070				1605				2140			
Angle from Forward Axis (°)		0	30	60	90	0	30	60	90	0	30	60	90
Harmonic Number (Hz)	1	50	40	50	40	50	57	60	65	73	N	--	--
	2	51	51	51	N	61	64	56	53	73	64	66	62
	4	50	46	45	N	59	59	52	53	68	63	59	54
	8	47	46	47	43	59	55	51	50	67	63	61	53
	12	47	N	47	N	57	55	53	N	64	63	60	53
	16	47	N	47	N	57	54	53	N	64	62	58	N
	20	47	N	N	N	55	54	51	N	60	N	N	N
	30	N	N	N	N	N	N	N	N	N	N	N	N
	40	N	N	N	N	N	N	N	N	N	N	N	N

(h) 4 Blades, Trapezoidal Tips, 8° Tip Angle										(W4 TR 8°)			
RPM:		1070				1605				2140			
Angle from Forward Axis (°)		0	30	60	90	0	30	60	90	0	30	60	90
Harmonic Number (Hz)	1	44	--	40	--	68	53	58	--	71	71	--	--
	2	49	--	44	--	68	54	55	N	64	66	53	51
	4	48	46	45	N	67	65	56	N	64	69	53	53
	8	48	41	43	N	58	51	54	N	69	61	54	53
	12	46	N	N	N	59	49	53	N	67	61	54	N
	16	N	N	N	N	58	50	51	N	62	58	N	N
	20	N	N	N	N	52	N	50	N	59	55	N	N
	30	N	N	N	N	51	N	N	N	55	N	N	N
	40	N	N	N	N	N	N	N	N	N	N	N	N

TABLE II.7 (Concluded)

HARMONIC LEVELS OF MODEL PROPELLER NOISE
SPECTRA AT 12 FT RADIUS FROM HUB

(Propeller diameter = 4 ft, Blade chord = 0.25 ft,
NACA 0012 section, Linear twist 7.5° from 0.3R to 1.0R)

(i) 2 Blades, Trapezoidal Tips, 8° Tip Angle										(W2 TR 8°)			
RPM:		1070				1605				2140			
Angle from Forward Axis ($^\circ$)		0	30	60	90	0	30	60	90	0	30	60	90
Harmonic Number (Hz)	1	56	--	--	--	62	--	--	--	69			
	2	52	50	43	N	60	61	61	60	73			
	4	56	55	N	N	61	61	58	54	70	70	68	60
	8	56	54	N	N	60	61	58	53	69	67	65	57
	12	55	51	N	N	59	61	56	50	68	67	65	55
	16	51	49	N	N	59	57	56	49	68	66	64	54
	20	51	N	N	N	59	57	54	N	66	66	61	50
	30	48	N	N	N	58	57	51	N	62	N	56	49
	40	N	N	N	N	56	N	N	N	N	N	N	N

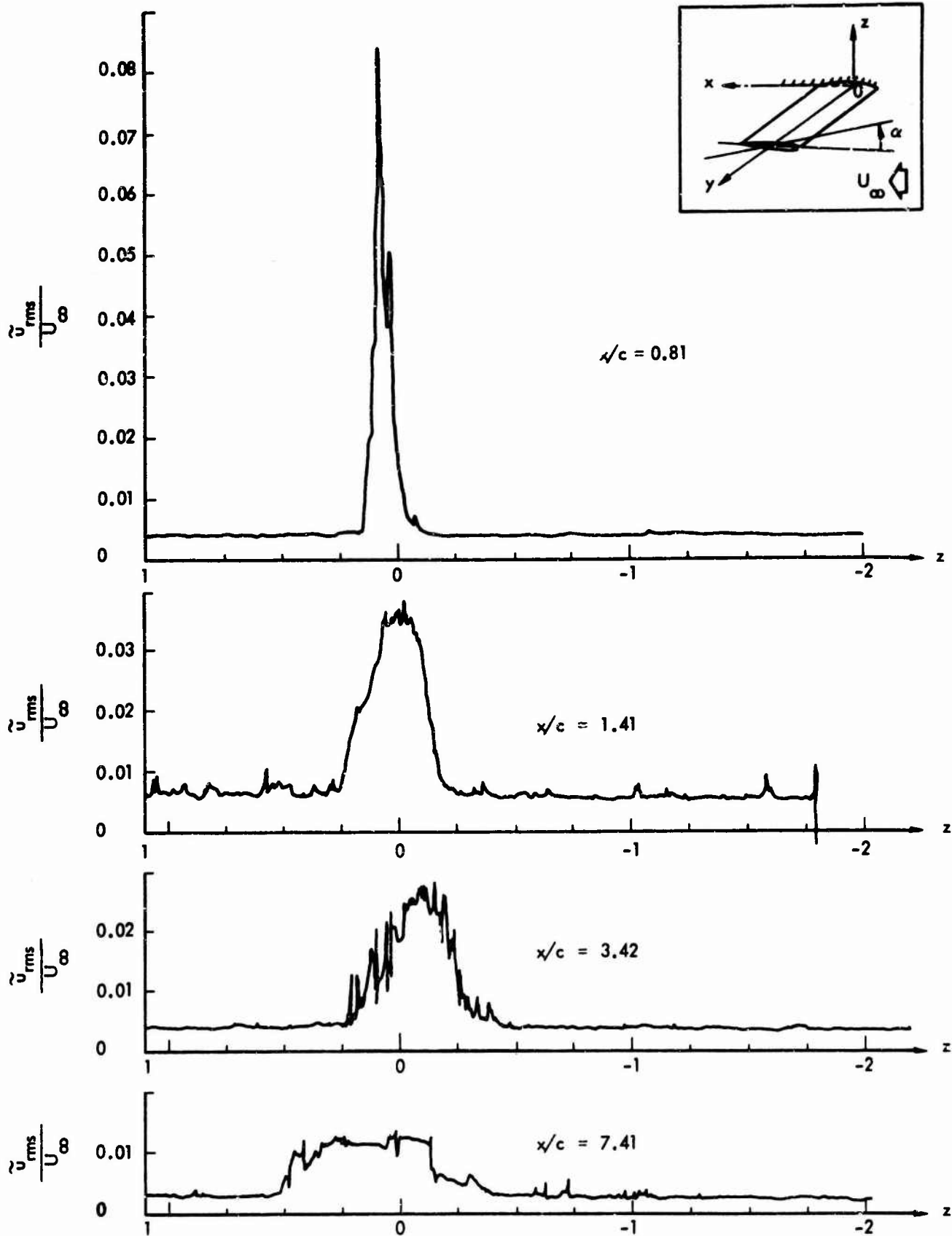
TABLE II.8

HARMONIC LEVELS OF SENSENICH PROPELLER NOISE
SPECTRA AT 12 FT RADIUS FROM HUB

(Propeller diameter = 4 ft)

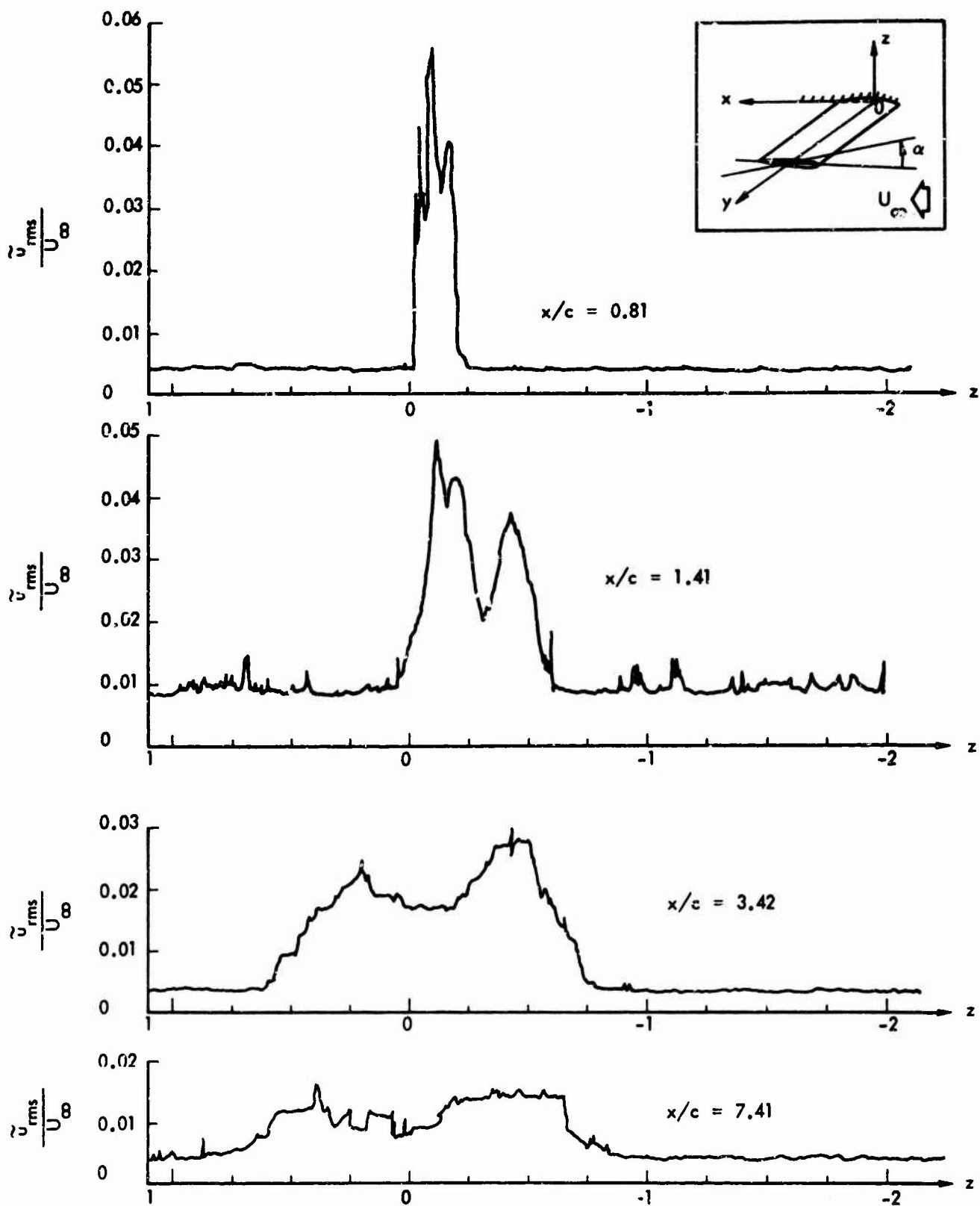
Sensenich W60 LK 18													
RPM:		1070				1605				2140			
Angle from Forward Axis (°)		0	30	60	90	0	30	60	90	0	30	60	90
Harmonic Number (Hz)	1	62		70		74		81	82	80	79	82	80
	2	62		55		74	70	60	67	81	79	78	83
	4	63		54		71	71	60	57	78	76	66	60
	8	62		49		70	65	61	53	78	75	66	55
	12	61		49		70	63	58	52	77	72	68	55
	16	60		50		69	62	59	N	76	69	64	54
	20	57		45		68	62	57	N	73	65	61	54
	30	55		N		65	59	56	N	70	61	58	50
40	51		N		56	N	N	N	68	60	N	N	

N - Not Distinguishable



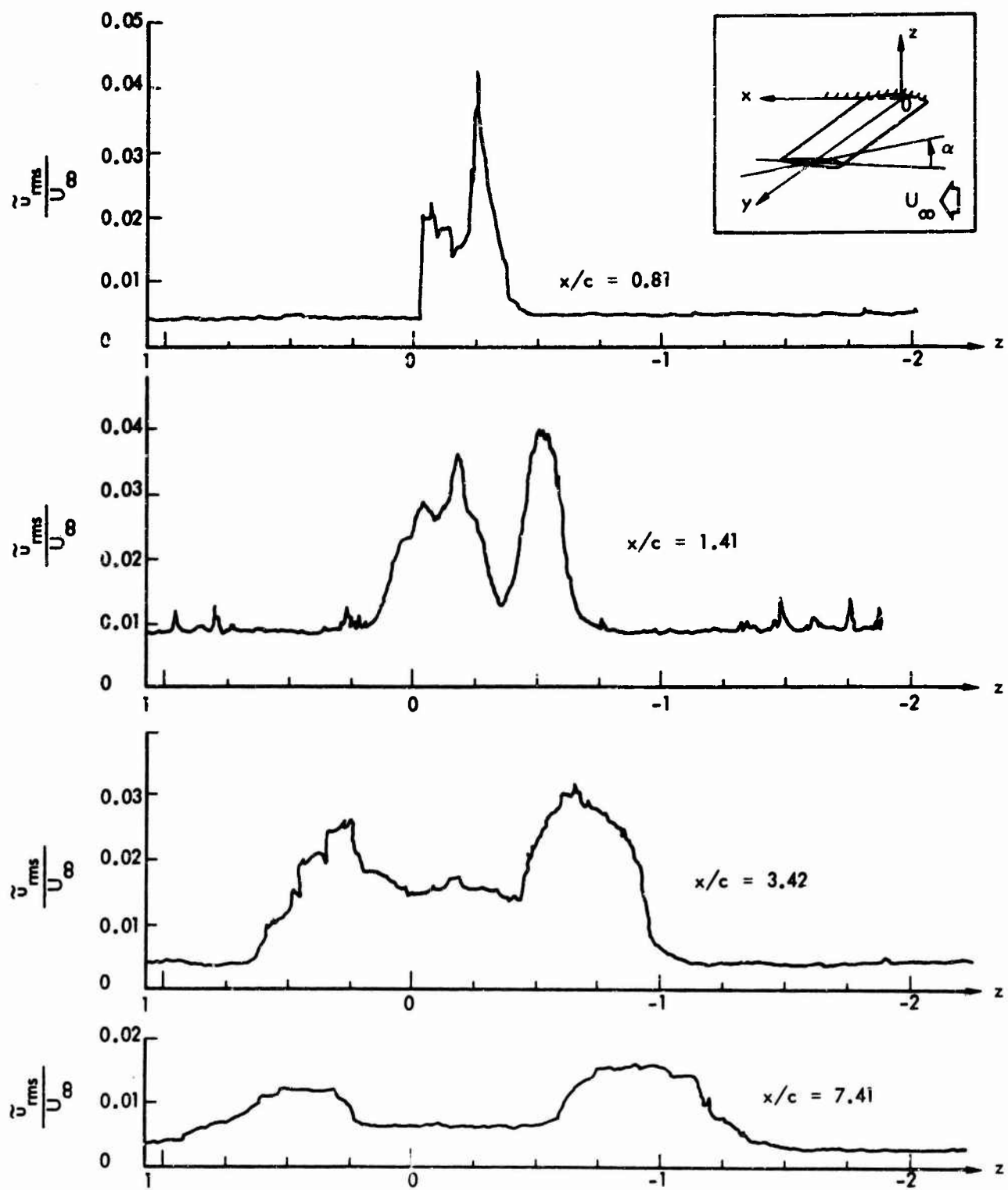
(a) Standard Blade Tip: $\alpha = 0^\circ$; $y = 5.75$ in.

Figure II.1. Turbulence Intensity Distributions at Different Stations Behind a Standard Blade-Tip Assembly. Wind Tunnel Data; $U_\infty = 150$ fps, $c = 3$ inch



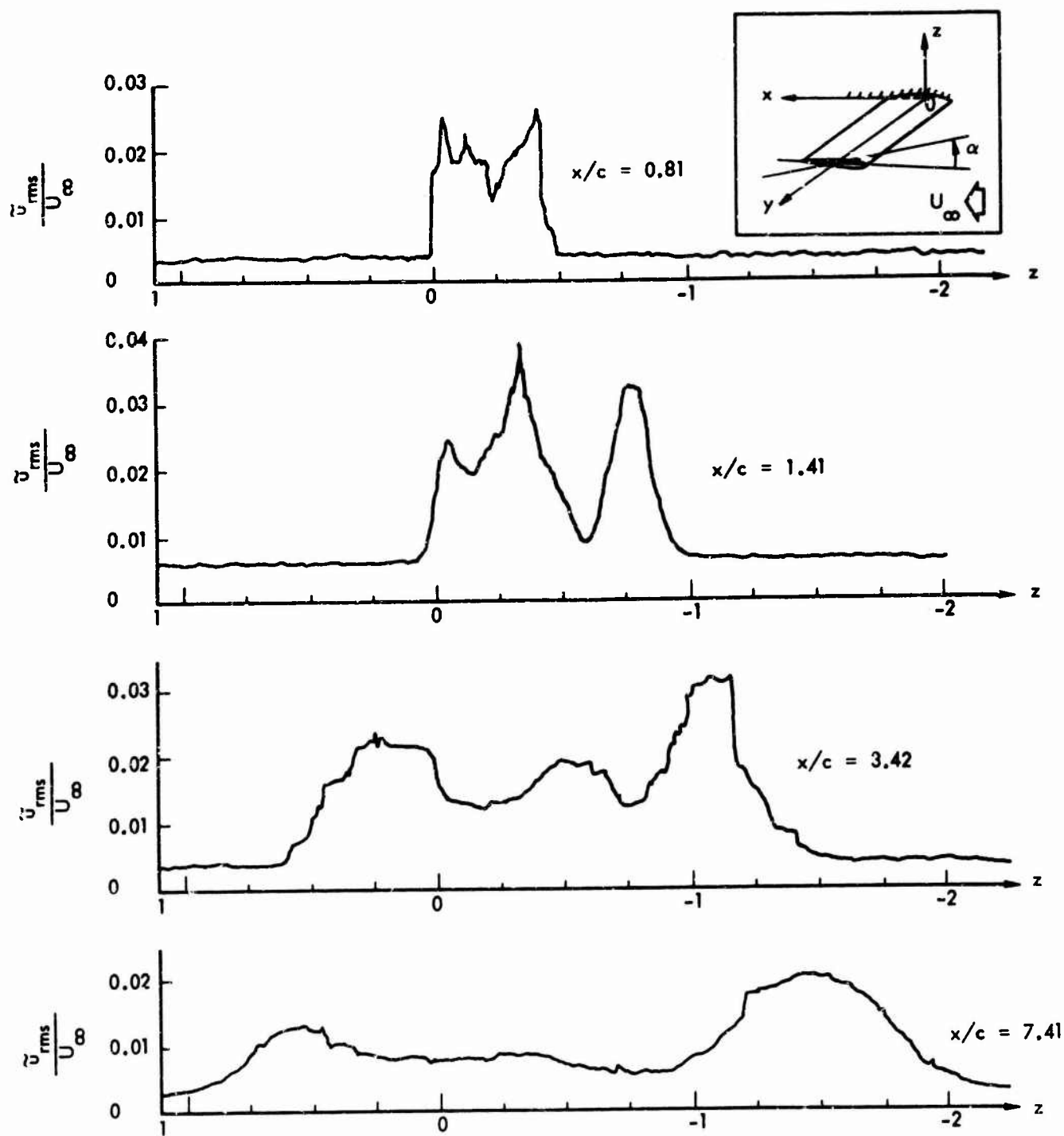
(b) Standard Blade Tip: $\alpha = 4^\circ$; $y = 5.75$ in.

Figure II.1. (Continued)



(c) Standard Blade Tip: $\alpha = 8^\circ$; $y = 5.75$ in.

Figure II.1. (Continued)



(d) Standard Blade Tip: $\alpha = 12^\circ$; $y = 5.75$ in.

Figure II.1. (Concluded)

APPENDIX III

METHODS FOR PREDICTING THE NOISE OF LOW SPEED PROPELLERS

Simplified methods are presented by which three components of propeller noise can be hand calculated. These involve a few straightforward computations and the use of a set of charts (figures III.1 through III.3). The charts have been prepared from machine computations based on equations (35), (46), and (75) in the main text, together with the optimized expressions for the aerodynamic loading terms. The three components are the harmonic sound generated by steady blade forces (Gutin), the harmonic sound generated by unsteady blade forces, and the random vortex noise component. For the convenience of summing the three terms, the random component is calculated as a spectrum level (constant 1 Hz bandwidth). However, instructions are provided for the conversion of the final result to octave or 1/3 octave band levels for comparison with the more commonly available experimental data. The methods are applicable to low tip speeds in the range $0.2 < M_t < 0.6$ although the accuracy of the results at the high end of this range is unknown. Also, levels will be underestimated for blade thrust coefficients ($C_{T_b} = T / \frac{1}{2} \rho_0 U_t^2 A_b$) less than about $0.1\sqrt{B}$ by an error which increases with diminishing C_{T_b} . This region should be avoided in a quiet propeller design because wake interference can cause an increase in noise radiation.

The propeller configuration and performance data required by the following procedures are as follows:

- Rotational tip Mach Number $M_t = \frac{\text{RPM}}{60} \times \frac{2 \pi R}{a_o}$
where a_o is the speed of sound.
- Propeller thrust T lb
- Propeller torque or power Q or P ft. lb or ft. lb./sec.
- Disc area A ft.²
- Total blade area A_b ft.²
- Blade chord at the 80% radius c ft.
- Number of blades B
- Distance of observer from the propeller hub (must be greater than 2 propeller diameters) r ft.
- Angle between the axis of rotation and the hub-to-observer vector θ

Note: For a propeller moving along the axis of rotation, adequate results are obtained by these methods provided the sound is calculated relative to the instantaneous position of the propeller (i.e., no attempt should be made to determine the earlier position of the aircraft when it generated the sound) and the appropriate forward flight loads are used.

Two sets of charts are presented which correspond to static (low inflow) and forward flight (high inflow) operation. These have been computed for thrust-to-in plane force ratios (in plane force = torque \div 0.8R) of 10 and 2 respectively. The main difference between the two cases occurs near the propeller disc plane and results for other ratios can probably be obtained with sufficient accuracy by interpolation.

1. HARMONIC RADIATION BY UNSTEADY LOADS

The harmonic noise spectrum at the observer position r, θ is obtained from figure III.1, which give relative levels L'_n of certain harmonics ($n = 2, 4, 8, 16, 32, 64$ and 128) for the tip rotational Mach Numbers $0.2, 0.4$ and 0.6 . Results for intermediate speeds must be obtained by interpolation. Each level read from the charts is adjusted according to the correction

$$L_n = L'_n + 20 \log_{10} \left(\frac{T}{100} \right) - 20 \log_{10} \left(\frac{r}{100} \right) - 10 \log_{10} \left(\frac{A}{10} \right) - 10 \log_{10} \left(\frac{B}{2} \right) \quad (A1)$$

The corrected values L_n should then be plotted against n (the latter preferably on a logarithmic scale) and a smooth curve faired through the points. The appropriate individual harmonic levels L_{mB} may then be read from this curve at all harmonic numbers mB (m is the harmonic number related to the blade passage frequency). Alternatively, the curve may be plotted directly on an absolute frequency scale $n f_0$, where f_0 the disc frequency, is $M_t a / 2\pi$

2. HARMONIC RADIATION BY STEADY LOADS

This component, defined G_n , increases in importance with tip speed and angle from the axis of rotation but generally has little influence beyond the first few harmonics. These levels are calculated (for mB up to 20) by the formula

$$G_{mB} = F_{mB} (M \sin \theta) + 20 \log_{10} (mB M) + 10 \log_{10} (\cos \theta - D/TM)^2 + 20 \log_{10} \left(\frac{T}{100} \right) - 20 \log_{10} \left(\frac{r}{100} \right) - 10 \log_{10} \left(\frac{A}{10} \right) + 103.6 \quad (A2)$$

Where $M = 0.8 M_t$ and $F_{mB} (M \sin \theta)$ is read from Figure III.2. Note that the thrust-to-in-plane force ratio T/D appears explicitly in the above expression.

Any terms L_{mB} which are smaller than the steady source terms G_{mB} are then replaced by G_{mB} .

3. RANDOM (VORTEX) NOISE RADIATION

Figure III.3 gives the spectrum level $w(f)$ of the random noise component at seven octave intervals about the center frequency $f_c = 0.35 Ma_0/c$ for the Mach numbers 0.2, 0.4 and 0.6. The band level $B(f)$ defining the level in any desired bandwidth Δf is calculated by the equation

$$B(f) = w(f) + 20 \log_{10} \left(\frac{T}{100} \right) + 10 \log_{10} c - 20 \log_{10} \left(\frac{r}{100} \right) - 10 \log_{10} \left(\frac{A_b}{10} \right) - 10 \log_{10} \left(\frac{B}{2} \right) + 10 \log_{10} \Delta f \quad (A3)$$

where $w(f)$ is read from figures III.3 through III.6 as a function of θ , M and f/f_c . For direct comparison with the harmonic data, a bandwidth Δf equal to the disc frequency f_c should be used. The band levels may then be plotted, at the frequencies $f_c/8$, $f_c/4$, $f_c/2$, f_c , $2f_c$, $4f_c$ and $8f_c$, directly over the harmonic results since the energy levels are equivalent.

4. CALCULATION OF COMPOSITE BAND LEVELS

The harmonic spectrum envelope and the spectrum level of the random noise (with a bandwidth equal to f_c) may be added together directly (i.e. decibel summation on an energy basis) to give the combined spectrum level. Conversion to one third octave band levels may be accomplished with sufficient accuracy in the high frequency by adding the increment $(10 \log_{10} f - 6.5)$ dB. This approximation breaks down at low frequencies where a 1/3 octave bandwidth ($= 0.23f$) reduces to the order of the blade passage frequency Bf_c . In this region each band must be inspected to determine whether or not a harmonic is present to be added to the broadband "background." Octave band levels may be obtained by the same procedure using the correction $(10 \log_{10} f - 1.5)$ dB or with greater accuracy by the appropriate summation of one third octave band levels.

5. EXAMPLE

As an example the noise spectrum will be calculated for a hypothetical propeller under the following conditions ($a_0 = 1117$ ft./sec.):

$M_t = 0.4$	$A = 20 \text{ ft}^2$	$B = 3$
$T = 50 \text{ lb}$	$A_b = 4 \text{ ft}^2$	$r = 50 \text{ ft}$
$P = 8 \text{ HP}$	$c = 0.5 \text{ ft}$	$\theta = 30^\circ$

The propeller radius $R = \sqrt{A/\pi} = 2.52 \text{ ft}^2$

In-plane force $F = \text{Power} \div \text{velocity at } 0.8 \text{ radius}$
 $= 8 \times 550 / 0.8 \times 0.4 \times 1117$
 $= 12.3 \text{ Lb.}$

And the ratio $T/D = 50/23.3 = 4.06$
 $= M_t A_o / 2\pi R = 28.2 \text{ Hz}$

(Therefore blade passage frequency $= Bf_o = 84.6 \text{ Hz.}$)

(a) Harmonic Radiation by Unsteady Loads

From equation (A1)

$$\begin{aligned} L_n &= L_n' + 20 \log_{10} \left(\frac{T}{100} \right) - 20 \log_{10} \left(\frac{r}{100} \right) - 10 \log_{10} \left(\frac{A}{10} \right) - 10 \log_{10} \left(\frac{B}{2} \right) \\ &= L_n' - 6.0 \quad + 6.0 \quad - 3.0 \quad - 1.8 \\ &= -5 \text{ dB} \end{aligned}$$

At $\theta = 30^\circ$ the curves for $T/D = 2$ and $T/D = 10$ are coincident in Figures III.1 and III.3.

From Figure III.1

$n = mB$	$f_{mB} = mBf_o$	L_n' dB SPL	L_n dB SPL
2	56.5	61	56
4	113	60	55
8	226	59	54
16	451	57	52
32	902	52	47
64	1805	44	39
128	3610	36	31

(b) Harmonic Radiation by Steady Loads

$M = 0.8 M_t = 0.32$

$$\begin{aligned} 10 \log_{10} \left(\cos \theta - \frac{D}{TM} \right)^2 + 20 \log_{10} \left(\frac{T}{100} \right) - 20 \log_{10} \left(\frac{r}{100} \right) - 10 \log_{10} \left(\frac{A}{10} \right) + 103.6 \\ = -20.2 - 6.0 + 6.0 - 3 + 103.6 \\ = 80.4 \end{aligned}$$

Therefore, from Equation A2

$$G_{mB} = F_{mB} (M \sin \theta) + 20 \log_{10} (mBM) + 80.4$$

And, using Figure I.2

mB	mBM	20 log mBM dB	F _{mB} Msin θ dB	G _{mB} dB SPL
3	.96	-0.4	-26	54
6	1.92	+5.6	-48	38
9	2.88	+9.2	*	

(c) Random Noise Radiation

$$f_c = 0.85 M_0 / c = 760 \text{ Hz}, \Delta f = f_0 = 28.2 \text{ Hz}.$$

From Equation A3

$$\begin{aligned} B(f) &= w(f) + 20 \log_{10} \left(\frac{T}{100} \right) - 20 \log_{10} \left(\frac{r}{100} \right) - 10 \log_{10} \left(\frac{B}{2} \right) \\ &\quad + 10 \log_{10} c + 10 \log_{10} \Delta f - 10 \log_{10} \left(\frac{A_b}{10} \right) \\ &= w(f) - 6.0 + 6.0 - 1.8 - 3.0 + 14.5 + 4.0 \\ &= w(f) + 13.7 \end{aligned}$$

Using Figure III.3:

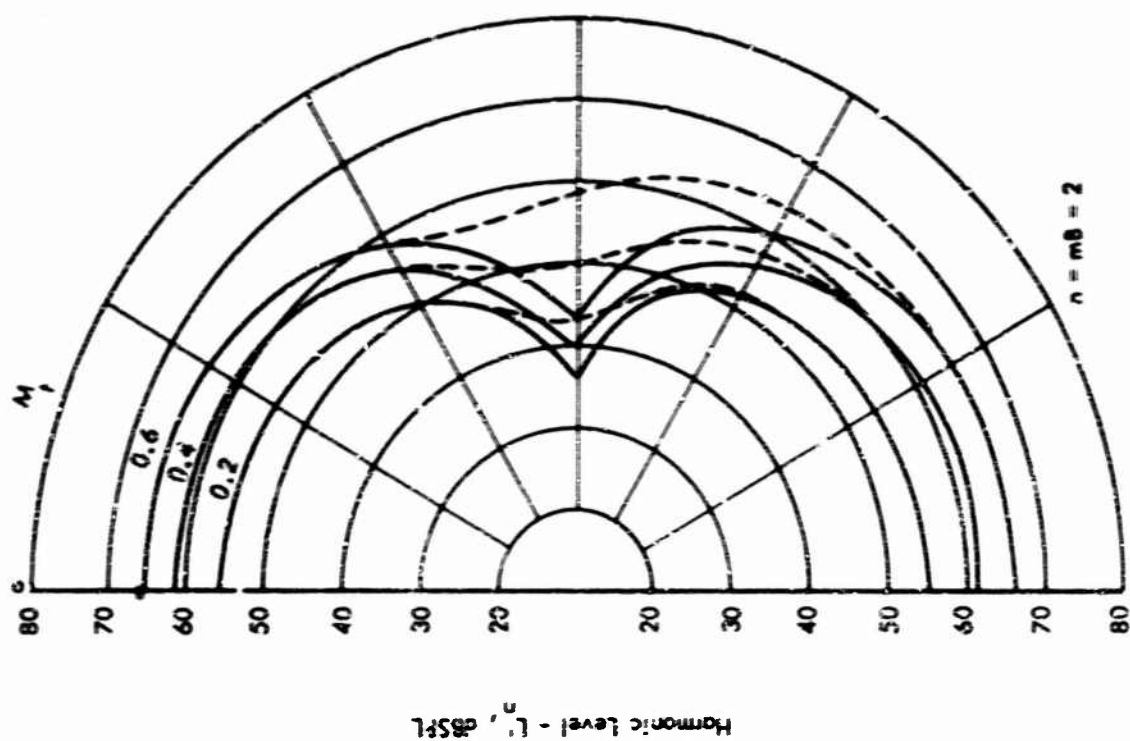
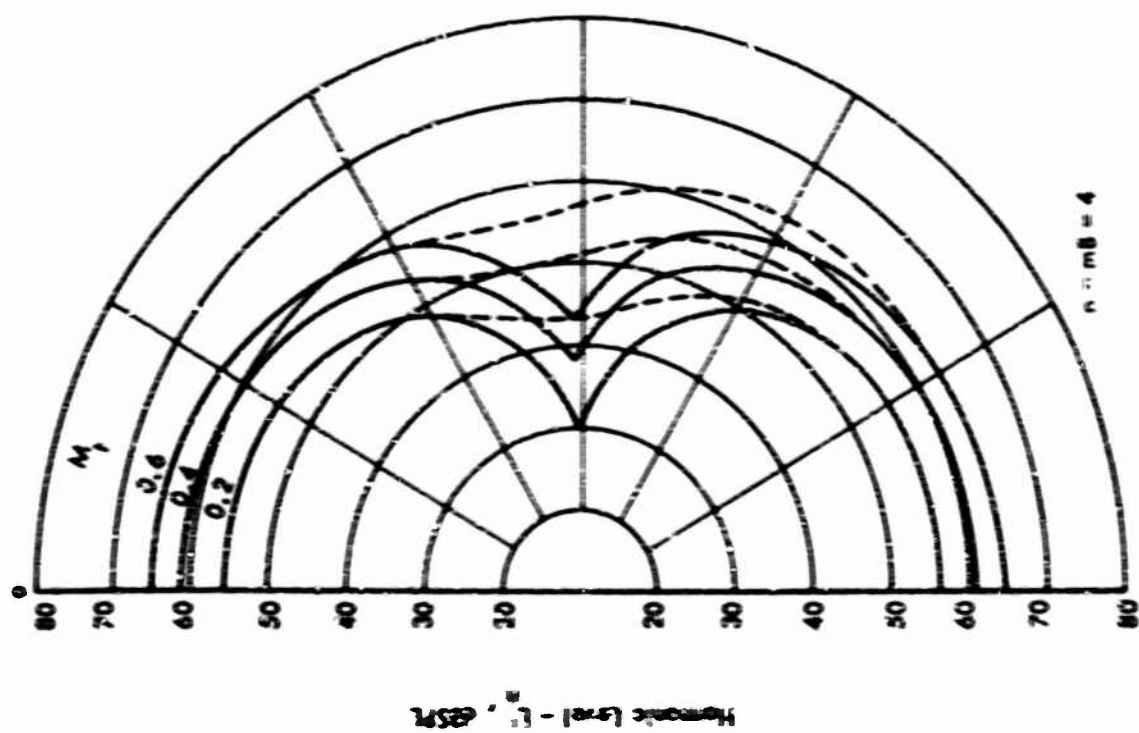
f/f_c	f Hz	w(f) dB	B(f) dB SPL
1/8	95	10	24
1/4	190	18	32
1/2	380	24	38
1	760	27	41
2	1520	25	39
4	3040	19	33
8	6080	11	25

(d) Spectrum Plot

The contributions from the three components to the total observed spectrum are identified separately in Figure III.4. The computed harmonic levels (a) for frequencies corresponding to $mB = 2, 4, 8, 16$, etc., are plotted and connected by a curve which represents the envelope of the harmonics generated by unsteady blade loads. The first ten harmonics have been drawn correctly, as spikes.

The steady source terms could only be calculated for the first two harmonics ($mB = 3$ and 6) and in both cases can be ignored since they are lower than the "unsteady" levels.

The random spectrum is also shown as a curve connecting the seven computed values. Since this represents the level measured in a bandwidth equal to the interharmonic spacing (f_0) it is compatible with the harmonic envelope on an energy basis.



--- } Thrust-to-in-plane force ratio $1/F$
 --- } $\frac{2}{10}$

Figure III.1.1. Harmonic Noise Levels Due to Unsteady Blade Forces

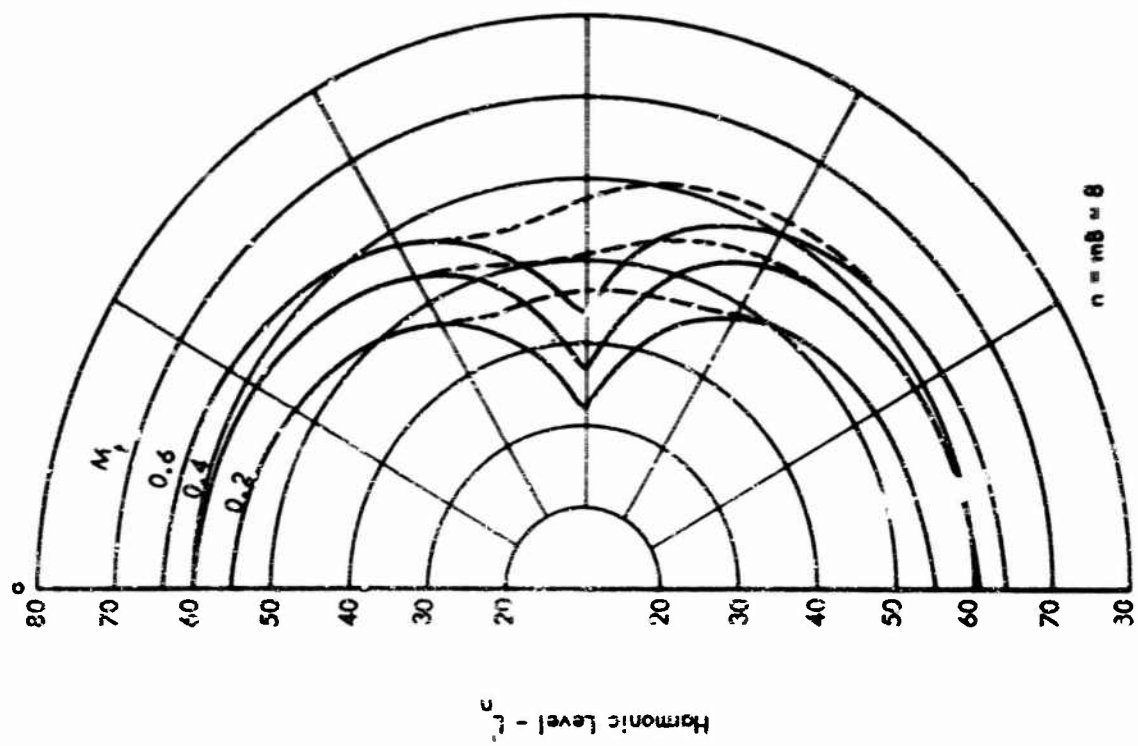
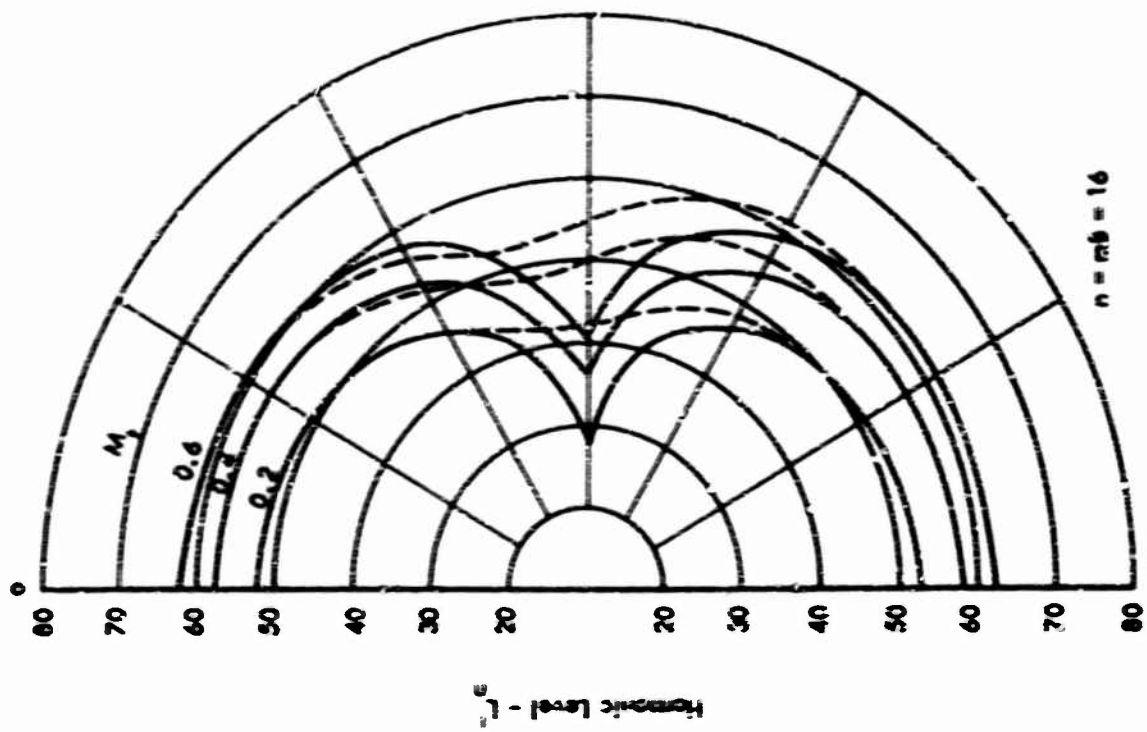


Figure III.1. (Continued)

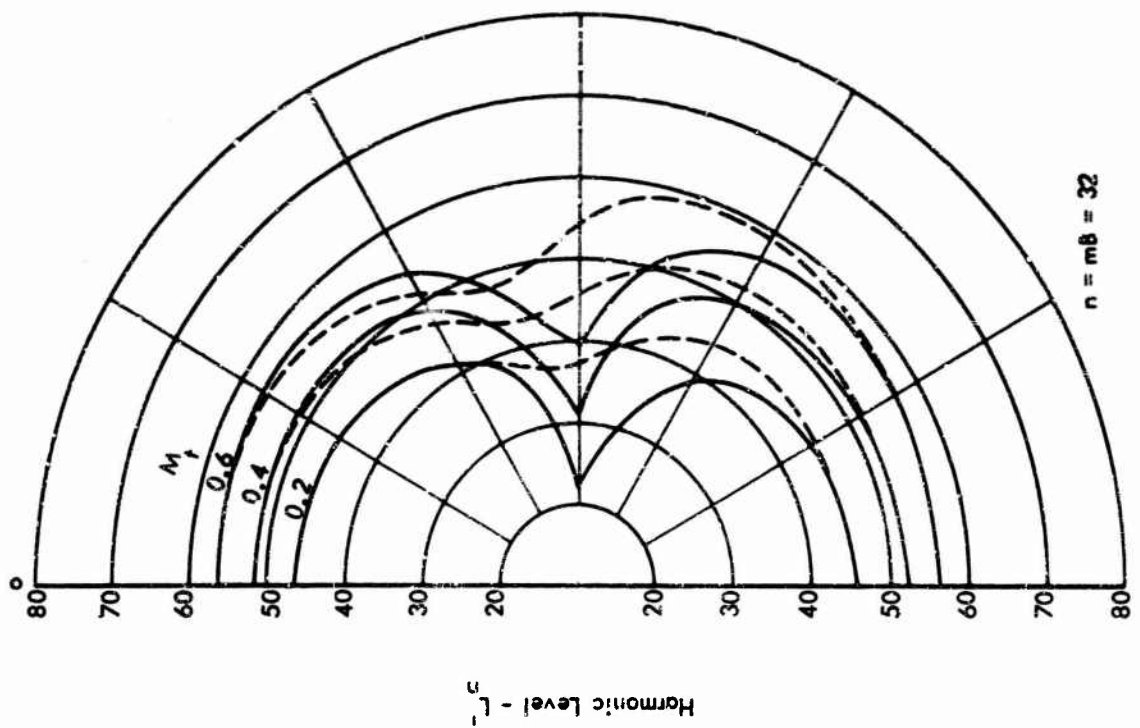
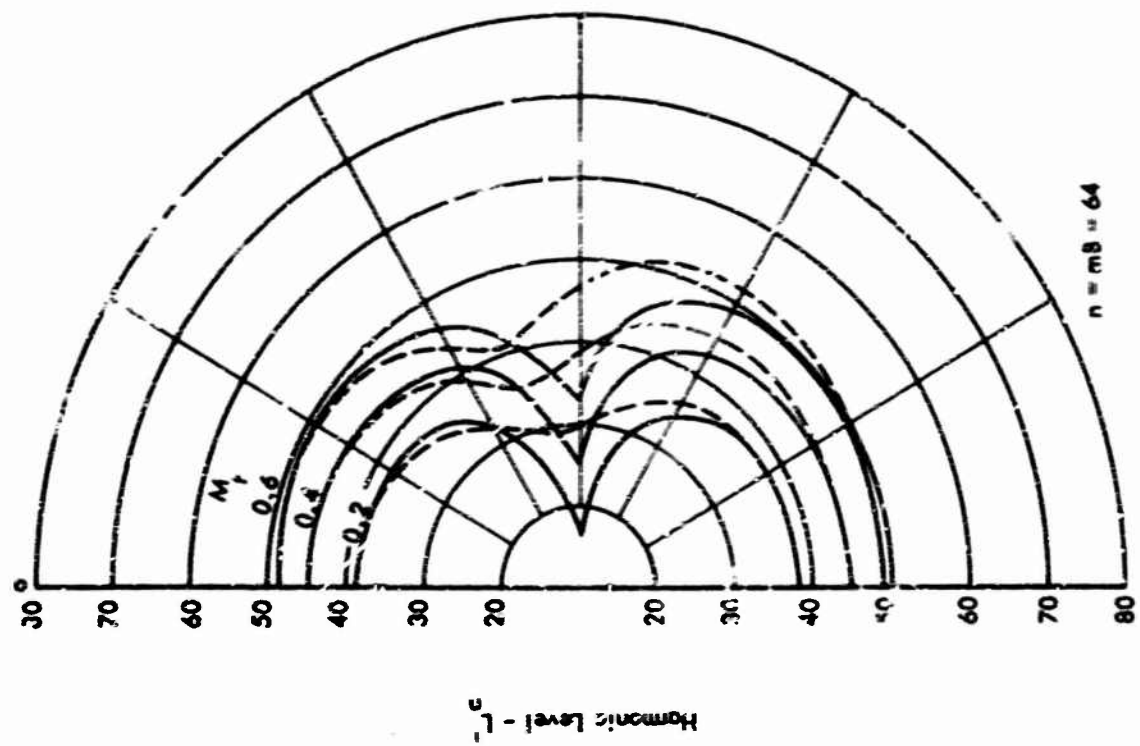


Figure III.1 (Continued)

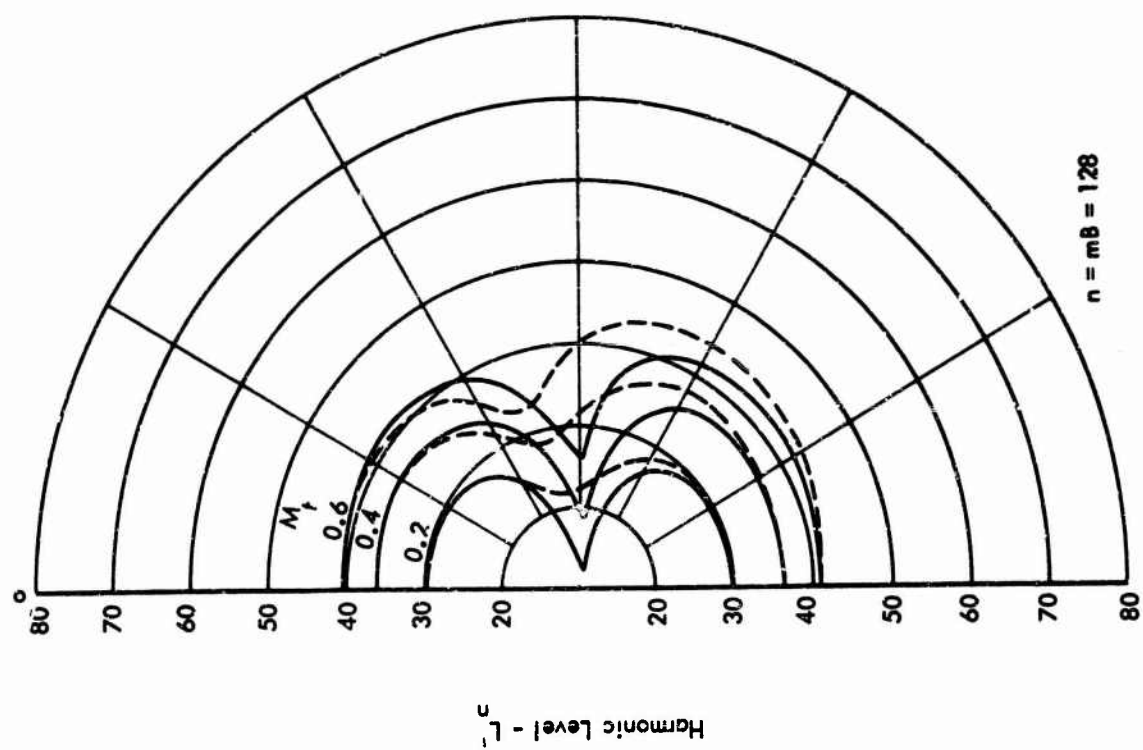


Figure III.1. (Concluded)

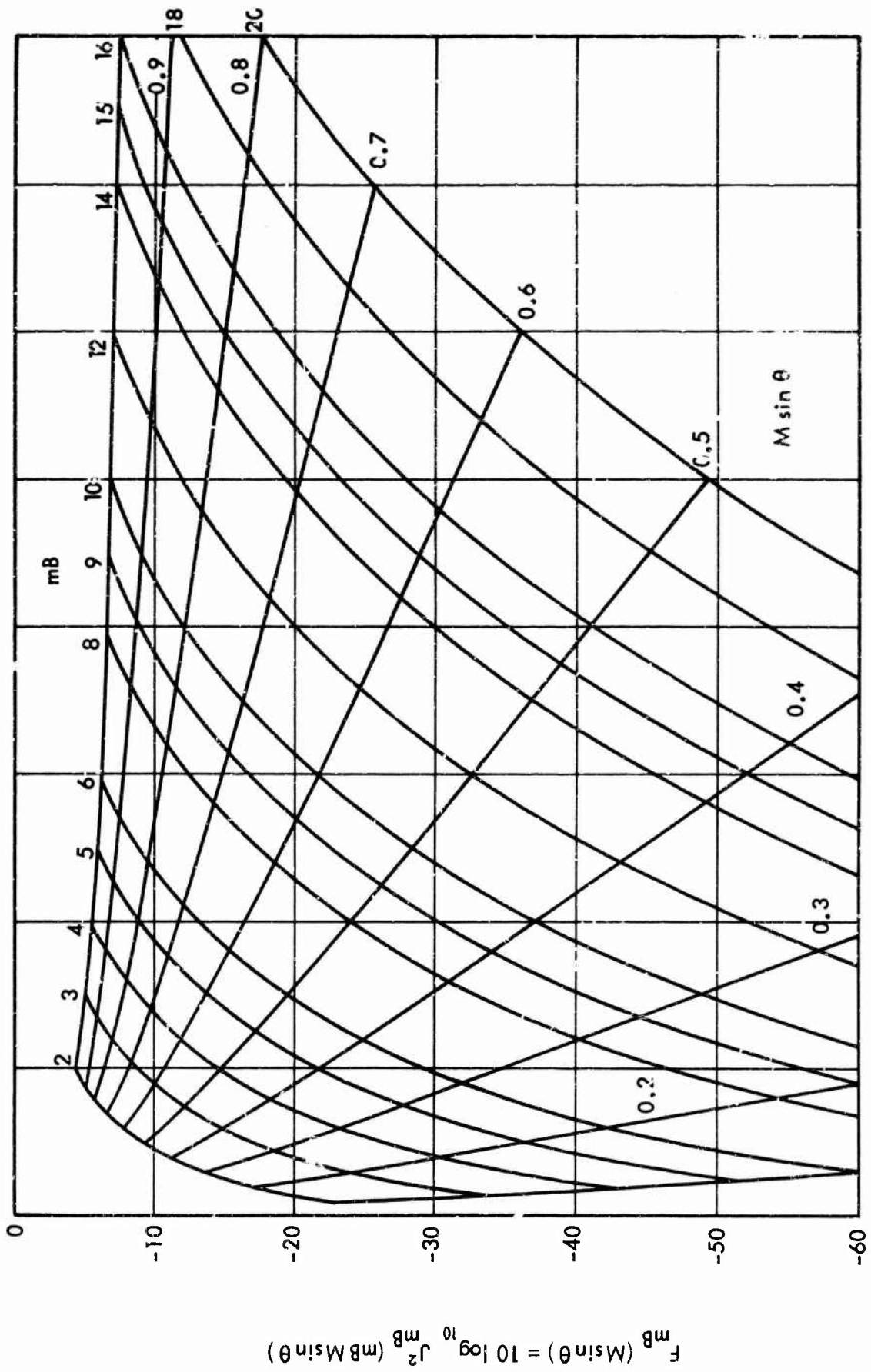
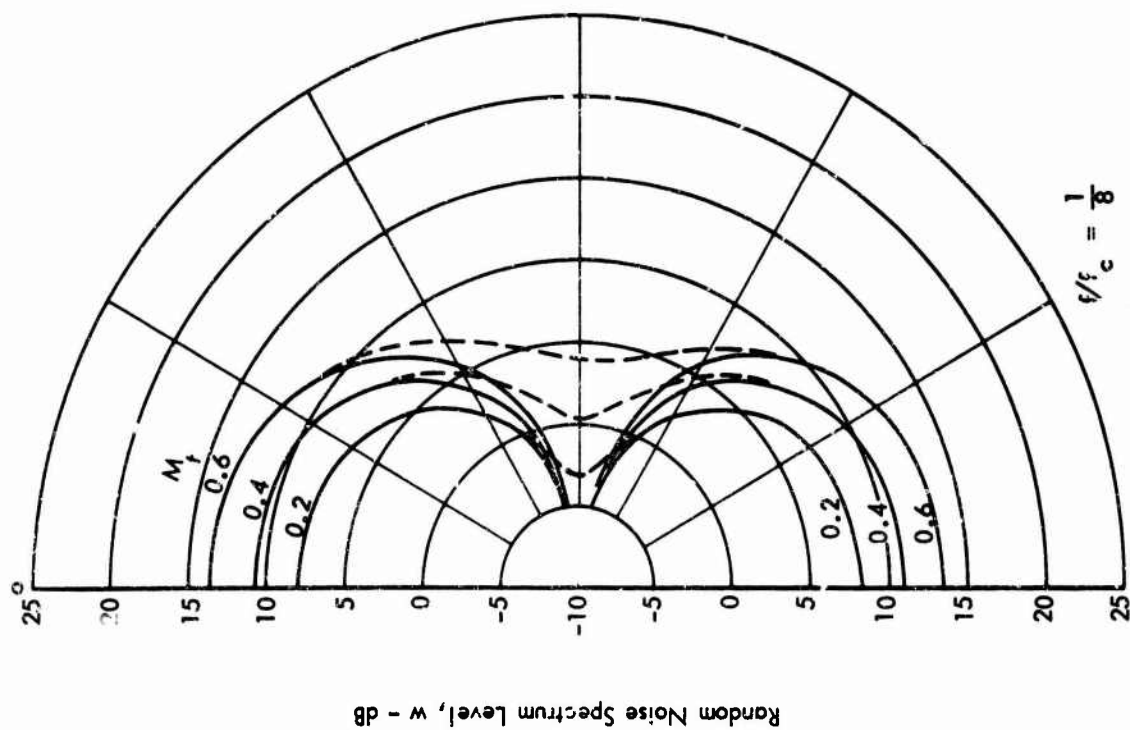
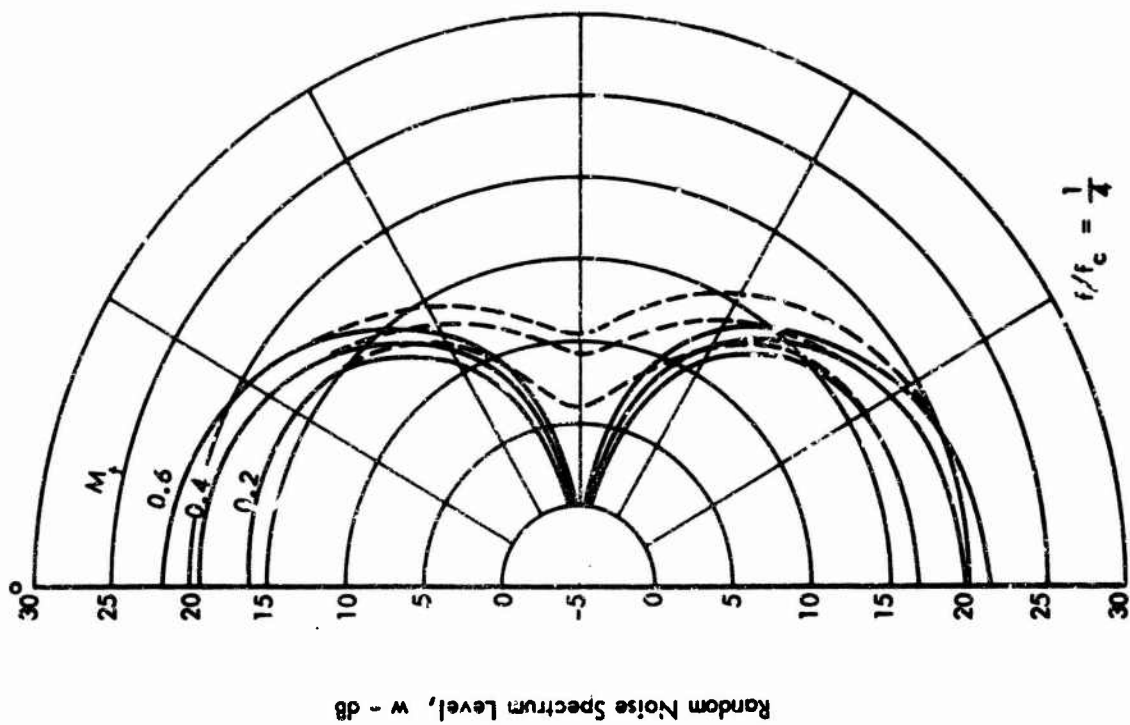


Figure III.2. Bessel Function Term $10 \log_{10} J_2^2 (mB M \sin \theta)$



--- 2 } Thrust-to-in-plane force ratio
 --- 10

Figure III.3. Spectrum Level (1 Hz Bandwidth) of Random Noise Radiation

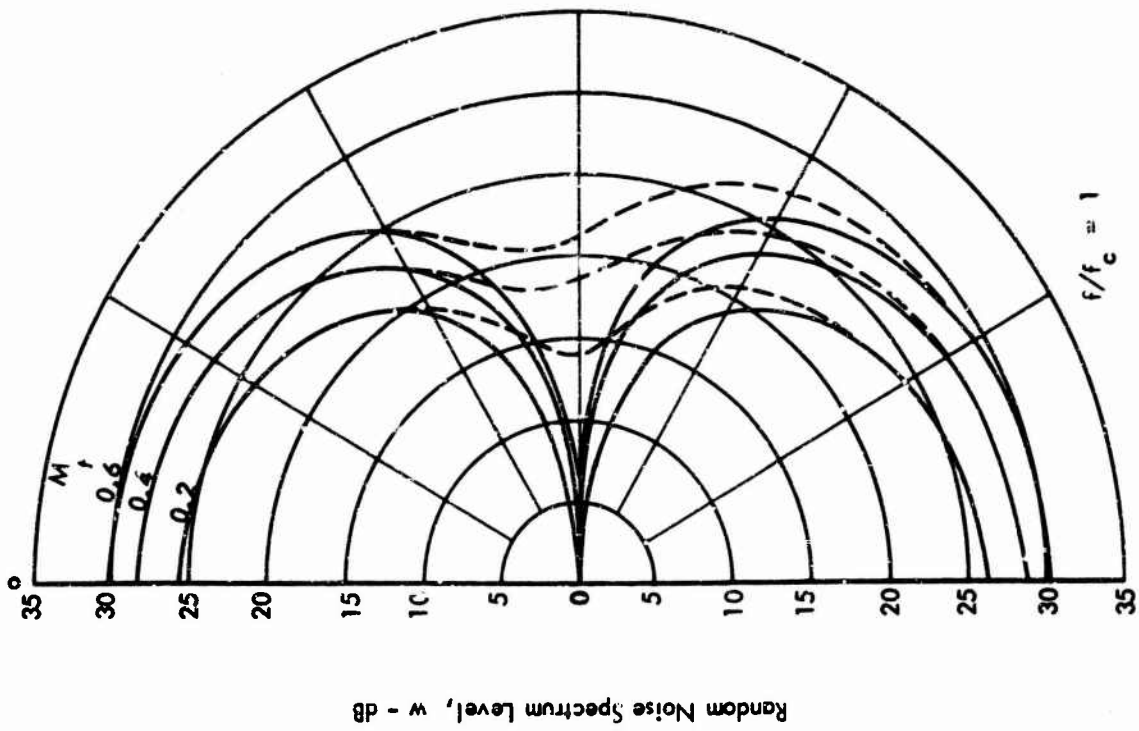
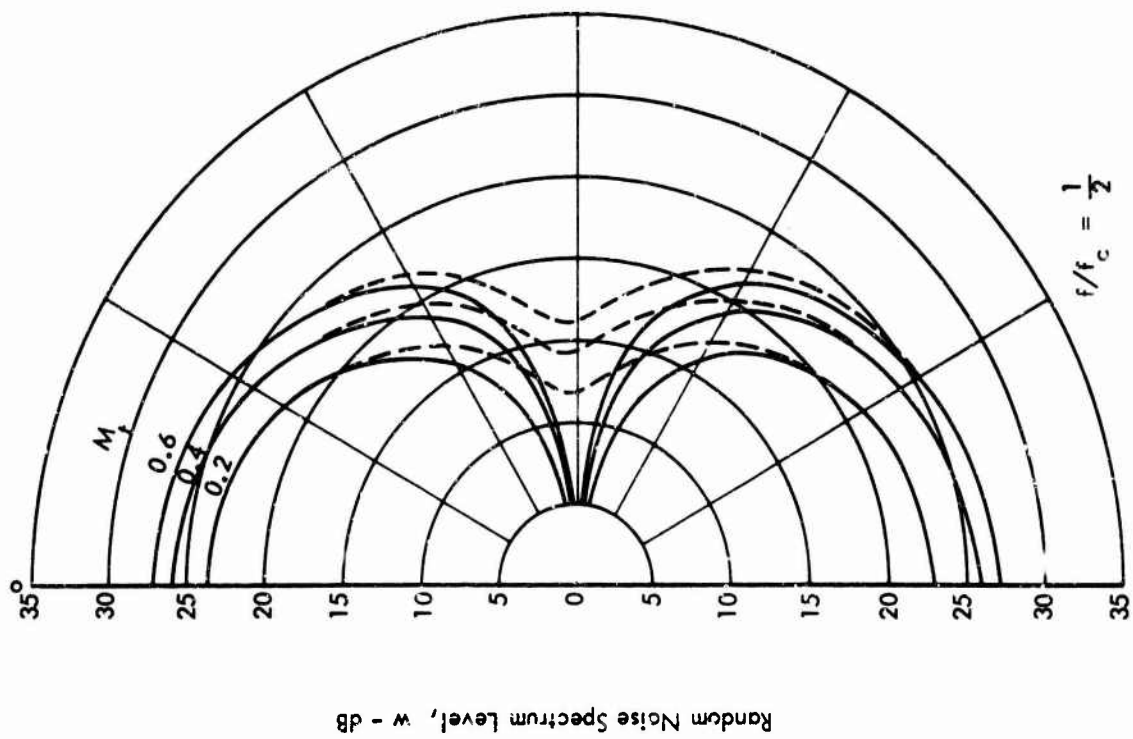


Figure III.3. (Continued)

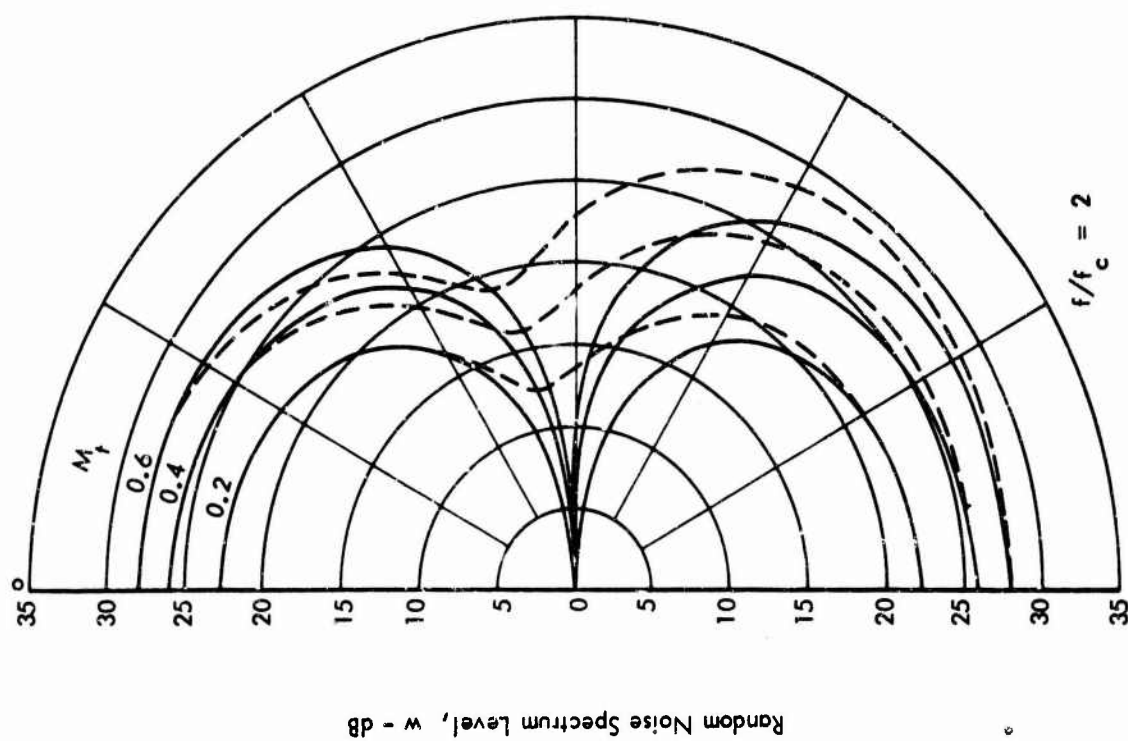
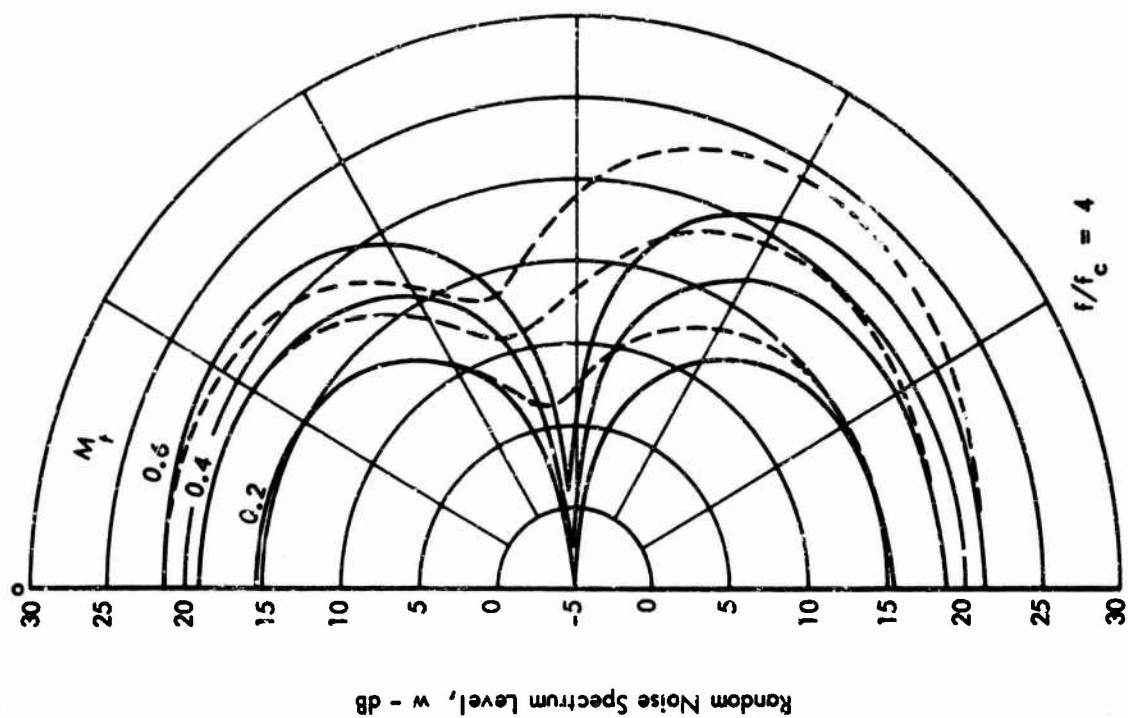


Figure III.3. (Continued)

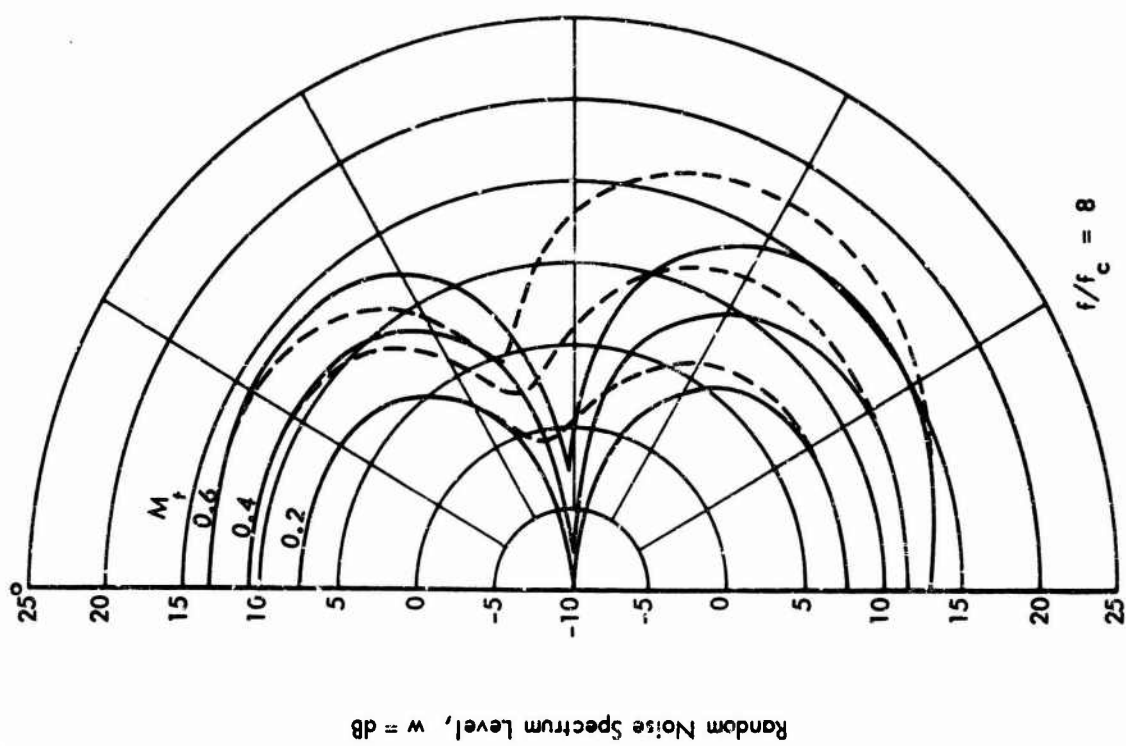


Figure III.3. (Concluded)

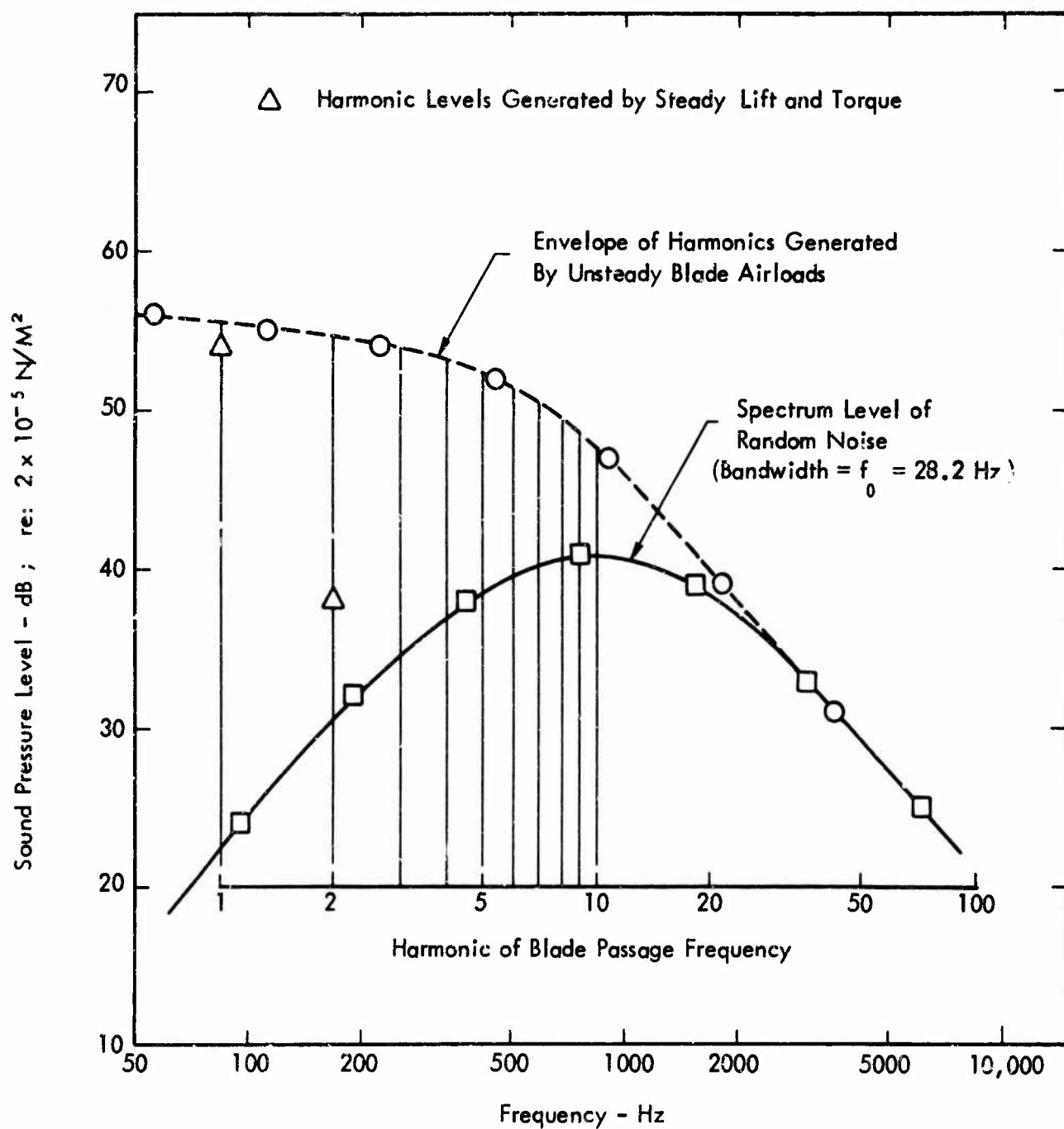


Figure III.4. Example Calculation of Propeller Noise Spectrum

APPENDIX IV

ADDITIONAL EXPERIMENTS ON PROPELLER NOISE CONTROL

Subsequent to the completion of the main study reported herein, it was decided to conduct a series of simple experiments to clarify the possible implications of boundary layer instability effects in terms of low-speed propeller noise reduction. These experiments comprised measurements of the noise radiated by model propellers (12 inch and 14 inch diameter) over a range of rotational speed, with various blade surface changes made to control boundary layer transition. The tests were conducted in a large anechoic chamber, with an electric motor drive installed outside the chamber and the drive shaft to the propeller projecting through the chamber wall. All tests and test instrumentation were identical except for the blade modifications, to allow direct comparison of the radiated noise levels. The noise data were evaluated by 1/3 octave real-time analysis and by dBA level measurements.

Test Procedures

(a) 12 inch Diameter Propellers

The noise of an unmodified (12" x 6") model propeller was measured and analyzed for each of 13 propeller speed settings over the range 5000 to 10,800 rpm. The measurement microphone was positioned at a distance of 24 inches from the propeller center, on the forward (thrust) axis. This procedure was identically repeated for a modified propeller on which the blade surface was crimped (roughened) over the leading edge region of the upper surface, and for a second modified propeller on which a small spanwise built-up ridge had been installed along the 1/8 chord line (approximately) of the blade's upper surface.

(b) 14 inch Diameter Propellers

The preceding tests indicated that a noise reduction was achieved by the modifications, relative to the unmodified propeller. In order to confirm these results, the above test procedures were identically repeated with two 14-inch diameter propellers, one being unmodified and the other being crimped in a manner similar to that of the 12-inch diameter modified propeller.

Test Results

Figure IV.1 shows a direct comparison of the dBA levels measured in each of the test series. Figure IV.2 shows 1/3 octave band spectra obtained for the 12-inch diameter propellers — unmodified, crimped and ridged, at a rotational speed of 9000 rpm.

The test results show that noise reduction of up to 5 dBA were obtained by modifying the blades. The spectral data showed that the reductions were generally predominant in the 3rd to 15th blade passage harmonic frequency range, and are consequently significant to the subjective aspects of propeller noise.

It is concluded that the stabilization of the blade boundary layer by induced (tripped) transition is beneficial in terms of low-speed propeller noise reduction. As these additional experiments were, of necessity, limited in scope, it is recommended that a more detailed study of the noise and performance characteristics of propeller boundary layer transitional effects be conducted.

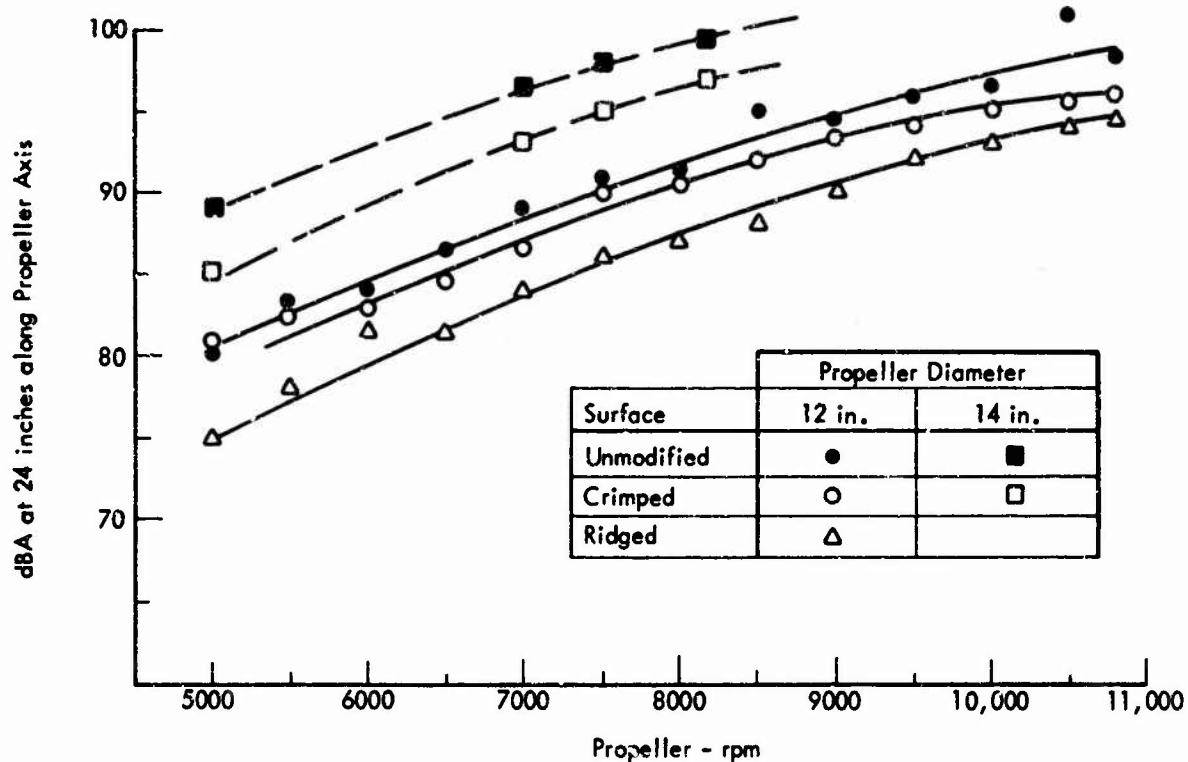
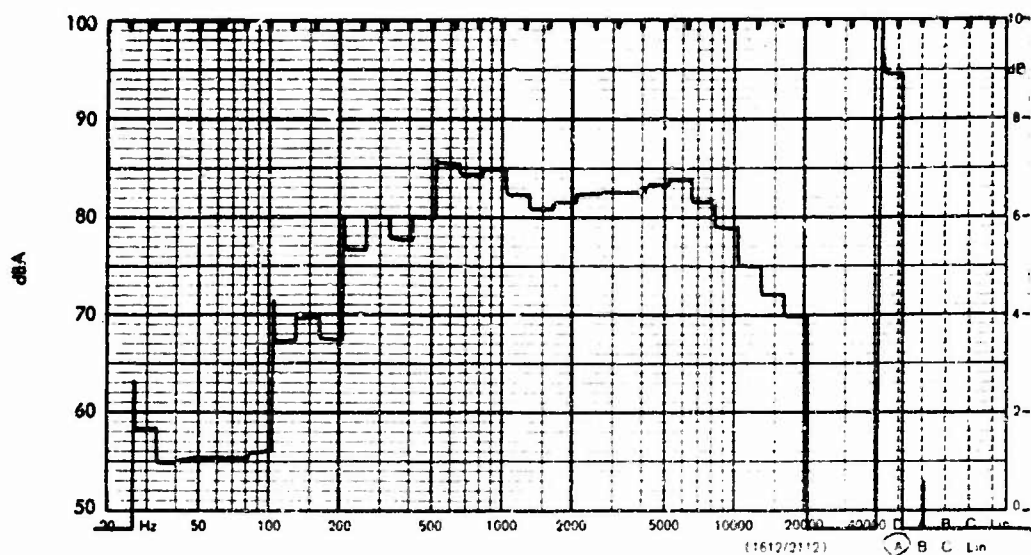
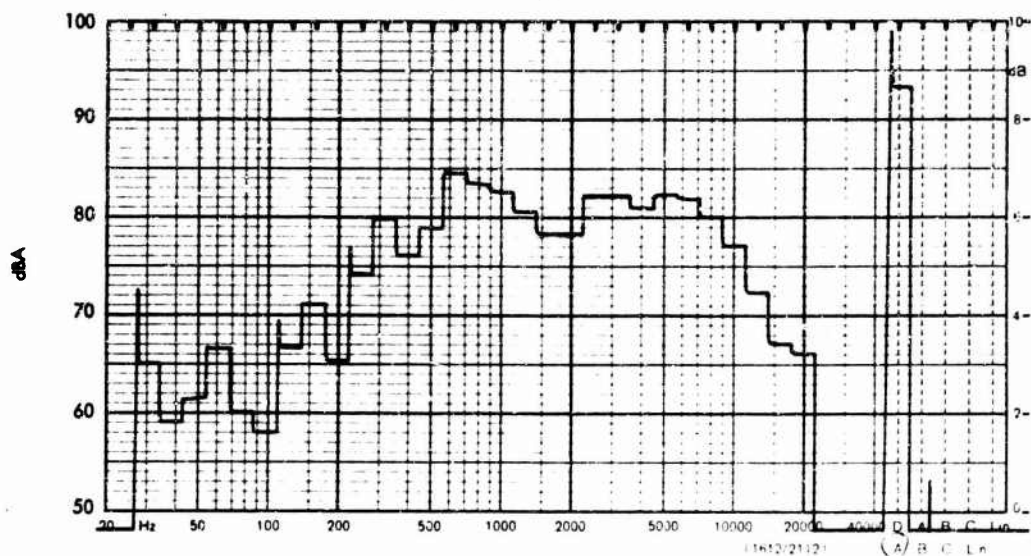


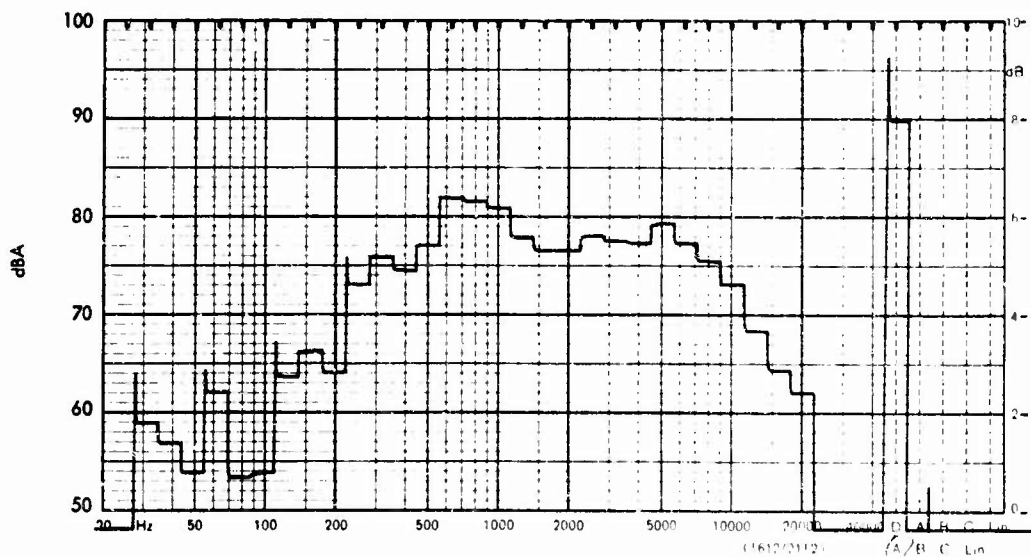
Figure IV-1. Comparison of Model Propeller Noise Levels (with Blade Surface Modifications)



(a) Unmodified



(b) Crimped Surface



(c) Ridged Blades

Figure IV-2. One Third Octave Band Noise Spectra of Model Propellers at 9000 rpm Speed